ASSESSMENT OF SIZE ASPECTS IN MODELLING MOLTEN FUEL COOLANT INTERACTION

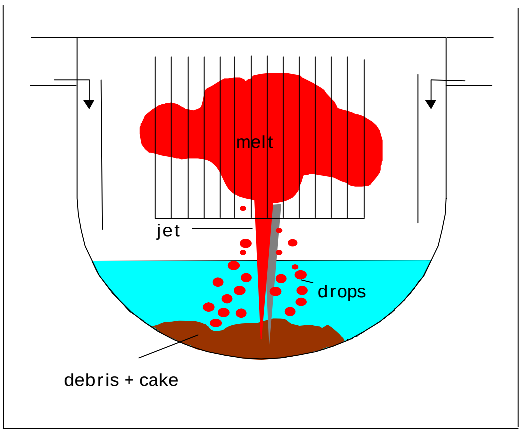

Student: **Patricia Pla Freixa**
PhD Director: **Francesc Reventós Puigjaner**
August 2003

Departament de Física i Enginyeria Nuclear
Universitat Politècnica de Catalunya

ACKNOWLEDGEMENTS

After all the years of research at the Joint Research Centre (JRC) of Ispra and at the Technical University of Catalonia (UPC), I would like to thank many people who contributed to the research and helped finalising this work. In particular, I would like to thank to:

Dr. Francesc Reventós, for being my supervisor and for his assistance, support, kindness and patient despite my absence. To all colleagues at the University for their company during my stays in Barcelona.

The JRC FARO team for welcoming me to their project and let me participate in the real laboratory experiences. Especially to Alessandro Annunziato, who has been my trainer and guide in the knowledge of MFCI phenomena; for his help during all these years, support, kindness, sincere interest and significant discussions and revisions to the manuscript. "*Grazie mille Alessandro!!*"

To all JRC FARO team: Carmelo Addabbo, Daniel Magallon, Giuseppe Leva, Werner Brewka, Rocco Silverii, Arnold Yerkess, Ilpo Huhtiniemi, Horst Weisshaeupl, Arturo Romor, Massimo Anselmi, Giovanni Sciamanna, Jean Ezan, George Nicol, Olivier Hubert, Colin Pantry, Antonio Leppeni, Alfredo Nalesso, Gian Piero Marzi, Zdzislaw Dzbikowicz, Gianpaolo Fraguglia, Raoul Kiefer, L. Bonomi, A. Renoldi, Valerio Ragazzoni, Arturo Signorelli for their enthusiasm and for engaging me in the FARO experiments activities, Karin Faber, Sara Brusamolin, Annie Mignot for their kindness and help, especially to Carola Piatti and Monica Leva for their friendship, company and free coffees.

To Chris Allison and Dick Wagner for their valuable help and constructive discussions about RELAP/SCDAP code use and understanding.

My parents, who always fully supported my work despite my stay abroad. All my Spanish friends living in Spain and around Europe, who supported my decision, and came to visit me in some occasions. And all friends and colleagues in and around Ispra and Milano, who created a pleasant atmosphere and social environment during my stay.

ABSTRACT

Severe accidents in light water nuclear reactors occur when reactor vessel water inventory decreases and there is no available additional water coolant to be delivered into the core. In general, during an extended severe accident sequence a period exists in which the reactor core, after a partial or total melt down, is poured into the lower plenum that can have some water present. The study of the interaction of the melt fuel with the water is the objective of MFCI (Melt Fuel Coolant Interaction) activities.

MFCI is one of the most important issues awaiting resolution in water cooled reactor safety analysis. The progression of a severe accident in a water cooled reactor can lead to energetic (steam explosion) or non-energetic (melt quenching) interactions as the molten fuel relocates and eventually interacts with the coolant either in the vessel lower head (in vessel) or in the cavity (ex-vessel).

The MFCI experiments at JRC Ispra site were conducted in the FARO (Furnace And Release Oven) test facility under realistic melt composition and prototypical accident conditions to provide basic information on underlying phenomena. The experimental programme was complemented by comprehensive pre-test and post-test analytical activities based on the development and application of the thermalhydraulic COMETA (COre MElt Thermalhydraulic Analysis) code. The code is developed and assessed on the basis of experimental information acquired in the FARO facility tests, and there are some limitations and uncertainties in their application to the full plant, which need to be identified and possibly quantified.

In general the main objective of the PhD research was achieved expanding the general knowledge in Melt Fuel Coolant Interaction. The knowledge was complemented collaborating and complementing the application of COMETA code under conditions not experimented before, developing and improving COMETA code sources and verifying the code consistency, analysing and unifying the COMETA simulations carried so far.

Also a further analytical study was carried out in order to illustrate the MFCI inside the general overview of a NPP (Nuclear Power Plant) severe accident sequence.

CONTENTS

1. INTRODUCTION

The present PhD Thesis in Nuclear Engineering deals with the methodology for calculate the characteristics and phenomenology of the interaction between core **molten or melt** material and residual **coolant** liquid (light water) located into the PWR (pressurized water reactor) vessel lower plenum during a severe accident progression. The study of the interaction of the melt fuel with the coolant water is the objective of **MFCI (Melt Fuel Coolant Interaction**) activities.

The core molten material, also called melt is formed by the core elements materials (U and Zr mainly) at about 3000 K of temperature. The melt relocation transient starts with the melt fall down from the core molten pool and ends when all molten material has reached the vessel bottom.

The exhaustive comprehension of the characteristic **Melt Fuel Coolant Interaction** phenomena is very important for the immediate effects assessment, for example sudden pressure increase, and also for the physical state of the material that reaches the bottom plenum, for example its temperature or fragmentation degree. This fragmentation defines the initial conditions of the lower plenum vessel thermal attack and the likely subsequent ex-vessel severe accident transient.

The Three Mile Island (TMI) reactor accident has been an important experience for the study and evolution of the light nuclear reactors (LWR) safety analyses. Theoretical studies supported by experimental facility tests, built up after the TMI accident, have allowed the expansion and verification of complex calculation codes, which are able to simulate a severe accident progression in a LWR. In this context the TMI experimental data are fundamental for the codes assessment.

The PhD research work was performed in its first part in the European Commission (EC) Joint Research Centre (JRC) of Ispra (Italy) as host site by means of a EC Marie Curie Research Training Grant (from march 1998 to march 2000) and a EC Auxiliary contract (from march 2000 to march 2001). The JRC researchers Alessandro Annunziato and Carmelo Addabbo supervised the work. Work was finished at the Technical University of Catalonia (UPC), Barcelona (Spain). The director of the PhD Thesis is the UPC professor Dr. Francesc Reventós.

In the field of reactor severe accident research, the European Commission carried out the FARO Research Programme specifically devoted to the characterization of MFCI, melt quenching as well as melt spreading phenomena. The MFCI experiments at JRC-Ispra site were conducted in the FARO test facility under realistic melt composition and prototypical accident conditions. The COMETA thermalhydraulic code was developed in the JRC-Ispra site in order to support FARO test preparation and execution with pre-test calculations and assist test results interpretation with post-test calculations.

PhD Thesis includes all the following items carried out during the stage in the Joint Research Centre - Ispra site: **a)** Complementing the application of COMETA code to the prediction of tests performed in the FARO facility under new conditions not experimented before (subcooled and triggered conditions). **b)** Simulation with COMETA of an extended MFCI accident in a hypothetical real size reactor with arbitrary geometry. **c)** Verification, analyses and unification of the COMETA simulations carried so far simulating again all the FARO experiments with the last available version of the COMETA code. All those subjects included the identification of simulation problems in the application of the COMETA code, which lead to a further development, and improvement of the code.

The general overview of the MFCI phenomena included in the PhD research was completed in the Technical University of Catalonia (UPC) with a study of a large LOCA accident in the overall view of a NPP with the RELAP5/SCDAP code. Focusing its interest in clarify how MFCI is placed in the context of a severe accident.

The document is structured in the following way:

Chapter 2 presents an explanation of the Melt Fuel Coolant Interaction (MFCI) phenomena.

Chapter 3 explains severe accidents phenomena and places the MFCI into the general overview of the severe accidents, this chapter also gives a brief of the severe accident research, mainly MFCI research, around the world, in terms of experimental facilities and analytical tools.

Chapter 4 presents the objectives of the PhD Thesis.

Chapter 5 presents the FARO facility, the main components and the simulation of accident phenomena into the facility.

Chapter 6 presents the models of the thermalhydraulic and melt fragmentation COMETA code.

Chapter 7 is a review of the PhD research activities. In particular:

COMETA pre-tests calculations are explained in chapters 7.1 and 7.2. In addition to give information for test experiment planning and execution in the FARO facility, the calculations gave results to improve COMETA code logic.

Chapter 7.3 summarizes the application of the COMETA code to reactor configurations, larger than scaled test facilities. This application was not performed before. The results lead to the identification of scale-up problems in the logic of the COMETA code. They also solved and explained one of MFCI related phenomena: the relation between the void fraction and the quenching rate.

To analyse and unify the experiment simulations with the last available version of the COMETA code another work is presented in chapter 7.4. Along the years the COMETA code was improved and changed to fit experimental results. This purpose was fulfilled simulating again tests from L-14 to L-31. This work gave some indications that help to choose the nodalization scheme in order to reduce the COMETA computer calculation time. The post-test analyses of the FARO experimental data increased the information for the assessment and qualification of the COMETA code.

In chapter 7.5 the calculations with RELAP5/SCDAP code complete the general overview of the MFCI phenomena included in the PhD research.

The application of COMETA code to the prediction of tests performed in the FARO facility and to reactor configurations, larger than scaled test facilities, lead to improve and develop COMETA code. Chapter 8 explains an important COMETA code improvement, particularly in the modification of the code to adjust *drops* radial movement, which is necessary in reproducing some local phenomena.

2. MELT FUEL COOLANT INTERACTION AND QUENCHING

The **MFCI (Melt Fuel Coolant Interaction)** is the sudden evaporation of a ***coolant liquid*** when interacts with another liquid, ***molten fuel***, less volatile and hotter. Phenomena present in nature could verify also this happening, for example falling volcanic magma emission in water. In a **MFCI** there is a rapid heat exchange from the molten fuel to the coolant through the large increase of the heat exchange surface due to the molten fuel fragmentation in a short period of time.

In a postulated severe accident in which the core melt-down partial or totally has occurred jets of molten material are poured into the lower plenum through the core support plate. The presence of residual water in the lower plenum can determine a fragmentation of the melt leading to interaction of melt particles with the coolant. This thermal interaction, depending on the fragmentation degree and the fragments size, could lead to a strong local vapour production that could eventually threaten the vessel integrity (steam explosion). However, if no steam explosion occurs, a strong vapour production and high system pressurization exists. On the other hand, if the melt reaches the bottom of the lower plenum unquenched potential exists for lower head penetration due to the residual power still produced in the debris bed.

The study of the interaction of the melt fuel with the water **MFCI (Melt Fuel Coolant Interaction)** activities is one of the most important issues awaiting resolution in water cooled reactor safety analysis. The progression of a severe accident in a water cooled reactor can lead to energetic (steam explosion) or non-energetic (melt quenching) interaction as the molten fuel relocates and eventually interacts with the coolant either in the vessel lower head (*in-vessel*) or in the cavity (*ex-vessel*). Referring to potential steam explosion, it is important to determine the melt-coolant mixture conditions in order to evaluate whether an explosion is conceivable or not. For melt coolability, the physical state of the molten fuel reaching the lower plenum bottom can seriously affect the possibility of coolability and vessel failure.

In MFCI experimental problems one of the main matters is the determination of the conditions of the melt when it arrives to the bottom plate of the vessel. If great fragmentation and quenching is produced in the water no big problems for vessel attack would occur. If instead a significant amount of melt would remain as a solid molten cake, potential for lower head penetration would exist.

In-vessel progressions take place into the pressure reactor vessel during a severe accident where initially core is degraded loosing geometry and melted down, the transient ends with molten pool formed slumping and interacting into the residual water in the lower plenum. Depending on the conditions of the molten material when it reaches the bottom vessel an energetic (steam explosion) or non-energetic (melt quenching) interaction could happen. Experimental studies have so far demonstrated that in-vessel steam explosion is retained very unlikely to occur. Only in cases when primary system pressure runs down to very low values steam explosion could be considered. In the working pressure ranges non-energetic (melt quenching) interaction is likely to occur.

Ex-vessel progressions take place outside pressure reactor vessel. They start when molten material slumps outside broken reactor vessel towards containment building. Molten material could interact with coolant water present in the containment pavement; water delivered from a primary circuit LOCA (Loss of coolant Accident) or present due to some emergency system procedure. Energetic interaction could occur because of low pressure in the containment building but in general is not considered due to the limited water quantity and only *spreading* of molten material over the water occurs.

Since the signing of the EURATOM treaty in 1957 the European Commission (EC) has been engaged in the support of reactor safety research activities, principally in the synchronization safety practices and methodologies among the EC member counties. The Commission promotes and conducts direct action research programmes performed in the JRC laboratories in close collaboration with research organizations.

In the severe accident research field, the MFCI experiments at JRC-Ispra site were conducted in the FARO test facility to provide basic information on fundamental phenomena. The Commission of the European Communities in order to characterize MFCI, melt quenching as well as melt spreading phenomena established the FARO Programme in September 1990. A first series of corium melt water quenching experiments was proposed in collaboration with US Nuclear Regulatory Commission (NRC), the Electric Power Research Institute (EPRI), and the Ente Nazionale per l'Energia Elettrica (ENEL, Italy). This programme was approved by the EC Member States and was followed by a group of EC experts.

KROTOS was another facility located in the JRC-Ispra site, it was a relatively small scale experimental installation dedicated to the study of molten fuel coolant pre-mixing with little masses of prototypic reactor melts or simulants as alumina (Al_2O_3). The progression of spontaneous and triggered energetic fuel coolant interactions (steam explosions) was also studied.

The experimental facilities programme was complemented by comprehensive pre-test and post-test analytical activities based on the development and application of the thermalhydraulic COMETA code.

From the MFCI experiences it is retained that a quite high pressurization rate has to occur in the interaction zone to have an energetic interaction (steam explosion); this would disturb the stability of the vapour film around the melt particles and possibly cause liquid-to-liquid contact with explosive consequences. The pressurization rate that can be achieved spontaneously or with a trigger is function of the pulse strength and the local void fraction.

FARO and KROTOS experiments shown that ***hydrogen generation*** due to several oxidation processes during the premixing phase of an interaction process of UO_2/ZrO_2 melts with water, would lead to increase void fraction formation within the mixture, which could suppress the propagation of triggered pulses and thus an eventual energetic escalation. Although there are considerable quantitative uncertainties on the behaviour of oxidic melts at high temperatures which need to be further assessed, COMETA calculations and KOTOS tests suggested that hydrogen generation and thus void formation in the interaction of Al_2O_3 base melts with water is less pronounced leading to thermalhydraulic conditions favourable to a steam explosion with energetic escalation.

In general, COMETA results indicated that non-condensable gases as H_2 have to be accounted for in the calculation for a proper representation of melt fuel coolant interaction and quenching processes.

3. STATE OF THE ART

3.1. SEVERE ACCIDENT UNDERSTANDING

The accident of Three Mile Island (TMI)-2 reactor in the United States on 28th march 1978 was the first nuclear accident with severe damage to the core. A severe accident in light water nuclear reactors occurs when the reactor vessel water inventory decreases and there is no available additional water coolant to be delivered into the core. In general during an extended severe accident sequence a period exists in which the reactor core, after a partial or total melt down, is poured into the lower plenum that can have some water present.

This accident shows that diagnostic and operation failing together with malfunctions in the operational systems could lead to serious consequences that were not expected in the design base accident scenarios. It is because severe accidents have now been studied worldwide for more than twenty years. Since TMI accident great effort has been devoted by manufacturers, exploiters and regulatory organizations to prevent and mitigate severe accidents: safeguards design, fission products confinement barriers, post-accident instrumentation, inspection and maintenance, emergency operation procedures, degraded accident management, operators training and formation among other subjects were generated or revised.

Multidisciplinary international projects have been raised to improve best understanding in the computational models that simulate phenomena correlated to severe accidents: core degradation, containment response, as well as to estimate the behaviour of gases, vapours and aerosols released in the accident progression.

3.2. MELT FUEL COOLANT INTERACTION IN LOWER WATER REACTOR SEVERE ACCIDENT PHENOMENOLOGY CONTEXT

A wide range of physical and chemical phenomena characterizes severe accidents. Knowledge of those phenomena and its interconnection can be acquired through experimental research at small and large scale and through analyses of the real experience.

Damage mechanisms exist during a severe accident in an LWR. They can change a reactor core from cylindrical fuel rods located in the centre of the reactor vessel to a deep debris bed located in the bottom of the vessel. The reactor vessel itself becomes vulnerable to heatup and damage after the core has relocated to the lower head.

The TMI-2 accident and severe fuel damage experiments have shown that reactor core damage proceeds through several stages before the core slumps to the lower head. These stages of damage progression include: (a) embrittlement of cladding due to oxidation, (b) melting of metallic cladding and dissolution of fuel in contact with liquefied cladding, (c) slumping of liquefied cladding and dissolved fuel due to failure of the oxide shell containing the liquefied mixture, (d) solidification of the slumped mixture at a lower and cooler location in the core and concurrent formation of a nonporous debris region that blocks the flow of coolant, (e) meltdown of the reactor core into a molten pool supported by the frozen previously molten ceramic material, and (f) melt-through or structural failure of the crust of frozen material that supported the molten pool and slumping of the molten pool to the bottom of the reactor vessel. An hour or more of time may elapse before damage has progressed through these six stages. This order of damage progression is established by the differences in melting temperatures of the metallic and ceramic parts of the reactor core.

Main severe accident associated well-known phenomena are represented in the schematic drawings of Figure 3.1.

Among the ***in-vessel*** phenomena:

Figure 3.1 a) represents cladding degradation when cooling system is not able to extract thermal energy produced in the fuel. Clad rod heats up, looses its mechanical properties, suffers ballooning, breaks due to internal pressure or does not break. Previous breaking sometimes occurs without ballooning. In any case, cladding zircalloy oxidizes in vapour presence, at temperatures above about 1500 K. Oxidation produces hydrogen and energy ($Zr + 2H_2O$? $ZrO_2 + 2H_2 + 586$ KJ/mol), which increases core heating rate and could produce temperature peaks that causes cladding melting. The oxidation increases also melting temperature of a-Zr(O) up to 2250 K and 2970 K for ZrO_2.

Figure 3.1 b) shows advance of cladding and fuel degradation. Oxidation energy and channels blocking due to cladding ballooning increase the fuel and cladding heating. A Zr-Fe and Zr-Ni eutectic is the first liquid formed. The In-Ag alloy also attacks Zr at 1500 K. Zirconium forms a eutectic with UO_2 that melts at 2500 K. The molten material drips over the intact clad rods and freezes in the cooler core parts as the plate that supports fuel rods.

The TMI-2 reactor core autopsy as well as the series of integral experiments SFD, CORA and PHEBUS-CSD have demonstrated that a metal solidified crust is formed, generally located on the lower plate (Figure 3.1 c)). This crust encloses a molten material pool, commonly oxides UO_2, ZrO_2 and steel components that form eutectic mixtures with low melting points (1670 K). Another crust, that contains oxides, is formed above the molten material pool. A porous debris bed, which is difficult to cooling, is formed above the crust.

Before damage has occurred, the configuration of the core is characterized by parameters such as rod spacing and rod diameter. After ***in-vessel*** damage has occurred, the configuration is characterized by parameters such as depth and porosity of debris. If the porosity is large and the debris is covered with water, then most of the decay heat in the debris can be removed by convective cooling. But, if the porosity is small and the debris bed is deep, then a large molten pool may develop. At this stage, there is the potential for rapid slumping of a large amount of hot material into the lower head of the reactor vessel and the possibility of a vigorous thermal attack of the lower head.

The damage progression can be either abated or intensified by the injection of water into the reactor vessel. On one hand, the injected water may cool the damaged core and stop damage progression. On the other hand, the injected water may break embrittled fuel rods so that the fuel rod fragments slump into the configuration of a porous debris bed. The injected water may also increase an excursion in the oxidation of fuel rod cladding in the parts of the reactor core where the oxidation was steam starved.

The last phenomenon recognized into the reactor vessel is the corium molten pool slumping into the bottom vessel (Figure 3.1 d)). In the TMI-2 accident the disintegration heat made the crust unstable due to thermal and mechanical stresses. The fluid pours in coherent shape into the bottom vessel. If there is residual water in the vessel at the slumping time, molten fuel interacts with water **(Melt Fuel Coolant Interaction)**, increasing pressure and continuing oxidation of zircalloy. A vapour explosion cannot be excluded. In other sequences hotter parts of the core can fall into the lower plenum due to lower plate destruction. These hot rests can form a liquid pool directly in the bottom vessel.

Among the ***ex-vessel*** phenomena:

Figure 3.1 e) shows molten corium expulsion outside pressure vessel. The interaction of fused and superheated corium with the bottom vessel steel can break it provoking fluid expulsion. Experts predict 3 methods, depending on pressure: (1) One vessel zone partial fusion. (2) Instrumentation tubes (PWR or BWR) fusion or control rods devices (BWR) fusion. (3) Bottom vessel break due to fluence at high temperature. TMI-2 vessel did not suffer degradation and only some tubes were melting. Probably melt fuel coolant interaction formed a fragmented debris bed, which was easy to cool. TMI-2 VEP project from NEA/OECD studied this important issue.

Figure 3.1 f) represents when molten corium is expulsed outside pressure vessel like a jet at high pressure and collides with the concrete pavement on the containment floor. Experts predict corium fragmentation in small hot particles and the particles diffusion in the containment environment. The non-oxidized zirconium can still react with the water steam present, releasing chemical energy and hydrogen. The atmosphere heating increases pressure and temperature on the containment walls threatening its integrity. The generated hydrogen increases the detonation risks. The detailed analyses of the associated phenomena and the containment break are being studied.

The hydrogen generated in the oxidation reactions; mainly from zirconium oxidation is accumulated in the containment room. It could reach the detonation threshold of the mixtures hydrogen-water steam-air. The shock waves generated can threaten vessel integrity (Figure 3.1 g)). Devices are installed for H_2 combustion in a controlled way to avoid the explosion risks. All the phenomena associated to hydrogen generation and transport, the detonation threshold, the transition from deflagration to detonation, the flames propagation, the shock waves physics, etc. is now object of deep study.

Figure 3.1 h) represents corium-concrete interaction. Corium poured on the containment floor produces concrete thermal disintegration, with water steam, CO_2 and silicon oxides release. These gases react with the corium metallic components producing hydrogen and CO. Oxides released in the concrete disintegration are incorporated to the corium reducing the melting temperature of the mixture. Corium molten mass cooling with water has not been demonstrated experimentally. Phenomena related to corium-concrete interaction has been studied in the EPRI-MACE project.

Among the ***gases, vapours and aerosols*** behaviour:

Gases, vapours and aerosols release (Figure 3.1 i)): 1) Cladding break releases gas and vapour that were accumulated in the gap, mainly noble gases and elements or chemical volatile substances. 2) Fuel melting releases vapours of the elements and components with lower boiling point, as caesium, iodine, tellurium, which lately become aerosols by condensation. 3) During the corium-concrete interaction, the higher temperatures and the gas bubbling lead to refractory oxides release, oxides that become aerosols of mechanical origin.

Gases, vapours and aerosols transport through primary system (Figure 3.1 j)): Gases, vapours and aerosols generated in the core, travel by pipes and components and arrive to the containment or outside the system. During transport gases could remain trapped by condensation, adsorption or precipitation in metallic surfaces. The gases, vapours and aerosols in the same way could break off from the walls when the hydraulic or thermal conditions change in the pipes and components or when physical properties change forming new chemical components.

Retention phenomena of gases, vapours an aerosols in water pools are represented in Figure 3.1 k). The bubbling of gases, vapours and aerosols in water pools is an efficient method to retain them. The document NUREG-1150 states decontamination factors from 1.2 to 4000. In PWR reactors these phenomena can happen in relief tanks, secondary side of steam generators and pressurizer. In BWR reactors it occurs in the relief pool. Gases vapours and aerosols in the bubbles can pass to the water through the separation membrane. The pass rate depends on the thermalhydraulic conditions of bubbles and mass of water. The LACE project investigated this subject.

Gases, vapours and aerosols retention phenomena in containment building are represented in Figure 3.1 l). Containment buildings have systems to retain gases vapours and aerosols released in accidents. Spray and filtration systems are the most commons. Water drops are created by the aspersion system and dissolve easily some components of iodine and caesium, while the high efficiency filters are much effective in retaining aerosols. Precipitation and adsorption are also used. Iodine can form inert organic molecules, which are difficult to retain. Radiation and disintegration heat introduce additional phenomena.

In-vessel phenomena:

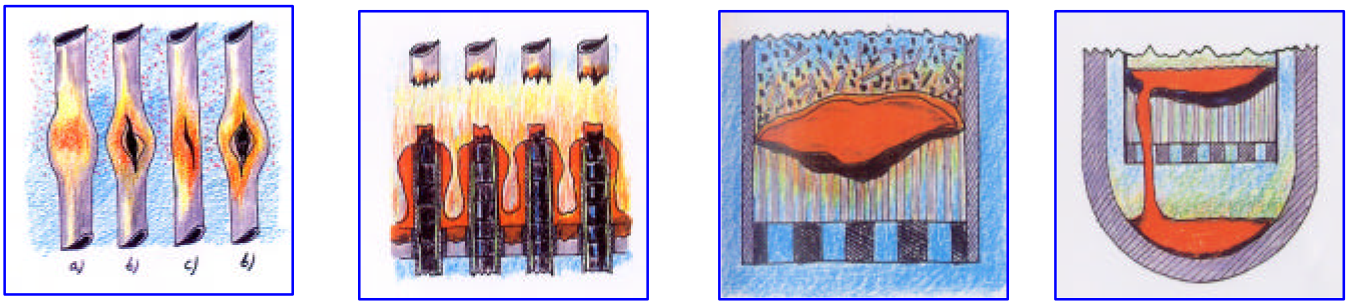

a) Cladding oxidation and ballooning

b) Fuel dissolution and melting

c) Crust, melt and debris bed formation

d) Corium relocation in the bottom vessel

Ex-vessel phenomena:

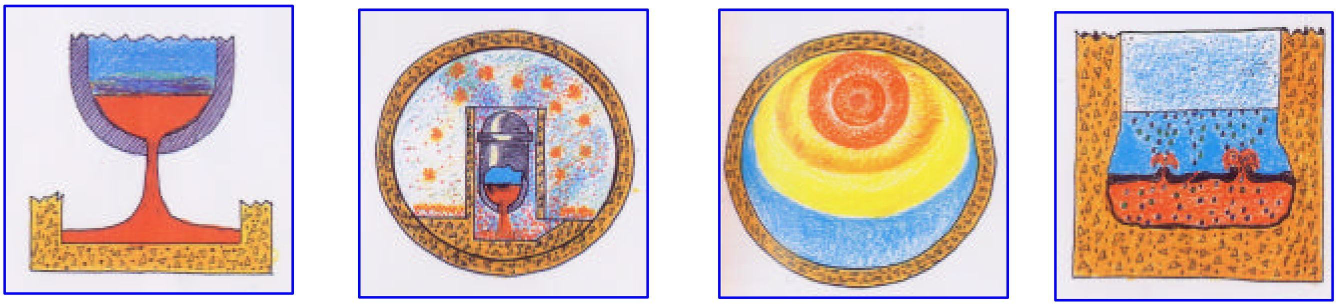

e) Expulsion of melt corium

f) Containment direct heating

g) Hydrogen explosions

h) Corium-concrete interaction

Gas, vapour and aerosol behaviour:

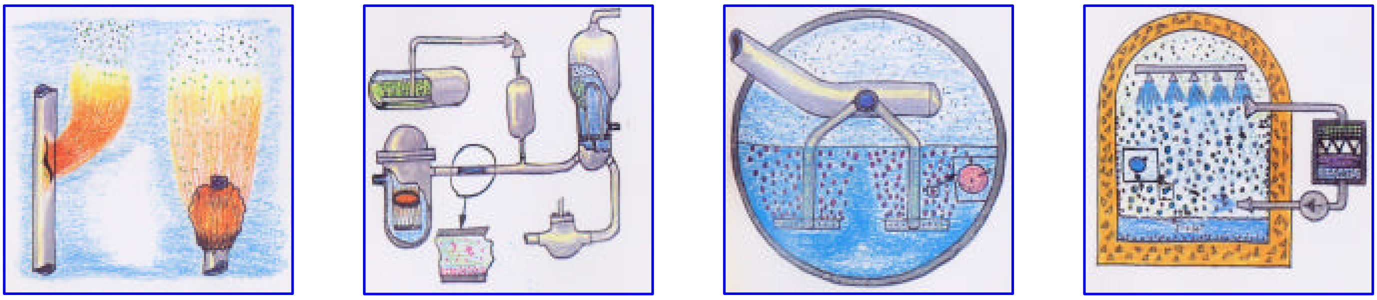

i) Gases, vapour and aerosol release

j) Gases, vapour and aerosol transport through primary system

k) Gases, vapour and aerosol retention phenomena in water pools

l) Gases, vapour and aerosol retention phenomena in containment buildings

Figure 3.1 - Severe accident associated phenomena [From [34]]

3.3. WORLD WIDE SEVERE ACCIDENT RESEARCH

3.3.1. EXPERIMENTAL FACILITIES

In 1996, the Senior Group of Experts on Nuclear Safety Research Capabilities and Facilities (SESAR/CAF) [28], which was investigating the ability of OECD Member Countries to sustain an adequate level of research, identified a number of facilities and programmes that were important for continuing research needed by the safety community during the coming decade. They also pointed out that many of these facilities and programmes were facing increasing budgetary constraints, and that some would cease to be supported at the national level in the near or medium-term future. Some of the facilities were of interest to more than one country. It therefore seemed logical to investigate the possibility of operating the facilities in an international context, in order to share the costs and the expertise, and to promote quicker and deeper international consensus on safety issues. It was in this context that in 1997 the NEA Committee on the Safety of Nuclear Installations (CSNI) decided to set up a Senior Group of Experts on Nuclear Safety Research Facilities and Programmes (SESAR/FAP). The new Senior Group of Experts was asked to identify facilities of potential interest for present or future international collaboration, to make specific recommendations regarding facilities, research programmes, and joint projects, and to discuss other possible forms of international collaboration. For efficiency, the group was restricted to the countries running the widest and most advanced research programmes. Some of the conclusions of the studies are presented in this chapter.

Severe accidents join three main topic areas: ***in-vessel phenomena***, ***ex-vessel phenomena*** and ***fission products***.

Due to the enormous extension of research topics in severe accidents only a little brief of the current state of the art following ***ex and in-vessel phenomena*** research facilities is given. Some of the in main subjects related to the ***in-vessel phenomena*** are:

1. ***Core Degradation and Melt Progression*****:** The facilities currently in operation conducting core melt progression experiments for PWRs are the QUENCH facility in Germany, PHEBUS in France and CODEX in Hungary.

QUENCH facility investigates the early phase of core melt progression, with emphasis on reflooding and the resulting fragmentation and H_2 generation. It was planned to operate in the near term.

PHEBUS had three tests remaining, primarily directed toward fission product transport; however, some information on early and late phase melt progression will be obtained, although at a small scale. Work on irradiated fuel is undertaken in PHEBUS. The continued conduct of core melt progression experiments will complement analytical code development and assessment and may be useful in addressing any concerns related to the changing operational characteristics of operating plants (e.g. higher burn-up fuels, higher power density).

2. ***Melt Fuel Coolant Interaction (MFCI):*** Currently there are several facilities in operation investigating MFCI.

Small-scale facilities (using simulant materials) exist in the US (University of California-Santa Barbara - MAGICO and SIGMA), Japan (ALPHA), Korea (CONVEX), Sweden (MIRA), COTELS (Kazakhstan, sponsored by Japan) and France (MICRONIS and TREPAM).

The ECO (Experiments on energy COnversion during a steam explosion) facility (FZK, Germany), housed inside the large FAUNA steel vessel, was designed for investigating energy conversion ratios up to 20%, related to 10 kg of melt under well-defined conditions after an energetic steam explosion. Alumina from a thermite re-action is used as a simulating material instead of corium.

The QUEOS (QUEnching Of Spheres) facility (FZK, Germany) serves to study premixing phenomena with solid spheres, i.e. without the danger of a steam explosion and the complication of melt fragmentation. In order to simulate melt jets as closely as possible, the spheres are released as a cylindrical jet into a three-dimensional test vessel.

The PREMIX (FZK, Germany) experiments have been performed to study the premixing of sizable amounts of very hot oxidic melts with water when being released as a jet in a reasonably characterized way and with full optical access. Alumina at 2600 K from a thermite reaction was used to simulate the corium melt. PREMIX involves the full physics of the mixing process including jet break-up and melt drop fragmentation.

Each of these facilities, with the possible exception of ALPHA, is projected to continue operation in the near term or be available, if needed.

The MISTEE (Micro Interactions STeam Explosion Experiment) (RIT, Sweden) facility is laboratory scale research on Molten Fuel-Coolant Interactions (MFCI) using a single molten drop. A new test facility was constructed. The objectives of this activity on single drop steam explosions are to investigate the triggerability and explosivity in a well-controlled facility with high temperature melts with an external trigger, to identify the influence of melt thermo-physical properties on triggerability, fragmentation and explosivity of the melts, to acquire quantitative data on the volume fractions of melt, coolant and vapour in the interaction zone and on the fine fragmentation process during the explosions, and eventually to develop scaling methodology for the steam explosions.

BILLEAU (CEA Grenoble, France) facility studies premixing phase of the vapour explosion phenomenon; study of the dispersion of hot plane jets into water; use of spheres (diameter 5 to 20 mm) heated up to 2200°C (analogies with QUEOS experiments which treat hot axisymetric jets). Measurement of the fraction of fragments, liquid water and steam.

The FARO (Furnace And Release Oven) and KROTOS in the European Commission JRC-Ispra (Italy) were shut down in 1999. The loss of FARO will eliminate large scale experimental data using prototypic material as well as useful data on melt quenching and spreading. KROTOS facility devoted to the study of molten fuel-coolant pre-mixing either with prototypic reactor melts or simulants such as alumina up to 5 kg and progression and energetics of spontaneous and triggered fuel-coolant interactions (vapour explosions) is relocated in France, where it will again be available for use.

In-vessel fuel coolant interactions can challenge reactor vessel integrity, if they are large enough. Knowledge sufficient to predict their occurrence and energy release is not mature and analytical tools based on MFCI fundamental physics need further development. However, there is general consensus that as long as the primary system is pressurized, large-scale in-vessel MFCI is very unlikely and additional research on this topic is not warranted. For low-pressure conditions there remains the potential for energetic MFCI. Therefore, the fundamentals of mixing and triggering (Trigger refers to potential steam explosion, it is important to determine the melt-coolant mixture conditions in order to evaluate whether an explosion is conceivable or not) MFCI still need investigation to develop adequate models to predict MFCI during unpressurized conditions (in-vessel and ex-vessel) and this is an area where additional experimental work is warranted to characterize under what conditions and to what extent MFCI will occur, including under what reactor vessel re-flood conditions. Also, confirmatory testing using prototypic materials are highly desirable to completely assess the analytical tools and resolve the remaining issues.

Work is continuing on the development of analytical tools and small-scale MFCI experiments. This work is directed toward understanding the fundamentals of MFCI. As discussed above, additional work on MFCI under low pressure conditions is warranted since MFCI is an important consideration in reactor vessel integrity and accident management (e.g. should the reactor cavity be flooded before or after vessel failure?) and in developing new designs. With the loss of the FARO facility at the end of 1999, large-scale experimental facilities, data and expertise in handling large amounts of prototypic materials needed to address MFCI will be lost. Therefore, there is a need to consider whether or not additional confirmatory experiments using prototypic materials under low-pressure conditions are needed. This would also help maintaining expertise in handling and understanding the effects of prototypic materials.

MFCI issues are relevant to safety aspects and related accident management strategies in current reactors as well as to the development of advanced safety features to be incorporated in new reactor concepts. The European Commission carried out for many years the FARO experimental facility program, which was specifically devoted to the characterization of MFCI, melt quenching as well as melt spreading phenomenologies. The program consisted of experimental and analytical activities at JRC-Ispra (Italy) and KFK-Kalsruhe (Germany). These activities support test preparation and execution with pre-test simulations, assist test results interpretation with post-test calculations and perform sensitivity analyses to point out the various parameters influence.

In Canada, a new programme is being established to investigate in-vessel fuel/water interactions in CANDU reactors for accident scenarios (e.g. flow blockage in a fuel channel) that can lead to molten fuel being forcibly ejected from fuel channels into the surrounding D_2O-filled Calandria vessel. A new facility, the Molten Fuel Moderator Interaction (MFMI) facility is currently being designed for this purpose at AECL's Chalk River Laboratories. The experimental programme will investigate the energetics associated with the ejection of up to 25 kg of prototypic molten CANDU corium into the moderator. This programme is expected to be completed by the end of 2005.

Among other Fuel Coolant Interaction facilities in present and past years:

At the Argonne National Laboratory the COEXIT facility allowed for FCI studies of 1-10 kg of corium. Series of experiments were focused on FCIs occurring in the ex-vessel reactor cavity and the associated containment pressurization from high and low pressure melt ejections into the cavity region, also tests were performed to investigate the coarse mixing and melt jet breakup for an in-vessel geometry.

At Winfrith large scale experiments were performed using corium thermite in the MFTF and MIXA facilities. MFTF facility was a large pressure vessel equipped with a thermite charge container. Melt was released in two ways: free and restricted release modes. Studies were focused on the effects of melt mass, ambient pressure and subcooling water, and explosion energetics. MIXA facility was designed for studying the mixing phase of FCI, in particular the corium melt poured through a droplet format, which produced various diameters of melt droplets before melt-water contact.

At the Sandia National Laboratories many large scale experiments were conducted in the EXO-FITS and FITS facilities, focusing on estimating the FCI energy conversion ratio, determining the triggering behaviour and explosion threshold.

At the University of Wisconsin it was constructed the WFCI facility to support FCI research as originally sponsored by the US NRC, in particular to perform fundamental experiments in energetic FCI. The experimental test chamber was designed as an approximate one dimensional geometry (L/D>10). It allows many measurements (fuel-coolant mixing and explosion propagation/escalation, mixture level swell, spatial and temporal shock pressure histories, explosion propagation velocities, expansion work and fragmented fuel debris distributions).

3. ***Debris Interaction with the reactor vessel Lower Plenum:*** Currently, work in this area is being conducted in the following places:

RASPLAV (Kurchatov Institute/Russia) - OECD co-operative project to investigate load to the reactor vessel lower head and chemical interaction between the reactor vessel steel and molten core debris, using prototypic materials. Separate effect tests and large scale real materials experiment up to 200 kg of UO_2 / ZrO_2 / Zr / Stainless steel heated up to 2300 - 2700 °C. Melt pool behaviour in the lower head with or without cooling. Corium lower head interaction.

COPO2 (Finland) - to investigate heat load to the reactor vessel using water as a simulant.

SNL-LHF (USA) - OECD co-operative project to investigate the mechanical behaviour failure modes of the reactor vessel lower head under high temperature pressurized conditions.

BALI (France) - to investigate the heat load to the reactor vessel using water as a simulant.

ALPHA (Japan) - to investigate in-vessel debris coolability.

FOREVER (Failure Of REactor VEssel Retention) (RIT, Sweden) experiment is an integral test investigating the creep failure of a 1:10 scale reactor pressure vessel under the combined thermal and pressure loadings. It simulates the late stages of in-vessel-melt progression under nuclear reactor severe accident scenario. The objectives of the EC-FOREVER tests are to obtain multi-axial creep deformation and vessel failure mode data for the prototypical vessel geometry (scaled 1:10), under prototypical thermal and pressure loading conditions.

The objective of the POMECO (POrous MEdia COolability) experiment is to investigate the effect of downcomer configuration on the dryout heat flux for an internally-heated particulate debris bed.

SONATA (Korea) - investigating interactions with the lower head. Currently using simulant materials.

RUPTHER (France) - investigating mechanical behaviour (creep rupture) under accident conditions.

The DISCO-C (DIspersion of Simulated COrium with Cold fluids) (FZK, Germany) facility serves to investigate melt dispersal from the reactor pit when the reactor pressure vessel lower head fails at low system pressure of less than 2 MPa. The fluid dynamics of the dispersion process is studied using model fluids, water or bismuth alloy instead of corium, and nitrogen or helium instead of steam. The effects of different breach sizes and locations, and different failure pressures on the dispersion can be studied.

The DISCO-H (DIspersion of Simulated COrium with Hot fluids) (FZK, Germany) test facility was set up to perform scaled experiments that simulate melt ejection scenarios under low system pressure in Severe Accidents in Pressurized Water Reactors (PWR). These experiments are designed to investigate the fluid-dynamic, thermal and chemical processes during melt ejection out of a breach in the lower head of a PWR pressure vessel at pressures below 2 MPa with an iron-alumina melt and steam.

The experimental programme named KAJET (Karlsruhe Jet Experiments, FZK, Germany) is being performed to investigate features of a pressurized melt jet and the interaction with substratum material (MCCI). Compact melt jets, rather than a spray-type melt release, are simulated using iron and aluminum oxide instead of corium. The experiments provide general information about erosion processes and data for the validation of computer codes (or, if possible, simplified correlations), which then are able to transfer the results to reactor conditions.

At present, in the general context of a nuclear severe accident (***ex and in-vessel phenomena***) and in the way to prevent radioactive release, the French Atomic Energy Commission (CEA) is pursuing an important programme on nuclear severe accidents for many years. It encompasses the development of models and codes, performance of experiments in simulant and prototypic materials and the analysis of international experiments.

The CEA severe accident studies on corium behaviour address the following topics: Molten Core Concrete Interaction (MCCI), Fuel Coolant Interaction (FCI), and In Vessel Retention with reactor pit flooding and Corium-Ceramic Interaction. The experiments with prototypic corium are performed in the PLINIUS experimental platform at CEA Cadarache (France).

The European Commission who financially supports Transnational Access to this Research Infrastructure has selected the PLINIUS platform. The 4 facilities of the PLINIUS experimental platform where are performed the experiments dedicated to the understanding of the corium behaviour are: VULCANO, COLIMA, VITI and KROTOS. Material analyses and code validation activities complement the experimental work, which is directed towards the analysis of new phenomena.

PLINIUS is an acronym that means: PLatform for Improvements in Nuclear Industry and Utility Safety. Four facilities are devoted to the corium behaviour and to the physical properties studies:

The VULCANO facility (Versatile UO_2 Lab for Corium ANalysis and Observation): it is a rotating plasma arc furnace able to melt about 80 kg of corium at temperatures of up to 3000°C (in or ex-vessel corium) and to pour the melt according to different configurations: spreading, interaction, solidification studies.

The COLIMA facility (COrium LIquid and MAterials): it is a 1.5 m 3 controlled atmosphere vessel, with an internal pressure, which can rise to 0.3 MPa. Induction heating can maintain some kilograms of corium at very high temperature (up to 3000°C) to study thermal exchanges, aerosol release and thermo-physicals interactions studies.

The VITI facility (VIscosity Temperature Installation) has been developed to perform viscosity and surface tension measurements on corium by aerodynamic levitation up to 2500°C. Samples of a few mg corium can be implemented.

The KROTOS facility: it is dedicated to steam explosion phenomenon studies. About 5 kg of corium at more than 2850°C are dropped in water. Thermal, optical and pressure instrumentation, along with fast imaging, constitute the instrumentation. The KROTOS facility for corium-water interaction tests has been transferred from JRC Ispra (Italy) and is being reinstalled at CEA-Cadarache on the PLINIUS platform.

3.3.2. ANALYTICAL TOOLS

Computer codes have been developed around the world to analyse nuclear severe accident phenomena and to support and simulate pre- and post- test carried out in the experimental facilities. Some examples:

The ICARE/CATHARE code [41] was developed by French Institut de Protection et de Sûreté Nucléaire (IPSN) in the framework of security research studies. The aim of the code is to predict the PWR core behaviour during an hypothetical severe accident. The severe accident can be result of a combined failure of reactor standard cooling system and security cooling system, and could lead to reactor core melting. ICARE code is used for the preparation and interpretation of the PHEBUS PF international program experiments.

Sandia National Laboratories (SNL) developed MELCOR for the USA Nuclear Regulatory Commission (NRC). It is a fully integrated, relatively fast-running code that models the progression severe accident in LWR. An entire spectrum of severe accident phenomena is modelled. Characteristics of severe accident progression that can be treated with MELCOR include the thermalhydraulic response in the reactor coolant system, reactor containment and confinement buildings; core heatup and degradation; radionuclide release and transport, hydrogen production, transport, and combustion; core concrete attack; and the impact of engineering safety features on thermalhydraulic and radionuclide behaviour.

The Idaho National Engineering and Environmental Laboratory (INEEL) developed the RELAP5/SCDAP code for the USA NRC. It was designed for best-estimate transient simulation of light water reactor coolant systems during a severe accident. The code models the coupled behaviour of the reactor coolant system, the core, fission products released during a severe accident transient as well as large and small break loss-of-coolant accidents, operational transients such as anticipated transient without SCRAM, loss of offsite power, loss of feedwater, and loss of flow. A generic modelling approach is used that permits as much of a particular system to be modelled as necessary. Control system and secondary system components are included to permit modelling of plant controls, turbines, condensers, and secondary feedwater conditioning systems.

The integral code ASTEC (Accident Source Term Evaluation Code) [12] [42] is being developed by IPSN (Institut de Protection et de Sûreté Nucléaire), France, and GRS (Gesellschaft für Anlagen und Reaktorsicherheit), Germany, since 1994. The aim of this close co-operation of both companies is the creation of a fast running integral code which allows the calculation of the entire sequence of a severe accident in a light water reactor from the initiating event up to the release of fission products into the environment, covering all important in-vessel and ex-vessel phenomena. The main fields of application of this code are probabilistic safety analysis level 2 studies, accident sequence studies, uncertainty and sensitivity studies and support to experiments.

Since the 1980s, a two tier approach has been applied by IPSN and GRS based on the simultaneous but independent development of both integral and detailed mechanistic codes. During this time IPSN has developed the integral code ESCADRE and GRS has modelled the containment behaviour using two codes, RALOC for the thermalhydraulics and the hydrogen distribution and FIPLOC for the aerosol behaviour. For the first ASTEC version (called V0), it has been decided to gather in the same system the best candidates, which can be provided by the two companies. Thus, ASTEC V0 consists in a combination of some modules of ESCADRE (for the reactor cooling system, core degradation, fission product release and transport, corium ejection from the vessel, direct containment heating and iodine chemistry in the containment), and of the module CPA (Containment Part of ASTEC), which combines the RALOC and FIPLOC codes.

The main code requirements are: best modelling available in both developing organizations, fast-running code, sufficient validation to cover the main physical phenomena, to account for safety systems and procedures, easy use to perform sensitivity analyses.

The European Validation of the Integral Code ASTEC (EVITA) project (5th EC FWP) has as main objective to distribute the severe accident integral code Accident Source Term Evaluation Code (ASTEC) to European partners in order to apply the validation strategy issued from the VASA project (4th EC FWP). Partners evaluate the code capability through validation on reference experiments and plant applications accounting for severe accident management (SAM) measures, and compare results with reference codes.

The basis version V0 of ASTEC commonly developed and basically validated by GRS and IRSN was made available in late 2000 for the EVITA partners on their individual platforms. The actual version V1 has been released to the EVITA partners by the end of June 2002. It allows simulating the front-end phase by two new modules.

Following modules are forming ASTEC V1: CESAR for thermal hydraulics in the reactor coolant system; DIVA for core degradation up to vessel lower head failure; ELSA for fission product release from fuel rods; SOPHAEROS for fission product vapour and aerosol transport in the reactor coolant system; RUPUICUV for direct containment heating (DCH); CORIUM for heat transfer between containment atmosphere and corium entrained out of the cavity by DCH; WEX (based on WECHSL) for molten-corium-concrete interaction (MCCI) in the cavity; Containment part of ASTEC (CPA) for thermal hydraulics, aerosol and fission product behaviour inside the containment; IODE for iodine behaviour in the containment; ISODOP for calculation of activity and decay heat in the reactor zones; SYSINT for management of engineered safety systems.

Among the specific codes for the **Melt Fuel Coolant Interaction** study:

At JRC-Ispra the development and application of the thermalhydraulic COMETA (Core Melt Thermalhydraulic Analysis) code [4] complemented the FARO experimental program by comprehensive pre-test and post-test analytical activities.

The COMETA code is composed of a two-phase flow field and a three phase corium field. The two-phase flow field is described in Eulerian coordinates by 6 equations (mass, momentum and energy conservation equations for each phase) and ‘n’ mass conservation equations for the non-condensable gases. The corium field, which is composed by the jet, the droplets and the debris bed are described in Lagrangian coordinates. Melt fragmentation and relocation model treats the jet, the droplets and the fused debris separately. The melt is assumed to be released in the form of a coherent jet, which has a conical shape, based on the initial discharge diameter. During its descent the jet accelerates and reduces in size as particles leave the jet surface; the erosion rate develops as function of the jet breakup length (Saito, Epstein-Fauske or mixed correlations are available in the current version of the code). The drops are created with an initial diameter to satisfy the Weber number criterion. Up to 500 groups of drops can be followed; each group is characterized by diameter, mass, temperature, velocity and position providing good basis for the analysis of the statistical distribution of the debris particles. The residual part of the jet, which reaches the bottom, relocates as a cake that then forms a conglomerate with the loosed debris. Although the heat transfer from the bottom conglomerate may be negligible during the initial phase, it becomes important and has to be properly accounted for the long-term energy balance. A simplified model to describe hydrogen generation during the interaction phase is included in the current version of the code.

The IKE version of the COMETA code builds up on the original version of the code and includes an additional jet fragmentation model developed at University of Stuttgart, Germany, which assumes as decisive mechanisms wave growth and wave crest stripping along the jet surface. Thereafter an erosion rate is determined leading to a coherent core of molten material surrounded by a cloud of fragments.

MC3D is a multicomponent 3D code developed by CEA, Grenoble, France, which describes within the Eulerian approach the behaviour of water, steam, hydrogen, fuel droplets and corium jet. The code has five continuity equations, four momentum equations and three internal energy equations. Steam and hydrogen are mixed in both momentum and energy equations. Each field can exchange momentum and energy with the other field, the exchange of mass being limited in this version between water and steam and between corium jet and droplets. The corium droplet population will undergo fragmentation described through an interfacial area transport equation. Jet fragmentation is calculated from an external analytical model dealing with the small scale instabilities initiated by the hot vapour film.

The IVA code, developed at Forschungszentrum Karlsruhe and at Siemens, Germany, models transient multiphase flows consisting of water, steam, non-condensable gases, microscopic and macroscopic solid particles and/or molten materials. Three material fields are modelled by the code; the first one contains a mixture of steam and air, the second one liquid water, and the third one a normally hot, heavy material (corium) in the liquid or solidus state. A Cartesian mesh is used. The model can be up to 3D, rectangular or cylindrical, and is to be subdivided in a number of cells in a rectangular grid. Time dependent volumes fractions of the three material fields (and their state variables, velocities, etc.) are calculated for each cell. A flow regime is assigned to each cell, depending on the volume fraction of the fields and in part on their physical state, and the modelling of the transfer of mass, momentum and energy depends on this flow regime. With reference to melt fragmentation/coalescence, the code does not contain an explicit jet model, but as long as the melt has not solidified a flow regime with continuous melt can occur. When changing from this regime to one with discontinuous melt, an initial particle size of 0.1 m is assumed. Further fragmentation and coalescence are calculated by the code until the melt cools down to 40% liquid, where solidification is assumed. Fragmentation tends to dominate as long as the melt moves, whereas coalescence tends to dominate in melt settling down. Particle sizes do not change any more after solidification except through thermal shrinking and mixing with particles from other calculation zones.

The IFCI (Integrated Fuel Coolant Interaction) code was developed under the auspices of the USNRC at Sandia National Laboratories, USA, to investigate fuel coolant interactions in an as mechanistic as possible manner. The code is intended to address all aspects of FCI phenomena, including coarse fragmentation and mixing of molten material with water, triggering, shock wave propagation and fine fragmentation, and expansion of the melt water system. The ultimate objective of the code is to predict rates of steam and hydrogen formation, melt fragmentation and dispersion, fission product release, shock wave generation and propagation, and system loading for explosive and non-explosive FCIs in reactor systems. To add generality, the fuel is divided in two fields: solid particles (corium debris) and molten corium (melt), while the gas component is a more properly a mixture of steam and hydrogen. The melt is described by a Eulerian field, interacting with the water and steam fields, which are also described in Eulerian coordinates.

The present version of JASMINE-pre (2.01) is a premixing simulation code for steam explosion analysis developed at JAERI, Japan. JASMINE-pre solves three sets of mass, momentum and energy conservation equations for steam, water and melt. These fundamental equations are formulated on Eulerian field, discretized by FDM. A simple flow regime map based on volume fractions was used in the analysis of ISP-39. The melt was always assumed to be a dispersed phase. Water was considered to be continuous if the void fraction was less than 0.3, while steam was considered to be continuous if the void fraction was more than 0.7. Constitutive models for water-continuous and steam-continuous regimes were averaged if the void fraction was between 0.3 and 0.7. The present version of JASMINE does not have any physical-based debris settling/packing model. The option used assumes that the melt is instantaneously spread on the floor if the temperature is above the melting point, so that the melt surface area is the same as the floor area. However, if the fully spread melt layer on the floor is thinner than the value defined (5 mm), the melt surface area was reduced keeping the defined layer thickness.

The TEXAS computer model was developed at the University of Wisconsin, USA, for the simulation of fuel coolant interaction during its mixing, triggering and explosion phases. TEXAS is based on a one-dimensional hydrodynamics code developed at Sandia National Laboratories and modified for fuel coolant interactions. The code solves the 1-D, three-field equations describing the fuel, coolant vapour and liquid. Two fields represent the coolant as a separate liquid and vapour in a Eulerian control volume, while one field models the fuel as discrete material volumes or master particles in a Lagrangian formulation within the Eulerian region. The ‘Lagrangian’ treatment for the fuel makes it quite straightforward to track the fuel particle movement and thus eliminates the numerical diffusion difficulties encountered in pure Eulerian codes. The two key constitutive relations involve hydrodynamic fragmentation during the mixing phase, and thermal fragmentation of the fuel and rapid quench during the explosion phase. The TEXAS thermal fragmentation model is a semi-empirical formulation based on the concept of vapour film boiling and coolant jet impingement on the fuel surface. The current model reflects the key features for the rapid escalation and propagation of the vapour explosion. As the pressure shock wave directly contributes to rapid fuel fragmentation, the fragmented fuel is quenched by the coolant generating more vapour which in turn increases the pressure sustaining the propagation of the shock wave to adjacent fuel coolant mixture regions.

The THIRMAL code has been developed at the Argonne National Laboratories, USA, to specifically address the physical processes related to melt breakup, quenching, steam generation, hydrogen generation and debris particle formation when the melt enters water as a circular stream. The code predicts conditions of melt stream impingement, debris collection at the bottom of a water pool and premixing conditions for the evaluation of steam explosion loadings. The code models are based upon observations of breakup/intermixing phenomena in visualization experiments performed by EDL and others using high-temperature reactor material melts and water. The melt stream is treated in Lagrangian coordinates with time-dependent release diameter, temperature and velocity.

The VAPEX code has been developed at the Electrogorsk Research and Engineering Center (Russia) to analyse steam explosion processes under severe accident conditions. The code permits to study both in-vessel and ex-vessel fuel coolant interaction processes. Premixing and propagation models of the VAPEX code are based on the three-dimensional multifluid approach. Three phases (melt droplets, water and steam) are considered. Melt droplets are described with the Lagrangian approach. Unsteady 3-D governing equations of mass, momentum and energy conservation for all species with a common pressure are used in the VAPEX model. The VAPEX melt fragmentation model is based on the critical Weber number concept; other correlations are, however, available as an option. Moving continuum is modelled by a system of liquid particles, coincident with Eulerian computational cells at the old time step. A transition to a new time level is realized by three stages: 1) determination of preliminary values of all the parameters without effect of flow movement, 2) mass flows through cell boundaries are calculated, 3) final new values for all parameters are determined. An explicit finite difference scheme is used for numerical solution of the governing equations. The scheme conserves mass, momentum and energy in each computational cell.

3.3.3. PRESERVATION OF SEVERE ACCIDENT DATA

All the considerable amount of resources devoted at the international level during the last few decades to the generation of experimental databases in order to provide reference information for the understanding of reactor safety relevant phenomenologies and for the development and/or assessment of related computational methodologies can be coupled to new technologies and modern methods to storage all these enormous information.

The extent to which these databases are preserved and can be accessed and retrieved is an issue of major concern. In particular, it has been recognized that new working methods and rapid advancement of computer hardware and software technologies require continuous upgrading of storage methods which can otherwise render access to and retrieve of the data unpractical and in some cases impaired. Similarly, code documentation including code sources and input decks as well as relevant assessment cases need to be properly preserved.

Within this overall context, the JRC-Ispra originally developed from 2001 the STRESA (Storage of Reactor Safety Analysis Data) [45] web-based informatics platform (http://asa2.jrc.it/stresa) in order to provide a secure repository of JRC Reactor Safety Facilities as well as COMETA code databases exploiting modern computer information technologies for access and retrieve of the data.

Some time later and in the field of Severe Accidents the European Commission EURSAFE (EUROPEAN NETWORK FOR THE REDUCTION OF UNCERTAINTIES IN SEVERE ACCIDENT SAFETY ISSUES) [11] project included also a JRC developed web-based informatics platform (http://asa2.jrc.it/eursafe), which preserves database and information about the main European severe accident facilities currently working.

4. OBJECTIVES

The work has been focused in the prediction through computer codes of the progression and consequences of severe accidents in water cooled reactors.

Taking into account the State of the Art of severe accident phenomena and particularly **Melt Fuel Coolant Interaction**, FARO facility experiments and COMETA code calculations have demonstrated to be worth mentioning in MFCI experience.

The main objective of the PhD research was focused in **expanding general knowledge in Melt Fuel Coolant Interaction** by means of the experience obtained in the three last FARO facility tests carried out at the Joint Research Centre of the Ispra site. The knowledge was complemented with the pre and post-test analytical activities based on the development and application of the COMETA code to the prediction of tests performed in the FARO facility. Also the application of the code to a full plant hypothetical severe accident increased MFCI knowledge. A further analytical study was carried out in order to illustrate the MFCI inside the general overview of a NPP severe accident sequence. Results were expected to be helpful in order to clarify the importance of the melt fuel-coolant interaction in the context of a severe accident.

To fulfil the above mentioned general objective some detailed goals were established as follows:

- Collaborating and complementing the application of COMETA code to the prediction of tests performed in the FARO facility under new conditions not experimented before (subcooled and triggered conditions).

- Verifying the code consistency, analysing and unifying the COMETA simulations carried so far.

- Developing and improving COMETA code. Both the application of COMETA code to the prediction of tests performed in the FARO facility and the identification of problems in scale-up to reactor configurations, larger than scaled test facilities, leaded to find COMETA code lacks and improvements. Solving this issue is part a matter of engineering analyses and part a matter of computer programming analyses.

- Application of the RELAP5/SCDAP 3.2 thermalhydraulic code in order to obtain a **deeper understanding** of the code MFCI modelling theory and its possible relationship with other detailed MFCI thermalhydraulic codes.

The following research activities were the tools to develop the above objectives:

Test L-29 was the first test performed in subcooled conditions. The general objective of the analysis was to investigate the behaviour of the facility for the selected test conditions and for a variety of parametric variations in order to provide reference information for test planning and execution. More specifically, the analysis aimed at providing a benchmark prediction for the verification and validation of the COMETA code.

Test L-33 was the third test performed in subcooled conditions and the first test including triggering. In this test an external trigger was applied to enhance the possibility of an energetic melt coolant interaction. In the case of failed triggering the test would have been considered as another quenching test.

Moreover in order to verify the consistency, analyse and unify the COMETA simulations carried so far, it was decided to simulate again all the FARO experiments with the last available version of the COMETA code and keeping as far as possible the same basic nodalization scheme for all the tests. Only changes due to different boundary conditions of facilities arrangements were performed. Tests calculations L-14, L-19, L-24, L-27, L-28, and L-31 were simulated again.

In order to study the phenomenological behaviour of the thermalhydraulic system in a large-scale accident, the work was focused in the simulation (with COMETA thermalhydraulic code) of an extended MFCI accident in a hypothetical reactor with arbitrary geometry. The objective was to correlate the initial conditions of the reactor with the phenomena evolution. The application of COMETA code to a full plant severe accident was not developed before. The reactor geometry chosen was typical of the Spanish reactor ASCO-1, a 3-loops 966 MW_e (2686 MW_{th}) Westinghouse PWR.

Finally an analytical activity reproducing a severe accident following a LOCA break in a generic PWR NPP (3 loops, 1000 MW_e) with the RELAP5/SCDAP 3.2 thermalhydraulic code was performed in order to obtain a better understanding of the MFCI modelling theory of RELAP5/SCDAP 3.2, to study the influence of the "low pressure injection system" (LPIS) in the LOCA sequence and to obtain the initial conditions just before the molten pool slumping into the lower plenum in order to introduce them in a specific MFCI code input so a detailed MFCI study could be later performed.

5. THE FARO TEST FACILITY

5.1. INTRODUCTION

FARO (Furnace And Release Oven) was an experimental facility operated by the Institute for Systems, Informatics and Safety (ISIS) at the JRC (Joint Research Centre) Ispra site of the European Commission.

The primary objectives of the FARO research program carried out were aimed at:

a) The acquisition of a reference experimental data base from tests performed in the FARO installation with realistic melt composition and under reactor typical accident conditions. The experimental reference is essential for the development and improvement of analytical models and the assessment of system codes used in LWR safety analysis.

b) The investigation of basic phenomena relevant to the progression of severe accidents in water cooled reactors with particular emphasis on the interaction of molten fuel with coolant and/or structures under both in-vessel and ex-vessel postulated severe accident conditions.

The test facility became operational in 1987 and was initially dedicated to the investigation of severe accident phenomena in liquid metal fast breeder reactors such as melt relocation and molten fuel-sodium interaction. Thereafter, the test facility was reconfigured to address emerging safety issues pertinent to fuel coolant interaction and melt quenching in light water reactors (LWR). FARO facility began the experiments or tests of the LWR-MFCI phenomena in 1990 in collaboration with several reactor safety research organizations from EC member countries and with the participation of the US Nuclear Regulatory Commission (USNRC) in the context of a Technical Exchange Agreement established with the Commission.

The interaction of large masses of prototypical corium melt mixtures (e.g.; UO_2/ZrO_2, UO_2/ZrO_2 /Zr) in the water under a variety of realistic accident conditions was studied. The reference scenario is relevant to a postulated in-vessel core melt down accident when jets of molten corium penetrate into the lower plenum water pool, fragment and settle on the lower head. Test conditions are such as system pressure, water subcooling, water pool depth and melt composition.

In the context of the investigation relevant to the fragmentation and quenching of molten material into the water coolant at different initial pressure and water subcooling, 12 quenching tests were performed in the FARO facility (Figure 5.1): 5 at 50 bar initial pressure, 1 at 20 bar and 6 tests at pressure lower than 5 bar. In the last test L-33 performed in July 1999 an external trigger was applied.

Another configuration was used, SARCOFAGO, (Figure 5.2) to investigate the impact on the core catcher of corium ejected after reactor pressure vessel failure during a core meltdown accident. The way melt spreads on the core catcher surface is important because of its effect on the long-term coolability of the melt. Two tests have been performed in the FARO facility, one with a dry surface and one with 1 cm of water layer.

The test facility is properly instrumented in order to characterize the evolution of the interaction process.

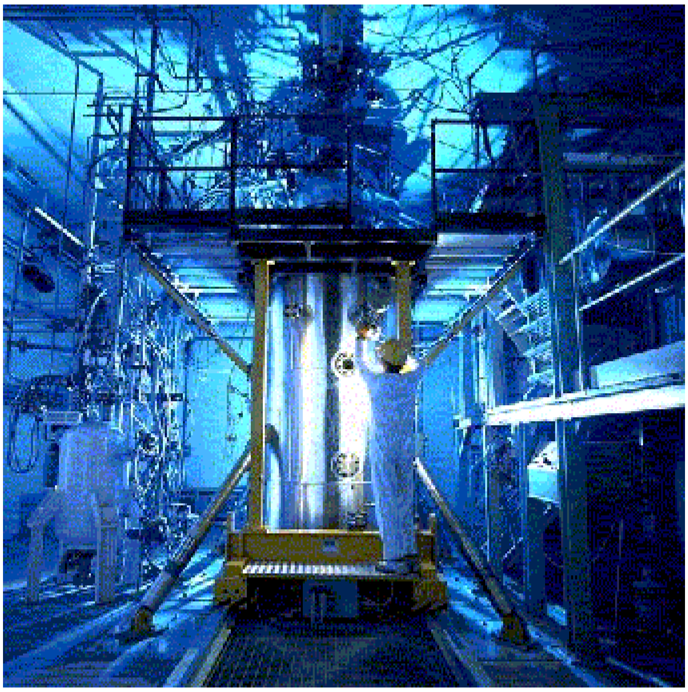

Figure 5.1 - Outside view of FARO Test facility with FAT release vessel for melt quenching experiments [From [25]]

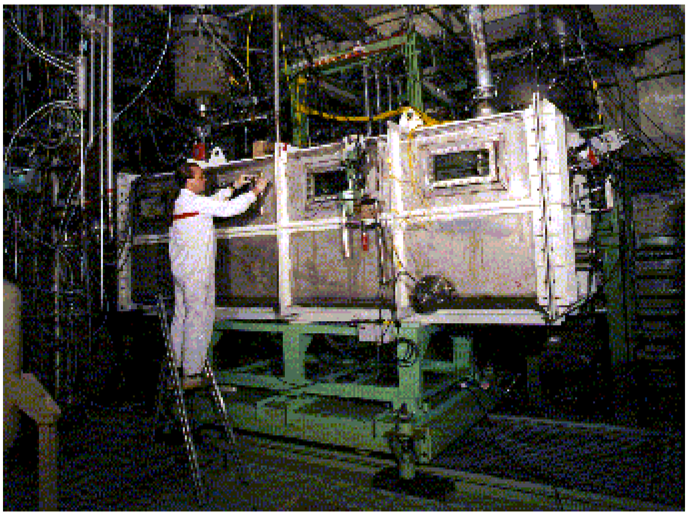

Figure 5.2 - The FARO SARCOFAGO test vessel for melt spreading experiments [From [25]]

5.2. FARO FACILITY COMPONENTS

In its initial configuration (Figure 5.3), the FARO test facility comprised five main major components that include the furnace, the intersection valve unit, the release vessel or melt catcher, the interaction test section and the venting system. From Test L-14 to L-24 the TERMOS interaction test section was used (0.71 m of diameter and about 1.5 m^3 of volume) (Figure 5.3). From Test L-27 it was changed to FAT test vessel (Figure 5.4), which consists of a pressure vessel of 1.5 m internal diameter and 2 m high, designed for a pressure of 8 MPa and a temperature of 300°C. To compare the FAT results with the TERMOS results, an internal cylinder was inserted in the FAT vessel. The cylinder internal diameter was the same of the previous TERMOS vessel, 0.71 m. This cylinder is filled with water and the outer annular space is part of the free board volume.

The FARO furnace consists of a pressure container, a melt mixture container, two electrodes and the release tube. A quantity in the order of up to 200 kg of prototypic oxide fuel melts can be produced in the FARO furnace possibly mixed with metallic components. Melt is generated by direct heating of a UO_2/ZrO_2 granulated variable mixture (in general consisted of 80% weight of UO_2 and 20% weight of ZrO_2) compacted between the electrodes. The lower electrode is provided with an orifice in the centre to transfer the melt through the release tube into the release vessel; during the heat up and melting phase, the orifice is closed by a tungsten disk mounted on the graphite cap of the lower electrode. Relatively large masses of oxide fuel type melts (up to 200 kg and 3000 °C) can be generated in the FARO furnace; as appropriate, the melt can be eventually mixed with metallic components in the release vessel. The heating process is depending on the mass quantity but generally is of about some hours. The corium is melted at low pressure (0.1-0.2 MPa) while the pressure and temperature in the test section TERMOS or FAT is as required by the experiment.

The intersection valve unit provides the means to isolate the furnace from the test section during the interaction phase. It consists of two slide valves, which are closed sequentially after the melt is transferred into the release vessel. An optical device is mounted in the upper part of the inter-section valve unit to survey the tungsten disk and to qualitatively monitor the melting process.

The release vessel is located inside the dome shaped upper head of the TERMOS or FAT test vessel. It is designed to hold the melt for the time necessary to isolate the furnace and balance the release vessel and the TERMOS or FAT test vessel pressures thus ensuring a gravity release of the melt. The release vessel is equipped with two flaps; the lower flap allows the discharge of the melt whereas the side flap ensures against built up of pressure differences between the release vessel and the test vessel during the release phase. The release orifice depending on the test was of diameter 5 cm or 10 cm.

At the end of the corium melting phase the melt is released from the furnace to the release vessel via the release tube and the valve S02 is closed. The release vessel is used as lock-chamber for pressure equalization. This is obtained bursting a double disk mounted on the communication line, which acts as a quick opening valve. Upon pressure balancing, the release vessel hinged-flap automatically opens, and the melt is delivered by gravity.

The interaction test section TERMOS test section consists of a pressure vessel designed for a pressure of 10 MPa at a temperature of 300°C and a debris catcher mounted on the lower part of the vessel. From Test L-27 it was changed to FAT test vessel (Figure 5.4), which consists of a pressure vessel of 1.5 m internal diameter and 2 m high, designed for a pressure of 8 MPa and a temperature of 300°C and a debris catcher mounted on the lower part of the vessel, the rest of the original facility was maintained. The test vessel is heated from the outside by trace heaters in order to establish the initial test conditions and is thermally insulated to minimize heat looses to the environment. It is connected to a steam-water separator during all the phases of the test.

A venting system connects the steam-water separator to a condenser through a set of four pressure relief valves to accommodate over-pressures in excess of the test vessel design pressure.

Three cameras are placed outside the test vessel to film the initial instants of the melt release and water interaction. These films are very important to analyse interaction phenomena and melt jet shape, melt fragmentation, etc.

A total of about 250 signals are generally recorded during a typical FARO test. They include pressures and temperatures both in the steam and water regions, vessel wall and debris catcher bottom plate temperatures as well as dedicated sensors for level swell measurement and hydrogen detectors.

5.3. SIMULATION OF ACCIDENT PHENOMENA IN THE FARO FACILITY

The severe accident phenomena can be divided in some stages, which are reproduced in the FARO facility:

The core molten material of the reactor (*melt*) pours by gravity into the lower plenum, in this first stage in the FARO facility melt is poured in *jet* shape through an orifice and falls by gravity in the gas space.

The *jet* enters into lower plenum water pool or in the FARO release vessel. The jet into the water fragments in little *drops* and melt fragments (*debris*) fall to the vessel bottom (*debris catcher*), at the same time in the vessel bottom a solid and dense mass (*cake*) is accumulated. This stage is characterized by high pressure and temperature increase and high heat exchange between *drops* and water, which is the *quenching rate*. The high *quenching rate* provokes void fraction and vessel *mixture level* increase.

Last stage is a medium and long term cooling, the high void fraction leads to a fragmentation (or *drops* production) decreasing, quenching rate, pressure and temperature increase become stable. *Drops* fall to the vessel bottom and *cake* increases in the debris catcher.

The FARO test objectives were to evaluate the steam generation rate associated to the melt heat transfer (*quenching*), to evaluate the hydrogen production associated to Zr oxidation, the heating of the bottom vessel structures and to evaluate the *debris* bed structure in the bottom plate.

The FARO tests with pure oxidic UO_2/ZrO_2 melts are characterized by a considerable amount of hydrogen generation which could be the result of either water dissociation at high temperature, reduction of UO_2/ZrO_2 during melt generation and subsequent oxidation in contact with steam/water, oxidation of UO_2 to U_3O_8, oxidation of the vessel material, a combination of the above or any other still unknown reason. Although pure oxidic melts such as UO_2/ZrO_2 or Al_2O_3 should form stable chemical compounds, at high temperatures chemical reduction reactions could result in changes to their molecular composition. In the performed FARO tests the quantity of hydrogen generated ranges between 1.2 and 3.4 g per kg of mixture.

Evidence of hydrogen generation in FARO has been given by mass spectrometer analysis; for some tests a quantitative evaluation has been performed comparing the saturation pressure to the actual system pressure or by venting the mixture of steam-argon-hydrogen from TERMOS into the condenser and evaluating the amount of hydrogen through the pressure increase in the condenser under the assumption of homogeneous conditions at the mean pressure of discharge. The evaluation of hydrogen generation in all FARO tests using the two methods has been performed.

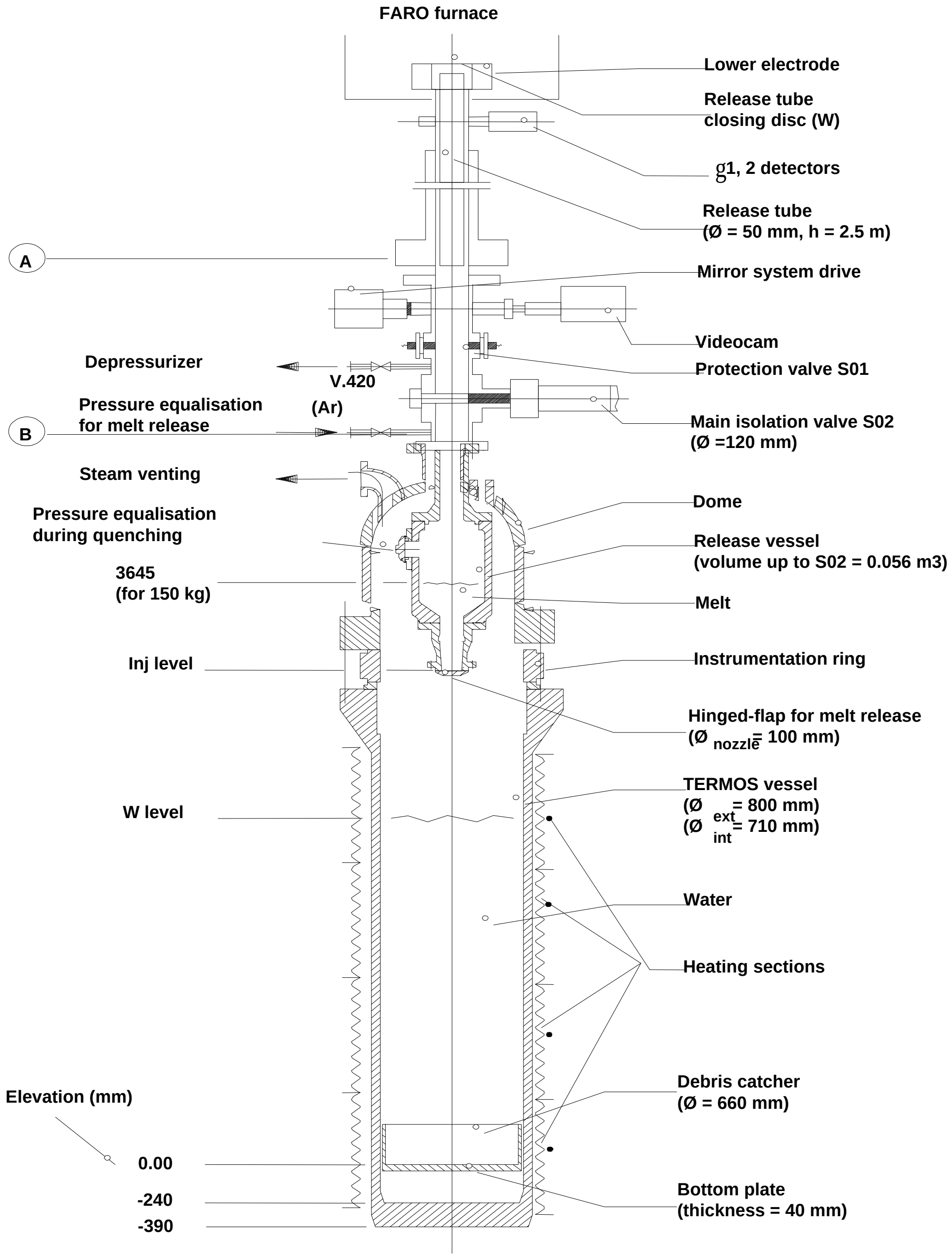

Figure 5.3 - FARO Test facility with TERMOS release vessel [From [17]]

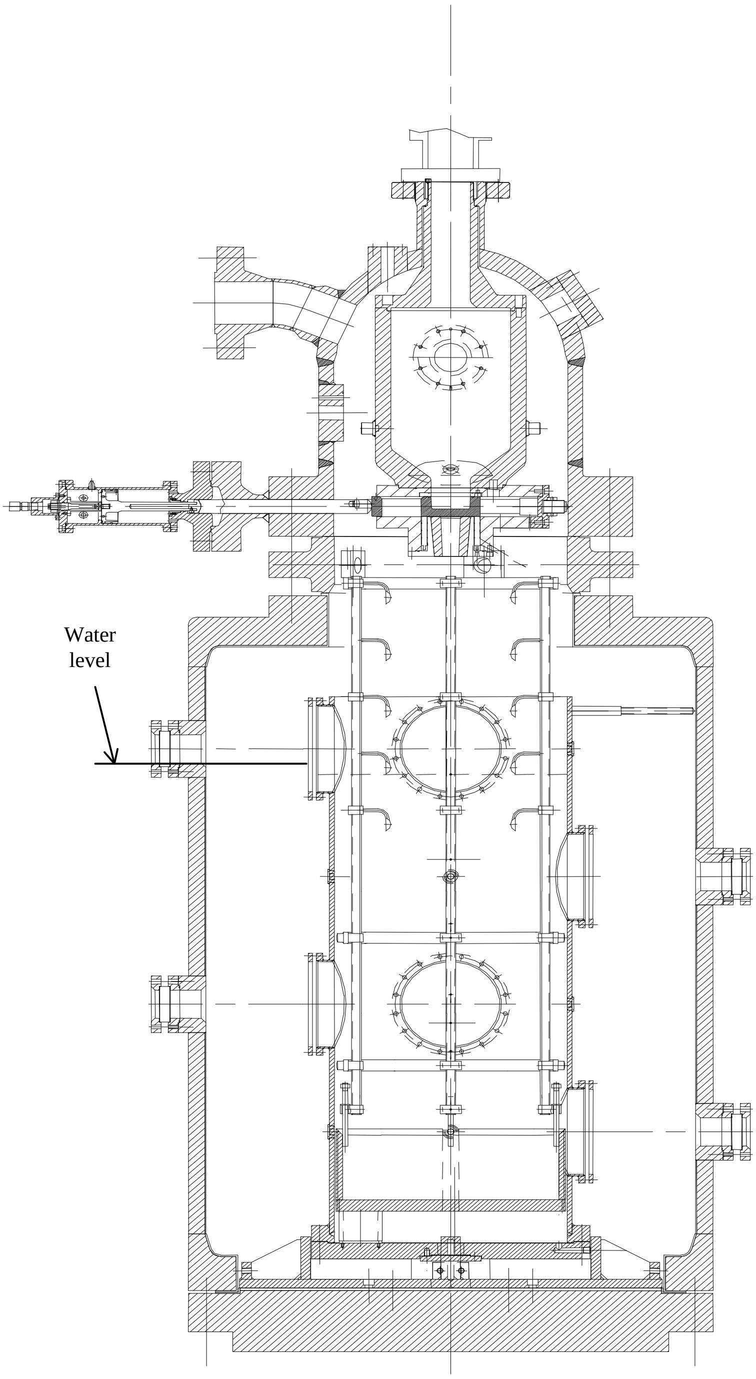

Figure 5.4 - FARO Test facility with FAT release vessel [From [20]]

6. THE COMETA CODE

6.1. INTRODUCTION

COMETA (COre MElt Thermalhydraulic Analysis) is a coupled thermalhydraulic and melt fragmentation code specifically conceived for the computational analysis of melt coolant interaction and quenching processes in LWR severe accident conditions.

It was written at the JRC Ispra in order to analyse with sufficient detail both the thermal-hydraulics and the fuel fragmentation phenomena of melt quenching tests as executed and/or planned in the FARO facility, including all the facility components considered necessary. Thus the immediate objective of the code is the prediction of the thermalhydraulic behaviour of FARO facility for design, definition of operational procedures and tests interpretation, and the long term objective of the code is to predict the behaviour of MFCI phenomena, including steam explosion events in any geometry 1d or 2d.

The overall structure of the COMETA code is complemented by the WinGraf data processing package.

The current version of the code has been extensively assessed against the FARO experimental data for the analysis of the integral aspects of melt-coolant interaction and against the LOBI test data for the verification of the related thermal-hydraulic. Also lately the code was also applied to real vessel reactor geometries.

The code runs both on a personal computer and on a workstation and it produces on-line plots (up to 9) and automatic nodalization drawing schemes showing volumes void fractions.

COMETA is structured in a thermalhydraulic two-phase flow model resolved in Eulerian coordinates and a melt fuel fragmentation model resolved in Lagrangian Coordinates.

The two-phase flow field is organized in a number of lumped volumes connected with junctions. A 2D nodalization can be built up connecting a number of macro-volumes (containing radial and axial volumes) and macro-junctions. Thermalhydraulic components, valves, pumps, separators and accumulators can be defined in order to represent the overall system configuration.

The melt field is described by the *jet*, the *drops* and the fused *debris bed*.

COMETA includes a model for hydrogen generation from metallic components based on validated correlations and also an empirical model for hydrogen generation from oxidric melts based on the experimental evidence provided by the FARO experiments.

6.2. THERMALHYDRAULIC MODEL

The two-phase flow field is described by “6+n” equations: mass, momentum and energy conservation equations for the liquid and vapour phases and mass conservation equations for “n” non-condensable gas present in the mixture. The model is derived for a 1d system (x direction) and is extended to 2d with use of radial junctions.

a) <u>Conservation Mass equations for the liquid, vapour and non-condensable phases:</u>

Liquid phase:

$$\frac{\partial(a_f r_f)}{\partial t} + \frac{1}{A}\frac{\partial(v_f a_f r_f A)}{\partial x} = -\Gamma_g \quad (1)$$

Steam phase:

$$\frac{\partial(a_g r_g)}{\partial t}+\frac{1}{A}\frac{\partial(v_g a_g r_g A)}{\partial x}=\Gamma_g \quad (2)$$

where:

g (subscript) = vapour
f (subscript) = liquid

a = void fraction

? = density (kg/m^3)

v = velocity (m/s)

A = flow area (m^2)

t = time (s)

x = coordinate (m)

? = volumetric vapour generation rate (kg/m^{3}s)

The equations considered in the code are the sum of (1) and (2) leading to the mixture conservation equation:

(1)+(2)

$$\frac{\partial(a_g r_g + a_f r_f)}{\partial t}+\frac{1}{A}\frac{\partial(v_g a_g r_g A + v_f a_f r_f A)}{\partial x}=0 \quad (3)$$

and the difference between equations (1) and (2). The choice of the sum and difference equations is in order to prevent a zero row in the resolution matrix when only one phase is present in a certain volume:

(1)-(2)

$$\frac{\partial(a_g r_g - a_f r_f)}{\partial t}+\frac{1}{A}\frac{\partial(v_g a_g r_g A - v_f a_f r_f A)}{\partial x}=2\Gamma_g \quad (4)$$

The mass conservation equations are integrated over a volume which is connected to other volumes via junctions that can be located at the inlet or outlet side (Figure 6.1 a) or at internal or external side in case of a 2D arrangement (Figure 6.1 b). The volume is assumed to have constant flow area.

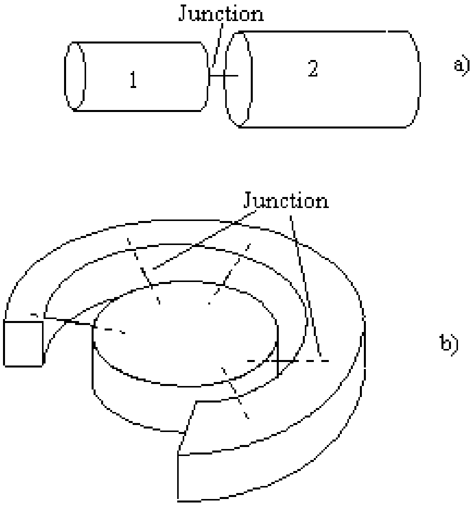

Figure 6.1 - Integration volumes [From [6]]

The non-condensable mass conservation equation can be written as:

$$\frac{\partial\left(a_{nc_i} r_{nc_i}\right)}{\partial t}+\frac{1}{A}\frac{\partial\left(v_g a_{nc_i} r_{nc_i} A\right)}{\partial x}=S_{nc_i} \quad (5)$$

for nc_i non-condensable gas

where:

S = volumetric source for non-condensable gas (kg/m^{3}s)

b) <u>Conservation Momentum equations for the liquid and vapour phases:</u>

The steam and liquid momentum equations are defined at the junctions and also in this case are the sum and difference forms. The momentum conservation equations are integrated between the centres of the volumes connected by the junction, using the donor cell technique to define the properties at the junctions.

Sum equation:

$$a_g r_g \frac{\partial v_g}{\partial t}+a_f r_f \frac{\partial v_f}{\partial t}+\frac{1}{2}a_g r_g \frac{\partial v_g^2}{\partial x}+\frac{1}{2}a_f r_f \frac{\partial v_f^2}{\partial x}=-\frac{\partial P}{\partial x}+\bar{r}g-a_g r_g FWGv_g+a_f r_f FWFv_f-\Gamma_g\left(v_g-v_f\right.$$

(6)

Difference equation:

$$\frac{\partial v_g}{\partial t}-\frac{\partial v_f}{\partial t}+\frac{1}{2}\frac{\partial v_g^2}{\partial x}-\frac{1}{2}\frac{\partial v_f^2}{\partial x}=-\left(\frac{1}{r_g}-\frac{1}{r_f}\right)\frac{\partial P}{\partial x}-FWGv_g+FWFv_f+\frac{\Gamma_g}{a_g r_g}\left(v_I-v_g\right)-\frac{\Gamma_g}{a_f r_f}\left(v_I-v_f\right)-\left(rFI\right)\left(v_g-v_f\right.$$

(7)

where:

g (subscript) = vapour
f (subscript) = liquid

P = pressure (Pa)

FWF, FWG = wall drag coefficients (1/s) for liquid and vapour

$\overline{r}$ = mean density (kg/m^3) = [$a\ ?_g$ + (1- $a\ ?_f$)]

? = interphase density (kg/m^3) = [$a_I\ ?_g$ + (1- $a_I\ ?_f$)]

FI = interphase liquid/vapour friction factor (m^3/kg s)

v_I = interphase velocity (m/s)

c) Conservation Energy equations for the liquid and vapour phases:

The energy conservation equations are kept separately for void fraction a = 0 or a = 1. In case of single phase the energy equation is substituted by the saturation equation. The energy conservation equations are also integrated over the control volumes.

In general, for the vapour phase:

$$\frac{\partial\left(a_g r_g U_g\right)}{\partial t}+\frac{1}{A}\frac{\partial\left(a_g r_g v_g U_g A\right)}{\partial x}=-P\frac{\partial a_g}{\partial t}-\frac{P}{A}\frac{\partial\left(a_g v_g A\right)}{\partial x}+Q_{wg}-Q_{wcond}+Q_{ig}+\Gamma_{g_{wall}}h_g+\Gamma_{g_{bulk}}h_g+DISS_g$$
(8)

For the liquid phase:

$$\frac{\partial\left(a_f r_f U_f\right)}{\partial t}+\frac{1}{A}\frac{\partial\left(a_f r_f v_f U_f A\right)}{\partial x}=-P\frac{\partial a_f}{\partial t}-\frac{P}{A}\frac{\partial\left(a_f v_f A\right)}{\partial x}+Q_{wf}-Q_{wboil}+Q_{if}+\Gamma_{g_{wall}}h_f+\Gamma_{g_{bulk}}h_f+DISS_f$$
(9)

where:

g (subscript) = vapour
f (subscript) = liquid

U = internal energy (J/kg)

Q_{if} = interphase heat transfer rate to liquid (W)

Q_{ig} = interphase heat transfer rate to gas (W)

Q_{wboil} = wall boiling heat transfer rate (W)

Q_{wcond} = wall condensation heat transfer rate (W)

Q_{wf}, Q_{wg} = wall heat transfer rate to liquid/gas (W)

h = enthalpy (J/kg)

DISS = dissipative terms in energy equation (W)

The unknown variables are:

- pressure
- void fraction
- gas and liquid velocities
- gas and liquid internal energies

The resolution is obtained by approximating the differential equations with finite differences and inverting the resultant matrix by a Gaussian elimination method. A system is used to reduce the initial 6n x 6n matrix to a n x n matrix by appropriate row linear combinations. The solution is therefore limited to the pressure solution that is then back substituted to determine the other unknowns.

The mass error is controlled via the time step reduction according to the actual error. The mass error is defined as the ratio between the mass obtained by integration of the partial differential equations and the mass obtained by the new temperature, pressure and void fraction values.

Additional relations are needed to characterize two-phase flow.

For the vapour generation rate the following formulation is used:

$$\Gamma_g = \Gamma_{g_{bulk}} + \Gamma_{g_{wall}} \quad (10)$$

where:

G_g = volumetric vapour generation rate (kg/m^3 s)

The term G_{gwall} is the vapour generated directly at the wall by wall heat transfer and it is determined according to the heat transfer mode.

The term G_{gbulk} is the vapour created in the bulk fluid due to the heat exchange between the liquid and the steam phase (depressurization, steam superheating or liquid subcooling):

$$\Gamma_{g_{bulk}} = -\frac{\frac{h_{ig}S_{ig}}{V}\left(T^{sat} - T_g\right) - \frac{h_{if}S_{if}}{V}\left(T^{sat} - T_f\right)}{h_g - h_f} \quad (11)$$

where:

if = liquid interphase
ig = gas interphase
sat (superscript) = saturation

T = temperature (K)

The terms *hS/V* are the heat transfer coefficient per unit volume and unit surface of interphase, *Ci*. A simple correlation is adopted for *Ci*:

where:

C = heat transfer coefficient per unit volume (W/m^{3}K)

if the void fraction is lower than 0.25

$$\begin{aligned} C_{if} &= \max\left(10^8 \alpha_g , 1.5 \cdot 10^5 \left(T_f - T_{sat}\right)\right) \\ C_{ig} &= 10^8 \alpha_g \end{aligned} \qquad (12)$$

if the void fraction is higher than 0.75

$$\begin{aligned} C_{if} &= 10^8 \alpha_f \\ C_{ig} &= \max\left(10^8 \alpha_f , 1.5 \cdot 10^5 \left(T_{sat} - T_g\right)\right) \end{aligned} \qquad (13)$$

a constant value $C_{ig}=C_{if}=C_i=2.3\ 10^5$ is used in case the void fraction is between 0.25 and 0.75.

For the interphase friction factor a model similar to the one present in RELAP5/MOD2 code is adopted.

Radial junctions can be specified in order to set up a 2D nodalization. The radial junctions are characterized by a slightly different momentum equation in which the gravity term is not considered and the interphase friction factor is minimized in order to allow mixing in the horizontal connected zones.

Heat slabs with different material composition can be specified in which the conduction and therefore the internal temperature distribution is accounted for. The Fourier equation is resolved in plane, cylindrical or spherical geometry and the geometry can be selected by input.

The heat exchange between structures (slabs, *jet, drops, debris*) and the coolant is described by the following correlations:

Single phase liquid convection	Dittus Boelter
Condensation model	Collier
Nucleate boiling	Chen
Transition/film boiling	Bromley-Pomeranz
Single phase vapour convection	Dittus Boelter

Additional models regard separator model and valve discharge/control model. These models allow the description of a complete test facility like FARO and the representation of a full complex transient.

6.3. MELT FUEL FRAGMENTATION MODEL

The melt field is composed of three phases for the description of melt: *jet, drops and fused debris bed* also called *cake* (Figure 6.2).

The melt is released from a tank (melt catcher) with an orifice and is fragmented during the fall keeping constant the ratio L/D, L is the distance from the injection orifice to the point where *jet* disappears and D is the initial diameter. The melt height is calculated at each time step according to the real actual dimensions of the melt catcher; it was found that the specification of the real dimensions of the melt catcher is important for the derivation of the discharge velocity:

$$V_{release}(t) = \sqrt{\frac{2gh_{melt}(t)}{K_{or}}} \quad (14)$$

where:

h_{melt} = Melt height in the melt catcher (m)

K_{or} = Melt orifice discharge coefficient (-)

g = gravity acceleration (9.81 m/s^2)

The melt is assumed to be released in the form of a coherent *jet*, which is conical shaped with a wavy and rough surface.

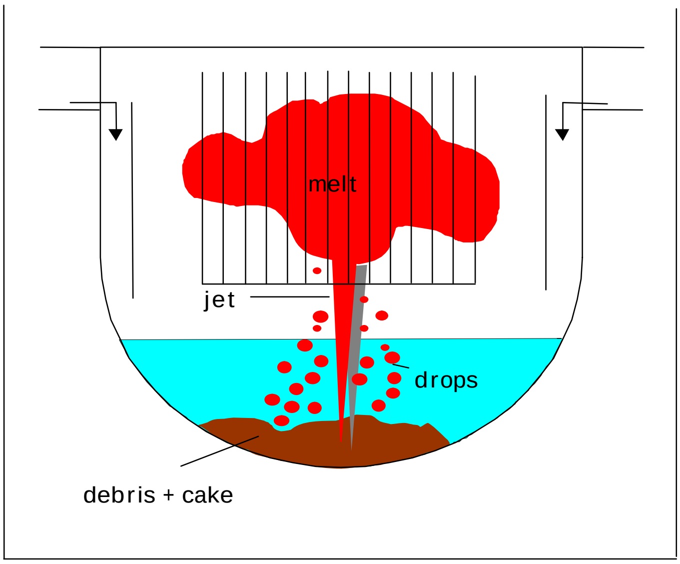

Figure 6.2 - Schematic melt field release description

a) Jet description:

Three models for *jet* fragmentation and fragments creation are included: the original COMETA model, based on the Jet Break-up Length concept, the Corradini-Tang model, similar to the model present in the TEXAS code (Chu and Corradini, 1989) and the IKEJET model (Bürger et al., 1995) developed by the University of Stuttgart.

The original COMETA model for *jet* melt fragmentation and erosion is based on an interpolated Jet Break-up Length criterion (Figure 6.3) with L/D evaluated at each position and time step. The local erosion rate is function of L/D.

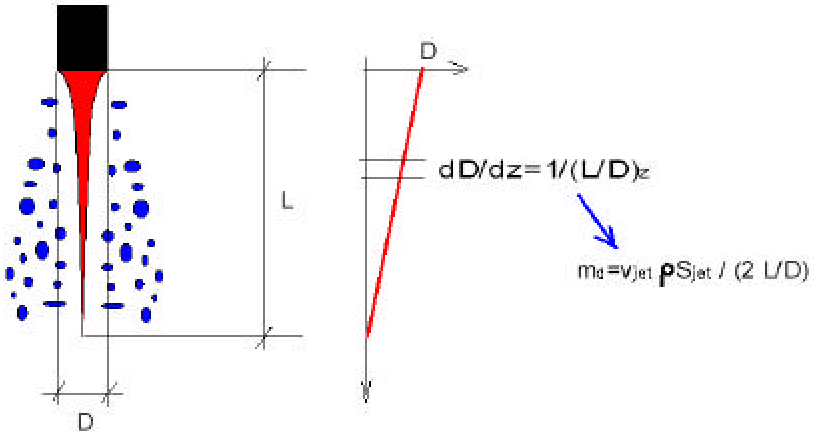

Figure 6.3 - Jet Break-up Length definition [From [6]]

The *jet* accelerates along its descent and reduces its size. Meanwhile some particles leave the *jet* surface at different axial positions. The erosion rate $\dot{m}$ is established to satisfy some of the available correlations for the Jet Break-up Length.

$$\frac{\dot{m}_d}{S_j} = \frac{v_j r_j}{2\left(\frac{L}{D}\right)} \quad (15)$$

$$\left(\frac{L}{D_j}\right) = f\left(We, Fr, x, ...\right) \quad (16)$$

where:

j (subscript) = melt jet

? = density (kg/m^3)

v = velocity (m/s)

S = surface (m^2)

L = length (m)

D = diameter (m^2)

We = Weber number

Fr = Froude number = $\frac{v_j^2}{gD_j}$

The correlation actually used in COMETA is a combination of two correlations: the Saito [14] correlation and the Epstein-Fauske [44] correlation.

The Saito L/D correlation is:

$$\frac{L}{D} = 2.1\sqrt{\frac{r_j}{r_c}}Fr^{0.5} \quad (17)$$

where:

j (subscript) = melt *jet*
c (subscript) = coolant

? = density (kg/m^3)

The Epstein-Fauske correlation for L/D is independent from the *jet* velocity:

$$\frac{L}{D} = \frac{\sqrt{3}}{2}\left(1+\frac{r_v}{r_j}\right)\sqrt{\frac{r_j}{r_v}} \quad (18)$$

The combined correlation is defined (Figure 6.4):

1 - Saito correlation is used up to Weber number 50, Epstein-Fauske above 100 and an interpolation in the transition between the two.

2 - In the two phase flow the Saito correlation is used for each Weber number.

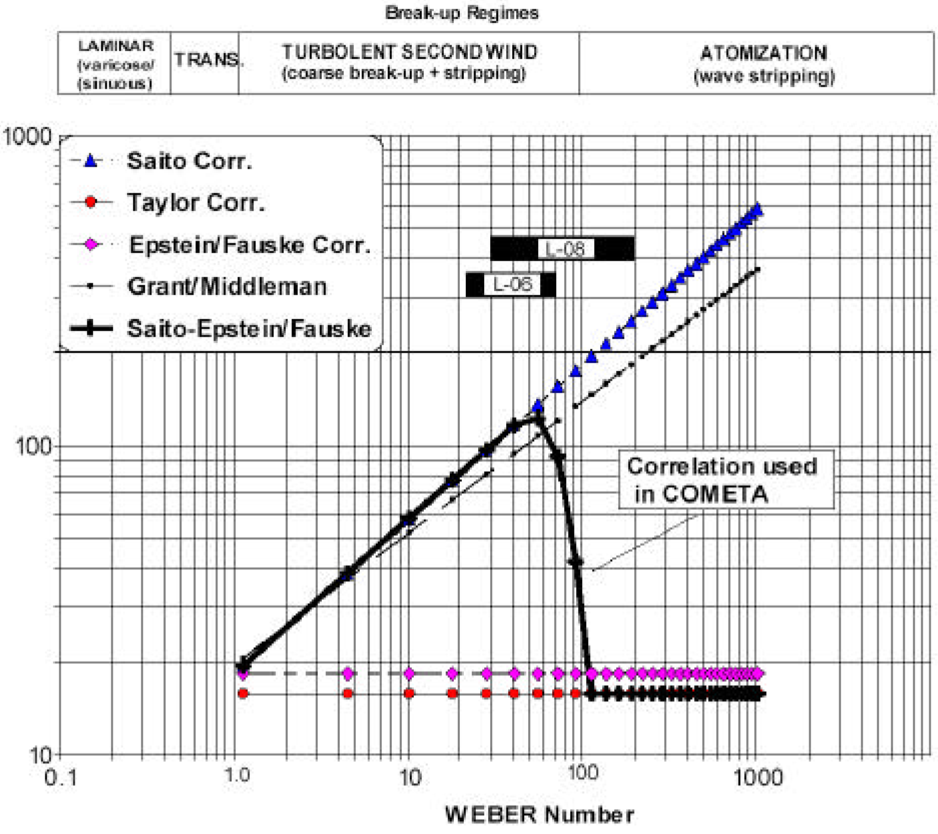

Figure 6.4 - Jet Break-up Length interpolated model [From [6]]

Both the *jet* and the *drop* particles released are moved in a Lagrangian framework of equations. The position is tracked along the transient and the corresponding Eulerian cell is identified and receives the heat source from the *jet* and *drop* particles.

The *jet* equations are represented by:

Jet mass conservation equation:

$$\frac{dM_j}{dt} = -\dot{m}_d \quad (19)$$

Jet momentum equation:

$$r_j V_j \left(\frac{dv_j}{dt} \right)_n = V_j \left(r_j - \bar{r} \right) g - F_j \quad (20)$$

$$F_j = \frac{1}{8} \left(c_d W_j \right) \bar{r} S_j \left(v_j - \bar{v} \right) | v_j - \bar{v} | \quad (21)$$

W_j is a multiplier that takes into account the surface roughness; at present however W_j=1.

Jet energy conservation:

$$r_j V_j c_{p_j} \frac{dT_j}{dt} = \left(q''_{jf} S_{jf} + q''_{jg} S_{jg} \right) W_j \quad (22)$$

where:

j (subscript) = melt *jet*
g (subscript) = vapour
f (subscript) = liquid

q'' = heat flux (W/m^2)

M = mass (kg)

V = volume (m^3)

T = temperature (K)

Wj = *jet* roughness parameter (-)

c_p = Specific heat (J/kg K)

c_d = Drag coefficient (-)

b) Drops description:

The melt *drops* are created with an initial diameter, which can be progressively halved to satisfy the Weber number criterion: i.e. the Weber number has to be lower than 12.

COMETA standard model is the fragmentation model with coefficients 6 for the diameters of the *drops* (it multiplies the equilibrium Weber number 12, and influences the final size of the fragments) and no multiplier for the *Jet* break-up length.

Up to 500 groups of *drops* characterised by diameter, mass, temperature, velocity and position can be accounted for. A unique *drop* temperature is assumed in each group. The residual part of the *jet* reaching the vessel bottom plate forms a fused *debris bed cake,* which can agglomerate eventual *drops* arriving with higher temperature than the solidification one.

If the *drops* are still liquid the diameter is controlled at each time step and if the Weber number increases above the limiting value (due to *drops* acceleration or different medium density) and the temperature is greater than solidification, the diameter is halved to satisfy Weber criterion.

The governing equations are:

Drop momentum equation:

$$r_d V_d \left(\frac{dv_d}{dt} \right)_n = V_d \left(r_d - \overline{r} \right) g - F \quad (23)$$

$$F = \frac{1}{8} c_d \overline{r} S_d \left(v_d - \overline{v} \right) | v_d - \overline{v} | \quad (24)$$

The value of c_d is obtained by a relation containing the Reynolds number.

Drop energy equation:

$$r_d V_d c_{p_d} \frac{dT_d}{dt} = \left(q''_{df} \, S_{df} + q''_{dg} \, S_{dg} \right) \quad (25)$$

where:

d (subscript) = melt *drops*

A unique *drop* temperature is adopted. This hypothesis is sufficient for small *drops* (<2mm) but it is probably not correct for larger *drops*. The only reason not to calculate the real temperature distribution is to avoid excessive iterations of the Fourier equation between time steps.

c) Fused-debris description:

The residual part of the *jet* that reaches the vessel bottom relocates in the so-called *fused-debris bed*. In this context the *fused-debris bed* is considered as the fused part of *debris bed* that represents only a portion of what is normally intended as *debris bed*, therefore not including the fragments.

The equations considered are:

Mass conservation equation:

$$\frac{dM_{deb}}{dT} = M_{j(Z=0)} + M_{d(Z=0, T_d > T_{melt})} \quad (26)$$

Energy conservation equation:

$$r_{deb} V_{deb} C_{p_{deb}} \frac{dT_{deb}}{dt} = q''_{debf} \, S_{debf} + q''_{debg} \, S_{debg} \quad (27)$$

where:

deb = melt *fused-debris*

The surface area of the *fused-debris* is assumed to be equal to 2.5 times the area of a hemisphere having the same volume; it is also possible to define a flat *cake*. The energy conservation equation takes into account the heat released to the coolant. Due to the different surfaces taking part in the heat exchange process during the initial phase of the transient the heat transferred from the *fused-debris* is negligible, while in the long term, after the quenching of the small *drops*, it becomes important for the total energy balance.

A model for H_2 generation based on the available end-of-test data of FARO tests was introduced into the code after L-20 post-test calculations. A first simple model is based on the consideration that oxidation potential is proportional to fragmented mass:

$$dM_{H_2} / dt = 0.003 dM_{fragm} / dt [kg/s] \quad (28)$$

The second model takes into account the surface generation and the chemical kinetics:

$$dM_{H_2} / dt = d(S\sqrt{2k_{H_2}t}) / dt [kg/s] \quad (29)$$

and relates the rate of H_2 mass production to the fuel surface *S* generated by the interaction and the reaction kinetic K_{H_2} that is obtained from the O_2 kinetic using the relationship:

$$K_{H_2} = K_{O_2} / 64 \ [kg^2 m^{-4} s^{-1}] \quad (30)$$

where the oxygen kinetic law is an exponential one:

$$K_{O_2} = a \exp\left(\frac{-b}{RT}\right) \quad (31)$$

The constants *a* and *b* are related to the type of the material considered; code uses the values present in the RELAP5/SCDAP MOD2 for metal oxidation. The maximum H_2 mass produced is limited to the experimental value, that is $2\ 10^{-3}$ kg of H_2 per kg of fragmented mass.

COMETA code includes the possibility to simulate vapour explosions. The threshold for the initiation of an explosive interaction in COMETA is based on a cell pressurization rate higher than 2 MPa/s; when this value is attained either in a spontaneous or triggered fashion, the melt present in the interested cell is fragmented in finer particles with a consequent increase of heat transfer and steam generation rate, enhancement of pressurization which eventually propagates to adjacent cells escalating the interaction.

The coupling between the fragmentation models and the thermal-hydraulic models is explicit, but the time step chosen is the minimum between the requirements of both fields. In particular the thermal-hydraulic models use as boundary condition the power transferred by the fuel fragments into the coolant, while the fuel fragmentation model use the local density, temperature and void fraction to calculate the fragmentation rate and the heat transmitted to the coolant. The volume occupied by the fuel is generally small compared to the coolant volume and therefore no volume reduction is taken into account. However some particular circumstances (as for example some KROTOS tests) could require taking into account the volume reduction.

7. RESEARCH ACTIVITIES SUMMARY

The PhD research activities were mainly concentrated in severe accident simulations with JRC-COMETA code, in one hand performing pre and post-test analysis of the FARO tests, in another hand performing code calculations applied to a large NPP reactor configuration. The application of RELAP5/SCDAP to a general NPP configuration completed the research activities.

Two important tests were performed in the FARO facility in 1998 and 1999: L-29 and L-33 under new conditions not experimented before (subcooled water for L-29 and triggered conditions for L-33). COMETA pre-tests calculations are explained in chapters 7.1 and 7.2. In addition to give information for test experiment planning and execution in the FARO facility, the calculations gave results to improve COMETA code logic.

Chapter 7.3 summarizes the application of the COMETA code to reactor configurations, larger than scaled test facilities. This application was not performed before. The results lead to the identification of scale-up problems in the logic of the COMETA code. They also solved and explained one of MFCI related phenomena: the relation between the void fraction and the quenching rate.

To analyse and unify the experiment simulations with the last available version of the COMETA code another work is presented in chapter 7.4. Along the years the COMETA code was improved and changed to fit experimental results. This purpose was fulfil simulating again tests from L-14 to L-31. This work also gave some indications that help to choose the nodalization scheme in order to reduce the COMETA computer calculation time.

In chapter 7.5 the calculations with RELAP5/SCDAP complete the general overview of the MFCI phenomena included in the PhD research.

7.1. COMETA PRE-TEST CALCULATION OF FARO TEST L-29

7.1.1. INTRODUCTION

Test L-29 was scheduled to be performed in the FARO facility in July 1998. It was the second test performed with the new FAT vessel. Test L-29 was the first test performed in the FARO facility in subcooled conditions. The general objective of the analysis was to investigate the behaviour of the facility for the selected test conditions and for a variety of parametric variations in order to provide reference information for test planning and execution. More specifically, the analysis aimed at providing a benchmark prediction for the verification and validation of the COMETA code.

There was a great interest in performing a subcooled test in the FARO test facility due to the potential for an energetic melt coolant interaction. This is supported by the recent results of the KROTOS Test 58, in which, for an UO_2 / ZrO_2 melt mixture, with conditions of 5 bar, 130°C subcooling a mild steam explosion occurred. Since there were uncertainties in the real initial test conditions, determined by the peculiarity of the test performed, a number of different hypotheses have been explored as initial conditions of the test, including saturation conditions cases.

The following hypotheses have been considered:

Subcooled Test

Pressure:	1, 2, 5 bar
Mass:	30, 50, 70, 150 kg (only for comparison purposes)

Saturated Test

Pressure:	2, 5 (only as a recalculation of L-28), 20 bar
Mass:	150 kg

Additional cases have been analysed to highlight the influence of enhanced fragmentation model, H_2 generation and the nodalization type (1d/2d).

Figure 5.4 shows the configuration of the facility for this test. An inner vessel with the same diameter as the TERMOS will be installed inside the FAT vessel. The venting lines to the separator will be closed.

7.1.2. RESULTS OF SUBCOOLED TEST OPTION FOR THE FARO TEST L-29

Initial and boundary conditions

In order to cover the possible range in the experimental conditions, calculations have been performed with different values of melt injected mass (Tmelt = 3073K) and 5 cm of discharge orifice. The first case, L29PR30N should be seen as a lower bound and case L29PR150N should be seen as an upper bound.

The so-called standard fragmentation model has been used for this test, i.e.: Cd=6, Cj=1, $f_{H2}=1.810^{-3} kgH_2/kg$ fragmented.

The following table summarises subcooled cases at 5 bar, 50°C and different melt mass:

Descriptor	Melt Mass (kg)	Melt temperature (K)	Initial Pressure (bar)	Initial water level (m)	Initial water temperature (K) and subcooling	Fragmentation Model
L29PR30N	30	3073	5	1.5	323 (100°C subc.)	Stand.
L29PR50N	**50**	**3073**	**5**	**1.5**	**323** (100°C subc.)	**Stand.**
L29PR70N	70	3073	5	1.5	323 (100°C subc.)	Stand.
L29P150N	150	3073	5	1.5	323 (100°C subc.)	Stand.

Table 7.1 - Performed L-29 pre-test subcooled calculations at 5 bar, 50°C

Other subcooled calculations have been performed to analyse effect of subcooling. Here, we consider four 50 kg melt mass cases with the subcooled water at different initial pressures and temperatures:

Descriptor	Melt mass (kg)	Melt temperature (K)	Initial Pressure (bar)	Initial water level (m)	Initial water temperature (K) and subcooling	Fragmentation Model
L291BSUB	50	3073	1	1.5	323 (50°C subc.)	Stand.
L292BSUB	50	3073	2	1.5	323 (70°C subc.)	Stand.
L29P2B20	50	3073	2	1.5	293 (100°C subc.)	Stand.
L29P5020	50	3073	5	1.5	293 (130°C subc.)	Stand.

Table 7.2 - Performed L-29 pre-test subcooled calculations

Due to the amount of figures it is impossible to present here all the case results, only the main results obtained in the calculations are graphically represented.

Results of the base case calculation (50 kg melt subcooled water)

Base case is **L29PR50N**: standard fragmentation model case of 50 kg melt mass at 3073K falling into 1.5 m of subcooled water at 50°C at 5 bar.

The void fraction is not very high and is mainly due to the non-condensable gas (H_2) and not to steam (Figure 7.1). The low void fraction causes great fragmentation and therefore low cake mass accumulation (Figure 7.2).

The jet leading edge position (Figure 7.3) shows that the melt falls down according to melt gravity release with 1m/s of initial velocity until 0.7 m. What happens is that the jet parcels are released at progressive increasing velocity from 0 to about 3 m/s. Some parcel can overcome the leading edge parcels, becoming leading edge. Therefore, the leading edge can become faster than the theoretical gravity release with initial velocity zero. This is a point that needs improvement in the code. It was not occurring with 10 cm jet because the velocity increase was smaller due to higher inertia. After the height of 0.7 m the friction becomes more and more important and deviation of the jet leading edge position from the theoretical gravity discharge curve occurs.

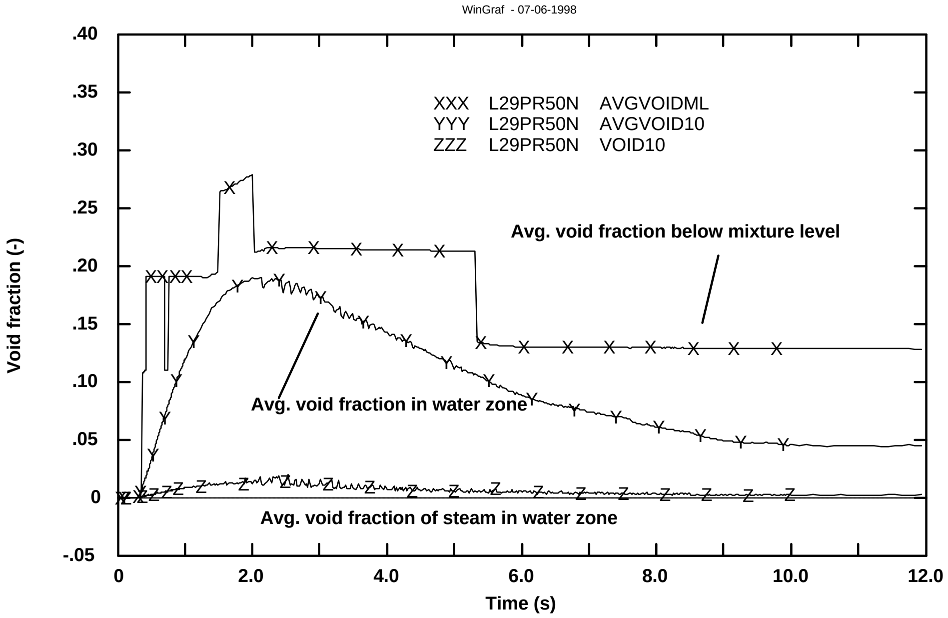

Figure 7.1 - Global average void fraction below mixture level (AVGVOIDML), global average void fraction in the water region (AVGVOID10) and average void fraction of steam in the water region (VOID10) in Test L-29

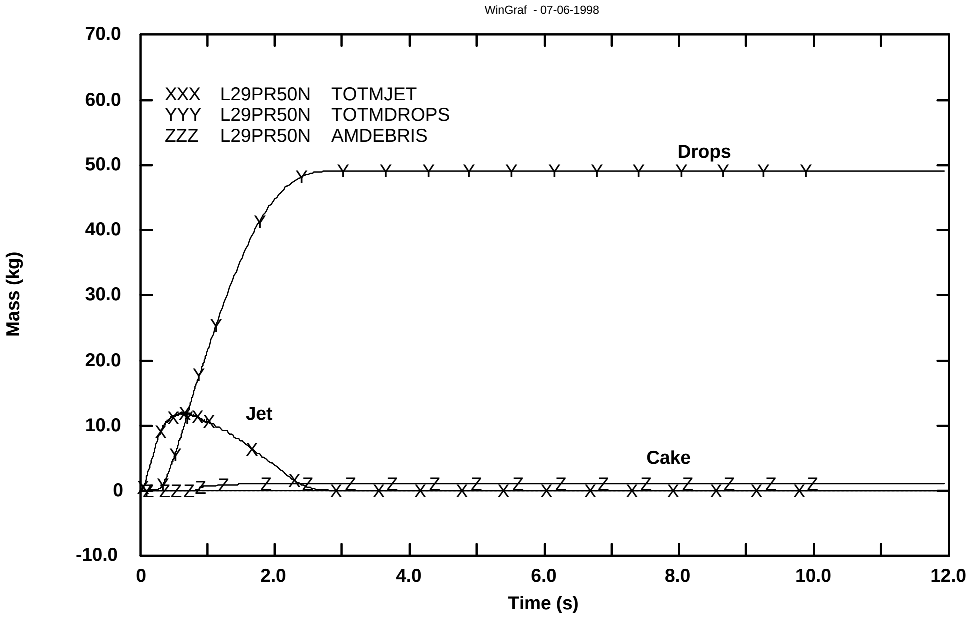

Figure 7.2 - Jet, Drops, and Molten Cake mass in the base case calculation in Test L-29

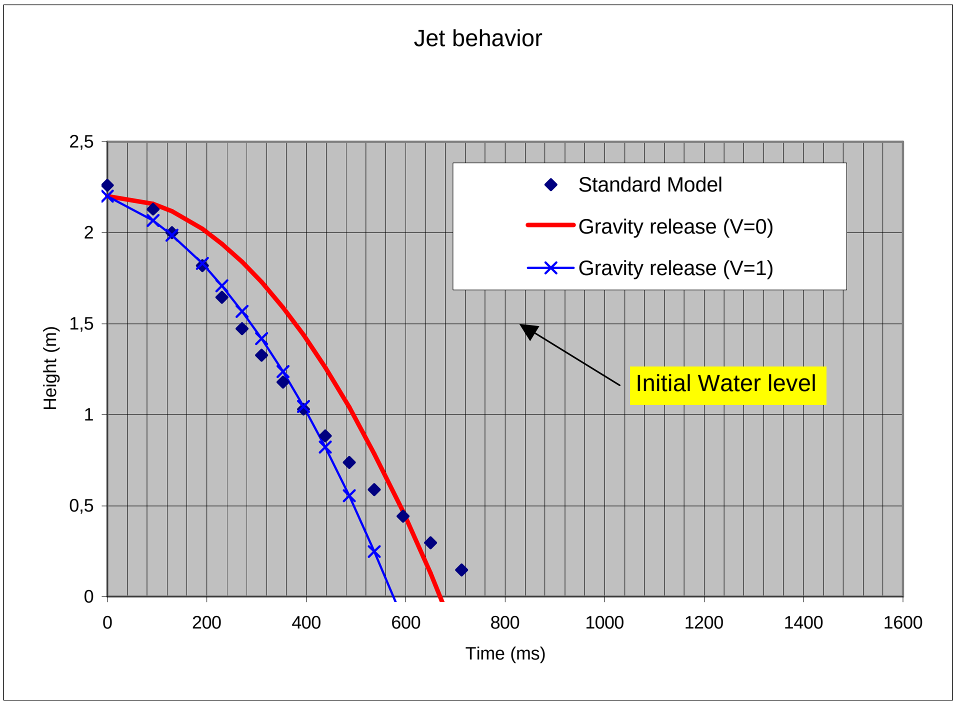

Figure 7.3 - Jet leading edge in the base case calculation in Test L-29

Results of the bounding calculations

In order to highlight the possible minimum and maximum energy release in this test three additional calculations have been performed with subcooled water (50°C) at 5 bar changing the quantity of melt mass injected. The minimum case was performed reducing the injected mass to 30 kg. In the other cases the mass was increased to 70 kg and 150 kg.

The mass reduction and increase of 20 kg do not show great differences. The increase in mass of 100 kg shows a higher pressure increase and also the energy released is greater in the upper boundary case with 150 kg. As injected mass increases more fragmentation is occurring. The cake mass produced is very limited, less than 5% of the total mass in the cases with 30, 50 and 70 kg. In the upper boundary case the cake mass increases up to 18 kg (12% of the total mass).

Global average void fraction is mainly due to H_2, it is higher as mass increases. Void fraction due to steam is practically zero in all cases.

Effect of subcooling and initial pressure

In order to check the possible influence of initial subcooling the following 50 kg mass melt cases are analysed. The base case L29PR50N (50°C at 5 bar, 100°C of subcooling), L291BSUB case (50°C at 1bar, 50°C of subcooling), L292BSUB case (50°C at 2bar, 70°C of subcooling), L29P2B20 case (20°C at 2bar, 100°C of subcooling), and L29P5020 case (20°C at 5bar, 130°C of subcooling).

Pressure is not affected by subcooling in the range 70°C to 100°C. The 100°C of subcooling case at 2 bar pressure is similar than case with 70°C of subcooling. The same occurs with the two subcooled cases at 5 bar.

Global void fraction is affected by pressure but not by subcooling. In Figure 7.4 it is possible to observe average void fraction of non-condensable gas (AVGVOISNC10) and of steam (AVGVOISST10) in the 10 lower volumes of FAT. Average void fraction of steam is very low in all cases; it increases as pressure and subcooling decrease (Figure 7.5). Average void fraction of H_2 is higher and decreases as pressure increases; However it is quite similar in the cases at the same pressure with different subcooling.

The fragmentation is very high in all cases and practically equal for the subcooled cases at the same pressure. It increases as pressure increases, due to lower void fraction.

Quenching rate shows moderate decreasing with pressure; and moderate increase as initial water temperature is lower at the same pressure, as subcooling increases. The quenching rate in the 1 bar subcooled case becomes unstable due to CCFL phenomena. High oscillations in the void fraction of the lowest volume are produced in the FAT vessel, which is continuously voided and refilled with water (Figure 7.6)

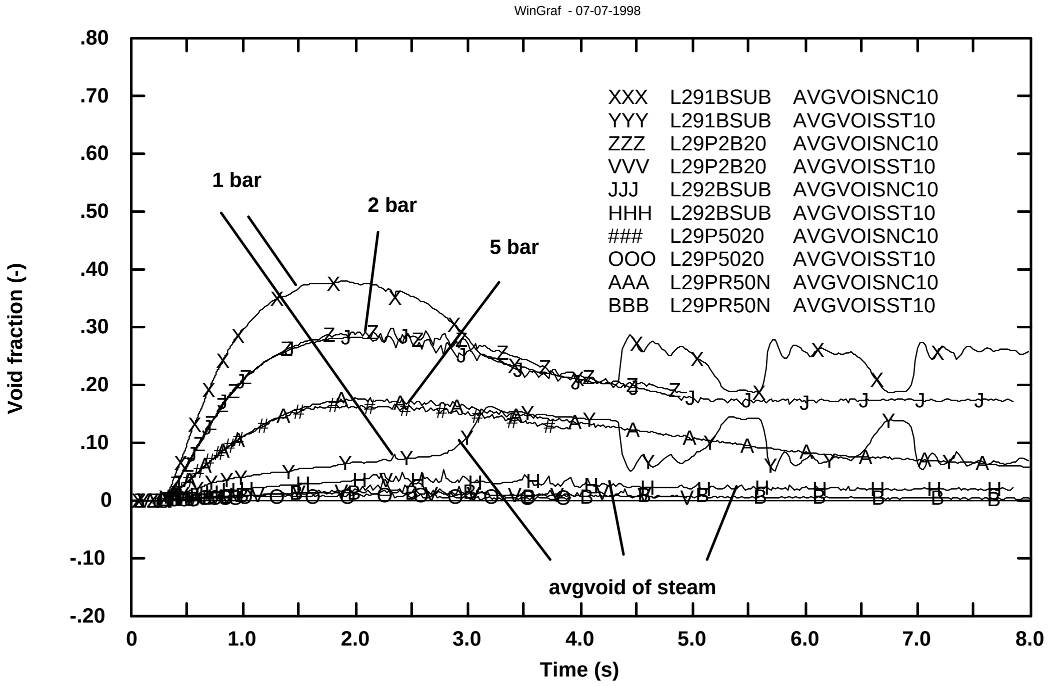

Figure 7.4 - Effect of subcooling and pressure on void fraction of non-condensable and steam in Test L-29

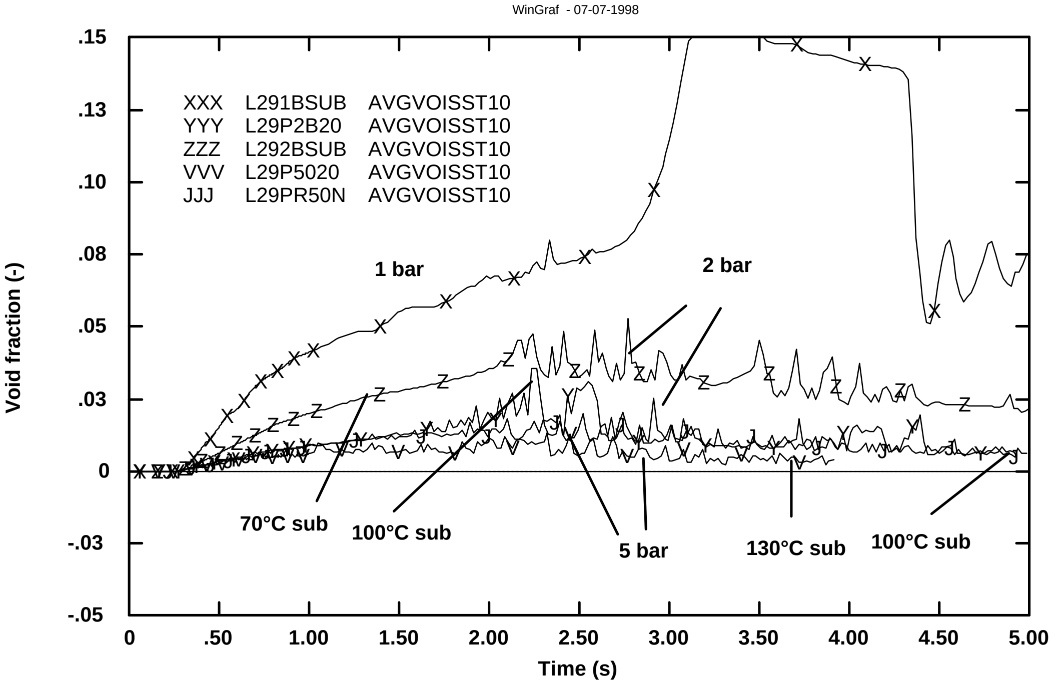

Figure 7.5 - Effect of subcooling and pressure on void fraction of steam in Test L-29

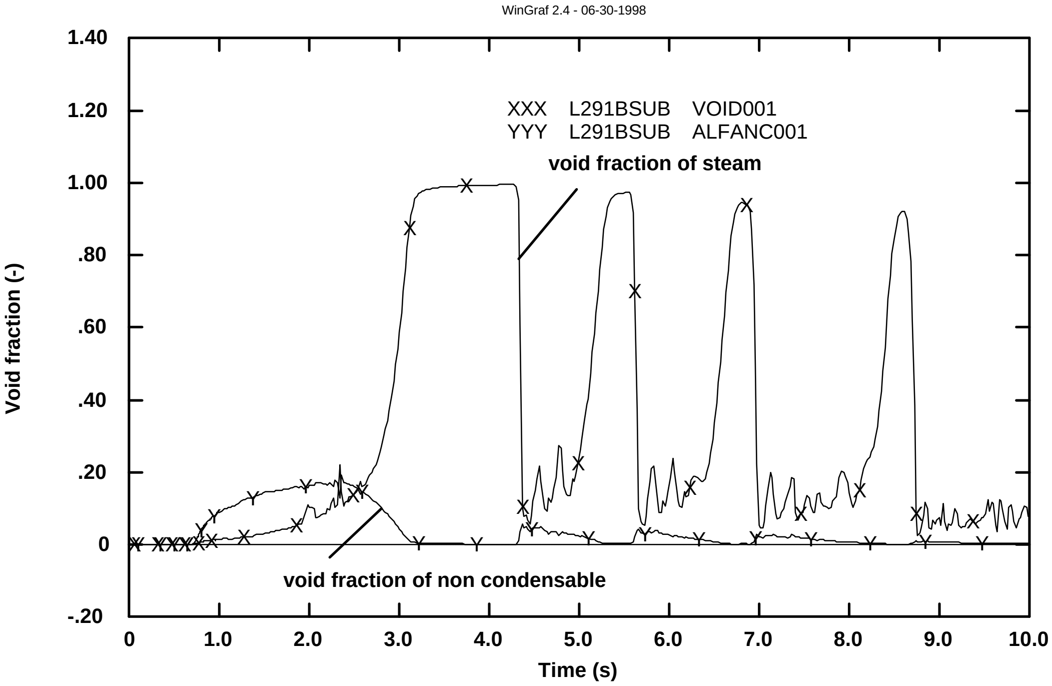

Figure 7.6 - Void fraction of steam and non-condensable in the FAT lowest volume for the 1 bar subcooled case in Test L-29

7.1.3. RESULTS OF SATURATED TEST OPTION FOR THE FARO TEST L-29

The following table summarises three 150 kg melt mass cases (5 cm discharge orifice) with saturated water at different initial pressures. It has been shown with Test L-28 prediction that is necessary to use the enhanced fragmentation model (Cd=3 instead of 6, Cj=0.5 instead of 1) to overcome the increased voiding caused by the lower pressure; therefore, the enhanced model has been used for these cases.

Descriptor	Melt mass (kg)	Melt temperature (K)	Initial Pressure (bar)	Initial water level (m)	Initial water temperature (K) and subcooling	Fragmentation Model
L292BAR	150	3073	2	1.5	Tsat.	Enhanced
L29P150S	150	3073	5	1.5	Tsat.	Enhanced
L2920BAR	150	3073	20	1.5	Tsat.	Enhanced

Table 7.3 - Performed L-29 pre-test saturated calculations

<u>Results of 150 kg mass saturation cases at different pressures</u>

The saturated cases were performed at different pressures and 150 kg melt mass (3073K). In order to have an idea of the influence of the subcooling the 150 kg saturated case at 5 bar (L29P150S) is compared with 150 kg subcooled (50°C at 5 bar, 100°C of subcooling) case: L29PR150N.

Cases are the following:

At 2 bar: L292BAR case; at 5 bar: L29P150S case and at 20 bar: L2920BAR case.

Pressure increases more as initial pressure is higher; it increases about 20 bar in the 20 bar initial pressure case. It is shown that the pressure is practically constant in the subcooled case with 150 kg mass at 5 bar. Also, quenching rate increases as initial pressure is higher and causes more fragmentation and less cake mass accumulation.

The quenching rate in the subcooled case is lower than the saturated one and becomes unstable due to high oscillations in the void fraction of the lowest volume in the FAT vessel, which is continuously voided and refilled with water (CCFL phenomena).

The void fraction below the mixture level increases as initial pressure decreases and so it does the accumulated cake mass. There is not a great influence of pressure on the global void fraction, which reaches about 70%. Void fraction in the subcooled case is much lower: the heat is transferred to subcooled water, which increases its temperature.

As conclusion it can be said that pressure increase in saturated test affects quenching rate and causes accumulated cake mass reduction as void fraction decreases.

7.1.4. ADDITIONAL CALCULATIONS PERFORMED FOR THE SUBCOOLED CASE

Additional cases have been analysed to highlight the influence of enhanced fragmentation model, H_2 generated and the nodalization type (1d/2d) in the subcooled case.

Effect of fragmentation model

The base case is compared with a case in which the enhanced fragmentation model has been used:

Descriptor	Melt Mass (kg)	Melt temperature (K)	Initial Pressure (bar)	Initial water level (m)	Initial water temperature (K) and subcooling	Fragmentation Model
L29PR50N	**50**	**3073**	**5**	**1.5**	**323 (100°C subc.)**	**Stand.**
L29PR50E	50	3073	5	1.5	323 (100°C subc.)	Enhanced

Table 7.4 - Performed L-29 pre-test base case calculations with standard and fragmentation model

Case L29PR50N: standard model case of 50 kg melt mass at 3073K falling into 1.5 m of subcooled water at 50°C at 5 bar, and L29PR50E case (same characteristics but using enhanced model).

The pressure starts to increase as the melt reaches the water at 0.27 s. In both cases, standard and enhanced, pressurisation are similar. In the enhanced fragmentation model case the pressurisation rate is initially greater, between 1.8 and 3 seconds pressure in the standard case is higher, but after 3 seconds and in the longer term the pressure in the enhanced case is maintained slightly greater.

It can be noted that in the standard model case the released energy is less than 65 MJ at 12 s. In the enhanced fragmentation case the amount is a little greater, about 70 MJ at 12 s. This little difference results in little differences in pressurisation rates.

In both cases, the average void fraction is between 12% and 18%, but is higher in standard fragmentation case. The reason is that in the enhanced fragmentation case the void fraction of single volumes of FAT increases much more in upper volumes, meanwhile is practically zero in the bottom volumes, in the standard case, it increases also in bottom volumes, and this makes the average value to increase.

Void fraction is mainly due to generation of non-condensable gas (H_2) and not to void fraction of the steam.

The melt components (jet, drops and cake) are presented in for the standard and enhanced fragmentation models. In the standard model most of the melt is fragmented and a little part is collected on the bottom as cake, with the enhanced model this trend is emphasized and the cake mass is practically zero. With the enhanced model the heat transfer surface is almost double than the other case.

To summarise, it can be said that calculations have shown that little difference exists in the application of the standard model or the enhanced fragmentation model when using initial subcooled water in the FAT vessel. A great quantity of drops is produced in both cases and little pressurisation and lower void fraction.

Effect of H_2 model, H_2 production

Also other case has been performed in order to analyse influence of H_2 production.

The base standard case without hydrogen production (L29P50NH) is compared with base case (L29PR50N):

Descriptor	Melt Mass (kg)	Melt temperature (K)	Initial Pressure (bar)	Initial water level (m)	Initial water temperature (K) and subcooling	Fragmentation Model
L29PR50N	**50**	**3073**	**5**	**1.5**	**323 (100°C subc.)**	**Stand.**
L29P50NH	50	3073	5	1.5	323 (100°C subc.)	Stand.No H_2

Table 7.5 - Performed L-29 pre-test base calculation using model with and without H_2 production

Two cases are compared to verify the influence of H_2 production during a subcooled transient. The base standard case L29PR50N (50 kg of melt mass, 1.5 m subcooled water at 50°C and 5 bar) and standard case L29P50NH (50 kg of melt mass, 1.5 m subcooled water at 50°C and 5 bar) using a model without H_2 production.

In both cases it is possible to observe similar quenching rate and fragmentation. Global void fraction (Figure 7.8) is much lower in the case without H_2 production. Pressure (Figure 7.7) is also lower in this case, and practically constant during the entire transient.

Summarising: it can be observed similar quenching rate and fragmentation with or without H_2 production model, but much lower void fraction (due to non-condensable gas and not to steam) and pressure in the case without H_2 production.

Effect of nodalization

In order to analyse the effect of the nodalization a case in 2d was run. This case was characterized by 5 radial volumes.

The pressure and quenching rate are very similar in the two cases. The only remarkable difference is in the void fraction distribution (Figure 7.9), which, in the 2d case, shows a central void fraction in the order of 30% and lateral void fraction about 8%, whereas in the 1d case is about 16%.

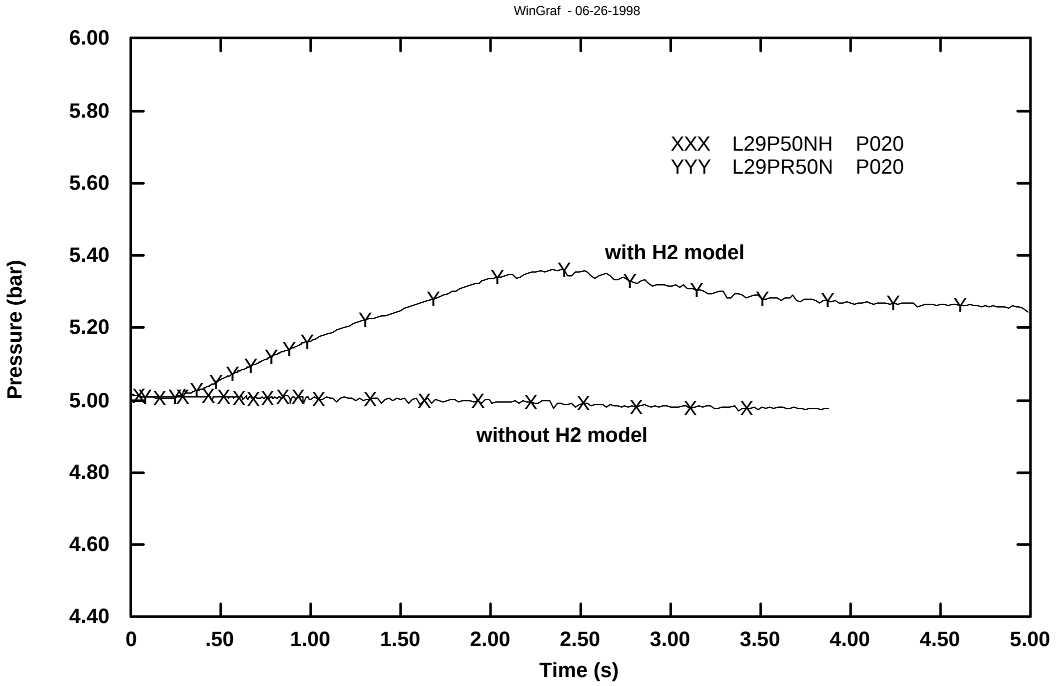

Figure 7.7 - Effect of the H2 production on pressure in Test the L-29

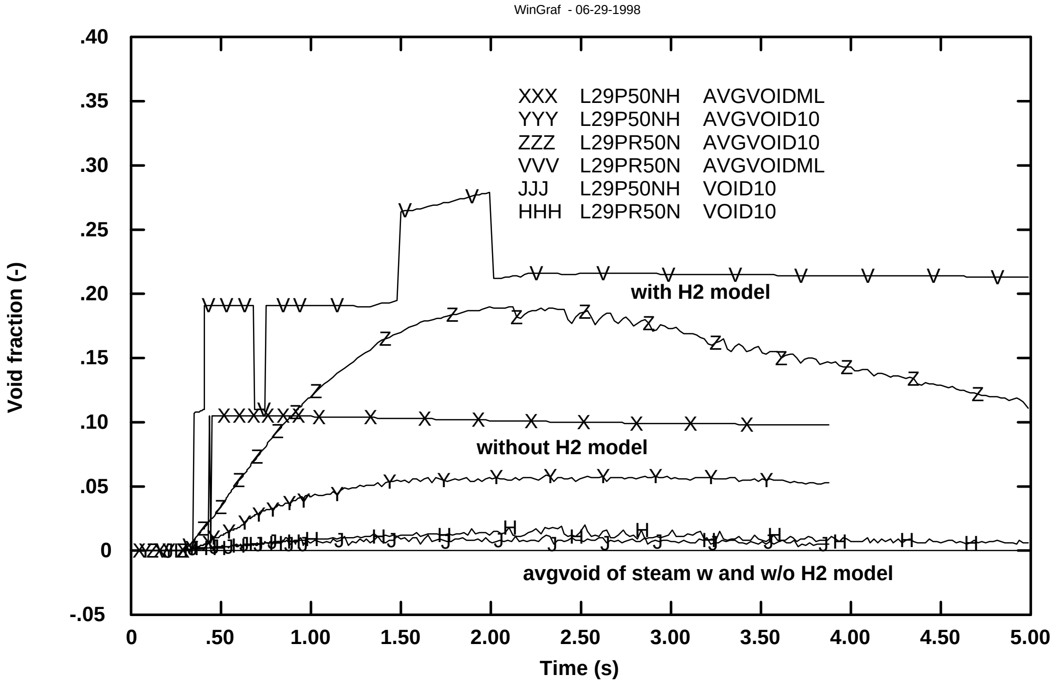

Figure 7.8 - Effect of the H2 production on the average void fraction in Test L-29

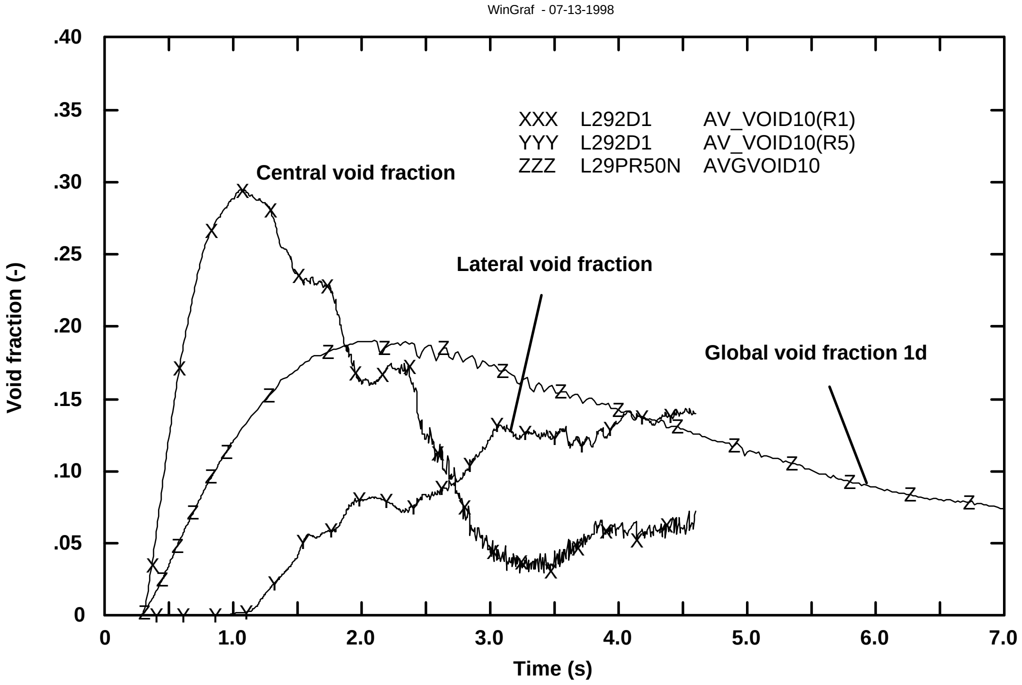

Figure 7.9 - Void fraction in the 2d calculation in Test L-29

7.1.5. CONCLUSIONS

The COMETA code was successfully applied to all the configurations prospected for the test L-29, that were basically:

Subcooled test with a reduced mass
Saturated test with the maximum available mass

In the subcooled test option it was shown the effect on the global void fraction of the selection of different pressure and/or temperature. The results indicate that the greater influence on the void fraction is caused by the pressure level (1 to 5 bar), which compressing the non-condensable void fraction, induces remarkable change in the global void fraction. No major influence is present in the quenching rate. Also, in subcooled conditions no significant difference resulted from the adoption of the standard or enhanced fragmentation model.

In the saturated test it was shown that the initial pressure influences the quenching rate and the amount of accumulated cake.

The code was able to calculate the subcooled conditions without innerving in major stability problems. However a point that needs improvement in the code is the jet parcels description in order to properly account for velocity differences among them.

Contrast between the 1-d and 2-d calculations showed no large overall influence of the nodalization scheme; difference in void fraction distribution between the central and pheripherical zones was, however, noticed.

7.2. COMETA PRE-TEST CALCULATION OF FARO TEST L-33

7.2.1. INTRODUCTION

Test L-33 was scheduled to be performed in the FARO facility in July 1999. There was a great interest in performing a subcooled test in the FARO test facility due to the potential for an energetic melt coolant interaction. In this test an external trigger was applied to enhance the possibility of this occurrence. This was supported by the results of the KROTOS Test 58, in which, for an UO_2 / ZrO_2 melt mixture, with conditions of 5 bar, 130°C subcooling a weak steam explosion occurred. In the case of failed triggering, the test will have been considered as another quenching test, the second one in subcooling conditions. Since there were uncertainties in the real initial test conditions, determined by the peculiarity of the test performed, a number of different hypotheses were explored as initial conditions of the test.

It is noted, however, that no spontaneous nor triggered steam explosions have been recorded so far with UO_2/ZrO_2 mixtures contrary to Al_2O_3 mixtures in the KROTOS facility which have exhibited spontaneous explosive interactions in subcooled conditions and triggered explosive interactions in nearly saturated conditions.

The following hypotheses were considered:

Subcooled Test

Initial Pressure:	3, 4, 5 bar
Mass:	176 kg
Initial Temperature	30°C
H_2 Production rate:	100% of what assumed for FARO tests ($1.8 \cdot 10^{-3}$ kg H_2 / kg $_{frag}$) 20% of what assumed for FARO tests ($0.36 \cdot 10^{-3}$ kg H_2 / kg $_{frag}$) for the 4 bar case.

Trigger Conditions

First trigger on the FAT vessel bottom, in the central volume, at 0.50 s.
Second trigger on the FAT vessel, at height 0.663 m, in the lateral volume, at 3 s.

Initially it was not yet decided if to perform the test with or without the internal cylinder in the FAT test section. Calculations were therefore performed in order to check the different behaviour in the two conditions. The relatively low influence of the internal cylinder and, even more important, safety reasons suggested to include the internal cylinder in the final test specifications. Only results with the internal cylinder in the FAT test section are here presented.

Figure 5.4 shows the configuration of the facility for this test. An inner vessel with the same diameter as the TERMOS will be installed inside the FAT vessel. The venting lines to the separator will be closed.

7.2.2. RESULTS OF TEST OPTION FOR THE FARO TEST L-33 BEFORE TRIGGERING

<u>Initial and boundary conditions</u>

The 2d nodalization adopted for the pre-test calculations for FARO Test L-33 is shown in Figure 7.10

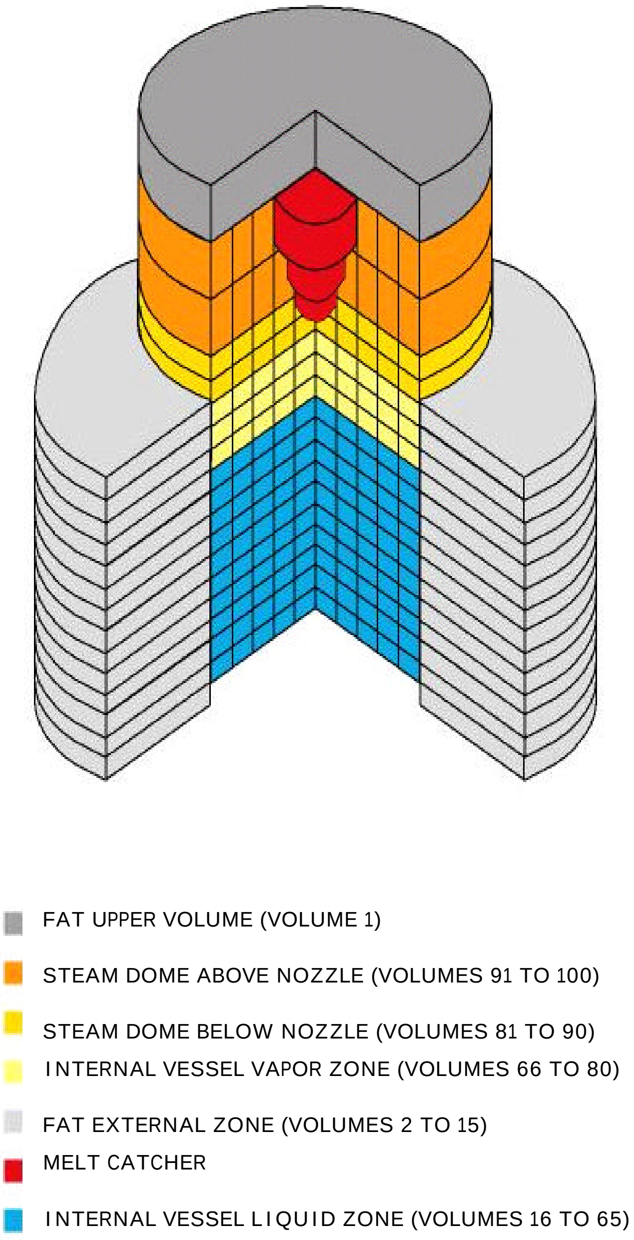

Figure 7.10 - COMETA 2d nodalization for FARO Test L-33

In order to cover the possible range in the experimental conditions, calculations have been performed with different values of initial pressure, with 176 kg of melt injected mass (Tmelt = 3073K) and 5 cm of discharge orifice. The case, L33INT3B should be seen as a lower bound and case L33INT5B should be seen as an upper bound.

The so-called standard fragmentation model has been used for this test, i.e.: Cd=6, Cj=1,$f_{H2}=1.8\cdot10^{-3}kgH_2/kg$ fragmented. For 4 bar case another case was performed in which the H_2 production rate was imposed to 20% of what assumed for standard tests ($f_{H2}=0.36\cdot10^{-3}kgH_2/kg$ fragmented). The reason for this change was due to the lower H_2 amount found in the first subcooled tests.

Calculations have been performed up to 3 s; in the following chapters several initial conditions for central and lateral triggering at 0.5 s and 3 s are show.

The following table summarises cases with 176 kg, at 30°C and different initial pressure:

Descriptor	Melt Mass (kg)	Melt temperature (K)	Initial Pressure (bar)	Initial water Level (m)	Initial water temperature (K) and subcooling	Fragmentation Model
L33INT3B	176	3073	3	1.5	303 (103ºC subc.)	Stand.
L33INT4B	**176**	**3073**	**4**	**1.5**	**303 (113ºC subc.)**	**Stand.**
L33INT5B	176	3073	5	1.5	303 (121ºC subc.)	Stand.
L33I4BNH	176	3073	4	1.5	303 (113ºC subc.)	Stand. 20% H_2 production

Table 7.6 - Performed pre-test calculations for Test L-33

<u>Results of the cases calculations up to 3 s</u>

Cases L33INT3B, L33INT4B, L33INT5B and L33I4BNH: standard fragmentation model cases of 176 kg melt mass at 3073K falling into 1.5 m of subcooled water at 30°C at 3, 4 and 5 bar. The 4 bar case was also performed with the H_2 production rate imposed to 20% of what assumed for standard tests.

The pressure increases about 1 bar in L33INT3B and L33INT4B cases and 2 bar in L33INT5B case at 3 seconds. In the case with 20% H_2 production this increase is only about 0.5 bar. The energy released is between 50 and 65 MJ at 3 s for all cases. Most of the melt is fragmented and a little part is collected on the bottom as cake.

The central void fraction is calculated in the central volumes of FAT vessel, where jet descends and fragments (vol.16 to 25). The global average void fraction (Figure 7.11) is calculated as the average void fraction of the 50 lower volumes (initially full of water) in the FAT vessel.

Void fraction is an important quantity in the study of possible steam explosions, since as the global void fraction is lower than a certain value, the steam explosion is likely to occur. In the three cases with higher H_2 production, the global void fraction reaches about 0.3 (30%) at 3 seconds, increasing as the initial pressure decreases. The void fraction in the central volumes is much less influenced by the initial pressure, being about 0.4 in all cases. A great influence is due to the amount of H_2 produced. Reducing it to 20% the void fraction in the central volumes reduces from 0.4 to 0.2.

The temperature increase is strongly dependent on the amount of energy released and therefore follows the same trend of this quantity. It can be noted that temperature increases faster in the bottom zone than in the upper zone.

The jet leading edge position (Figure 7.12) shows that initially the melt falls down according to melt gravity release as for Test L-31. What happens is that the jet parcels are released at progressive increasing velocity. Some parcel can overcome the leading edge parcels, becoming leading edge. Therefore, the leading edge can become faster than the theoretical gravity release with initial velocity zero (Figure 7.13).

In order to remove this discrepancy a modification in the logic of the COMETA logic was introduced and if one parcel reaches the one before it, the interference part between the two is broken up and the faster jet is slowed down. Therefore the leading edge proceeds with the gravity discharge trend (Figure 7.14). With this new logic the comparison with L-31 is much better. Figure 7.15 shows that the leading edge position with the modification of the COMETA logic for 4 bar case (performed with the H_2 production rate imposed to 20% of what assumed for standard tests) is similar to jet behaviour for Test L-31.

Pressure behaviour increases in the first seconds for case with this modification in the COMETA logic, because the jet travels slowly and produces more fragmentation: in this case the heat transfer surface is higher.

Conditions at the expected time of activation of the Central Trigger (0.50 s)

Figure 7.16 to Figure 7.18 show the curves of some quantities obtained in the four calculations at 0.50 seconds versus the height in the FAT vessel up to the point of injection of the melt. These would be the initial conditions for the trigger at 0.5 seconds.

Figure 7.16 shows central void fraction; it is zero in the bottom volumes because the jet has not yet arrived at that location. It would be better to trigger before the jet arrives to the bottom to avoid the vapour to absorb the impulse of the trigger.

Figure 7.17 shows the lateral void fraction, only different from zero in the upper volumes. Figure 7.18 presents the mass of drops in the central volumes; drops are mainly present in the volumes at medium height. The jet mass at 0.50 s has not arrived at the bottom.

Conditions at the expected time of activation of the Lateral Trigger (3 s)

Figure 7.19 to Figure 7.22 present the initial conditions for lateral trigger at 3 seconds and at height 0.663 m. Central and lateral void fractions are higher in the upper volumes. In this case also the mass of drops in the lateral volumes is represented (Figure 7.22). The jet has arrived at the bottom except for case at 5 bar. The reason is due to a greater fragmentation with this higher pressure (more drops present, Figure 7.21).

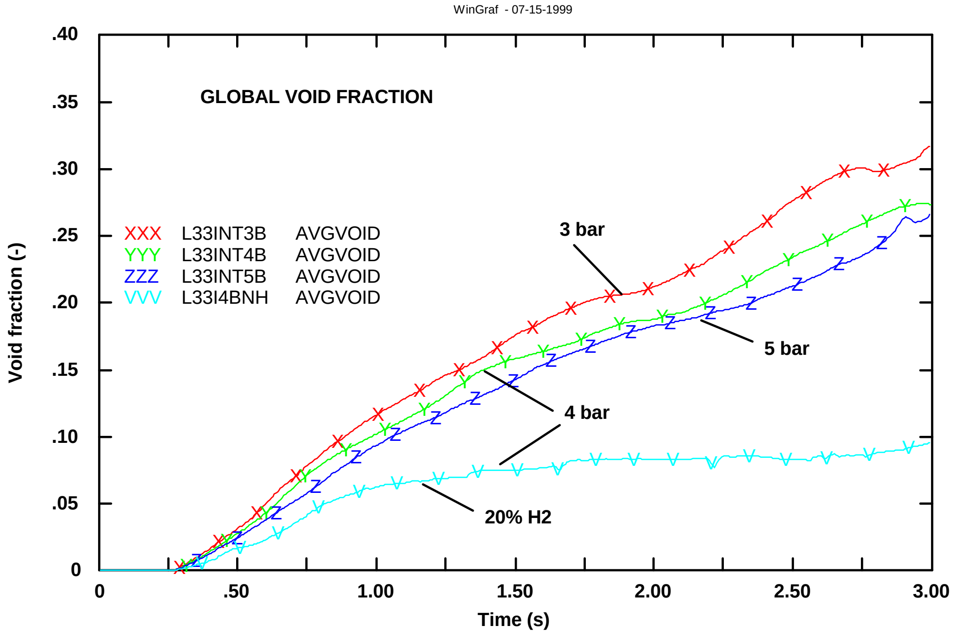

Figure 7.11 - Global void fraction for Test L-33

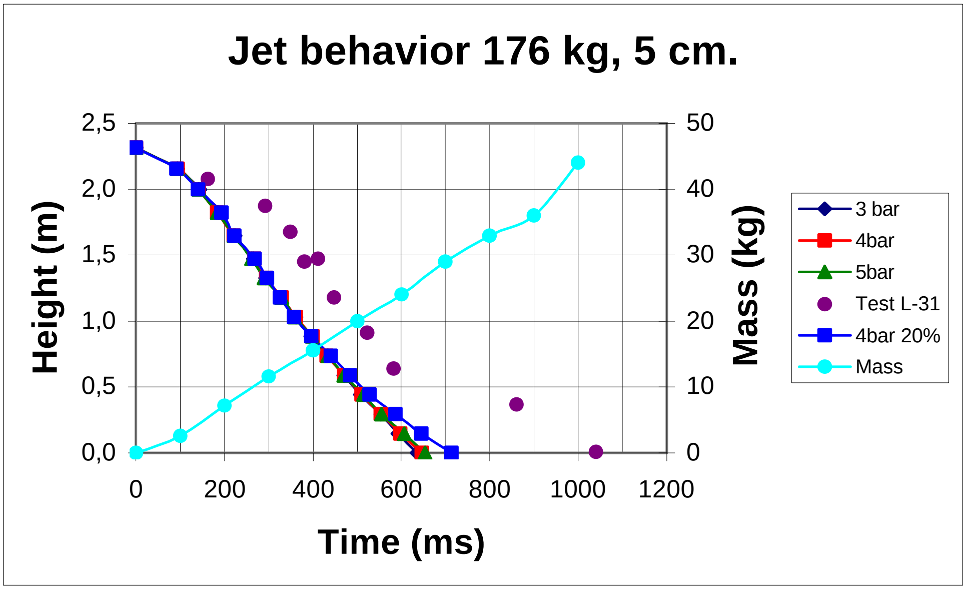

Figure 7.12 - Jet leading edge for Test L-33

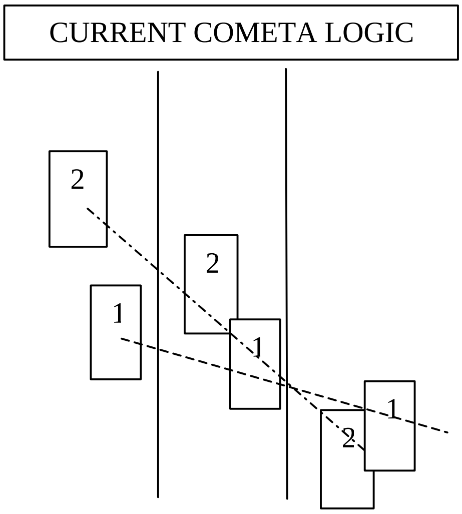

The faster jet piece (2) can overpass the slower one (1)

Figure 7.13 - Current COMETA logic for leading edge behaviour

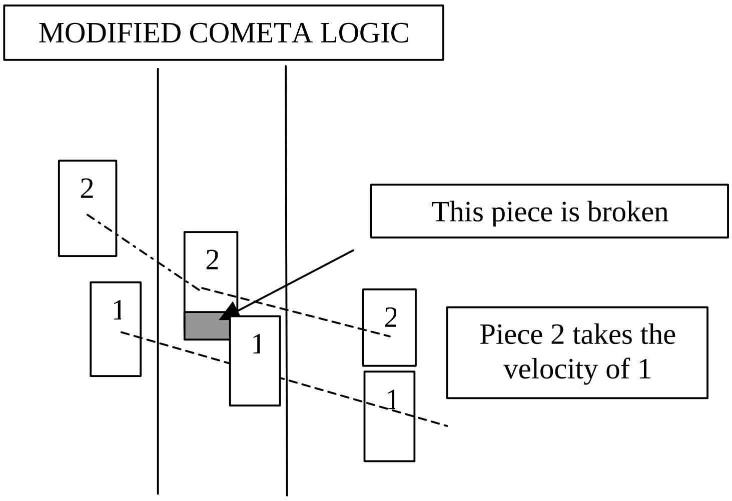

The faster jet piece (2) cannot overpass the slower one (1)

Figure 7.14 - Modified COMETA logic for leading edge behaviour

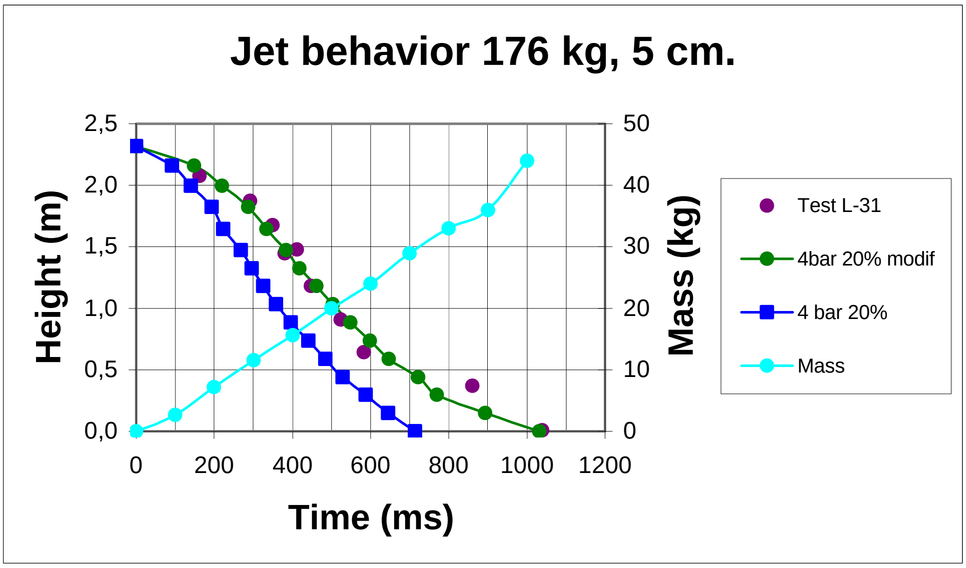

Figure 7.15 - Jet leading edge for Test L-33 with modified COMETA logic

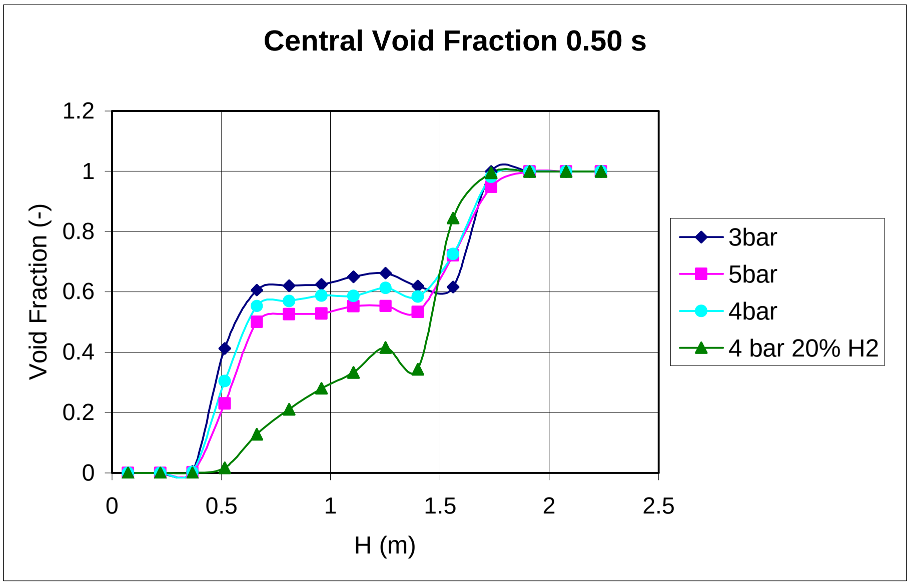

Figure 7.16 - Central void fraction vs. height at 0.5 s for Test L-33

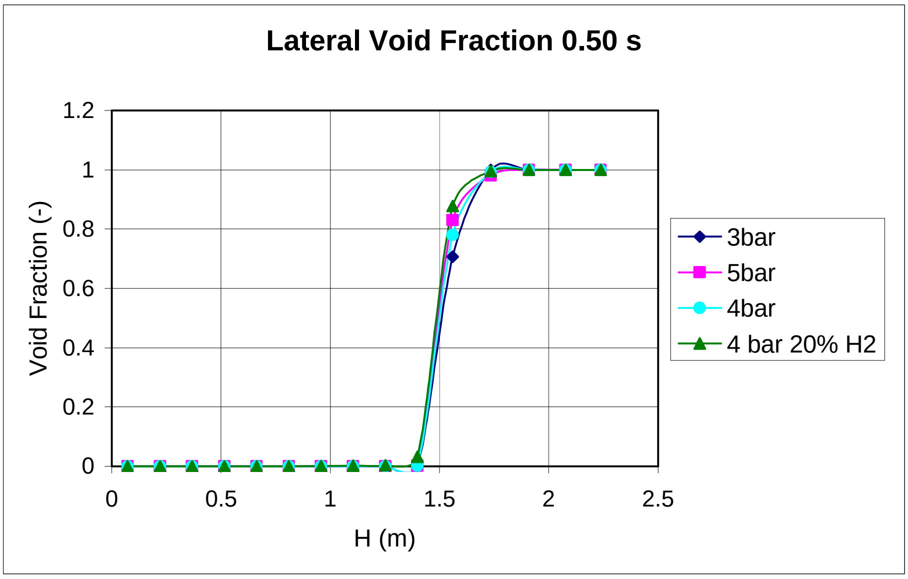

Figure 7.17 - Lateral void fraction vs. height at 0.5 s for Test L-33

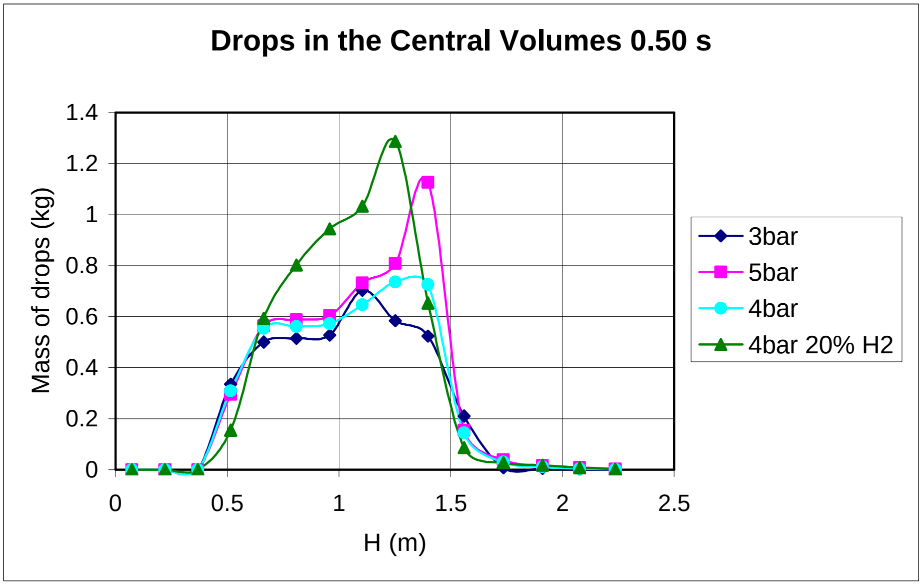

Figure 7.18 - Drops in the central volumes vs. height at 0.5 s for Test L-33

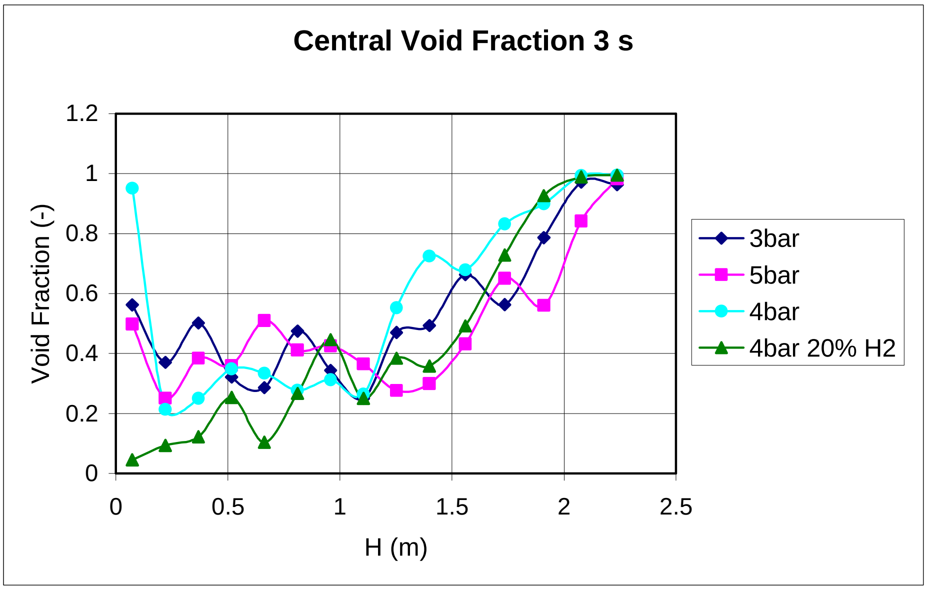

Figure 7.19 - Central void fraction vs. height at 3 s for Test L-33

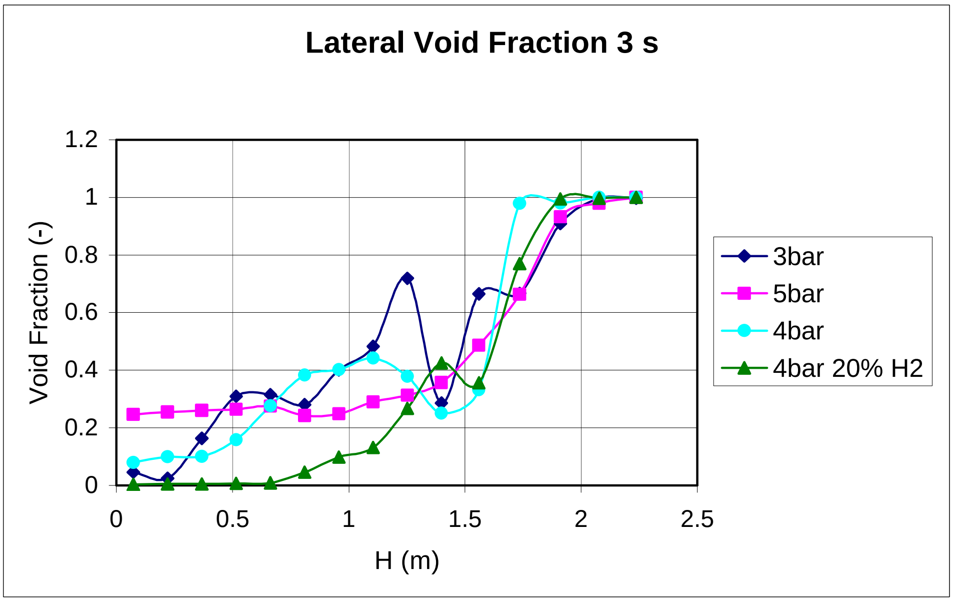

Figure 7.20 - Lateral void fraction vs. height at 3 s for Test L-33

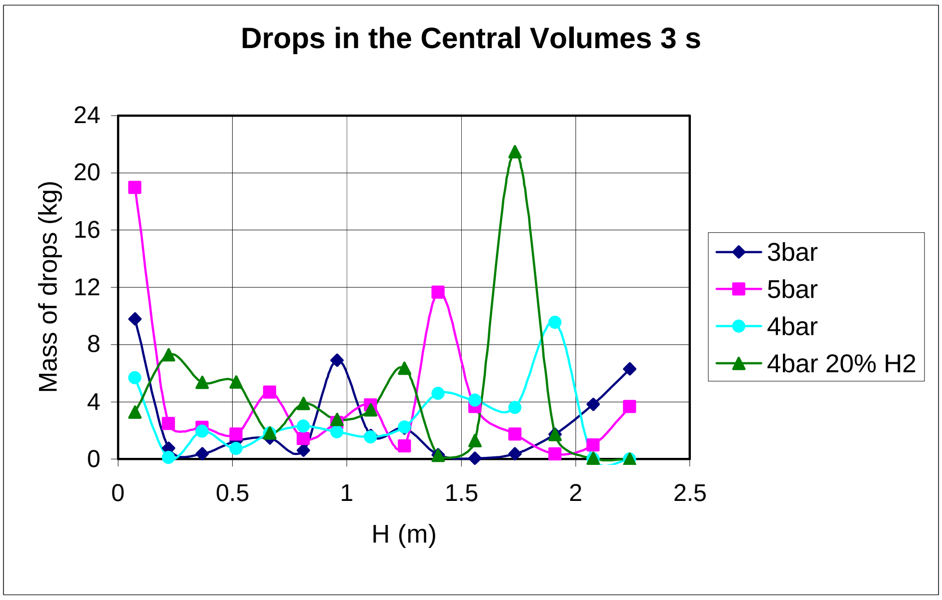

Figure 7.21 - Drops in the central volumes vs. height at 3 s for Test L-33

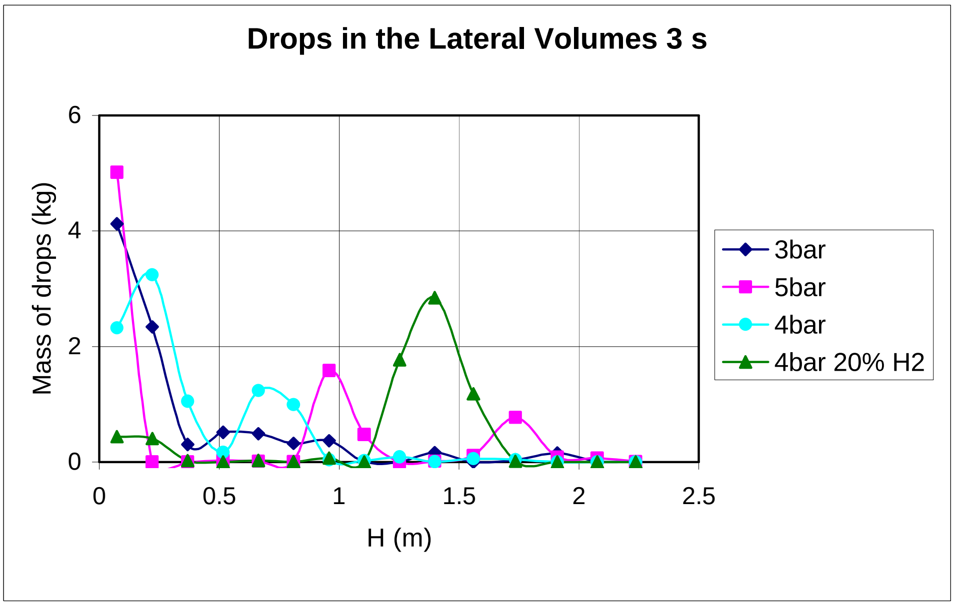

Figure 7.22 - Drops in the lateral volumes vs. height at 3 s for Test L-33

7.2.3. TRIGGER CALCULATION TESTS WITH WATER

Several shapes of trigger were tested in the FAT vessel with the internal cylinder and without releasing melt, to choose the appropriated one. In the experiment it was planned to use a plastic charge whose form in terms of pressurization was quite different from previously used gas triggers like in KROTOS. Figure 7.23 shows the triangular mass flow shape of the vapour trigger initially tested, injecting vapour at 1 bar and 293 K, with a maximum peak of 167 kg/s. This trigger causes pressure behaviour in the central volumes shown in Figure 7.24. This impulse was strong enough but the shape of the pressure peak was not as short as in the case of the planned plastic trigger.

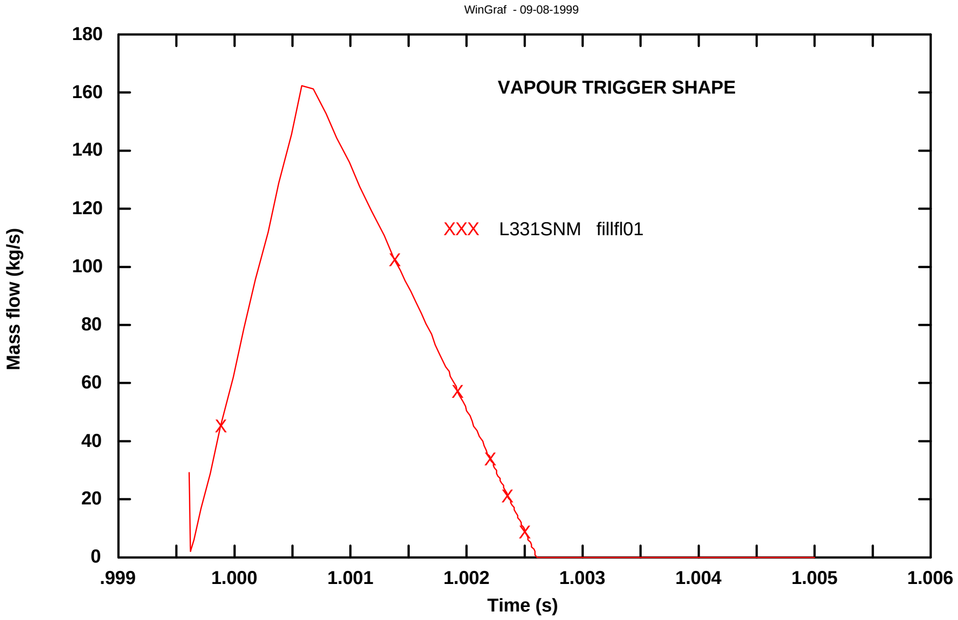

Figure 7.23 - Vapour trigger mass flow shape for Test L-33

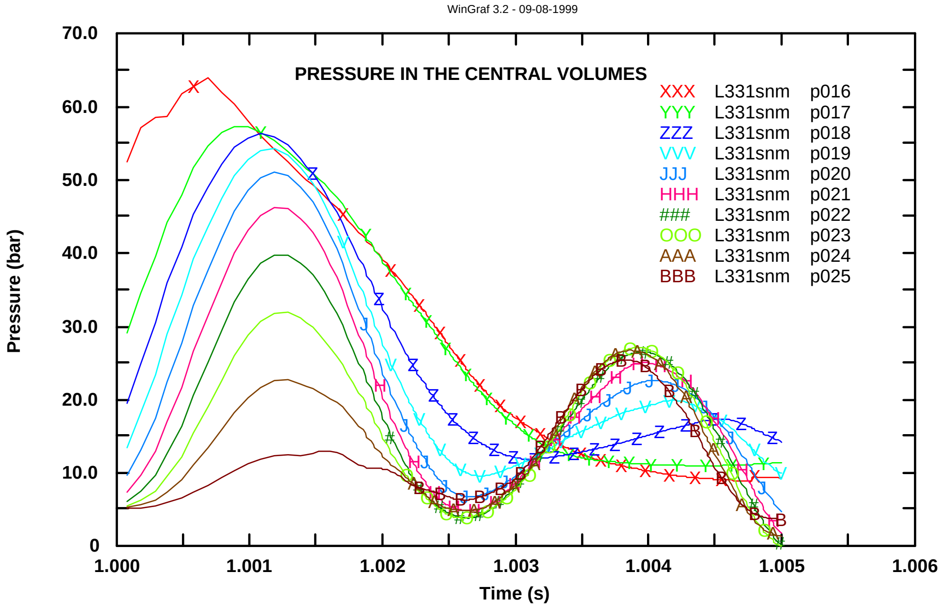

Figure 7.24 - Pressure in the central volumes triggering with vapour mass flow

Another trigger shape (Figure 7.25) was tested in the same conditions but injecting water instead of vapour at 200 bar and 293 K, during 0.251 ms in a rectangular shape, and a mass flow maximum of 1350 kg/s. This impulse causes the pressure behaviour shown in Figure 7.26. A high pressure of 250 bar was reach in the bottom central volume. This was the selected trigger shape for the calculations.

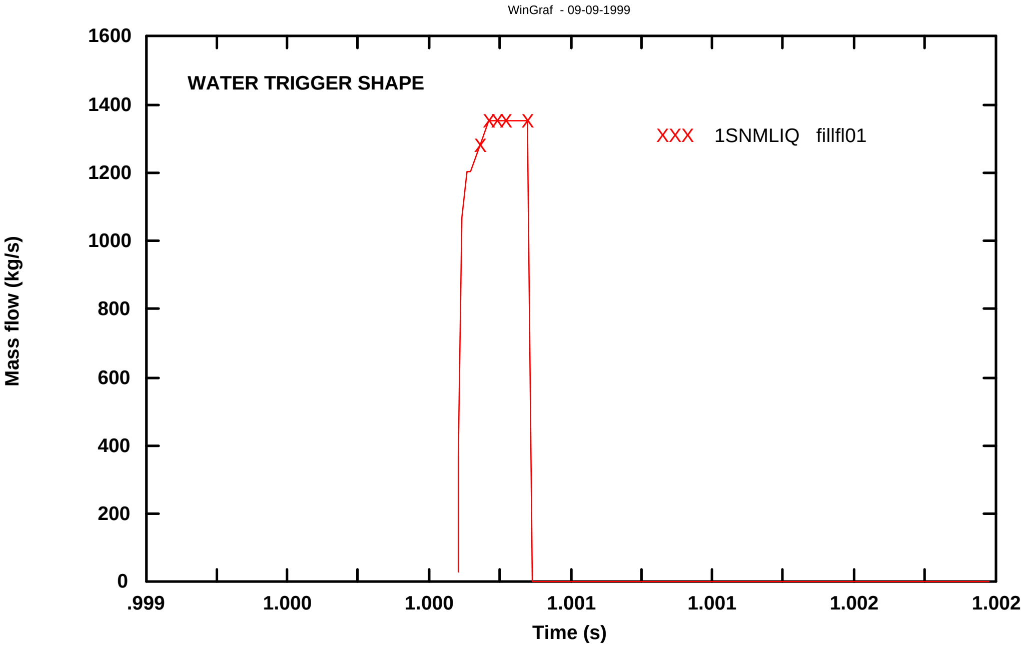

Figure 7.25 - Water trigger mass flow shape for Test L-33

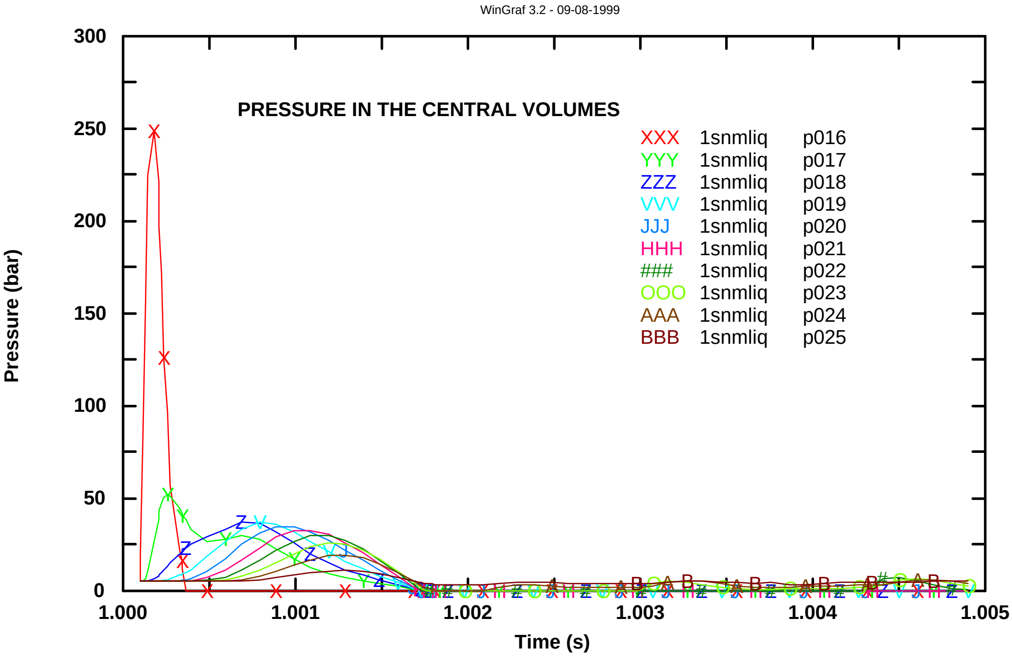

Figure 7.26 - Pressure in the central volumes triggering with water mass flow

Figure 7.27 shows pressure behaviour in the central bottom volume 17 triggering with the triangular vapour mass flow and the rectangular water mass flow. A thinner shape is obtained triggering with water.

Figure 7.28 shows the final trigger shape used for all calculations, injecting water at 200 bar and 293 K during 0.251 ms in the bottom central volume of the FAT vessel at 0.5 s and in the lateral volume at 3 s.

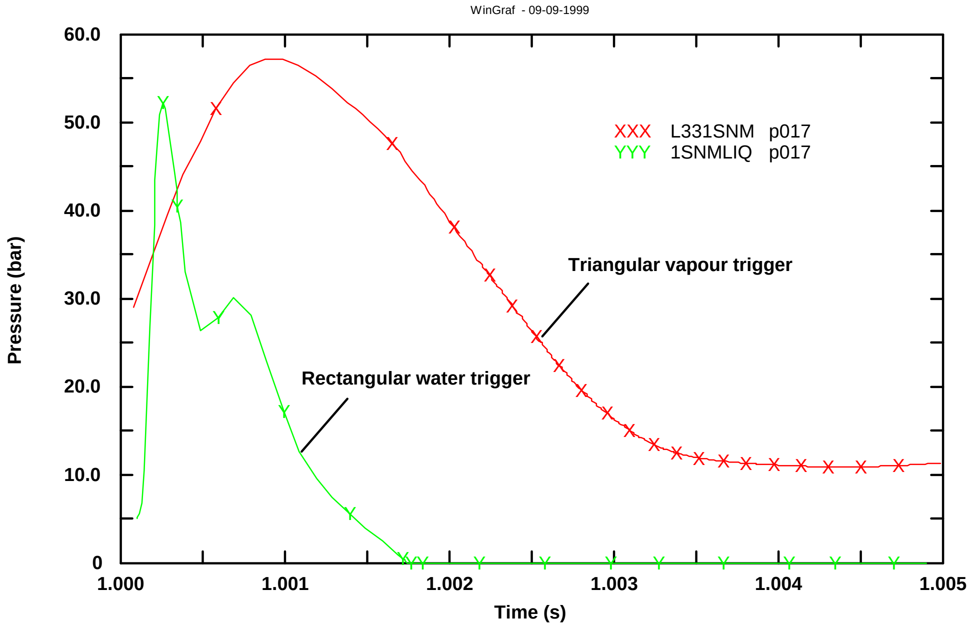

Figure 7.27 - Pressure in two central volumes triggering with vapour and water mass flows

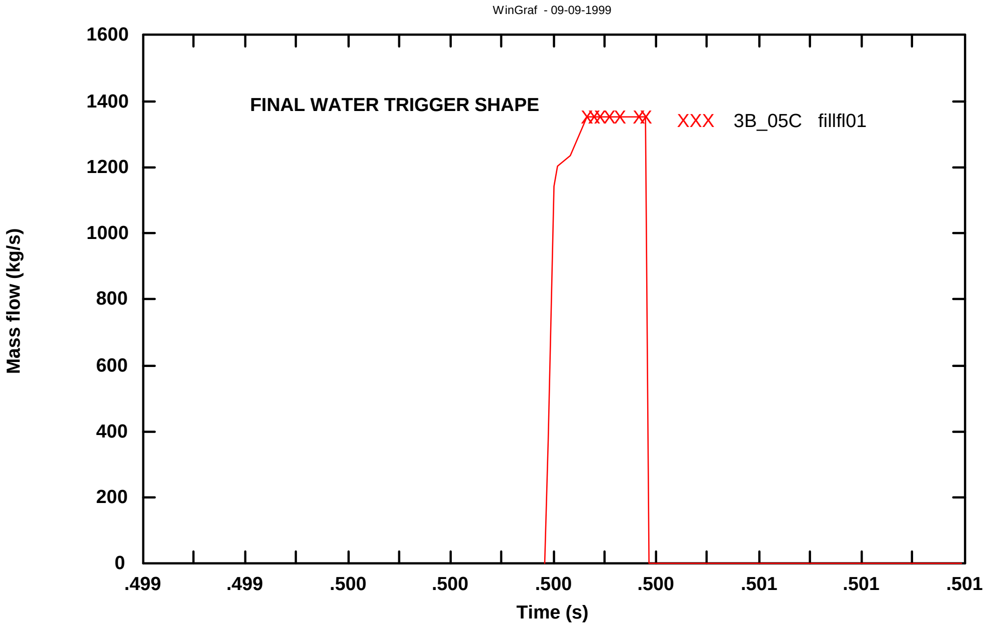

Figure 7.28 - Selected water trigger mass flow shape for Test L-33

7.2.4. CALCULATION OF THE TRIGGERING EVENT FOR THE FARO TEST L-33

Results of 176 kg mass cases at different pressures

Two different triggers have been simulated with COMETA code. The first one at 0.5 seconds of calculation, simulated injecting water at 200 bar and 293 K during 0.251 ms in the bottom central volume of the FAT vessel (volume 16) and the second one at 3 seconds injecting water with the same characteristics in the lateral volume at height 0.663 m (vol. 60).

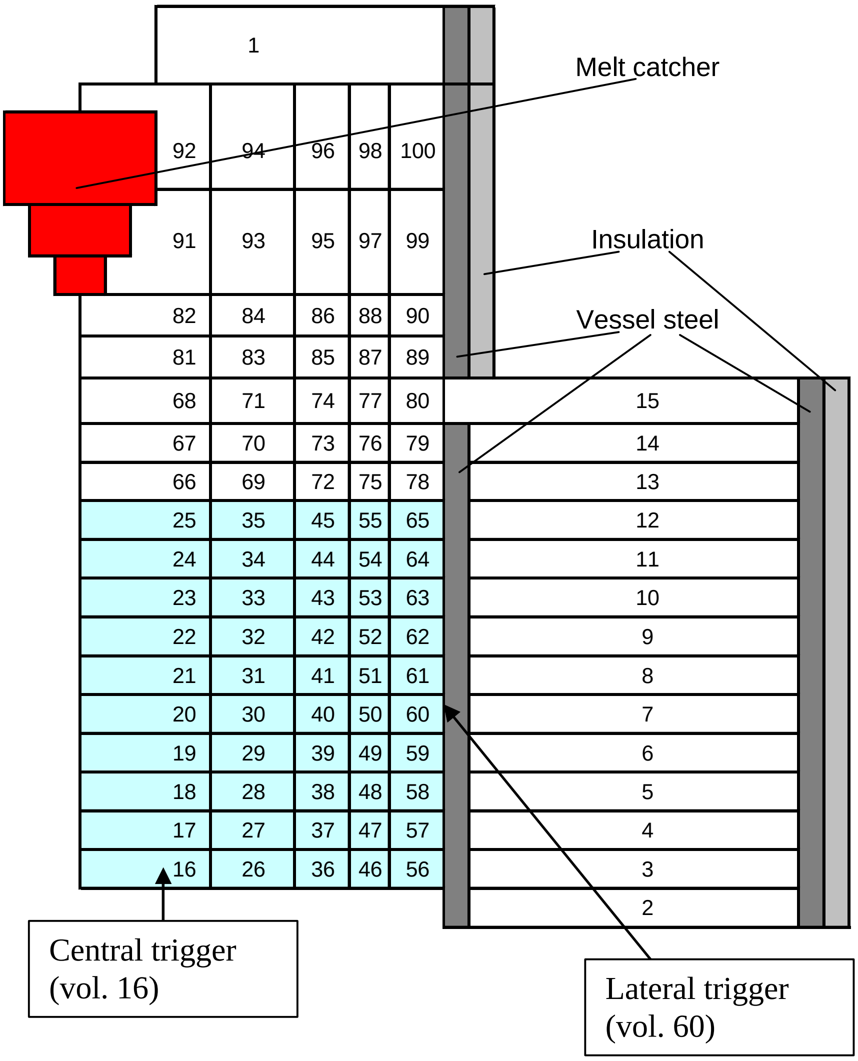

Figure 7.29 - COMETA 2d nodalization and triggering position

The trigger causes pressure pick that should be transmitted to the upper and lateral volumes.

Pressure behaviour is studied after central triggering in the central (vol. 16 to 25) and lateral volumes (vol. 56 to 65) initially full of water. For the case at 3 bar of initial pressure (L33INT3B), after the central trigger, the pressure reaches 250 bar in the central zone and about 60 bar in the lateral zone. But this impulse is not propagated, is absorbed almost completely by the vapour present in the central volumes.

In case at 4 bar initial pressure (L33INT4B), and case at 5 bar initial pressure (L33INT5B) occur the same problem, pressure reaches a high value (about 250 and 60 bar in central and lateral bottom volumes, respectively) but this impulse is not propagated.

Case at 4 bar initial pressure with the H_2 production rate reduced to 20% of what assumed for FARO standard tests (L33I4BNH) is presented in Figure 7.30 and Figure 7.31 (central and lateral pressure evolution). It is observed that a propagation is present and it is possible to see the progression of the pressure along the mixture.

Central and lateral pressures in the four cases after lateral trigger at medium height (0.663 m) are studied. All cases show low increase of pressure and little transmission of the impulse (Figure 7.32 and Figure 7.33).

In the standard cases the pressure increase only in the bottom volume and the void fraction is sufficiently high to suppress any propagation. In the case with reduced H_2 production, instead, a propagation is present and it is possible to see the progression of the pressure along the mixture. The calculation could not be continued after 20 ms because the pressure of 250 bar has been reached and the code stops at that value.

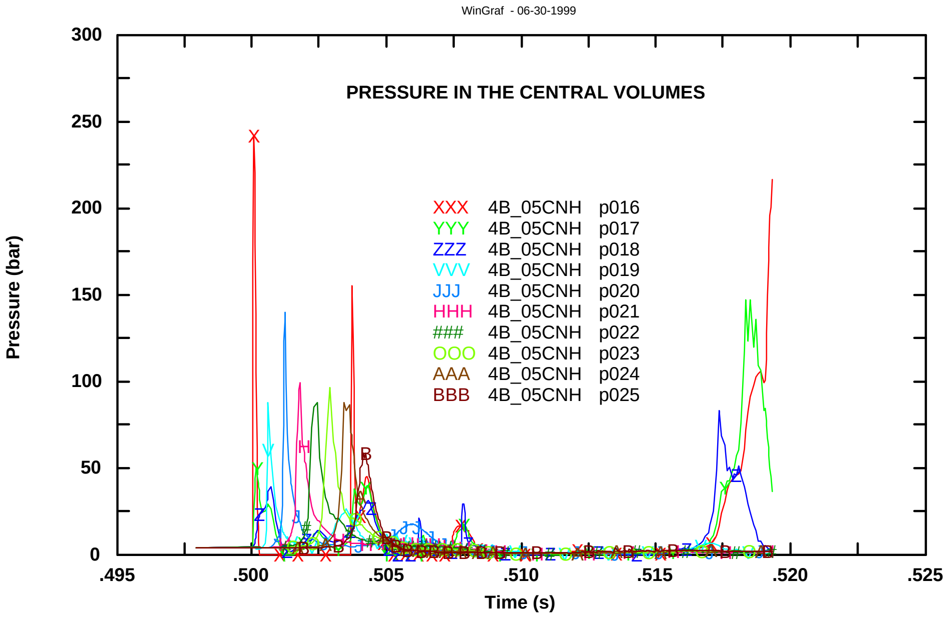

Figure 7.30 - Pressure behaviour in the central volumes after triggering at 0.5 s in the 4 bar case calculation with 20% of H_2 production

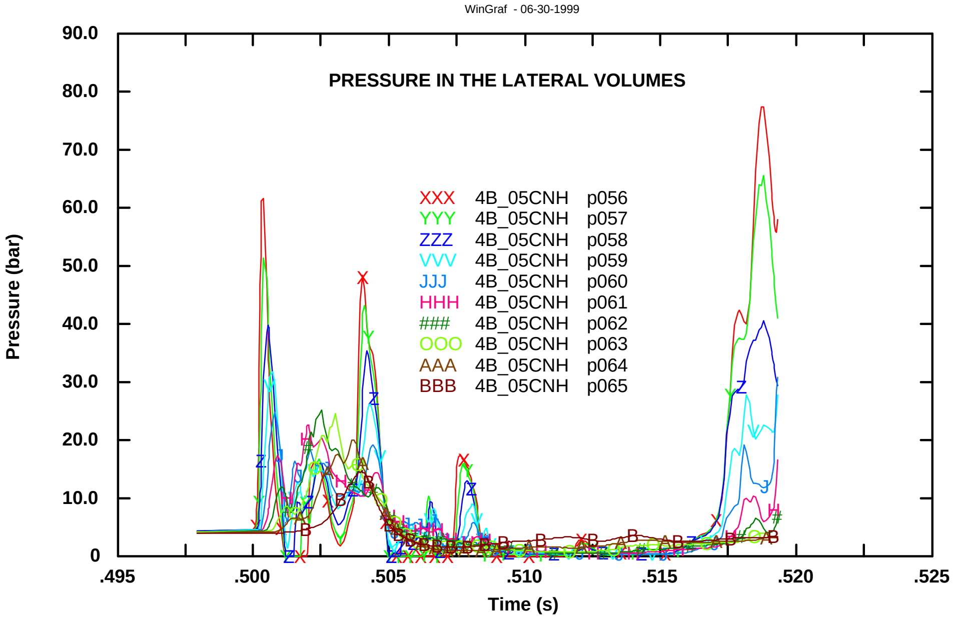

Figure 7.31 - Pressure behaviour in the lateral volumes after triggering at 0.5 s in the 4 bar case calculation with 20% of H_2 production

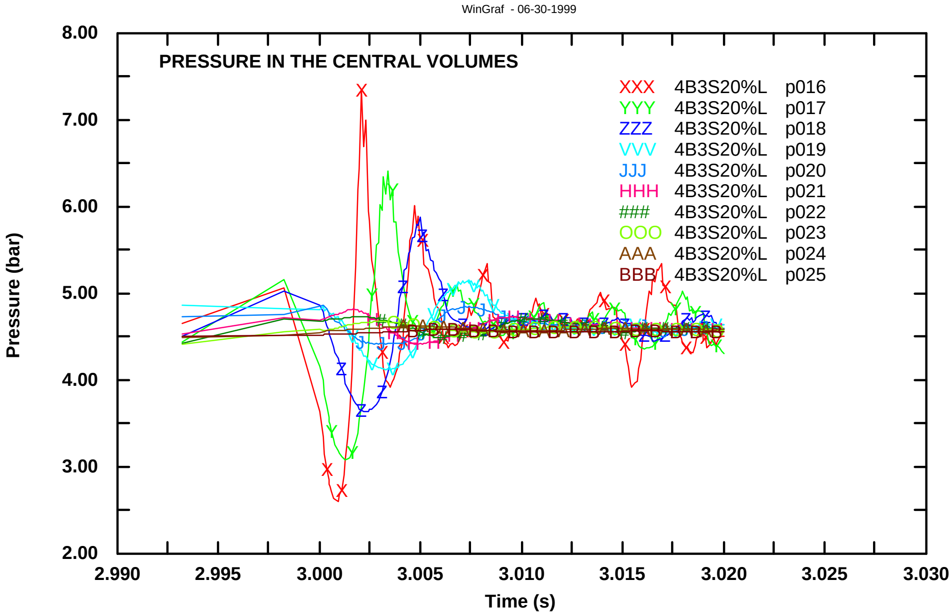

Figure 7.32 - Pressure behaviour in the central volumes after triggering at 3 s in the 4 bar case calculation with 20% of H_2 production

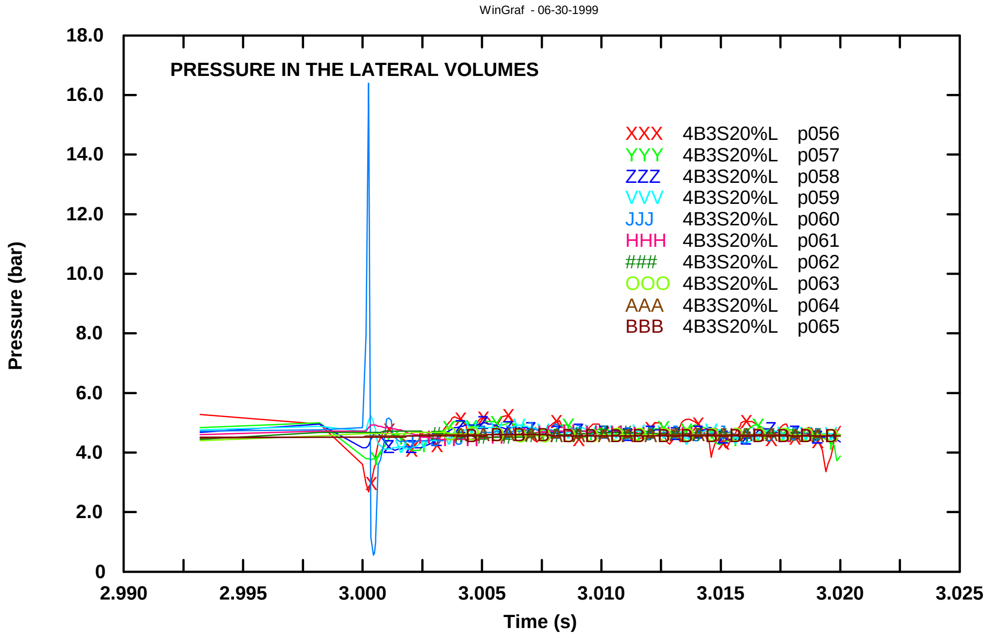

Figure 7.33 - Pressure behaviour in the lateral volumes after triggering at 3 s in the 4 bar case calculation with 20% of H_2 production

7.2.5. CONCLUSIONS

The COMETA code has been used to calculate the conditions foreseen for the FARO Test L-33. According to the initial specifications this facility configurations were prospected: one with the internal vessel and one without it. The calculations indicated no major differences as far as regards the central part of the test section. Therefore the solution with the internal cylinder was chosen.

The code has been also applied to simulate the triggering and the response due to a possible explosion. No propagation was calculated if the H_2 generation model was the same as applied for previous saturated tests. If the amount is reduced to values typical of the last subcooled Test L-31 or even less a propagation of the explosion seems possible.

7.3. ANALYSIS OF FUEL-COOLANT QUENCHING PHENOMENA BY COMETA CODE IN REACTOR GEOMETRY

7.3.1. INTRODUCTION

During the progression of a severe accident in water cooled reactors, molten fuel resulting from overheating the core, in absence of adequate cooling, can relocate and interact with coolant in the reactor pressure vessel lower plenum or in the reactor cavity.

The document reports some simulation results of an extended melt coolant interaction accident in a reactor geometry typical of the Spanish reactor ASCO-1, a 3-loops 966 MW_e (2686 MW_{th}) Westinghouse PWR (*Asociación Nuclear ASCÓ, A.I.E - "Private communication. Data trasmission" - 1998*) [33] [49]. 1-d and 2-d calculations have been performed with the last version of JRC-Ispra COMETA code, simulating 30.000 kg of melt that fall into the central part of the core inlet and lower plenum. The melt mixture consisted of 80% weight of UO_2 and 20% weight of ZrO_2 at 3073K released by a 10 cm diameter discharge orifice into saturated water at a pressure of 50 bar and at different water levels. Boundary cases in which completely full or completely empty conditions were also considered.

Emphasis is placed on overall thermal-hydraulic system response and melt fragmentation behaviour in order to correlate pertinent phenomena to a range of accident initial and boundary conditions such as residual water level depth, melt discharge rate and exchanged power.

7.3.2. INITIAL AND BOUNDARY CONDITIONS. ANALYSED CASES

The following case was analysed: a molten pool is formed in the central core region and starts to be released through a hole of diameter 10 cm into the core inlet and the lower plenum that are considered full of water or partially full, depending on the case. The melt is assumed to be discharged in the central part of the vessel and eventual fragmented pieces are kept in the central zone for the 2-d cases, which is 0.37 m wide. In 1-d cases fragmented pieces can be found in all core inlet and lower plenum volumes. No heat exchange is assumed above the injection point. The melt does not occupy volume, i.e. no reduction of the volume due to the presence of the melt is assumed in the lower plenum.

The following conditions were considered:

Pressure:	50 bar.
Temperature:	Tsaturation.
Melt mass:	30.000 kg.
Melt temperature:	3073K.
Orifice size:	10 cm.

1-D Descriptor	Initial Water level (m)	Nodalization
ACQPL2	2.969 (vol.: 19 to 33, 34 to 45 and 46 to 57)	1D (57 nodes)
ACQ2M37	2.37 (vol.: 19 to 33, 34 to 38 and 46 to 50)	1D (57 nodes)
ACQ2M	2 (vol.: 19 to 33, 34 and 46)	1D (57 nodes)
ACQ129M	1.29 (vol.: 19 to 28)	1D (57 nodes)
ACQ1M	1 (vol.: 19 to 26)	1D (57 nodes)
ACQ05M	0.5 (vol.: 19 to 22)	1D (57 nodes)
VAPOR	0.26 (vol. 19 and 20)	1D (57 nodes)
BOUND	All lower plenum (vol.: 19 to 33), core inlet (vol.: 46 to 57), downcomer (vol.: 1 to 8 and 34 to 45), riser and upper plenum (vol.: 11 to 18) full of water	1D (57 nodes)

2-D Descriptor	Initial Water level (m)	Nodalization
2DASCOFULL	8.1 (vol.: 1 to 8, 11 to 18, 19 to 52, 53 to 57 and 58 to 77)	2D (77 nodes)
2DASCOHALF	5.51 (vol.: 1 to 4, 11 to 14, 19 to 52, 53 to 57 and 58 to 77)	2D (77 nodes)
2DASCOBASE	2.969 (vol.: 19 to 52, 53 to 57, and 58 to 77)	2D (77 nodes)
2DASCO1M	1 (vol.: 19 to 48)	2D (77 nodes)

The initial conditions assumed in the calculations are depicted in Figure 7.34 for 1-d calculations: only extreme cases VAPOR (0.26 m water level) and BOUND (Vessel full, 8.1 m water level). The rest of the cases are between those ones (0.5 m, 1 m, 1.29 m, 2 m, 2.37 m and 2.969 m). Initial conditions for 2-d calculations are shown in Figure 7.35: Vessel full (2DASCOFULL, 8.1 m), half vessel full (2DASCOHALF, 5.51 m), base case (2DASCOBASE, 2.969 m) and 1 m case (2DASCO1M).

In specific sequences like TMI, however, after core melt down, relocation into the lower plenum occurred with a vessel full condition since the primary system water inventory was being replenished during the evolution of the accident. So it was decided to perform cases with all vessel full of water up to upper head level: BOUND and 2DASCOFULL cases in 1-d and 2-d nodalization, respectively. One case with half vessel full of water in 2-d nodalization (2DASCOHALF) was also performed.

The nodalization chosen for all calculations is presented in Figure 7.36 and Figure 7.37 for the 1-d and for the 2-d cases; great detail has been devoted to the simulation of the reactor vessel lower downcomer, core inlet and lower plenum.

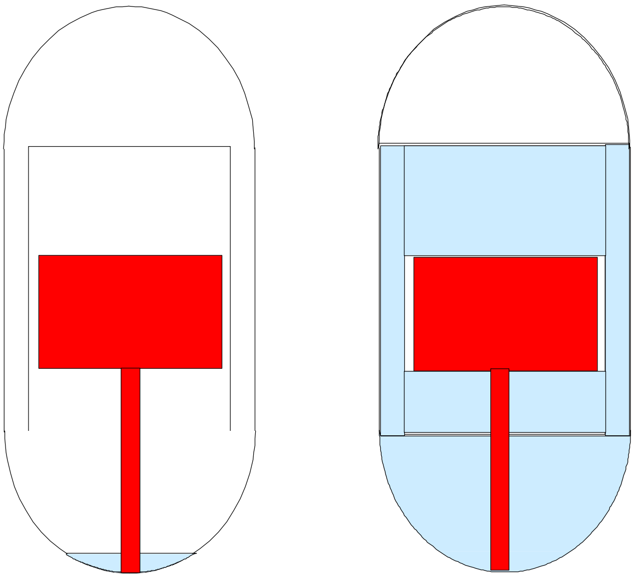

a) 0.26 m water (VAPOR) b) Vessel Full (BOUND)

Figure 7.34 - Initial conditions for extreme 1-d calculations in COMETA reactor calculation

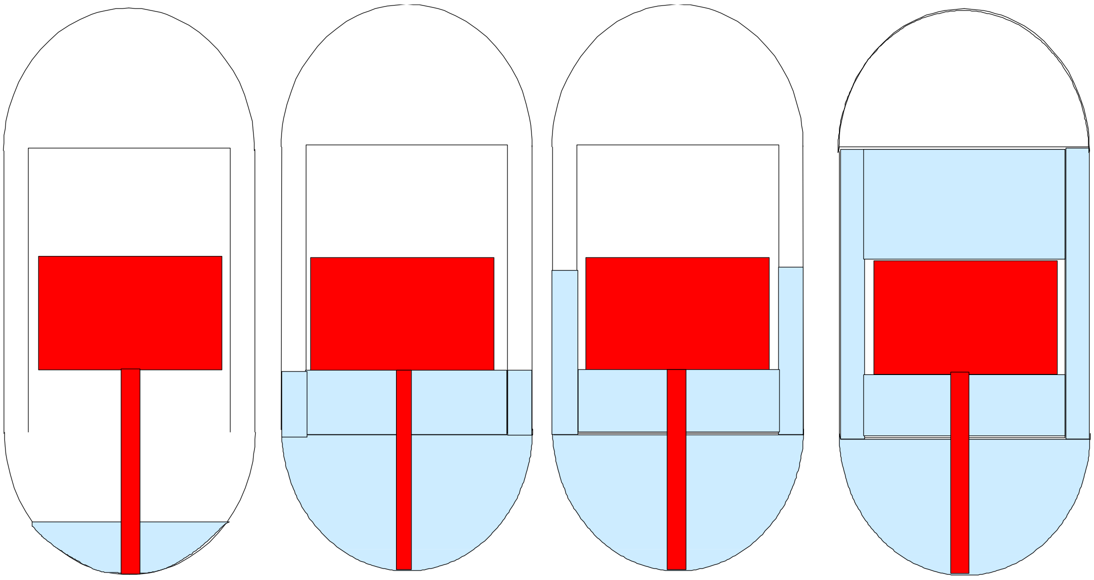

a) 1 m water (2DASCO1M) b) Lower plenum and core inlet full (2DASCOBASE) c) Half vessel full (2DASCOHALF) d) Vessel Full (2DASCOFULL)

Figure 7.35 - Initial conditions for 2-d calculations in COMETA reactor calculation

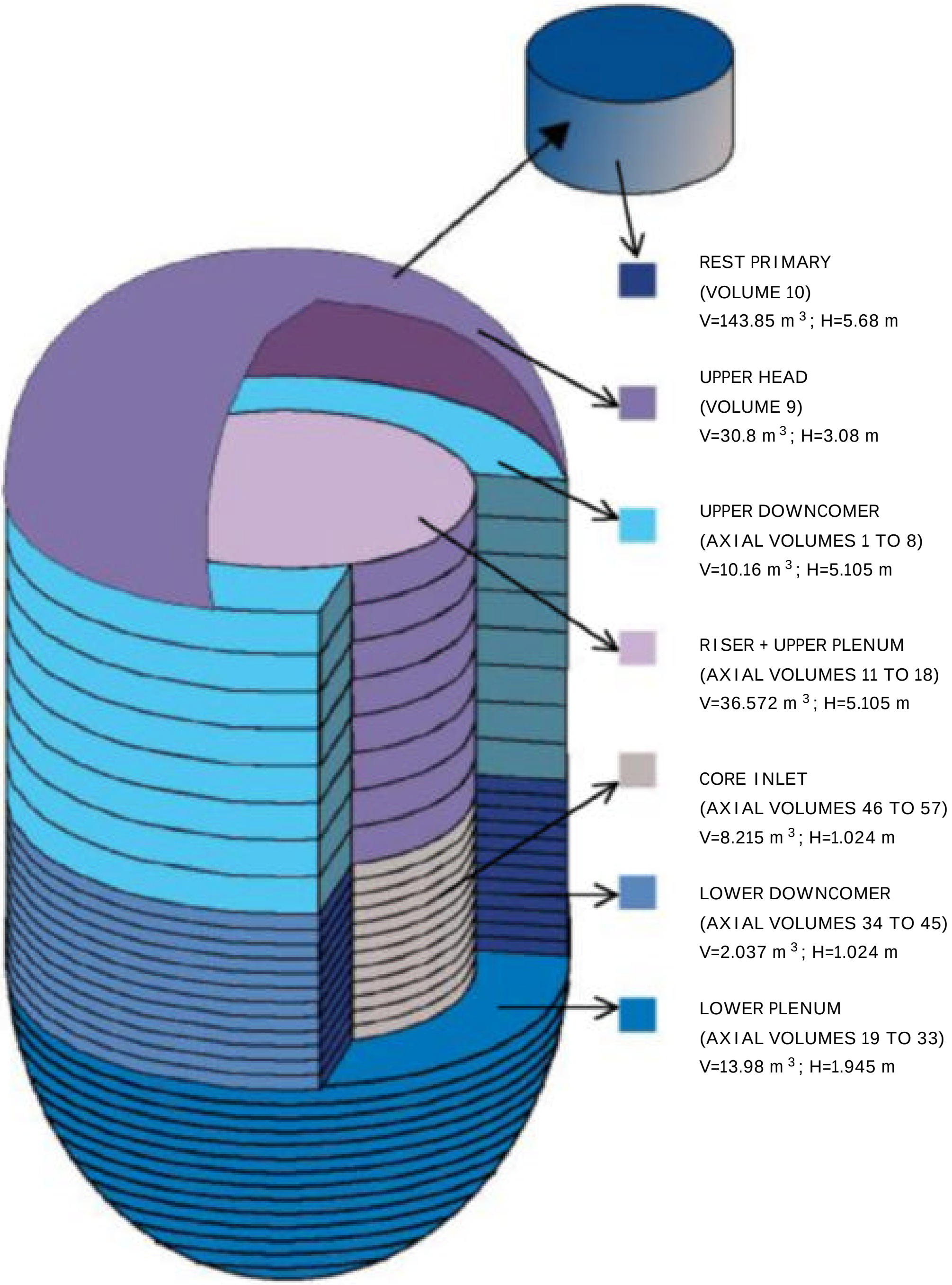

Figure 7.36 - COMETA 1-d nodalization in reactor calculation

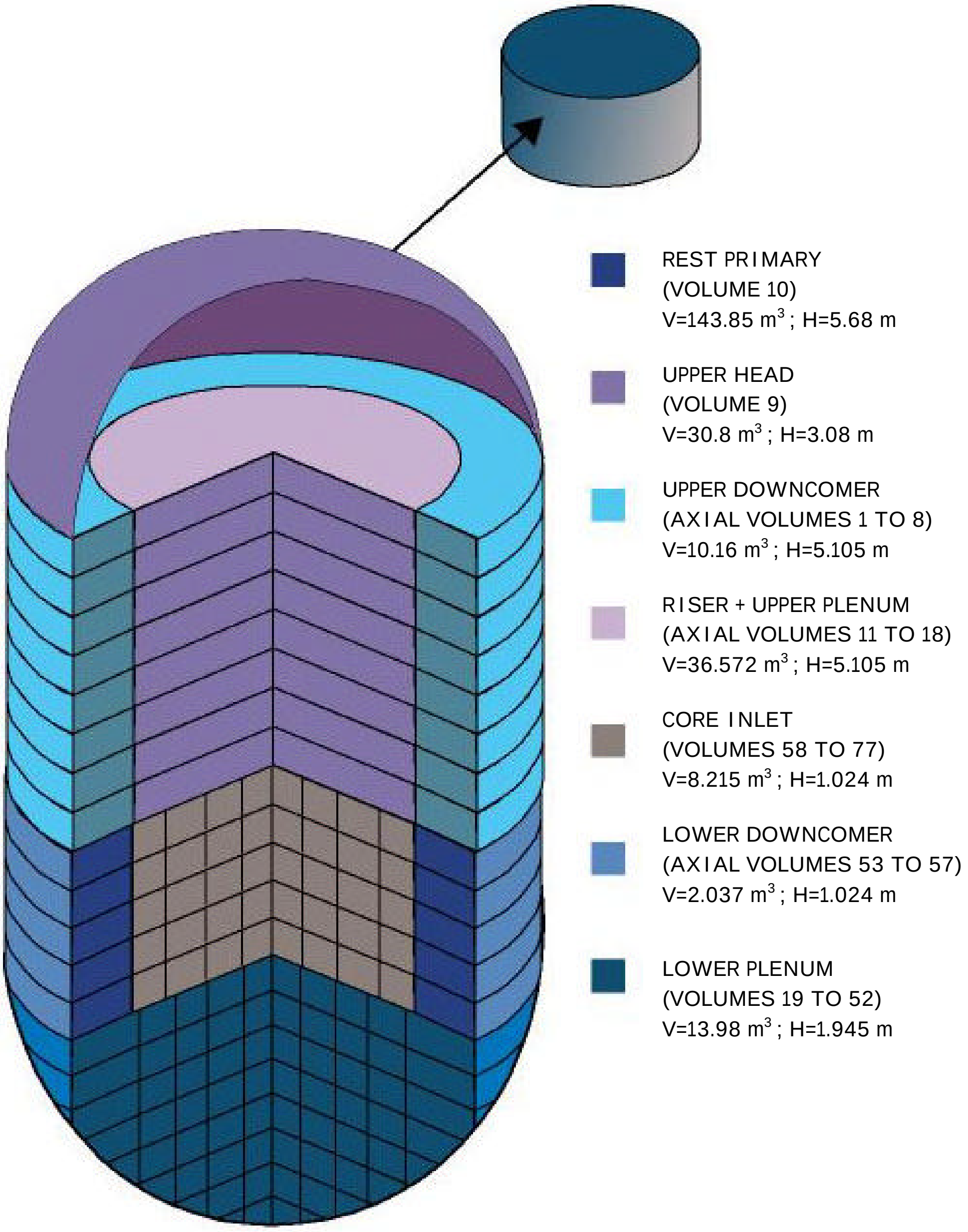

Figure 7.37 - COMETA 2-d nodalization in reactor calculation

7.3.3. CALCULATION RESULTS

All calculations, 1-d and 2-d, were performed until about 130 seconds. The melt mass released (30000 kg), increases up quickly to a constant injection period of about 50 seconds with a mass flow rate of 250 kg/s and after, it reduces to 0 at about 200 seconds.

The case with water filling lower and upper plenum, riser and downcomer (BOUND) was prolonged up to 300 seconds to observe the behaviour in the longer term.

Results of 1-d cases at different water levels (from 2.969 m down to 0.26 m)

The next table indicates distribution mass at 40 seconds of transient:

Case	Initial Water level (m)	Fragmented mass (kg)	Molten Cake mass (kg)	Molten Cake mass/Total mass (%)
ACQPL2	2.969	6203	3627	37
ACQ2M37	2.37	6161	3712	38
ACQ2M	2	6008	3945	40
ACQ129M	1.29	5729	4182	42
ACQ1M	1.0	5245	4712	47
ACQ05M	0.5	67	9805	99.3
VAPOR	0.26	50	10034	99.5

The pressure (Figure 7.38) increases initially in a similar way for 2.969, 2.37, 2, 1.29 and 1 m level cases. In the long term in the first three cases it continues to increase while in the 1.29 and 1 m level cases trends to a stabilisation. The stabilisation is due to the completely voiding of the lower plenum, for case with 1 m level and for case with 1.29 m level, from a certain time no fragmentation and heat exchange occurs.

The pressurisation in the 0.5 m level case (ACQ05M) and in the case with 0.26 m of initial level (VAPOR) is much lower than in the other cases, due to the lower quenching rate, as explained later. In these two cases about 70 and 60 bar are reached respectively at 130 seconds.

The mass of fragmented melt (drops) grows initially in a similar way for cases with 2.969, 2.37, 2, 1.29 and 1 m initial water level. In the 0.5 m and 0.26 m water level cases it is very low, less than 100 kg. In 1.29 and 1 m level the fragmentation mass is stabilised after about 100 and 80 seconds, respectively.

The production rate of drops (kg/s) can be observed in Figure 7.39 for the lower plenum. In the core inlet, in the first seconds, it becomes null in all cases. In the 1.29 m and, 1 m level cases, the production rate in the lower plenum increases rapidly due to the earlier arrive of the jet to the water. In those cases the production rate becomes null and consequently fragmentation mass is stabilized.

In cases with initial water level above the lower plenum height (2.969 m, 2.37 m and 2m) manometric flow oscillations occur between core inlet and lower downcomer.

From Figure 7.40 can be verified these phenomena observing velocity oscillations (gas and liquid) in junctions 19 (from lower plenum towards core inlet) and 20 (from lower plenum towards lower downcomer) for 2 m initial water level cases.

The heat exchange (Figure 7.41), which is related to hot drops production, is almost equal for all cases with higher initial water level (2.969 m, 2.37 m and 2 m). As the initial water level is reduced (0.5 m and 0.26 m) the quenching rate decreases due to the lower drops production. After 40 seconds it decreases, in all cases, as melt mass injection flow is reduced.

The mixture level, in the lower plenum and core inlet, is calculated up to a maximum of 2.969 m, the injection point. It reaches the core bottom level or injection point (2.969 m) for cases with 2.969, 2.37 and 2 m initial water level in the first seconds of transient and remains at that value or above for a longer period as the initial level is higher. After about 20 seconds (2 m level case), 60 seconds (2.37 m level case), and 150 seconds (2.696 m level case), the mixture level decreases below the injection point. The mixture level in the rest cases reaches levels below the injection point and also below the lower plenum height (1.945 m).

To resume, Figure 7.42 shows the mixture level at 10 seconds transient versus initial water level. If the initial water level is above 1.9 m, the heat exchange is able to increase the mixture level above the injection point.

The global mean void fraction in lower downcomer, core inlet and lower plenum (Figure 7.43) increases quickly up to an equilibrium value near 0.4 for the cases with higher initial water level (2.969 m, 2.37 m and 2 m). As the mixture level decreases in all these cases, the void fraction starts to increase (at about 150 seconds, 60 seconds and 20 seconds, depending on the case).

The 1.29 and 1 m level cases start from a higher mean value and reach stability at the maximum value of void fraction, 1.0. For the 0.5 m and 0.26 m water level cases, initial value is almost 1.0 and after small increase, they reach equilibrium.

The un-fragmented mass production ratio (cake), calculated as un-fragmented mass/injection melt mass flow, is high for the cases with lower initial water level (0.5 m and 0.26 m), where lower drops are produced, it fast increases, reaching almost 100% of the discharged melt mass in these cases. The cases with higher initial level increase up to about 40% (Figure 7.44).

The void fraction of the upper volumes indicate that when the mixture level exceeds the lower downcomer, the core inlet or the lower plenum volumes the water is delivered to the upper downcomer or riser or upper volumes of lower downcomer, core inlet or lower plenum.

As conclusion: All these cases show decreasing fragmentation and energy production as the initial water level in the core inlet and lower plenum is reduced. With an initial water level below a value between 1 m and 0.5 m, the fragmentation and the quenching rate progressively decrease and the cake mass accumulation increases (Figure 7.45).

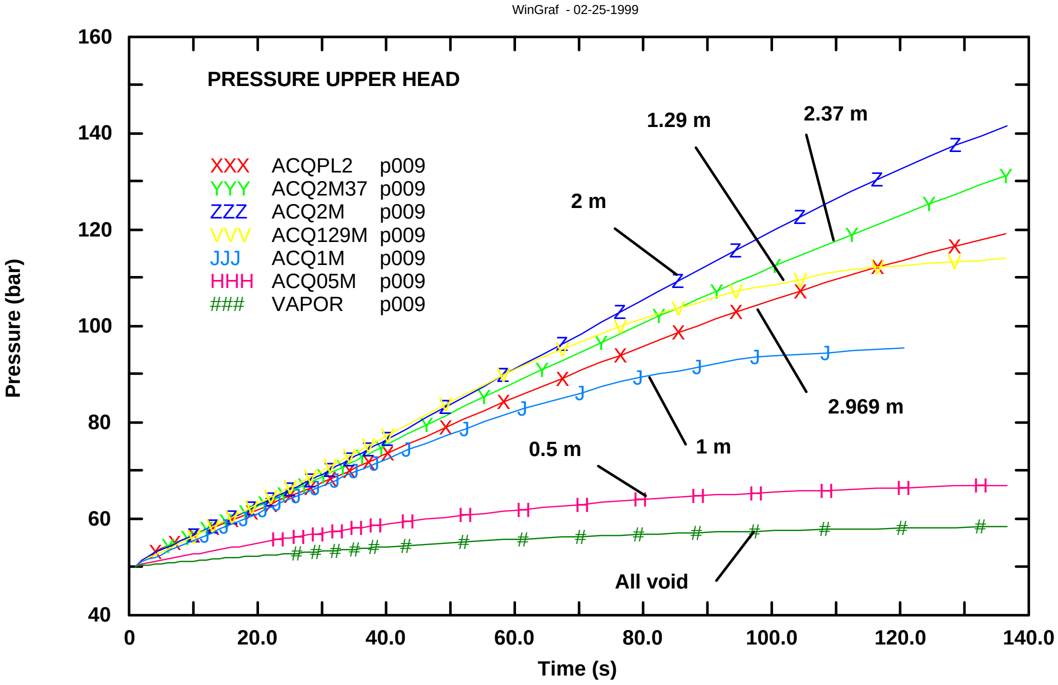

Figure 7.38 - Pressure in the upper head at different initial water levels

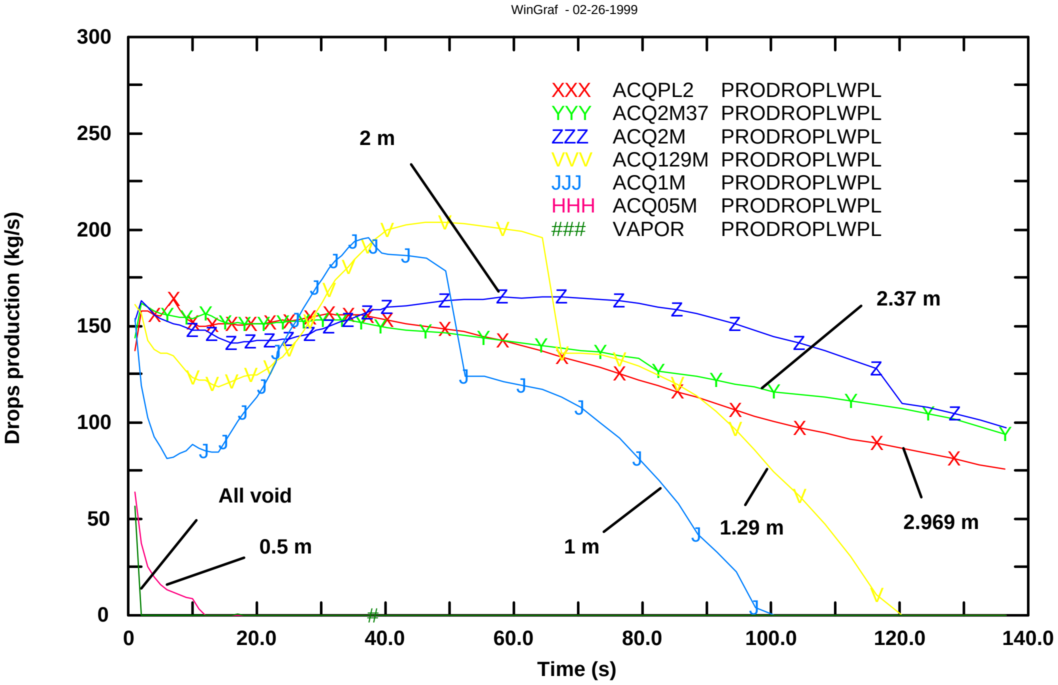

Figure 7.39 - Drops production rate in lower plenum at different initial water levels

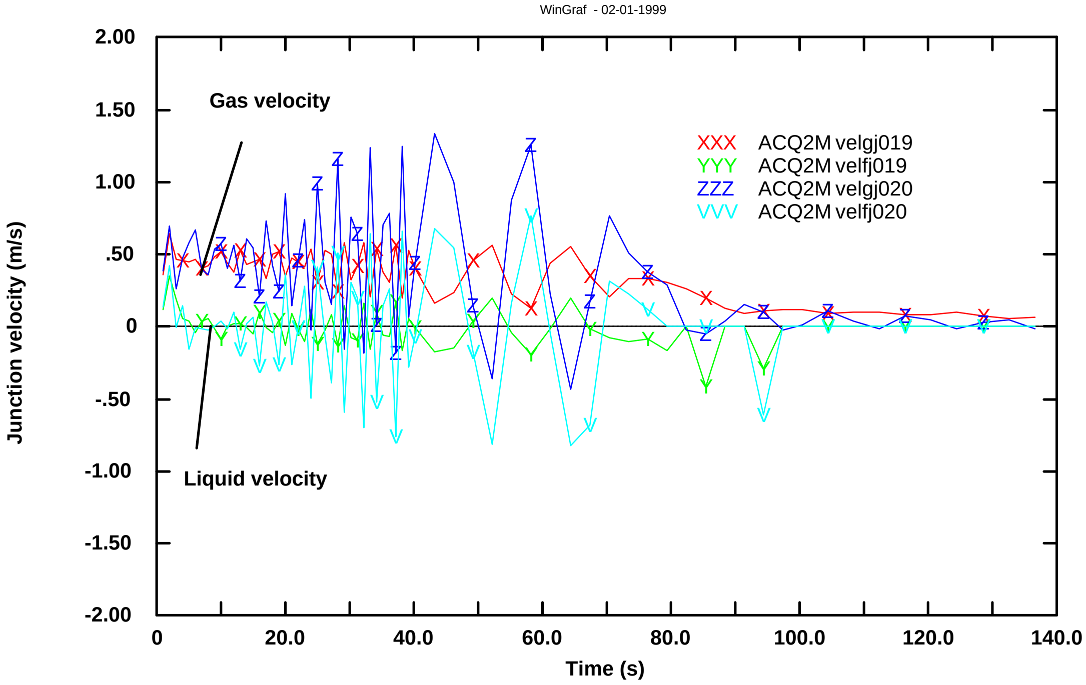

Figure 7.40 - Velocity in junctions 19 and 20 in 2 m initial water level case

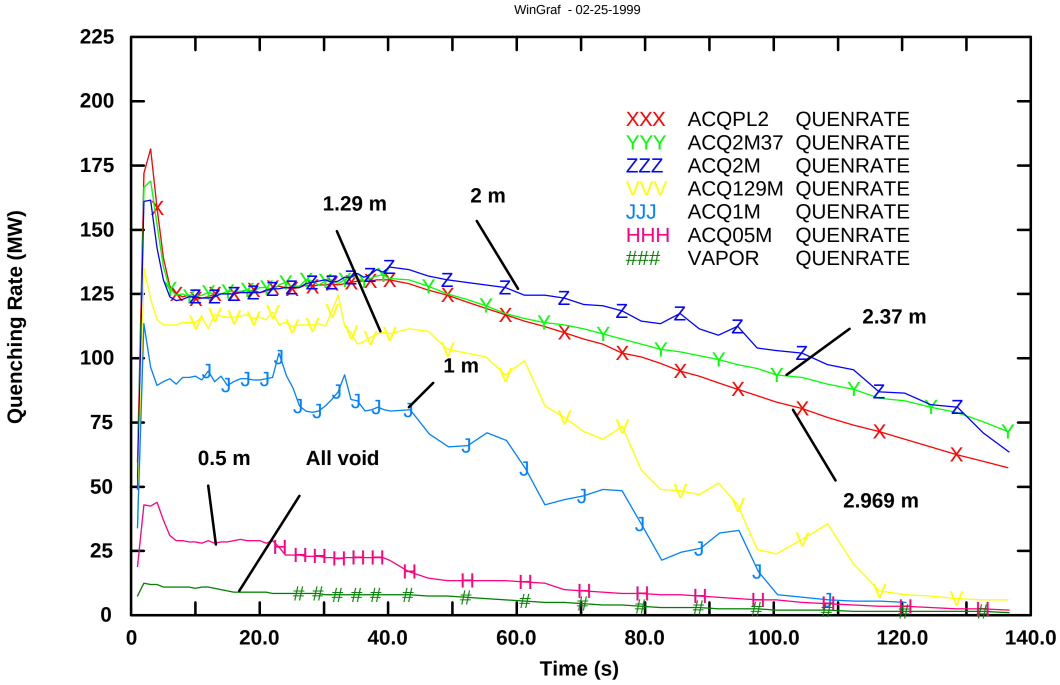

Figure 7.41 - Quenching rate at different initial water levels

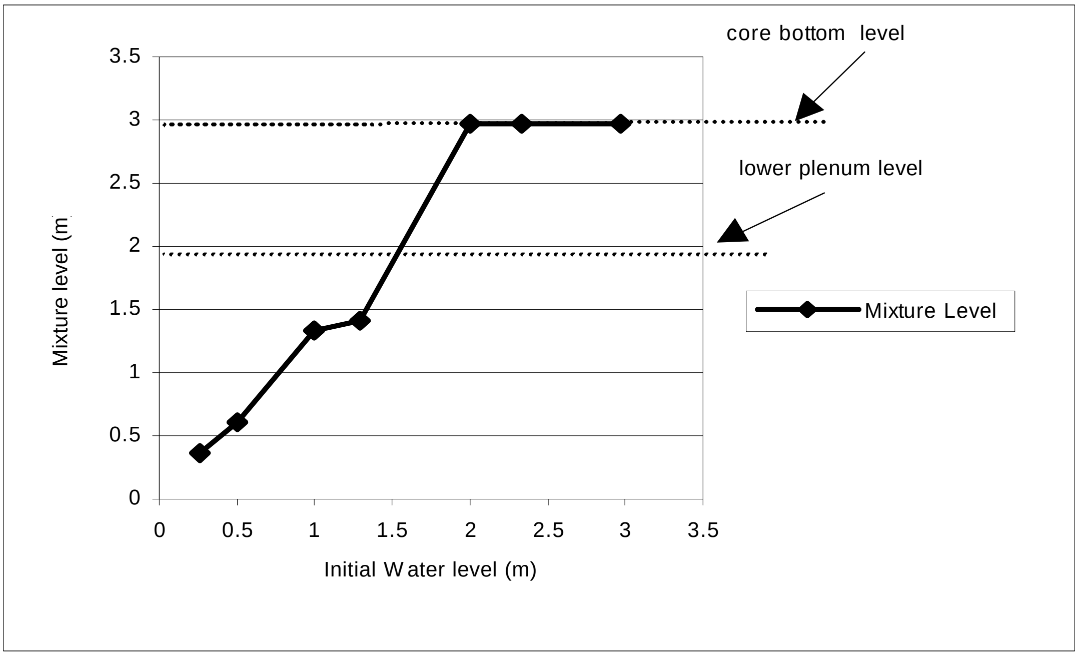

Figure 7.42 - Mixture level vs. initial water level

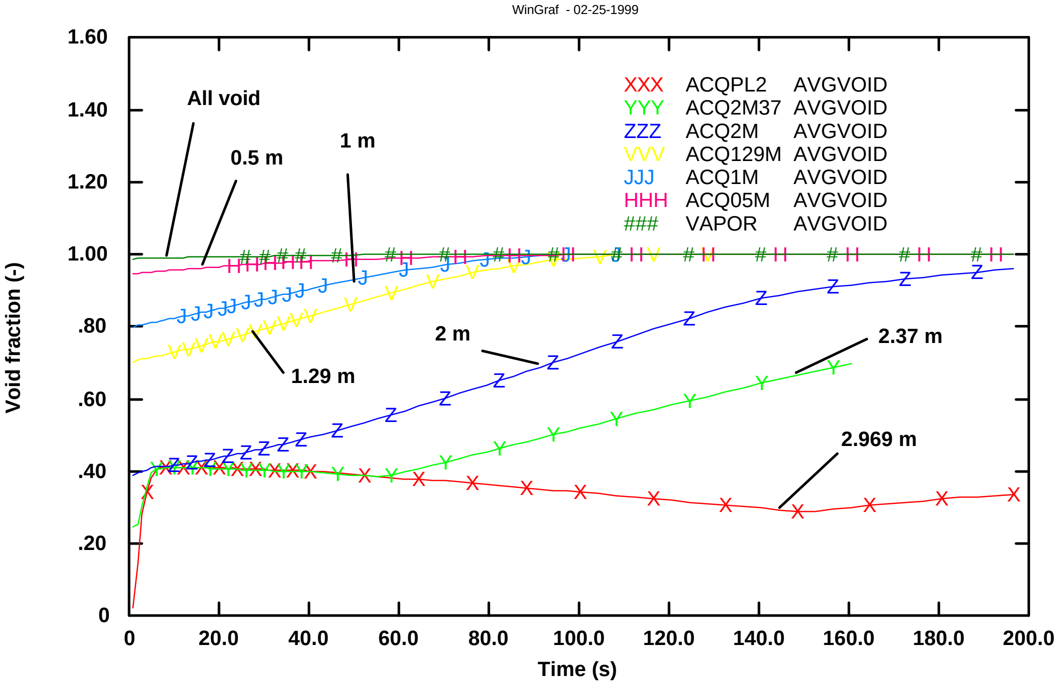

Figure 7.43 - Global mean void fraction in lower downcomer, core inlet and lower plenum at different initial water levels.

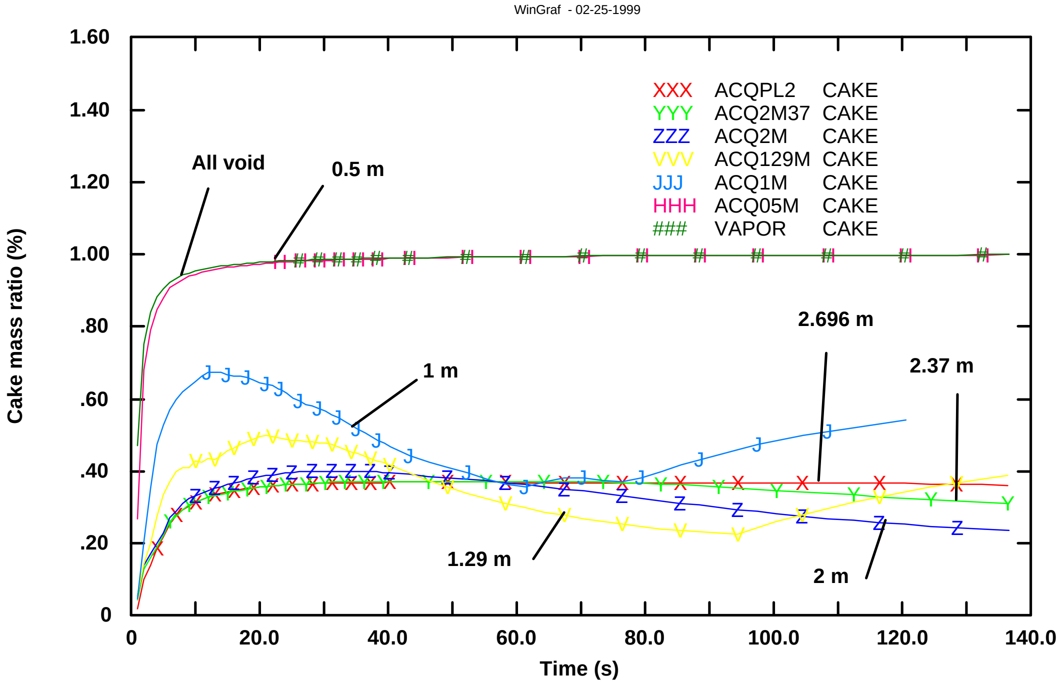

Figure 7.44 - Cake mass ratio at different initial water levels

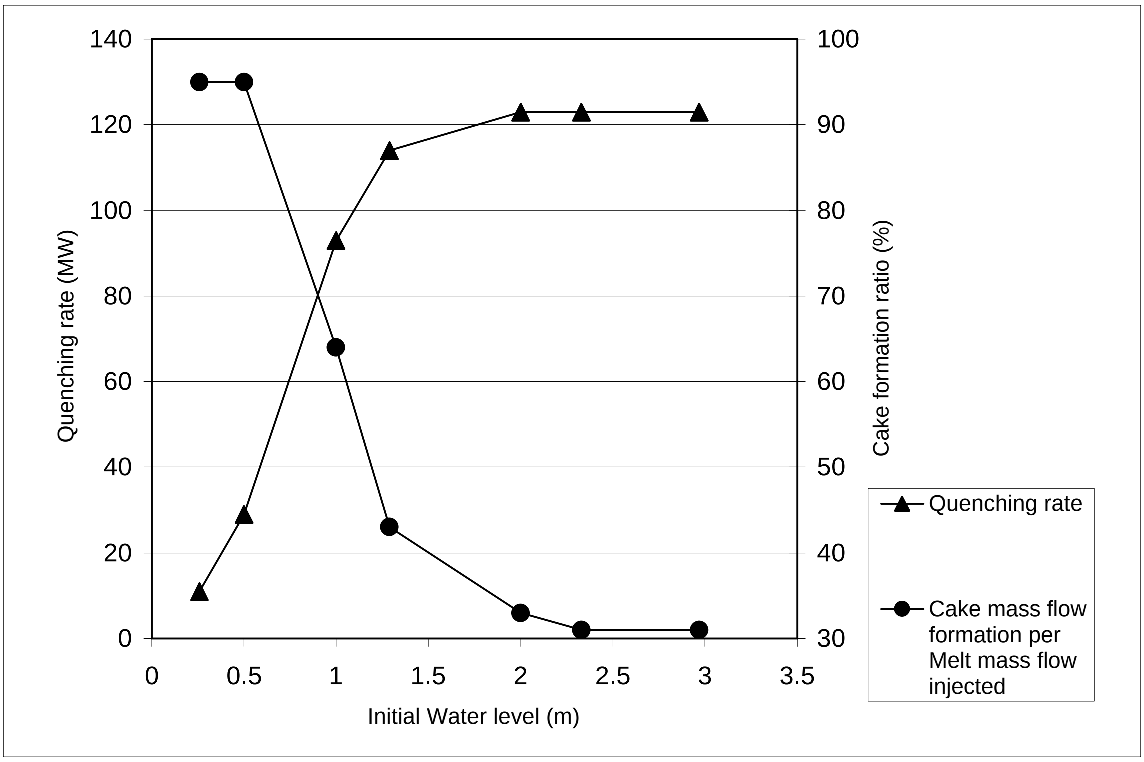

Figure 7.45 - Quenching rate and cake mass flow per melt mass flow versus initial water level

Boundary case: downcomer, riser, upper plenum, core inlet and lower plenum full of water

For the boundary case (riser, upper plenum and upper downcomer full of water) the calculation has been continued up to 300 seconds to analyse the behaviour in the longer term, with particular interest on quenching and mean void fraction behaviour.

Pressure (Figure 7.46) increases slower than in the other cases. The reason for the lower pressurisation is not due to the smaller quenching rate achieved, but is due to the greater void condensation in the upper volumes. Pressure tends to a stabilisation. As the injected mass flow rate decreases fragmentation stabilises, producing constant quantity of drops.

Fragmentation in boundary case is similar to cases with higher initial water level.

The quenching rate achieved (Figure 7.47) is initially similar to cases with higher initial water level, after about 5 seconds it can be observed an increasing of quenching due to drops accumulation in the core inlet (Figure 7.48). Heat exchange does not disappear; it reaches a minimum steady value close to 12 MW at about 200 seconds.

Figure 7.49 shows that natural circulation is established in this case; water is moving from lower downcomer to core inlet through junctions number 20 (from lower downcomer to lower plenum) and junction number 19 (from lower plenum to core inlet). Liquid mass flow in those junctions cause drops accumulation in volumes of core inlet, as it was observed in Figure 7.48. Natural circulation continues up to about 210 seconds. After that time void fraction in lower downcomer and core inlet are balanced and no more natural circulation is produced.

The global mean void fraction (Figure 7.50) shows for the boundary the same initial steady value of 0.4 than cases with higher initial water level. In this case, the initial level (8.074 m) is much higher than the injection point (2.969 m) and the mixture level, due to boiling, never goes below that point. Therefore, global mean void fraction continues to decrease. A minimum steady value close to 0.07 is obtained at about 200 seconds.

The cake mass production is similar to cases with higher initial water level, increasing up to about 40% of discharged mass.

Water is transferred mainly to upper head (volume 9) and some to the rest primary system (volume 10). The void fraction in the upper head (volume 9) and in the rest of primary system (volume 10) is shown in Figure 7.51 for the boundary case in the longer term. The water, which had been transferred in the upper head (volume 9), turns back into the riser, core inlet and lower plenum as the quenching rate and steam evaporation decrease.

To summarise: In the boundary case pressure increase is lower due to condensation, quenching rate is higher and drops mass, void fraction and cake mass accumulation are similar to cases with higher initial water level. The difference in this case is the onset of natural circulation in the vessel that causes a redistribution of the drops mass in the system.

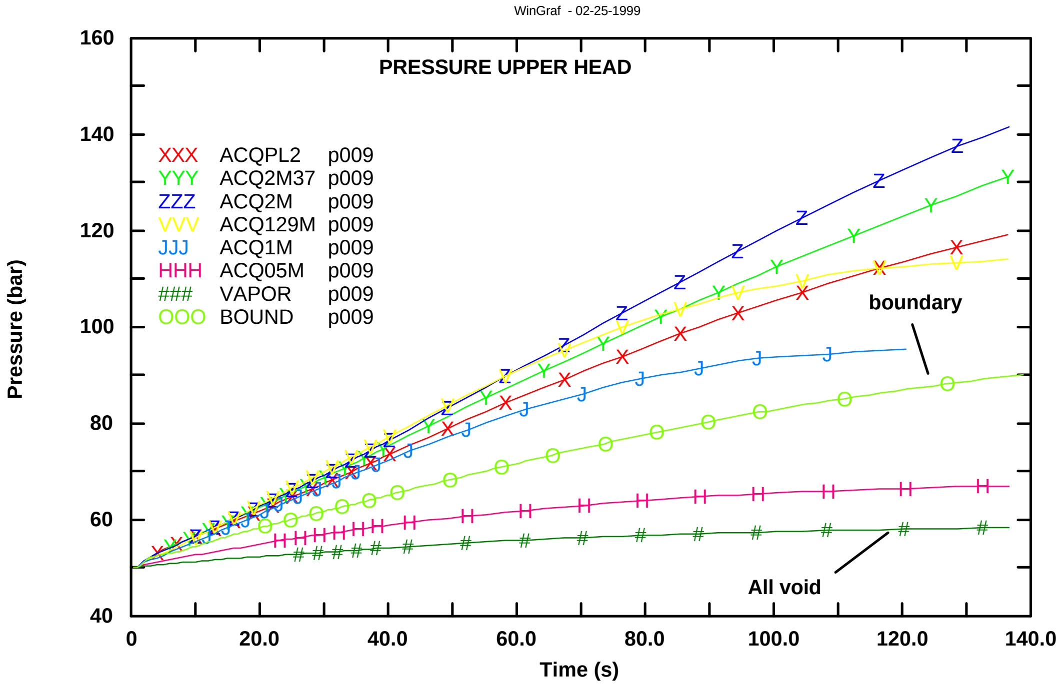

Figure 7.46 - Pressure in the upper head in boundary case

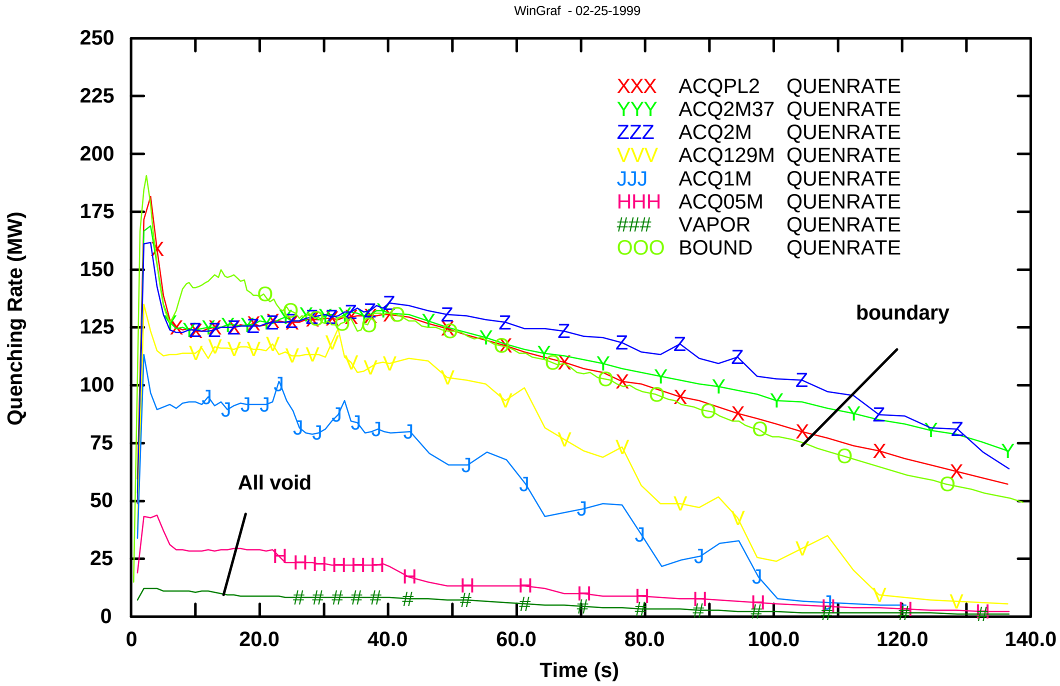

Figure 7.47 - Quenching rate in boundary case.

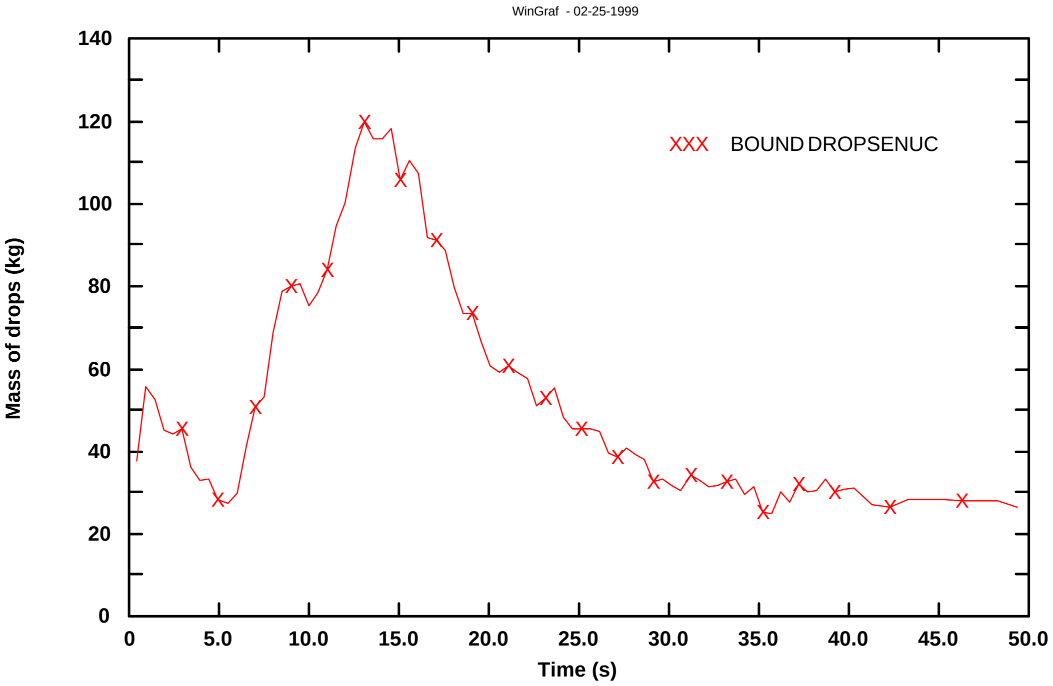

Figure 7.48 - Drops mass in core inlet in boundary case

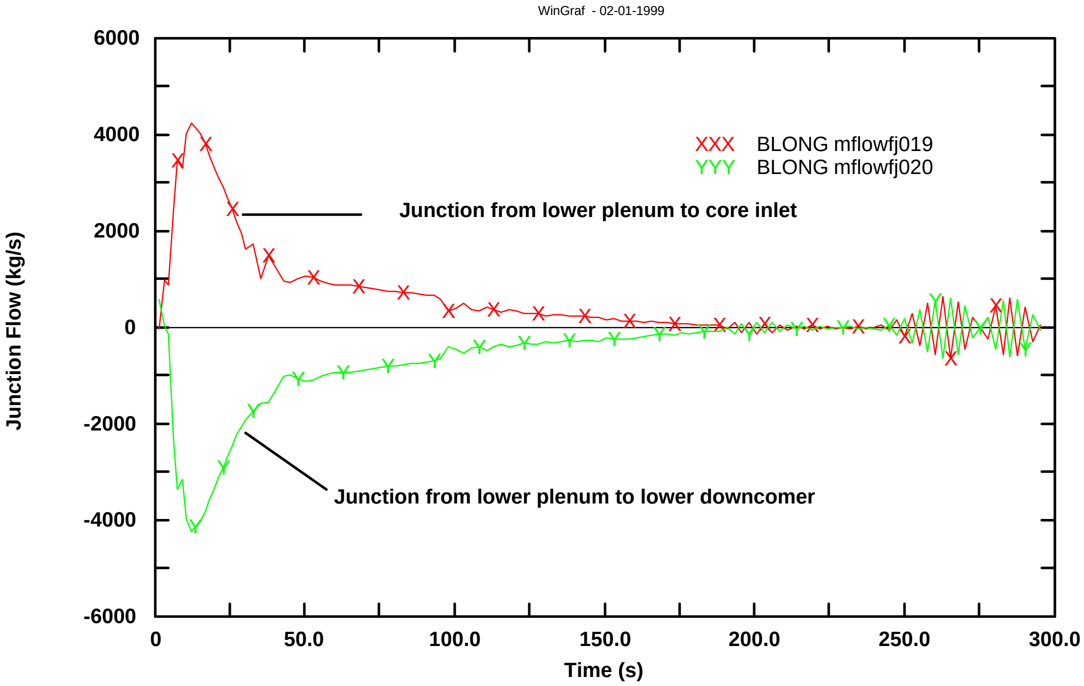

Figure 7.49 - Liquid mass flow in junctions 19 and 20 in boundary case in the longer term

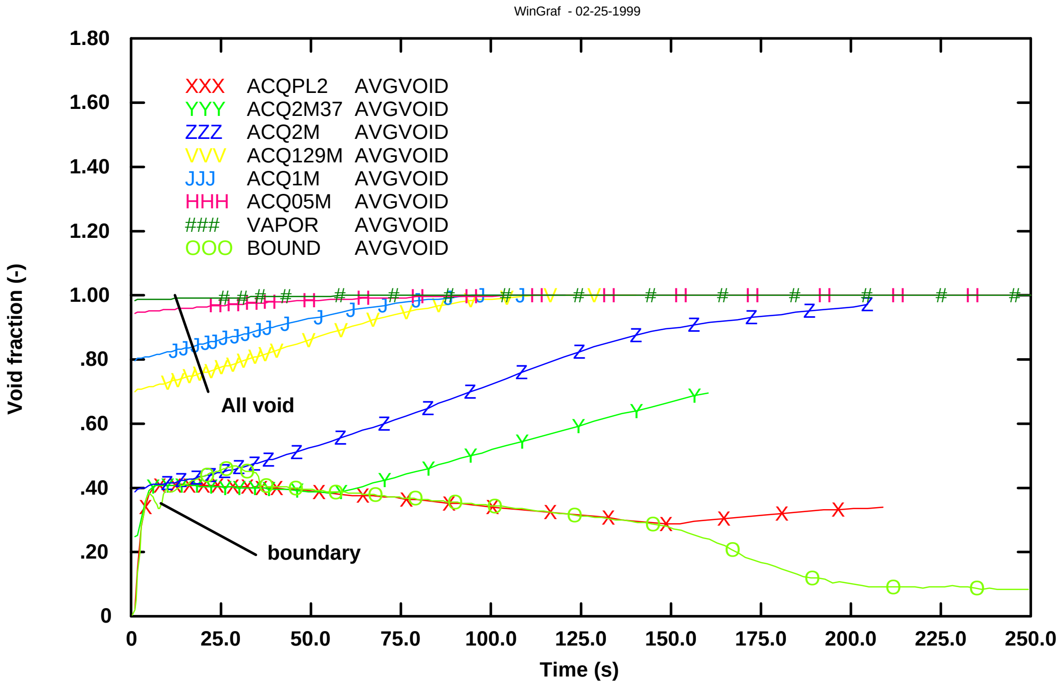

Figure 7.50 - Global mean void fraction in lower downcomer, core inlet and lower plenum in boundary case

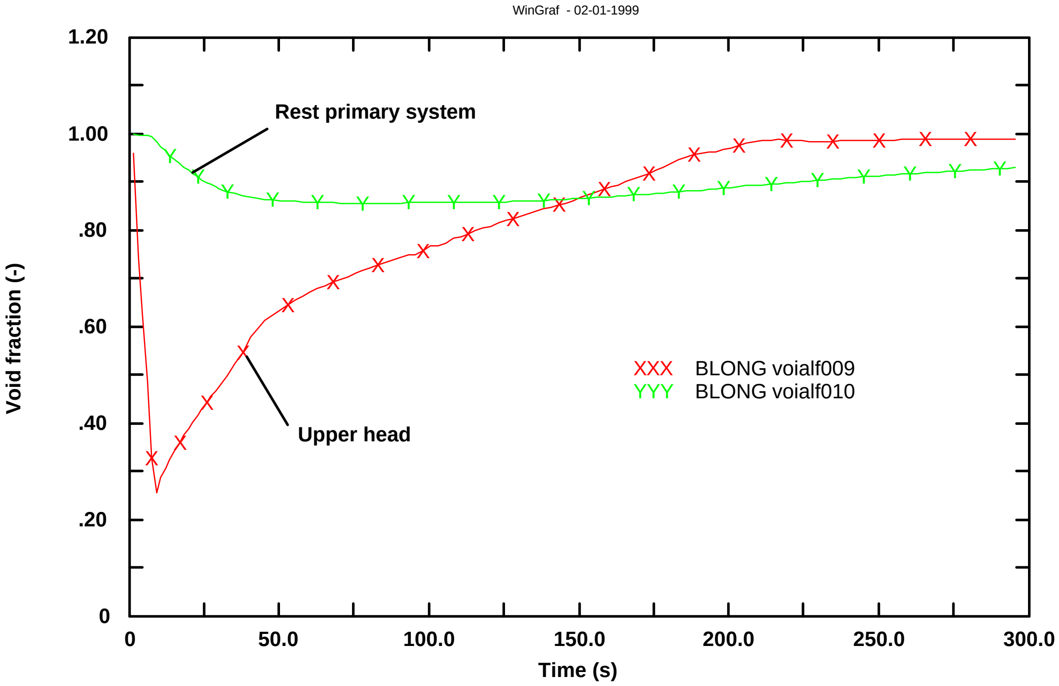

Figure 7.51 - Void fraction in the upper head (9) and rest primary system (10) in boundary case in the longer term

Results of 2-d cases at different water levels (from 8.1 m down to 1m)

Pressurisation due to power exchange in 2-d cases (Figure 7.52) is higher in 2.969 m case (Base case), reaching about 150 bar at 140 seconds. In “full case” and “half full case” the greater void condensation in the upper volumes leads to a slower pressurisation as it occurred in 1-d boundary case. The pressure in the lower level case (1 m case) after an initial increase trends to a stabilisation, at about 60 seconds, due to voiding of lower plenum as it occurred in 1-d case.

The heat exchanged (Figure 7.53) increases quickly up to a similar value for “full”, “half full” and “base” case, reaching about 160 MW. In the 1 m case the lower plenum is rapidly voided and fragmentation produced is lower, corresponding to a lower quenching rate achieved.

In the cases “full”, “half full” and “base”, cases with the mixture level during the melt discharge up to or above the injection point, the reduction of quenching rate occurs after about 50 seconds, when the melt mass flow injected is also reduced. In the 1 m case this reduction of power exchange starts before, due to the lower mixture level reached, below the injection point, and subsequent more void produced.

The fragmented mass (total drops mass, Figure 7.54) increases in a similar way for cases “full”, “half full” and “base”. In 1 m case, fragmented mass increases up to 6000 kg and at about 60 seconds it stabilises due to voiding of the lower plenum.

For 2-d cases the mean void fraction in lower plenum, core inlet and lower downcomer is presented as global void fraction, which is the result of the heat transferred to all lower plenum, core inlet and lower downcomer. It has been also calculated a local mean void fraction for volumes 19 to 26 (central lower plenum) and volumes 58 to 62 (central core inlet) as central void fraction, which is responsible for the fragmentation produced (fragmentation is assumed only in central part of lower plenum and central part of core inlet).

In Figure 7.55 and Figure 7.56 mean void fraction (global and central) for 2-d cases is shown. Central void fraction increases rapidly until a steady value of 0.5 due to the heat transferred by drops fragmented in the central volumes. The void fraction does not increase above this value and equilibrium is reached in which the void fraction, the power exchanged and the pressurisation rate are almost constant. In the 1m case the initial void fraction starts from a higher value and continues to increase, the mixture level is reduced and the lower plenum is voided. In the base case after about 100 seconds void fraction starts to increase because the mixture level becomes lower than the injection point. In “full” and “half full” cases the mixture level never becomes lower than the injection point and void fraction does not increase.

Production rate of drops (kg/s) is observed in Figure 7.57 for the lower plenum and for the core inlet. In the core inlet, in the first seconds, it becomes null in all cases. In “full”, “half full” and “base” cases production rate is similar in the lower plenum and in 1m case it is lower, becoming zero at about 60 seconds, and stabilising fragmented mass (Figure 7.54).

The un-fragmented mass produced (cake ratio, Figure 7.58) is similar for “full”, “half full” and “base” cases, reaching about 50% of discharged mass in the first seconds. 1 m case reaches a higher cake mass production, about 70%.

To summarise it can be said that “full”, “half full” and “base” cases showed similar energy exchange, drops production and cake mass accumulation. In these three cases, the mixture level is up or above the injection point (for base case up to about 100 seconds), allowing equilibrium in void fraction, heat exchange and pressurisation rate. In 1 m case the mixture level is continuously reduced and lower plenum is voided, it shows lower heat exchange and fragmentation than other cases and higher cake mass accumulation.

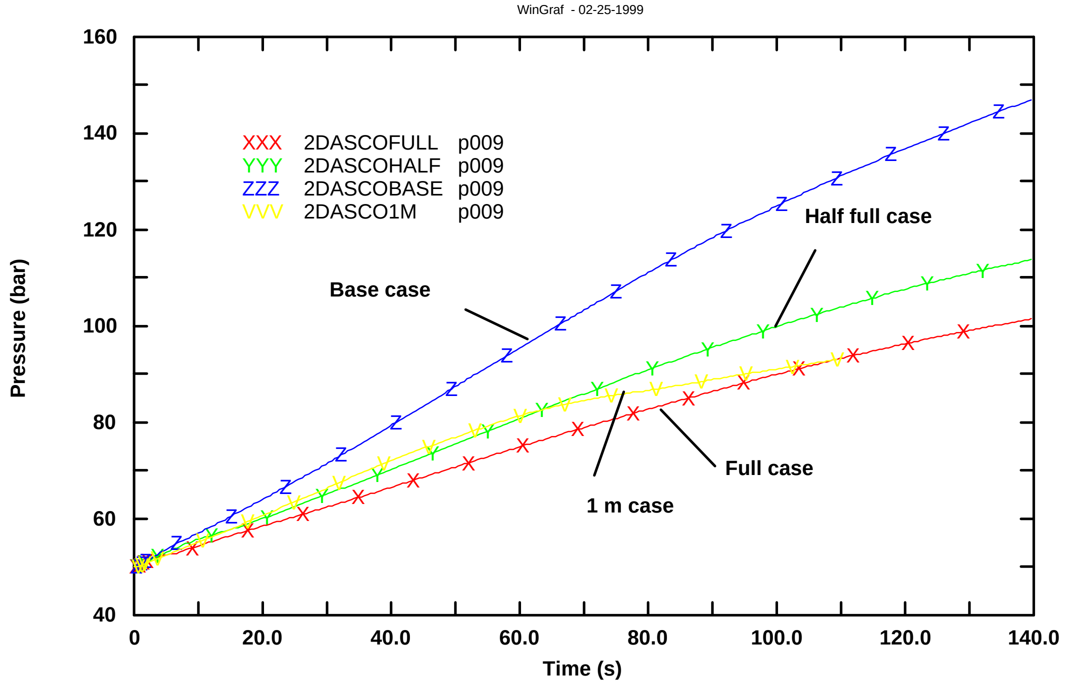

Figure 7.52 - Pressure in the upper head in “full”, “half full”, “base” and 1 m cases with 2-d nodalization

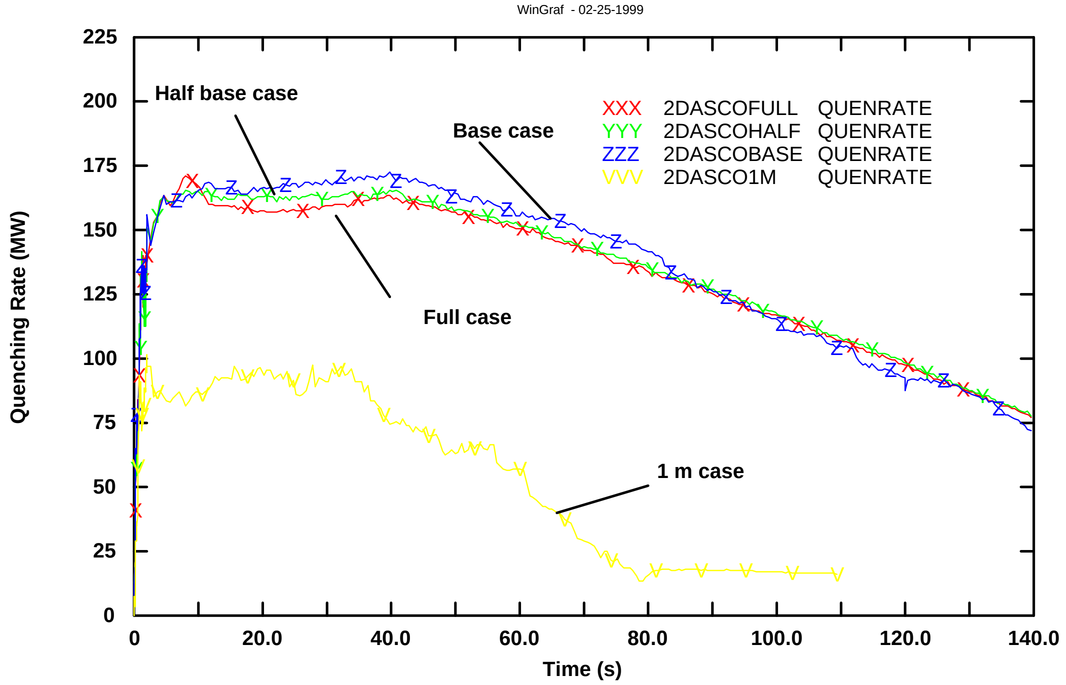

Figure 7.53 - Quenching rate in “full”, “half full”, “base” and 1 m cases with 2-d nodalization

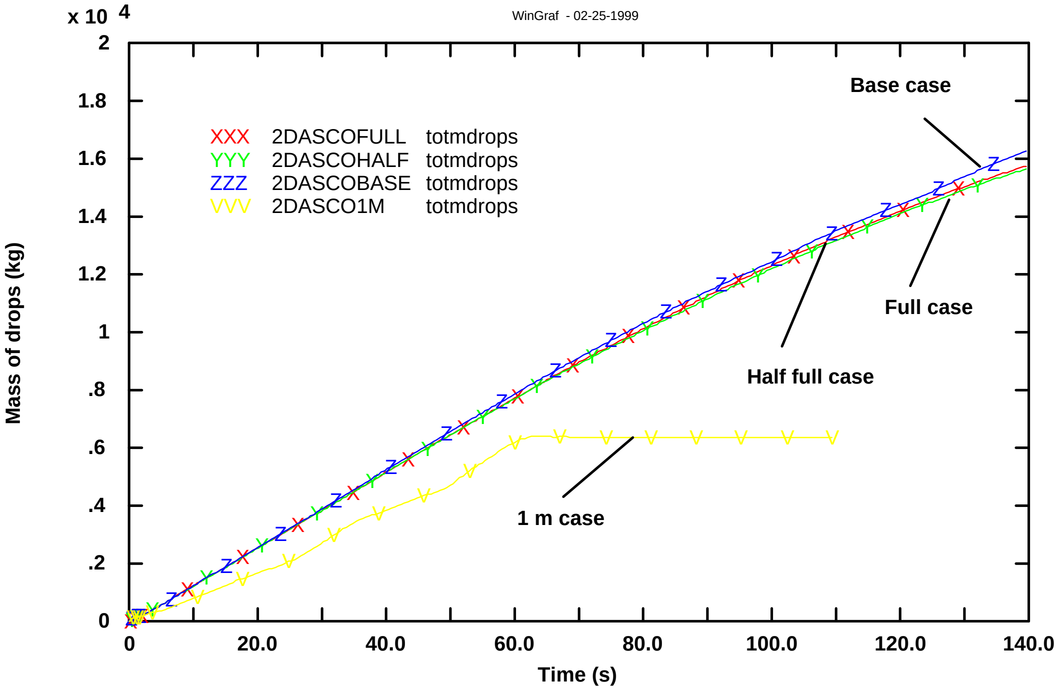

Figure 7.54 - Total drops mass in “full”, “half full”, “base” and 1 m cases with 2-d nodalization

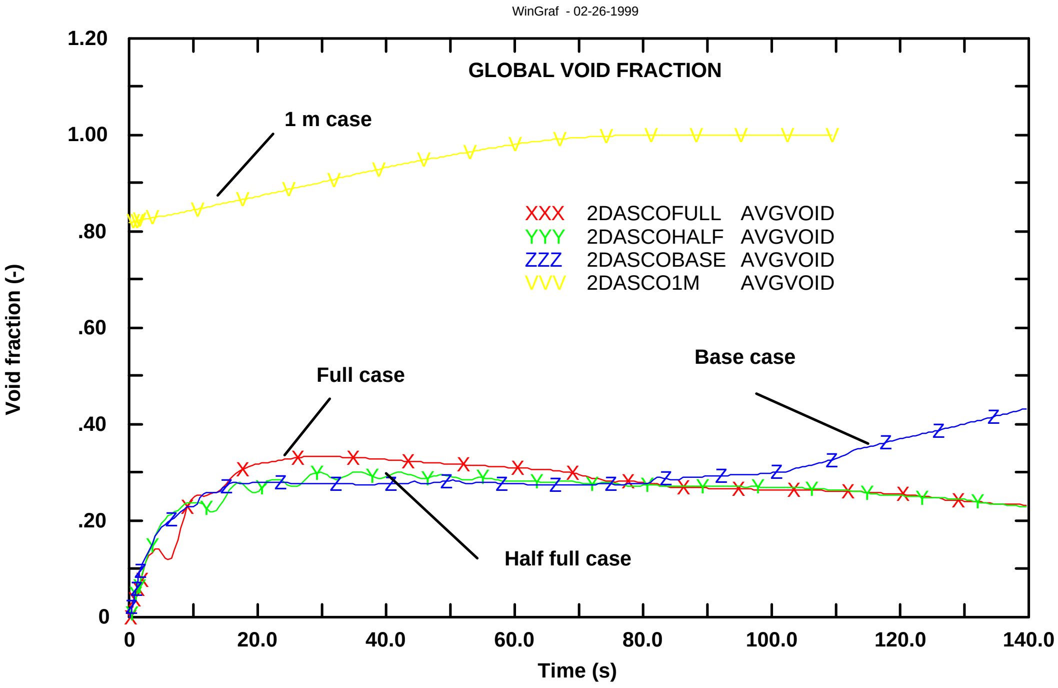

Figure 7.55 - Global mean void fraction in “full”, “half full”, “base” and 1 m cases with 2-d nodalization

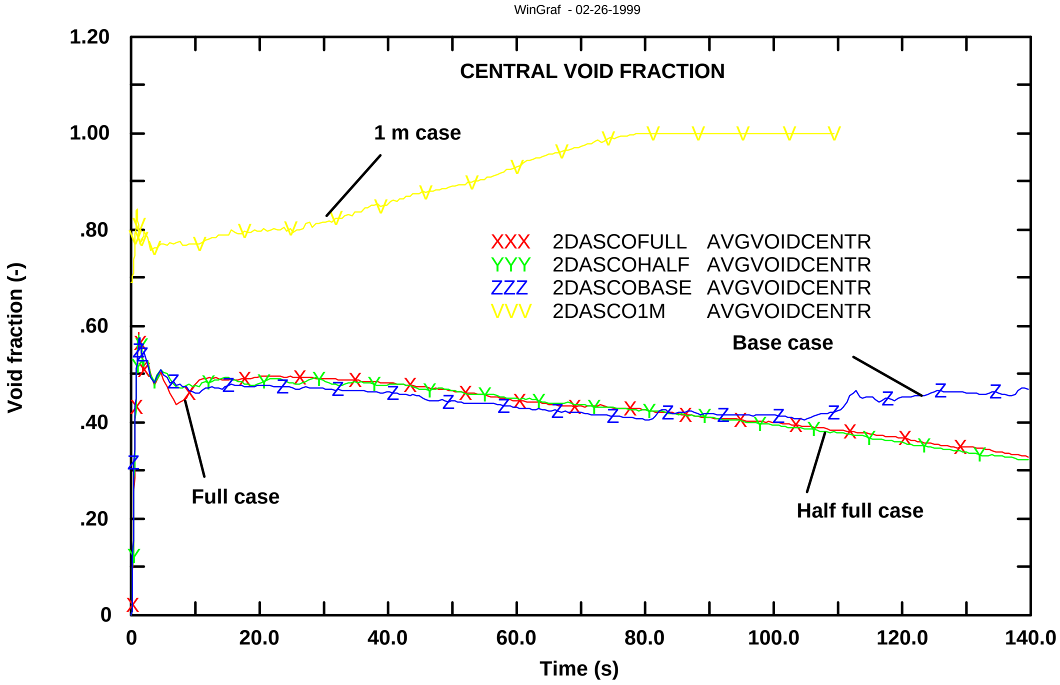

Figure 7.56 - Mean void fraction in the central side of lower plenum and core inlet in “full”, “half full”, “base” and 1 m cases with 2-d nodalization

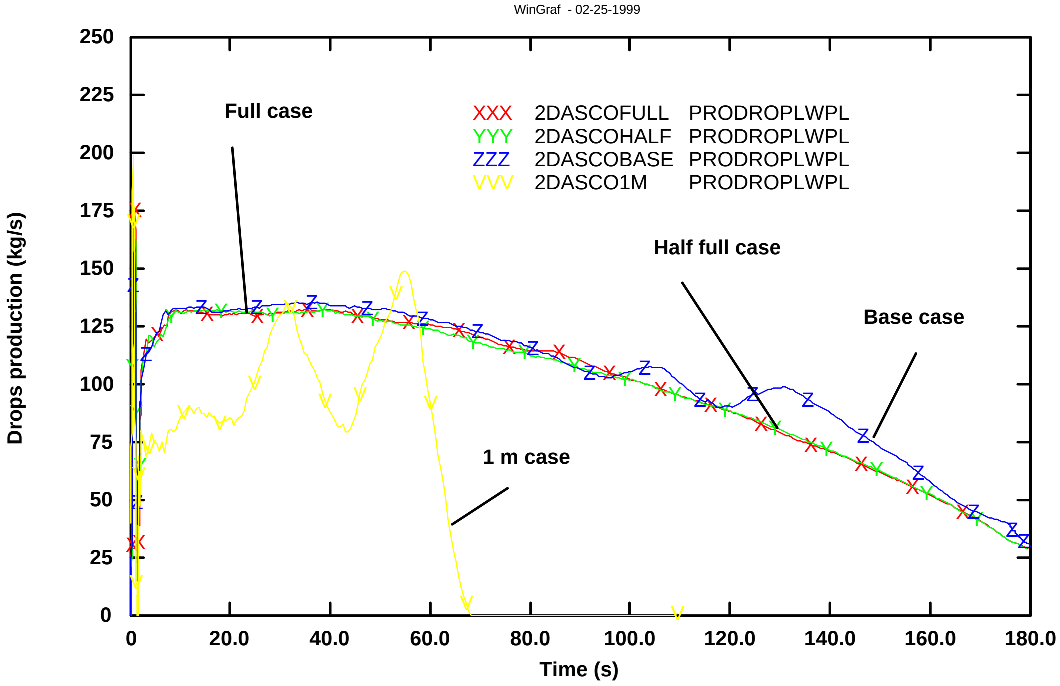

Figure 7.57 - Drops production rate in lower plenum in “full”, “half full”, “base” and 1 m cases with 2-d nodalization

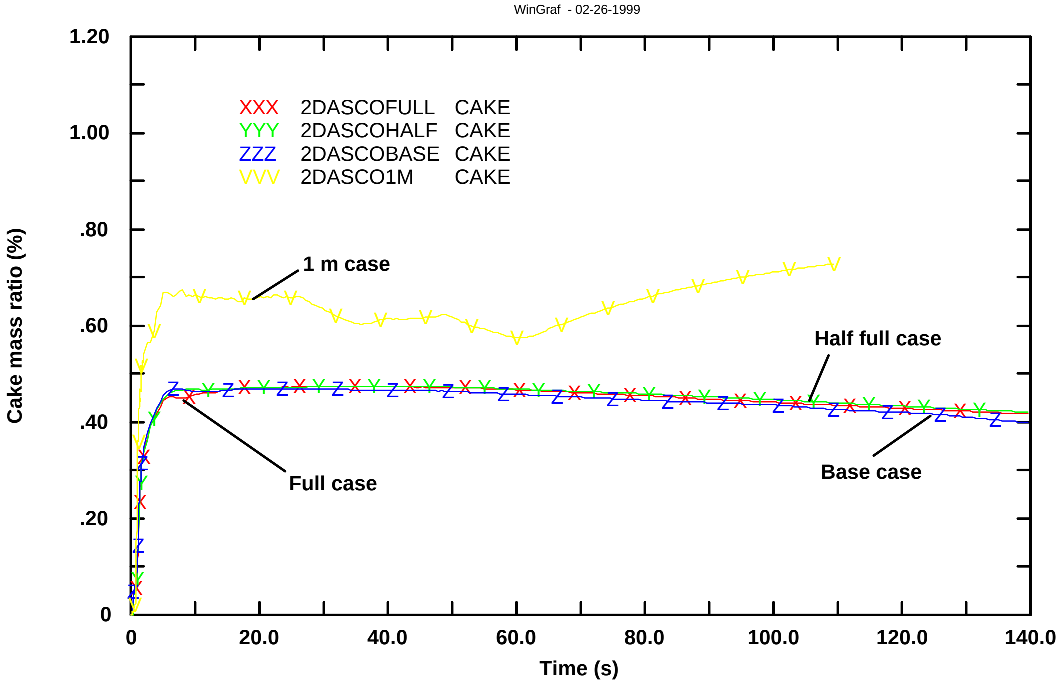

Figure 7.58 - Cake mass ratio in “full”, “half full”, “base” and 1 m cases with 2-d nodalization

The thermal-hydraulic equilibrium plot

In this chapter the relation between the void fraction and the quenching rate is analysed to show why the various cases trend to an equilibrium value, arriving to it in two different ways depending on the initial conditions.

Let’s consider a system in which the power is imposed and the resulting mixture level is arbitrary. The power is imposed only below the mixture level, Figure 7.59. At a certain power corresponds a certain void fraction in the mixture. As the power applied increases, the void fraction increases. It is therefore possible to draw a line relating the various power states and the related void fraction. However, if the same power is applied and the mixture level is reduced, the global void fraction is higher for two reasons; firstly, because locally the heat transfer coefficient is higher and secondly, because if the mixture level is lower the specific power will be higher. Therefore; another line can be drawn corresponding to a different mixture level. Therefore a family of curves exist corresponding to the various mixture levels. The upper bound curve is the one corresponding to the maximum mixture level, i.e. up to the injection point.

Let us suppose now a different situation, in which melt is injected into a constant density medium. Imposing an arbitrary void fraction to a steam-water system, the melt injected with a certain mass flow rate, will fragment and create drops that will exchange heat with the medium. Therefore, it is possible to draw a line corresponding to the power exchanged by the melt at a fixed injection mass flow rate and at a fixed void fraction (independent of the power exchanged), Figure 7.60. If the mass flow rate is reduced, the fragmentation is reduced and also the power exchanged; therefore another family of curves corresponding to various injected mass flow rates can be generated.

The two simultaneous processes described in Figure 7.59 and Figure 7.60 can be merged in the chart of Figure 7.61. At higher mass flow rate and higher mixture level corresponds the equilibrium point A. If the system is so that a reduction of the mass flow rate occurs with a constant mixture level, the system will move from point A to point B', on the left-down of point A. If instead the mixture level is decreasing with a constant injection flow, the point will move from point A to point B", i.e. right-down. Of course, if both the injection flow and the mixture level are reduced, the representative point will move from A to B"'.

The cases analysed so far indicate that equilibrium in terms of injected mass, quenching rate and void fraction is reached after some initial seconds of stabilisation. This process can be well seen in a plot showing the observed quenching rate versus mean void fraction.

Figure 7.62 and Figure 7.63 show the calculated behaviour for the reactor in the plane void fraction-power for cases performed in 1-d and 2-d, respectively.

In Figure 7.63 the curve A represents the power that is determined by the fragmentation process as a function of the void fraction at an injected mass flow rate of 250 kg/s, while curve B represents the equilibrium void fraction at various imposed power levels (distributed uniformly in the central part of a lower plenum) with the maximum mixture level in saturation conditions.

Figure 7.62 represents in the plane void fraction-power all the 1-d cases. The three cases with higher initial water level, boundary case (BOUND), all lower plenum and core inlet full (ACQPL2) and 2.37 m initial water level (ACQ2M37) behave in the following way: they start with void fraction and power null (BOUND and ACQPL2) and void fraction 0.25 and power null (ACQ2M37), as the transient proceeds, the power exchanged and the void fraction increase tending to an equilibrium point in all cases (void fraction ≈ 0.4 and power ≈ 120 MW).

Since the mixture level is constant in the period of constant injection, the three cases will move down-left (like A to B'), because the reduction of the injected mass flow rate occurs. In the boundary case, the mixture level never becomes lower than the injection point and the behaviour continues along the curve B, while in the 2.969 m initial water level (ACQPL2) case after about 150 s the representative point moves down (like A to B'''), because the mixture level became lower than the injection point and void fraction below this point starts to increase. The same occurs for 2.37 m initial level case, but earlier, at about 60 seconds.

In the other cases, those with lower initial water level (2 m, 1.29 m, 1 m 0.5 m and 0.26 m), at the beginning the representative point on the thermal-hydraulic plot is a not null void fraction and power 0. As the transient proceeds, the power exchanged and the void fraction increase tending to an equilibrium point but on different B-type curves. All the representative points move down-right (like A to B''), because, due to boiling the mixture level continues to decrease and void fraction increases.

Figure 7.63 represents in the plane void fraction-power all the 2-d cases. In the “full” case, “half full” case and “base” case, at the beginning the representative point on the thermal-hydraulic plot is void fraction and power null; as the transient proceeds, the power exchanged and the void fraction increase tending to an equilibrium point in all three cases (void fraction ≈ 0.5 and power ≈ 160 MW), then they will move down-left (like A to B'), because the reduction of the injected mass flow rate occurs. The base case, after 100 s, moves down (like A to B'''), because the mixture level became lower than the injection point. The half and full cases will continue along the so called curve B, because the mixture level never becomes lower than the injection point.

In 1 m initial water level case, at the beginning the representative point on the thermal-hydraulic plot is the void fraction 0.7 and power 0. The representative points in this case of low level move down-right (like A to B''), because due to boiling, the mixture level continues to decrease.

To summarise: All the cases with mixture level higher than the orifice injection will behave similarly with an equilibrium point which moves down-left (like A to B'), while the cases with lower mixture level will move down-right (like A to B'') because of reduced inventory in the interaction zone. Depending on the case, in some cases with initially mixture level higher than injection point, this mixture level starts to reduce and void fraction starts to increase after a particularly time depending on the initial water level and then they move down right (like A to B''').

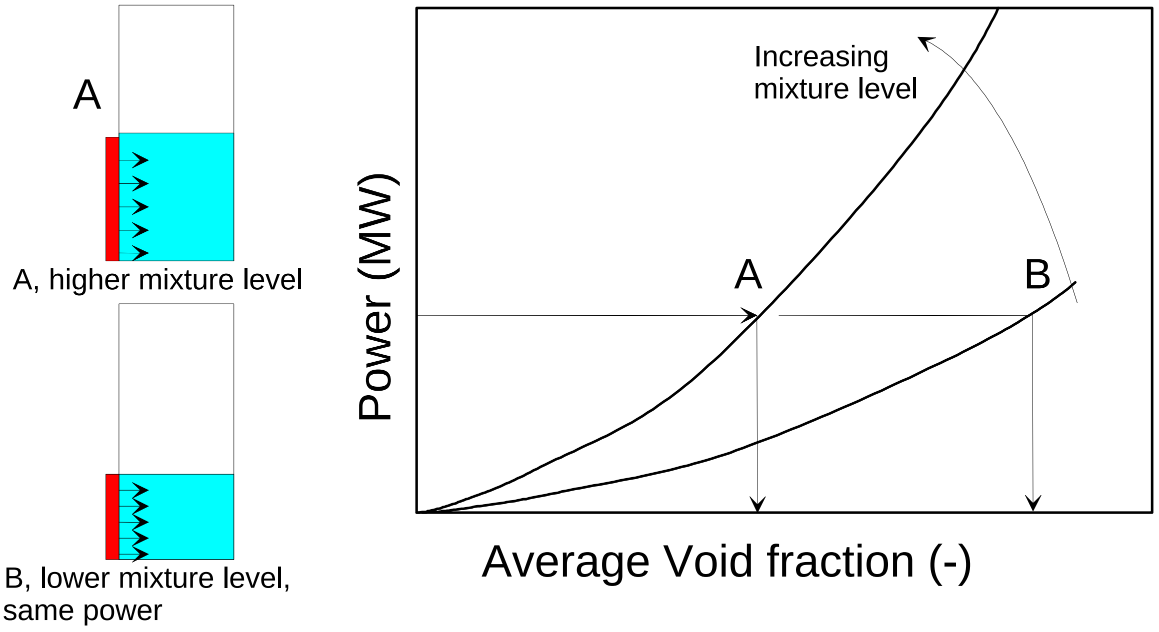

Figure 7.59 - Resulting void fraction by applying a constant power

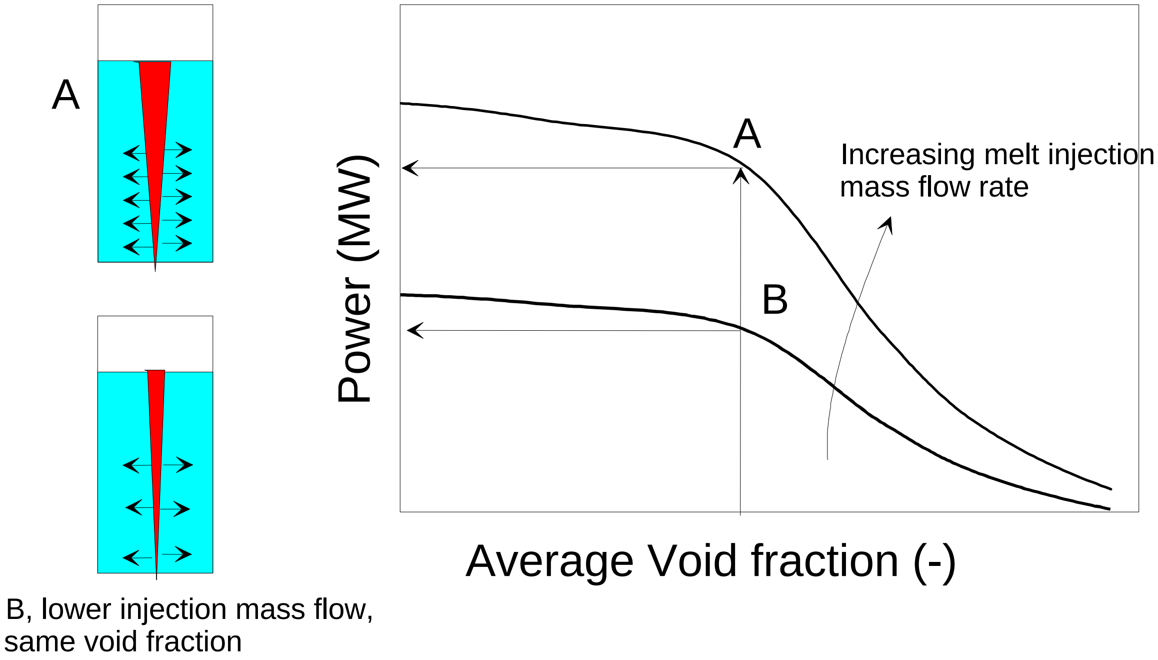

Figure 7.60 - Resulting power exchanged fragmenting melt in a constant void fraction medium

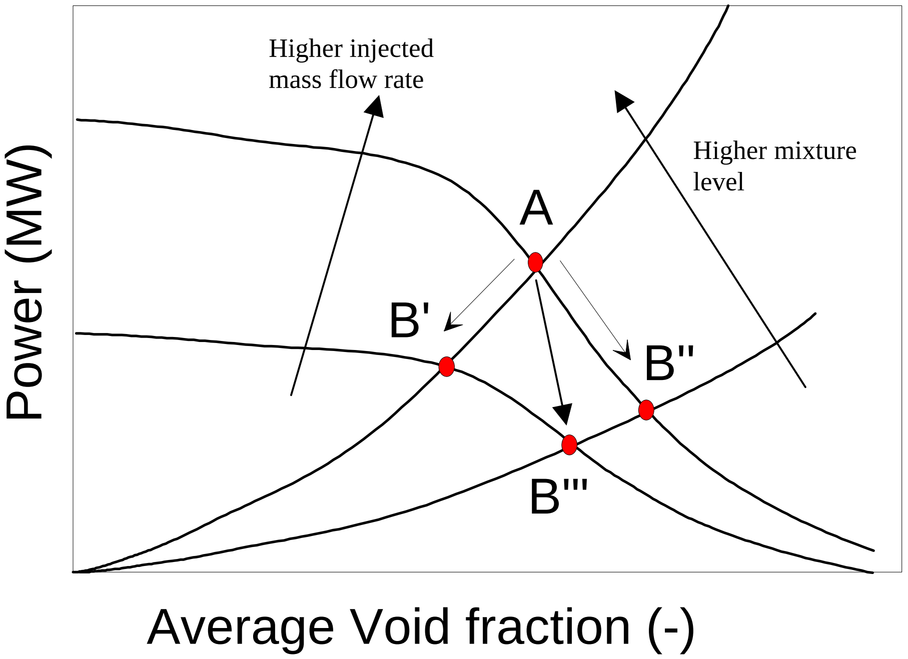

Figure 7.61 - Power exchanged versus void fraction plan

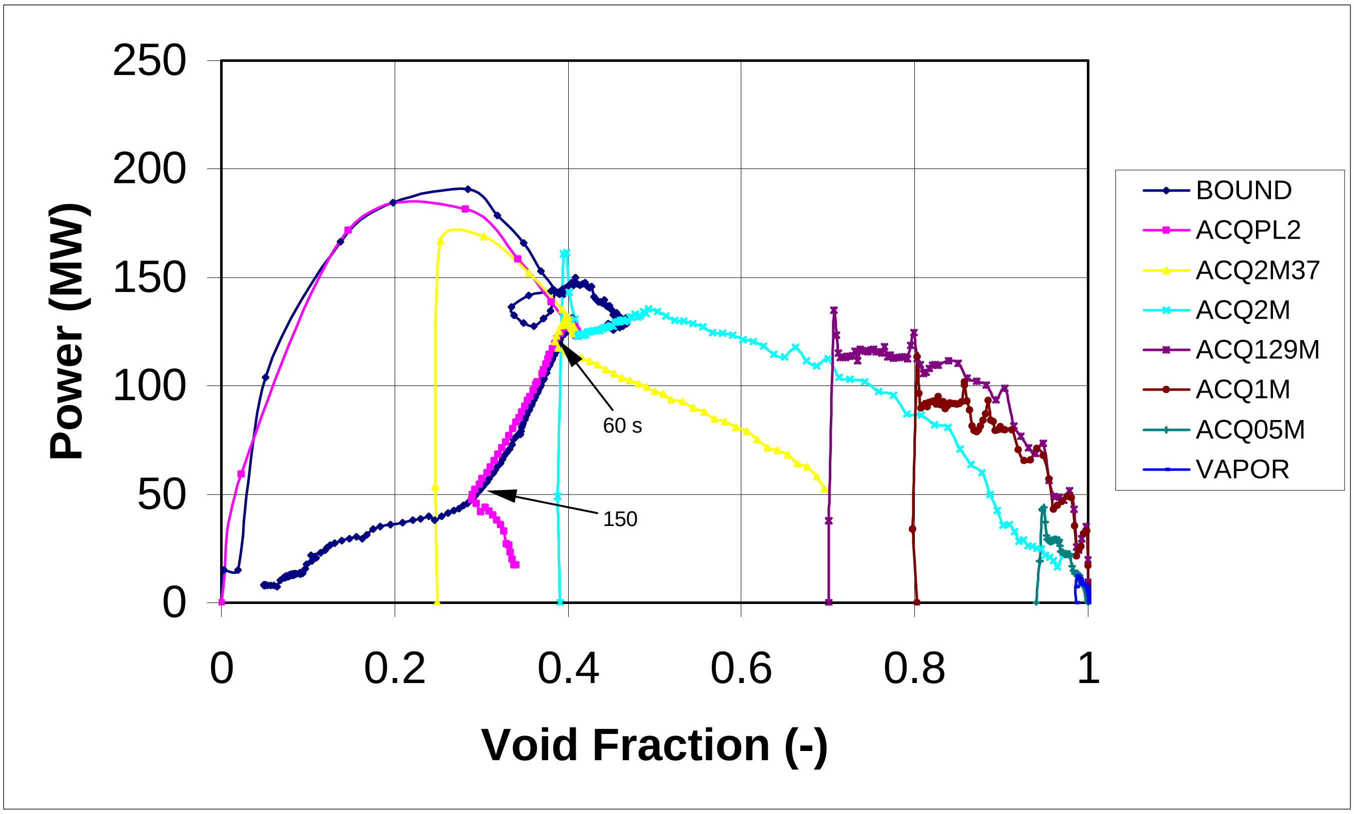

Figure 7.62 - Quenching rate versus global mean void fraction in cases 1-d

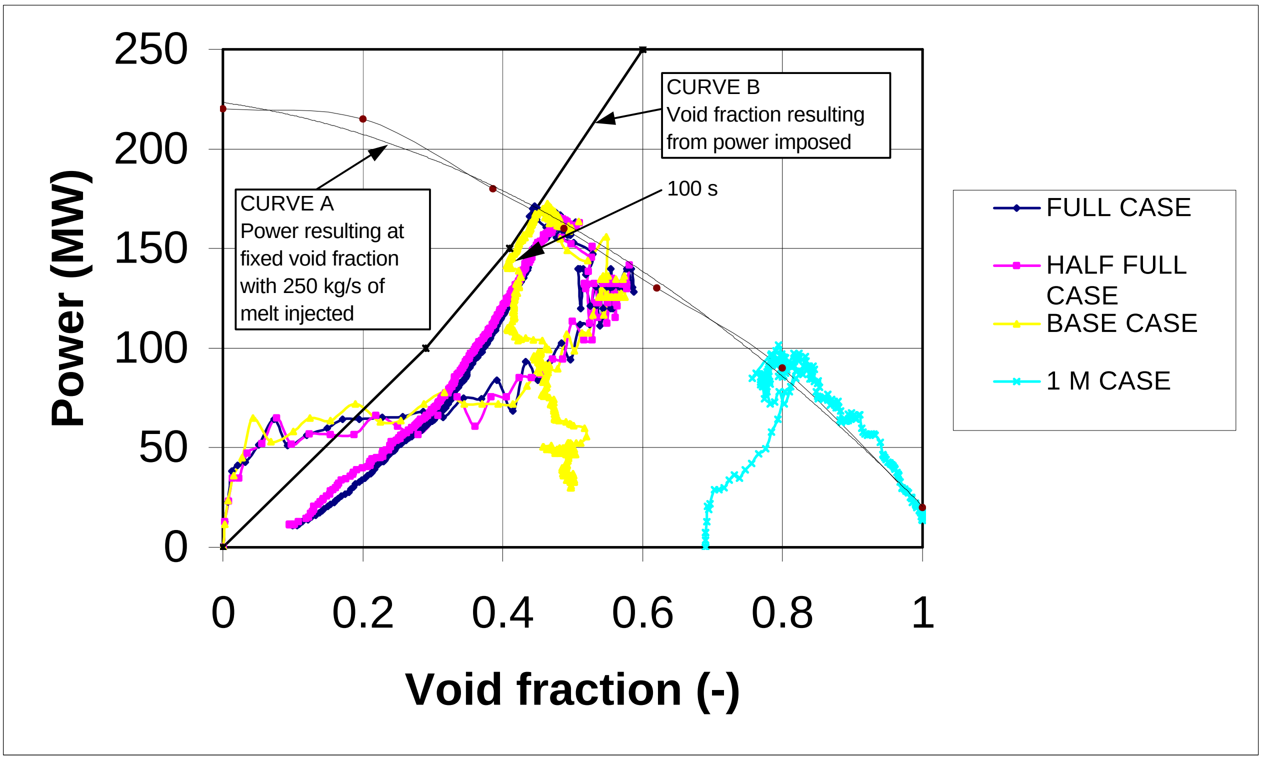

Figure 7.63 - Quenching rate versus global mean void fraction in cases 2-d

7.3.4. CONCLUSIONS

As conclusions of the study, the following items can be pointed:

All the cases show decreasing fragmentation and energy production as the initial water level in the core inlet and lower plenum is reduced. With an initial water level below a value between 1 m and 0.5 m, the fragmentation and the quenching rate progressively decrease and the cake mass accumulation increases.

In the boundary case pressure increase is lower due to condensation, quenching rate is higher and drops mass, void fraction and cake mass accumulation are similar to cases with higher initial water level. The difference in this case is the onset of natural circulation in the vessel that causes a redistribution of the drops mass in the system.

The relation between the void fraction and the quenching rate has been clarified. An equilibrium value is generally attained and is possible only if increase and decrease of void fraction is allowed; that is if the mixture level is at or above the injection point (flooded regime). On the contrary, if the mixture level is too low, the power exchanged will continuously decrease and tend to zero as the water level decreases (depleted regime).

7.4. COMETA CODE CALCULATIONS OF THE FARO QUENCHING TESTS

7.4.1. INTRODUCTION

The work has been focused in the simulation (with COMETA thermalhydraulic code) of the MFCI test series carried out in the FARO facility. The objective is to analyse and to unify the experiment simulations with the last available version of the COMETA code.

The interaction of big melt masses in the water under realistic accident conditions was the objective of the FARO experiments. FARO facility began the experiments of the LWR-MFCI phenomena in 1991. The last test was performed in 1999.

In this context the COMETA thermalhydraulic code was developed in order to support test preparation and execution with pre-test calculations and simulation, assist test results interpretation with post-test calculations and perform sensitive analyses to point out the influence of various parameters on the test facilities response.

During the time the COMETA code models and input decks changed as a result of additional analyses and in some cases of errors correction.

In order to analyse and unify the COMETA simulations carried so far, it was decided to simulate again all the FARO experiments with the last available version of the COMETA code and keeping as far as possible the same basic nodalization scheme for all the tests. Only changes due to different boundary conditions of facilities arrangements were performed. This chapter summarises the Tests calculations (L-14, L-19, L-24, L-27, L-28, and L-31). Test L-33 was not included in this document because, due to the specific nature of the test (steam explosion) the analysis was performed in a separate document.

7.4.2. EXPERIMENTS IN THE FARO FACILITY

The series of experiments in the FARO facility were part of the research activities in severe accidents in LWR carried out by the Institute for Systems, Informatics and Safety (ISIS) of the JRC. The reference situation is an accident in which one or more mass melt jets pour into the water of the lower plenum, fragment and settle down in the bottom. The objectives of the tests were to evaluate the steam generation rate associated to the melt heat transfer (quenching), to evaluate the hydrogen production associated to Zr oxidation, the heating of the bottom vessel structures and to evaluate the debris bed in the bottom plate.

The experiments simulated with the last version of the COMETA code are presented in Table 7.7, which summarises the experimental conditions for each experiment. From Test L-14 to L-24 the TERMOS test section was used (0.71 m of diameter) (Figure 5.3). From Test L-27 it was changed to FAT test vessel (Figure 5.4), which consists of a pressure vessel of 1.5 m internal diameter and 2 m high, designed for a pressure of 8 MPa and a temperature of 300°C. To compare the results with the ones of the previous configuration TERMOS, an internal cylinder was inserted in the FAT vessel. The cylinder internal diameter was the same of the previous TERMOS vessel, 0.71 m. This cylinder is filled with water and the outer annular space is part of the free board volume.

Tests L-14, L-19 and L-20 were performed under a relative medium and high pressure, lower pressure was imposed from Test L-24 until L-33. Test L-31 and L-33 were the only ones performed under subcooled conditions in the pool of water. In Test L-33 an external trigger was applied at 1.1 s. Due to the peculiar type of phenomena, this test has not been included in this study.

Test L-28, L-31 and L-33 were performed with a 5 cm melt orifice discharge, the rest with a larger one (10 cm). This reduction determined a longer discharge time of the melt.

EXPERIMENT	**L-14**	**L-19**	**L-20**	**L-24**	**L-27**	**L-28**	**L-31**	**L-33 (**)**
Initial pressure (bar)	50.4	50.4	20.4	5.1	4.9	5.1	2.2	4.1
Mass (kg)	125	157	96	177.1	128.7	174.9	92	100
Melt temperature (K)	~3073	3073	3173	3023	3023	3052	2988	3073
Initial water level (m)	2.05	1.1	1.97	2.02	1.47	1.44	1.45	1.62
Initial water temperature	Tsat	Tsat	Tsat	Tsat	Tsat	Tsat	290.8 K	294 K
Free fall in gas (m)	1.04	1.99	1.115	1.065	0.73	0.89	0.77	0.77
Injection elevation (m)	3.09	3.09	3.085	3.085	2.2	2.33	2.22	2.39
Orifice diameter (m) (*)	0.092	0.092	0.092	0.094	0.094	0.044	0.046	0.044
Vessel geometry	TERMOS	TERMOS	TERMOS	TERMOS	FAT	FAT	FAT	FAT
Test date	June 23rd1994	June 22nd 1995	January 30th 1996	December 5th 1996	Dec. 3rd 1997	Apr 2nd 1998	Nov 11th 1998	July 1st 1999

Table 7.7 - Experimental conditions in the series of experiments in the FARO facility

(*) The initial orifice diameters are 0.1 m and 0.05 m but due to the formation of crusts before the melt injection, at the time of release, the effective orifice diameter is smaller.

(**) This test has not been included in this study.

7.4.3. COMETA CODE SIMULATIONS OF THE FARO TESTS

Calculations were performed with the last version of the COMETA code. The original jet fragmentation model was applied. The IKE jet fragmentation model, developed at the University of Stuttgart, Germany, was also tested.

Other calculations were performed for low pressure tests to account for the initial higher fragmentation rate. The Enhanced fragmentation model, in which a lower critical Weber number multiplier and a lower jet break-up length coefficient were used during the initial phase of calculation (i.e. less than 1s). After that time, the standard values adopted for high pressure calculation were used (*).

The following Table describes the COMETA calculations performed:

EXPERIMENT	L-14	L-19	L-20	L-24	L-27	L-28	L-31
Descriptor 1d original COMETA model	L14N_1D	L191D05A	L20N_1D	L24N_1D	L27N_1D	L28N_1D	L31N_1D
Descriptor 2d original COMETA model	L14N_2D	L192D05A	L20N_2D	L24N_2D	L27N_2D	L28N_2D	L31N_2D
Descriptor 1d IKEJET fragmentation model	L141DIKE	L191DI0A	L201DIKE	L241DIKE	L271DIKE	L281DIKE	-
Descriptor 2d IKEJET fragmentation model	L142DIKE	L192DI0A	L202DIKE	L242DIKE	L272DIKE	-	-
Descriptor 1d ENHANCED fragmentation model	-	-	-	L241DENH	1D_PROV3	L281DENH	-
Descriptor 2d ENHANCED fragmentation model	-	-	-	L242DENH	PROVA3	L282DENH	-

Table 7.8 - Experiment calculations with COMETA code

The detailed calculation results [Publication [3]] are not presented in this document due to the big amount of information, only summary results, general conclusions and overall recommendations extracted from the results are commented.

(*) It was never clarified if the initial higher fragmentation, which was measured from Test L-24, was due to the lower pressure conditions or due to the melt release mode. The priorities in other research topics and the anticipated closure of the FARO project prevented a clear understanding of this issue, which could have been resolved by performing a new test at high pressure with the new melt release device.

7.4.4. EFFECT OF THE NODALIZATION SCHEMES ON THE RESULTS

The next table shows a first assessment summary of the overall results after performing all the Test simulations. The objective is to give some general conclusions and to help to choose the nodalization scheme to reduce the computer calculation time. It may be helpful to simulate other similar quenching cases.

TEST	PRESSURE	ORIFICE DIAMETER	WATER CONDITIONS	COMETA ORIGINAL MODEL	IKEJET FRAGMENTATION MODEL	VESSEL GEOMETRY
L-14, L-19 and L-20	High	10 cm	Saturated	**1d nodalization ~ 2 d nodalization**	**1d ? 2d: effect of vapour-liquid junction velocity**	TERMOS
FARO Test missing	High	5 cm	Saturated	Not assessed	Not assessed	-
FARO Test missing	High	5 cm	Subcooled	Not assessed	Not assessed	-
L-24 and L-27	Low	10 cm	Saturated	**Very good results using 2d Enhanced frag.** **1d not defined**	**1d ? 2d: effect of vapour-liquid junction velocity**	TERMOS and FAT
L-28	Low	5 cm	Saturated	**Better results with 2d nodalization**	Only performed 1d nodalization	FAT
L-31	Low	5 cm	Subcooled	**Good calculation results.** **1d nodalization ~ 2 d nodalization**	Not performed	FAT

Table 7.9 - Assessment summary of the simulation results

- Tests performed at ***high*** pressure, ***10 cm*** orifice diameter and ***saturated*** initial water conditions: no great differences on the main quantities (pressure, energy, quenching fragmented mass) are observed between calculations using 1d or 2d nodalization scheme with the original COMETA model. With the same initial conditions, the COMETA-IKEJET model shows differences between 1d and 2d nodalization scheme: calculations with the 2d COMETA-IKEJET model show an initial pressure high jump due to the effect on this 2d model of the liquid-vapour junction velocity.

The influence on the results of the melt discharge orifice diameter was not performed at high pressure, in saturated or subcooled conditions because no FARO Test with 5 cm orifice diameter was available in these conditions.

- Tests performed at ***low*** pressure, ***10 cm*** orifice diameter and initial water ***saturated*** conditions: Very good results are obtained using the 2d Enhanced fragmentation model. 1d nodalization does not show differences respect to 2d nodalization in Test L-27. Calculations with the 2d COMETA-IKEJET model show an initial pressure high jump due to the effect on this 2d model of the liquid-vapour junction velocity, 1d and 2d nodalization show differences.

- Tests performed at ***low*** pressure, ***5 cm*** orifice diameter and initial water ***saturated*** conditions: There are great differences on the main quantities between 1d and 2d COMETA original model, 2d calculations are much better. The same is true using the Enhanced fragmentation model.

- Tests performed at ***low*** pressure, ***5 cm*** orifice diameter and ***subcooled*** initial water conditions: In this Test only COMETA original model was used for the simulations. Using 1d or 2d nodalization scheme it shows no major differences in the main results although they are, in some cases, seen amplified by the small plotting scale i.e. pressure.

So, in general it seems better to use 2d nodalization scheme for Test performed at low pressure, saturated conditions, and small diameter. At high pressure and saturated conditions it is better to use a simpler 1d nodalization, because there are not great differences versus 2d and it allows reducing the computer calculation time.

7.4.5. CONCLUSIONS

The work was focused in the simulation of the quenching test series carried so far in the FARO facility (L-14, L-19, L-24, L-27, L-28, and L-31) with the last version of the COMETA thermalhydraulic code. The objective of the simulation was to keep as far as possible the same basic nodalization scheme code models and options for all the tests. Only changes due to different boundary conditions were included. Test L-33 was not included in this document because, due to the specific phenomena included in the test (steam explosion) the analysis was performed in a separate document.

The COMETA original jet fragmentation model was applied to all Tests. The COMETA-IKEJET fragmentation model, developed at the University of Stuttgart, Germany, was also tested.

The Tests L-14, L-19 and L-20 were performed with water at the beginning in saturated conditions above 20 bar in the TERMOS vessel.

a) In 1d calculations the rising ramp and the overall trend for pressure are well predicted; long term values are also close to experimental value, except for L-19 that are slightly higher. Energy release and quenching rate overall trend are well predicted by the calculations; long term values for L-20 are slightly lower. The calculated fragmented mass is slightly underpredicted in some cases.

b) In 2d calculations pressure overall trend is well predicted; calculations with the COMETA-IKEJET model show an initial high jump due to the effect on this model of the liquid-vapour junction velocity. Energy release and quenching rate overall trend are well predicted by the original COMETA and IKEJET-COMETA models; long term values for L-20 are slightly lower. The fragmented mass in the COMETA-IKEJET calculations shows values closer to the experimental ones.

In Tests at high pressure, with 10 cm orifice diameter and saturated water initial conditions, 1d and 2d nodalization differences are shown in Table 7.9.

The Tests L-24, L-27, L-28 and L-31 were performed below 20 bar: L-24 was performed in the TERMOS vessel, the others in the FAT vessel. All these Tests were performed with water at the beginning in saturated conditions, with the exception of Test L-31, in which the water was subcooled. Some calculations were performed to account for the initial higher fragmentation rate (Enhanced fragmentation model).

a) In 1d calculations the initial pressure rising ramp is very well predicted with the Enhanced fragmentation model. In Test L-27, the long term behaviour with the Enhanced fragmentation model is also very well predicted. COMETA original calculation for subcooled Test L-31 shows pressure value very close to the experimental one. In general, the pressure increase for subcooled tests is much lower than for saturated cases. In Test L-31 the differences between experimental and calculated values are less than 0.2 bar. Energy release and quenching rate show values very well predicted by the Enhanced fragmentation model in Test L-27 and by the original COMETA model in Test L-31.

b) In 2d calculations the pressure overall trend is very well predicted with the Enhanced fragmentation model; calculations using the COMETA-IKEJET model show in Test L-24 pressure an initial high jump due to the effect of the liquid-vapour junction velocity. As it was shown for 1d case, 2d COMETA original model calculation for subcooled Test L-31 shows pressure value very close to the experimental one. Energy release, quenching rate and fragmented mass show calculated values closer to the experimental ones with the Enhanced fragmentation model and COMETA-IKEJET model in Tests L-24, L-27 and L-28.

In Tests at low pressure, 10 or 5 cm orifice diameter and saturated or subcooled water initial conditions, 1d and 2d nodalization differences are shown in Table 7.9.

In general, as a main conclusion: the COMETA code was successfully applied to all the FARO configurations reaching the main objective: to analyse and unify the COMETA calculations carried so far. Also some indicative advises, related to the model or the 1d - 2d nodalization, are given. The post-tests simulations also gave significant information for the assessment and qualification of the COMETA code.

7.5. CHARACTERIZING MELT FUEL-COOLANT INTERACTION IN A NPP CONTEXT WITH RELAP5/SCDAP 3.2 CODE

7.5.1. INTRODUCTION

After concluding FCI studies from the reactor vessel standpoint, a wider overview of these phenomena and others related to a severe accident may be of interest. Because of this it was decided to complete the research studying the severe accident progression in a nuclear power plant. This work may help to clarify the importance of the melt fuel-coolant interaction (MFCI) in the context of a severe accident.

The study presented aims to illustrate the MFCI inside the general overview of a severe accident sequence and the overall view of the NPP.

RELAP5/SCDAP 3.2 is the code chosen for the calculations [31] [32] [48] [50]. It is being used by the Technical University of Catalonia (Universitat Politècnica de Catalunya, UPC) thanks to the agreement between the Spanish Nuclear Security Council (Consejo de Seguridad Nuclear, CSN) and the American Idaho Innovative Systems Software (ISS) Company.

Three objectives are aimed to reach:

a) Deeper understanding of the MFCI modelling theory of RELAP5/SCDAP 3.2 and how the code models all the associated phenomena to the melt fuel coolant interaction.

b) Study the influence of the “low pressure injection system” (LPIS) in the sequence of a large “loss of coolant accident” (LOCA) in the cold leg, followed by core uncover and degradation. It is also interesting to study up to what point it is possible to minimize core degradation and to avoid its meltdown (with the LPIS) and in the same way to quantify the LPIS effect on the cladding oxidation, hydrogen production and core additional heating due to the exothermic reaction.

c) Obtain the initial conditions (pressure, coolant temperature, molten mass temperature, molten mass composition, water level in the lower plenum, etc.) just before the molten pool slumping into the lower plenum in order to introduce them in a specific MFCI code input (as JRC-COMETA [6]) so a detailed MFCI study could be later performed.

A generic PWR NPP (3 loops, 1000 MW_e) is chosen to perform the calculations.

7.5.2. THE LOSS OF COOLANT ACCIDENT (LOCA)

In the event called “loss of coolant” [26], the reactor cooling fluid is escaping from a leak or a break within the primary cooling system and can cause an imbalance between heat production and heat removed leading to a potential risk of inadmissible high fuel temperatures.

A loss of coolant caused by a major rupture within the primary cooling system is one of several “limiting fault conditions occurrences”. These are faults, which are not expected to occur but are postulated because their consequences could include the risk of a major release of radioactive material.

The loss of coolant accident (LOCA) caused by a double ended break of a main coolant inlet pipe (cold leg between pump and reactor pressure vessel, RPV) of the primary cooling system of a PWR is the most dangerous fault against which the safety systems have to be designed; it is a design basis accident (DBA) determining the specifications for the limiting, safety related design of the reactor plant, particularly of the emergency core cooling system (ECCS).

The severity of a LWR LOCA in the primary cooling system and its possible consequences is essentially determined by the rupture characteristics in terms of break location and break size.

Possible break sizes range from a double ended or guillotine rupture of a main coolant pipe which is referred to as a 2x100% (of the main coolant pipe flow cross section) break, down to a break of a single steam generator tube (about 0.1%).

Within this wide rupture size spectrum, a distinction can be made between small (<2%, <80 cm^2 break area), intermediate (2%-10%, 80-400 cm^2 break area) and large (>10%, >400 cm^2 break area) LOCAs according to break size. The quantitative values for the break size area and percentage should not be considered fixed; they certainly vary between plants from different manufacturers.

In addition, for the case of a rupture of the main coolant piping, distinction is made between cold leg ruptures, pump and reactor pressure vessel (RPV) or between steam generator (SG) and pump, and hot leg ruptures between RPV and SG.

In general the ECCS are designed to cope any of these type of accident.

For the calculations here considered the loss of coolant accident (LOCA) is caused by a break with the 60% flow area (0.23 m^2) of a main coolant inlet pipe (cold leg between pump and reactor pressure vessel, RPV) of the primary cooling system of a PWR in which not all the emergency systems are in operation. As a consequence the core experiences a severe accidental sequence.

7.5.3. THE RELAP5/SCDAP 3.2 CODE

The Idaho National Engineering and Environmental Laboratory (INEEL) initially developed the RELAP5/SCDAP code [38][39][40] for the USA NRC. It was designed for best-estimate transient simulation of light water reactor coolant systems during a severe accident.

The RELAP5/SCDAP code models the coupled behaviour of the reactor coolant system, the core kinetics, fission products released during a severe accident transient as well as large and small break loss-of-coolant accidents, operational transients such as anticipated transient without SCRAM, loss of offsite power, loss of feedwater, and loss of flow; and SCDAP models the core melting phases up to melt relocation in the lower head.

The core degradation includes models of cladding oxidation, materials relocation in the core, cladding rupture, molten pool formation and its relocation in the lower head.

Calculation results (at the moment of the relocation) performed with codes as RELAP5/SCDAP 3.2 could be seen as initial conditions for JRC-COMETA code calculations to simulate detailed MFCI phenomena.

RELAP5/SCDAP 3.2 modelling theory in the late phase damage progression

The uncertainties involved in modelling the late phase damage progression make it useful to perform bounding studies on the calculated times of molten pool slumping and failure of the lower head, that include the next areas: strength and configuration of solidified material that supports a pool of molten core material, fragmentation temperature of embrittled fuel rods that are quenched, configuration of slumping molten material, heat transfer coefficient between debris and the lower head of the reactor vessel.

The code user can define a parameter for each of these areas of modelling, so that a series of analyses can be performed to bind the possible behaviour of the reactor.

From the code version 3.1, in the models that determine when material from a molten pool in the core region slumps from this region to the lower head of the reactor vessel three events are considered to trigger this slumping:

1- The first event is the melting of structural failure of the vertically oriented crust at the periphery of the core that was containing the molten pool and keeping it from slumping into the core bypass region.

2- The second event is the structure failure of the crust at the top of the molten pool that was supporting core material above the molten pool. This event is considered to cause slumping of the molten pool to the lower head only when the molten pool had already spread to the periphery of the code.

3- The third event is the propagation of the molten pool to the elevation of the bottom of the core.

The calculated time of slumping of a molten pool to the lower head should be regarded as having a large degree of uncertainty, it is very difficult to predict even for a well defined manufactured structure. This large uncertainty in the calculation of crust failure requires that the severe accident analyst examine the effect of the failure criteria upon the calculated course of a severe accident. It is also possible to set this slumping time and the duration of the slumping (10s by default) by the code user as an input parameter.

The code user also defines the degree of interaction of the slumping material with the water through which it falls.

If the user defines that no interaction takes place, then the slumping core material is considered to fall with no transfer of internal energy from the slumping material to water. The slumped material that accumulates in the lower head is considered to have no porosity.

If the user defines a complete interaction between slumping material and the water through which it falls, then the slumping material is considered to break up into small particles and transfer all of its internal energy instantly to the water, then the molten material is cool when it impacts the lower head. By default the slumped material that accumulates in the lower head is considered to have a porosity of 0.5 and a particle size of 10 mm. These values are an input parameter than could be settled by the code user. The transfer of internal energy from the slumping material to water may cause a large amount of vapour generation and may significantly increase the pressure in the reactor vessel.

Since that time interval of the slumping is arbitrary, the pressure increase caused by the energy addition may or may not be conservative. However, the total energy added to the water is still conserved. The option to predict the minimum heat transfer to the water assumes that all of the stored energy remains in the melt and is only removed by heat transfer from the surfaces of the resulting debris in the lower plenum. This option is the most conservative in a possible study about lower head failure and want the maximum amount of energy in the melt when it interacts with the vessel.

7.5.4. NODALIZATION. ANALYSED CASES

For the calculations the loss of coolant accident (LOCA) chosen is caused by a break with the 60% flow area (0.23 m^2) of a main coolant inlet pipe of the primary cooling system. Break transient time is 460s.

The nodalization adopted in all calculations for some NPP parts (the reactor vessel, break and three loops LPIS) is shown in Figure 7.64. It includes a detailed core nodalization in 5 thermalhydraulic radial channels, two for the centre core (number 111 and 114), two for the middle core (112 and 115) and one for the outer core (113) connected by cross-flow junctions and divided in 10 axial nodes, numbered from 1 (core bottom) to 10 (core top). Each core channel includes two SCDAP components, one that simulates fuel rod (components number 1, 3, 5, 7, 9) and other that simulates control rod (2, 4, 6, 8, 10). The total reactor thermal power is 2.686e9 W.

In all cases performed, accumulators are available; they open below about 5 MPa. In the so-called “Base Case” **(DEBRIS_NOBK, DEBRIS_BK)** low pressure injection system (LPIS) is not available, so core degradation and meltdown occurs. The other cases include the manual action of LPIS system at different times after the break (from 15 min up to 34 min).

For the “Base Case” two calculations were performed **(DEBRIS_NOBK, DEBRIS_BK)** in order to highlight the difference in the degree of interaction (of the slumping material with the water through which it falls) that could be obtained setting two different values in an input parameter.

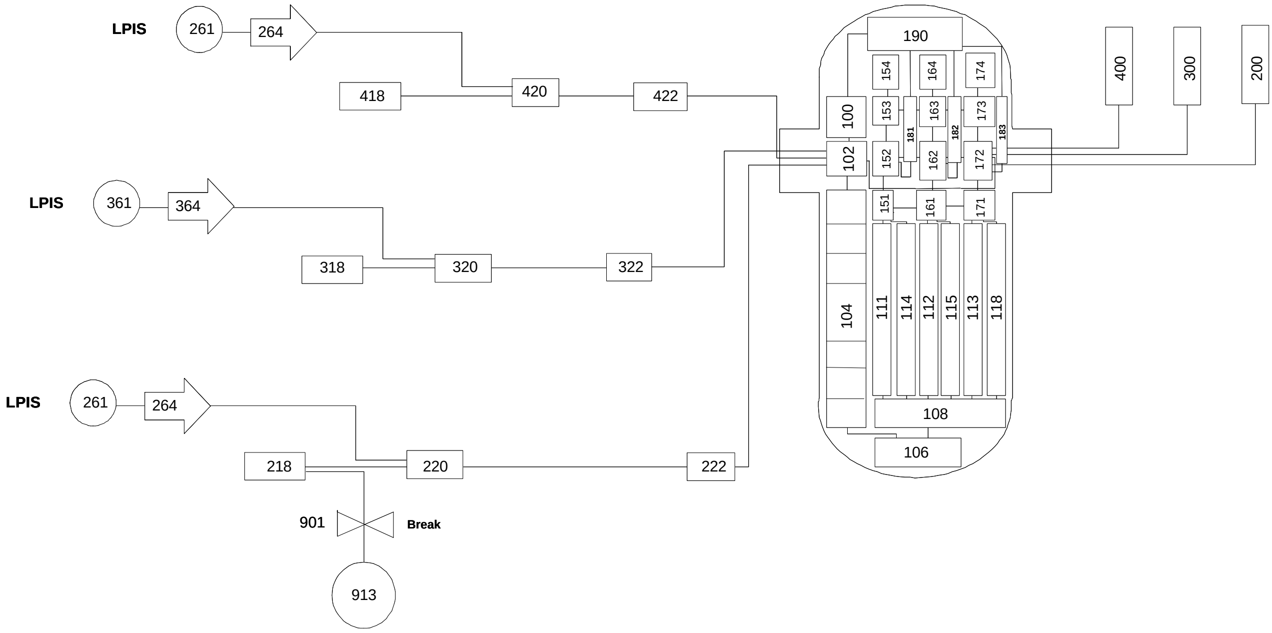

Figure 7.64 - Vessel, LPIS and break RELAP5/SCDAP nodalization

The following Table 7.10 summarises the performed cases. These cases provide the initial conditions that could be set in an input code for a detailed MFCI study, like JRC-COMETA code [6]. Initially cases with LPIS were performed in order to study which is the maximum LPIS action time that prevents core meltdown.

Descriptor	Break size (%)	LPIS	LPIS injection time after transient beginning (t=0s)	LPIS injection time after break (t=460s)	Calculation purpose
DEBRIS_NOBK (Base Case)	60	NO	-	-	Understand RELAP5/SCDAP 3.2 model for MFCI. Initial conditions for COMETA code
DEBRIS_BK (Base Case)	60	NO	-	-	Understand RELAP5/SCDAP 3.2 model for MFCI
LPIS_2000	60	YES	2000s	1540s	LPIS influence. Initial conditions for COMETA code
LPIS_1500	60	YES	1500s	1040s	"
LPIS_1300	60	YES	1300s	840s	"
LPIS_1200	60	YES	1200s	740s	"
LPIS_1150	60	YES	1150s	690s	"
LPIS_1125	60	YES	1125s	665s	"
LPIS_1121	60	YES	1121s	661s	"
LPIS_1120	60	YES	1120s	660s	"
LPIS_1119	60	YES	1119s	659s	"
LPIS_1115	60	YES	1115s	655s	"
LPIS_1110	60	YES	1110s	650s	"
LPIS_1100	60	YES	1100s	640s	"
LPIS_900	60	YES	900s	440s	"

Table 7.10 - Performed RELAP5/SCDAP calculations

7.5.5. CALCULATION RESULTS

Calculation results are presented in four different chapters:

The first one (a) discusses the two calculations of the “Base Case” **(DEBRIS_NOBK, DEBRIS_BK)** in order to study the SCDAP models for a possible MFCI of the slumping material towards the lower plenum with the water through which it falls and to show the difference in the degree of interaction that could be obtained setting two different values in an input parameter.

The second and third chapter (b) and (c) show calculation results for all cases in which LPIS does not avoid (after core degradation) molten pool formation and subsequent slumping to the lower plenum. That is up to a LPIS injection time of 660s (1120s from t = 0). In chapter (b) all cases that are clearly far from core recovery are presented: from case LPIS_1150, injection time 690s after the break (1150s from t = 0) up to LPIS_2000, injection time 1540s after the break (2000s from t = 0). In chapter (c) the three cases that are closer to the core recovery are presented together (LPIS_1120, LPIS_1121 and LPIS_1125) because they are a little different from the rest after the LPIS injection time.

Chapter (d) presents cases in which LPIS could avoid core degradation and melting.

Figure 7.65 shows that if LPIS injection time is lower than 659s after the break (case LPIS_1119) core temperature increase can be mitigated.

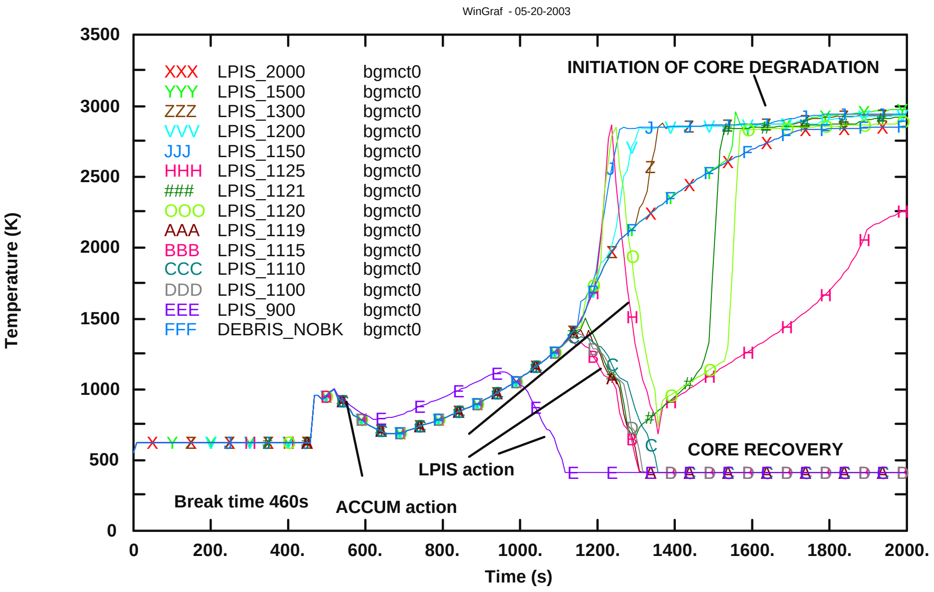

Figure 7.65 - Core maximum temperature in all SCDAP calculations

a) “Base Case” (DEBRIS_NOBK, DEBRIS_BK cases). MFCI with RELAP5/SCDAP 3.2

Two “Base Case” calculations were performed with the code. The chosen scenario is a LOCA without LPIS leading the vessel to a progressive voiding and the core to a complete uncover. Core melting and molten pool formation that pours into the lower plenum will be also observed.

The first case **DEBRIS_NOBK** is a calculation performed with the input option in the code (w4 = 1 on card 51010000) that predicts the minimum heat transfer from the slumped material to the water in the lower plenum. This option is the most conservative for a study about lower head failure because the melt contains the maximum amount of energy when it interacts with the vessel.

The second case **DEBRIS_BK** is a calculation performed with the input option in the code (w4 = 0 on card 51010000) that predicts that maximum heat transfer from the debris (as it slumps) to the water is caused when the debris breaks up in little particles. All the stored energy from the melt is added to the water over a time interval of about 10 seconds. Linked to this option two parameters can be settled in the core input, debris porosity and particle size. By default the debris material is considered to have a porosity of 0.5 and a particle size of 10 mm and these are the values used to perform the calculation.

After LOCA break (at 460s) some parameters are plotted in both cases. Obviously both calculations are identical up to the moment of slumping. LOCA break mass flow is presented in Figure 7.69. It reaches a peak of about 3200 kg/s 15 seconds after the break. In Figure 7.66 pressure in the primary system is shown. It decreases in few seconds from 16 MPa up to stabilization at about 0.2 MPa. Figure 7.67 shows water temperature in the primary system after break. In Figure 7.68 downcomer water level is presented, it can be also observed the initial increase of water level due to accumulators injection.

At the time of the slumping, the higher interaction between molten material and water in the lower plenum and higher energy transferred to it causes a large amount of vapour generation. This may increase pressure and temperature significantly in the reactor vessel. Figure 7.70 and Figure 7.71 show lower plenum pressure in both cases. The higher pressure peak during slumping is obtained in case DEBRIS_BK (from 0.25 to 0.9 MPa) where molten material transfers instantly all the energy to the water. The calculation is performed in an open system (break) so the pressure increase is small (Figure 7.71).

Void fraction (Figure 7.72) in case DEBRIS_BK reaches the value 1 in few seconds, almost instantly lower plenum is voided due to the heat transfer from the fragmented little particles to the water, in case DEBRIS_NOBK lower plenum is voided progressively due to the debris heat transfer. The first slumping of control material (some kg of Ag) before the real so-called molten pool slumping is shown.

Figure 7.73 shows lower plenum temperature, higher during slumping for the DEBRIS_BK case.

From Figure 7.74 and Figure 7.75 case DEBRIS_NOBK shows that power and energy still stored in the slumped debris are transferred by convection from top surface and to fluid at boundaries of debris and structural material. In DEBRIS_BK both values are small because most molten pool energy was transferred form the fragmented particles to the water and less debris mass is expected to be in the lower plenum bottom.

The two calculations have shown the MFCI study possibilities with RELAP5/SCDAP 3.2. However in general it is more interesting to study the grade of interaction (a point between total interaction, total fragmentation of the slumping material instead of no interaction or no fragmentation) as a result from the initial conditions in the time just before the slumping of the molten pool and the evolution of the interaction transient instead of to impose this interaction grade as an input parameter. More accuracy can be achieved using detailed MFCI codes but on the other hand these codes do not have the capacities to run full detailed NPP transients as RELAP5/SCDAP 3.2 has. So the combined use of two codes could be a good solution to study MFCI phenomena in a full NPP transient.

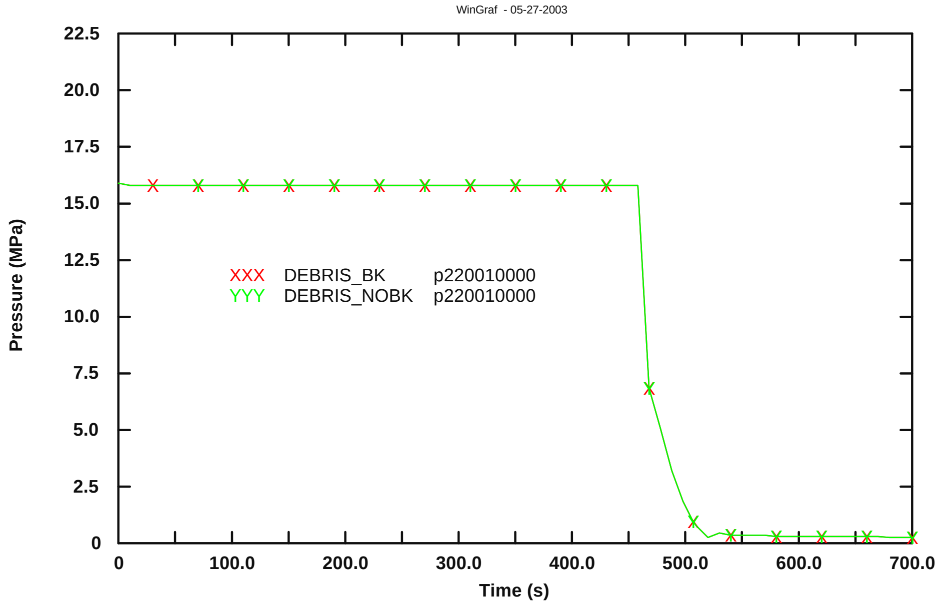

Figure 7.66 - Pressure of primary system after break

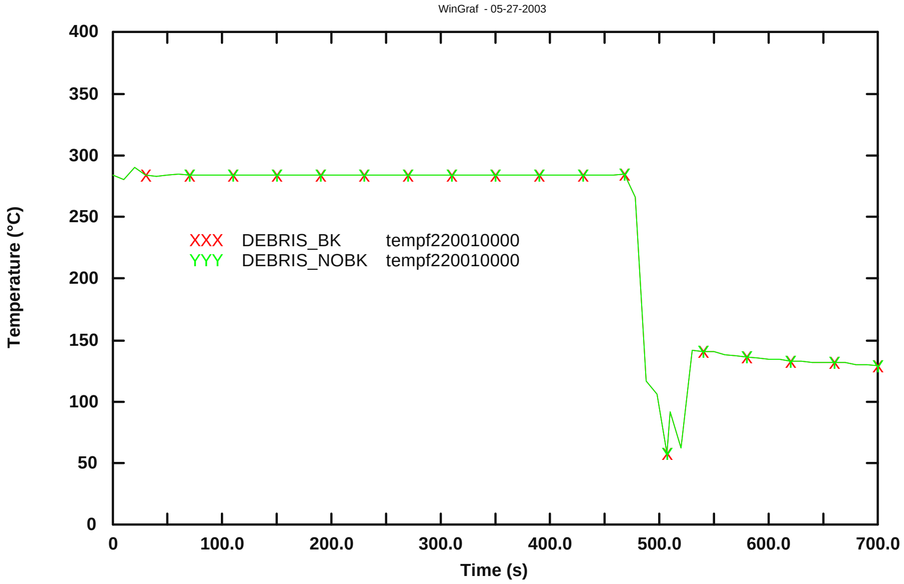

Figure 7.67 - Temperature in primary system after break

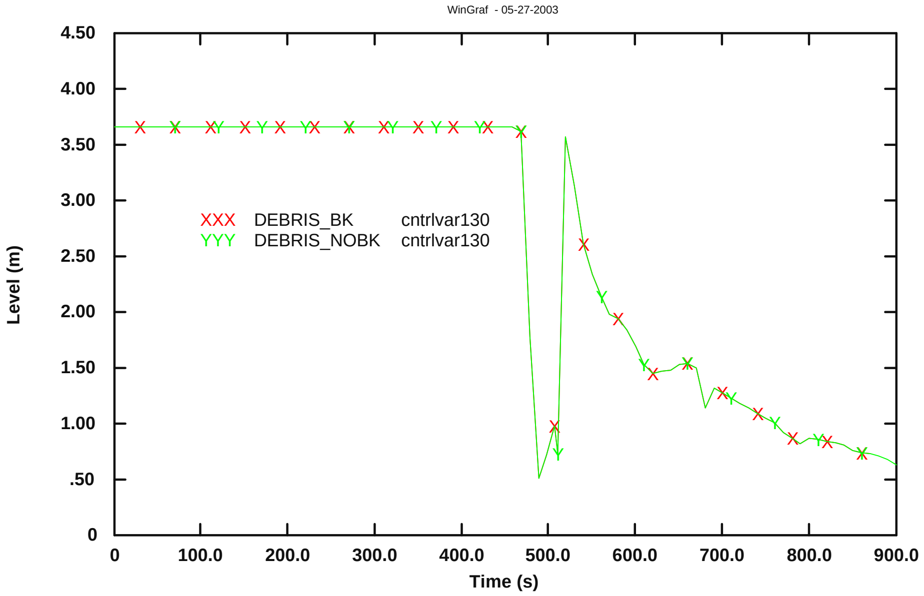

Figure 7.68 - Downcomer level after the break

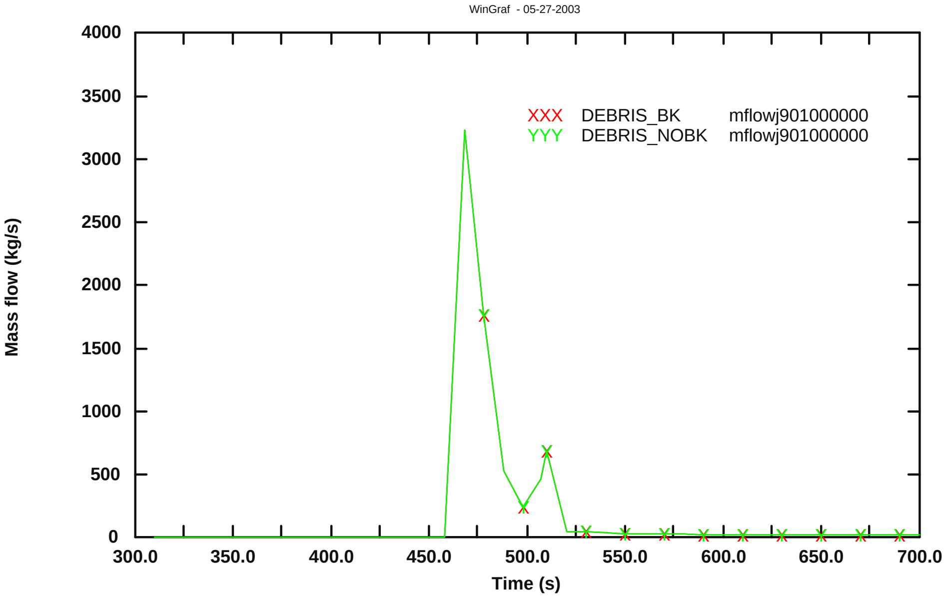

Figure 7.69 - Break mass flow

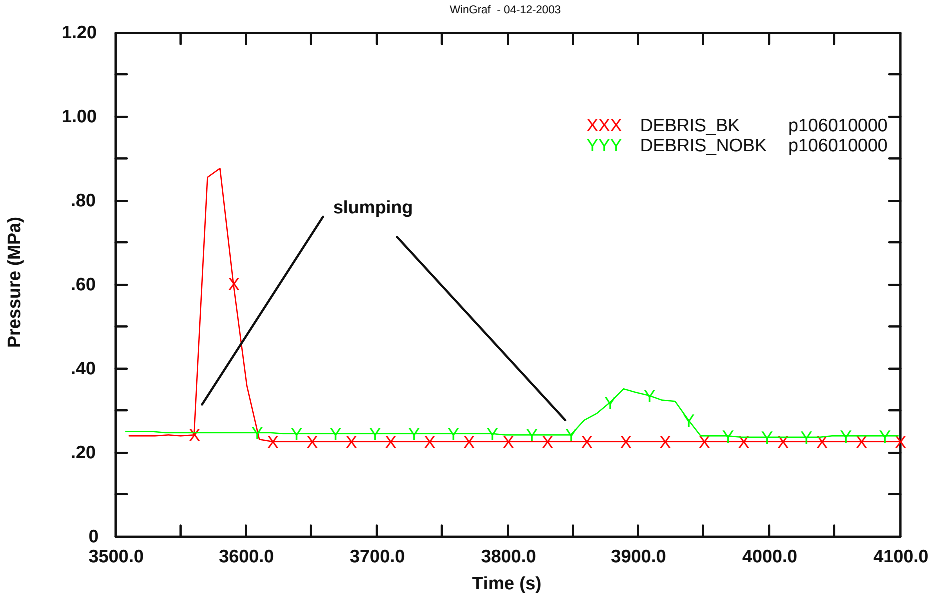

Figure 7.70 - Pressure in the lower plenum at the slumping time in MFCI SCDAP calculations

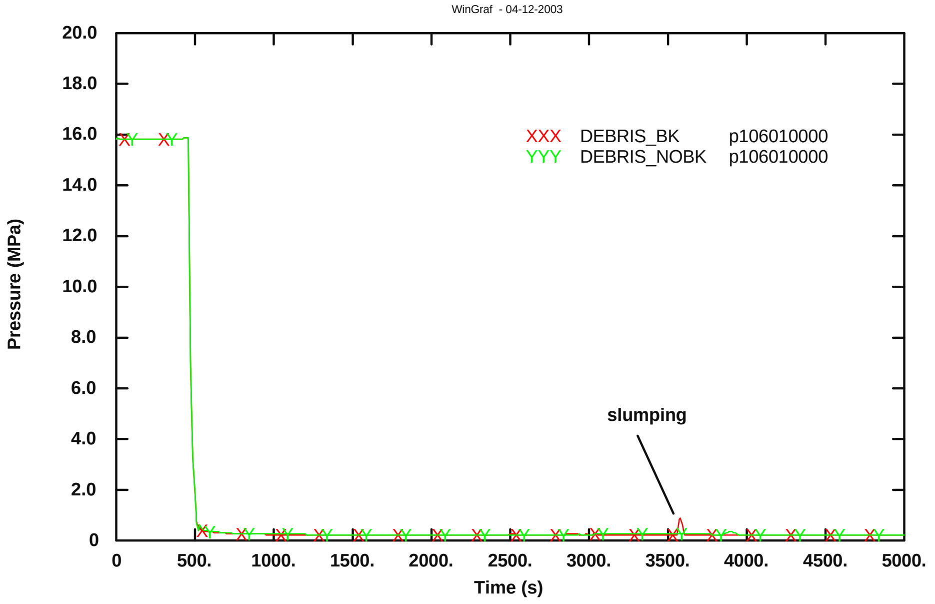

Figure 7.71 - Pressure in the lower plenum in MFCI SCDAP calculations

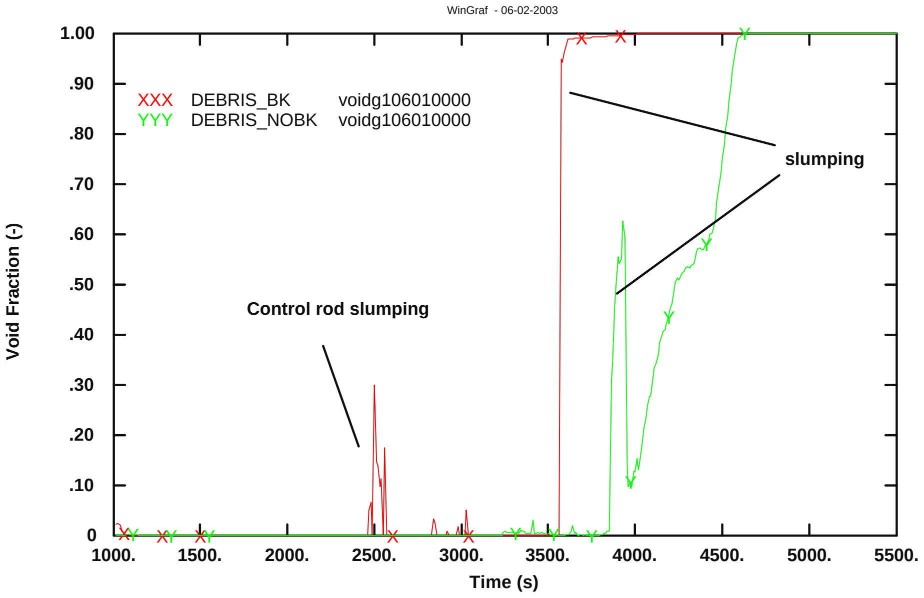

Figure 7.72 - Void fraction in the lower plenum at the slumping time in MFCI SCDAP calculations

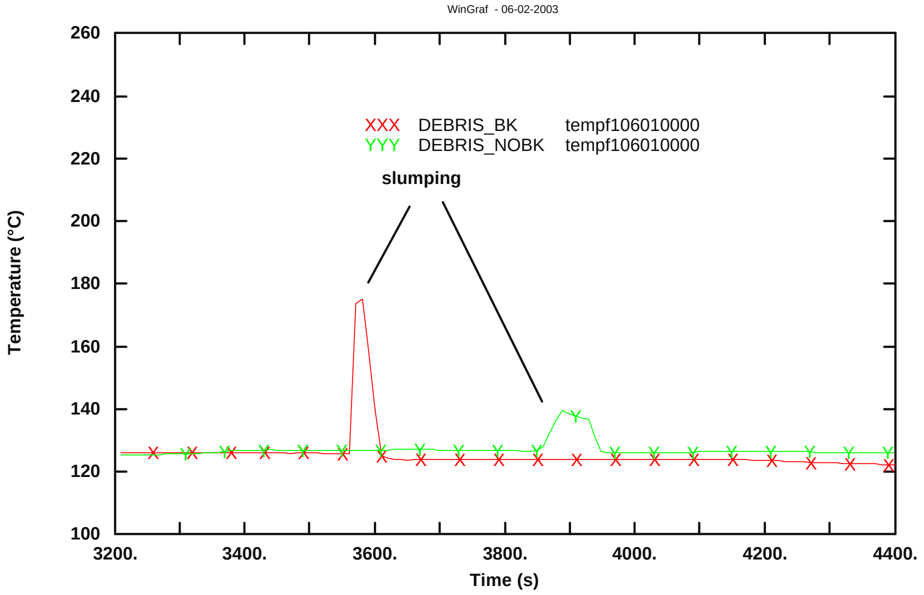

Figure 7.73 - Water temperature in the lower plenum at the slumping time in MFCI SCDAP calculations

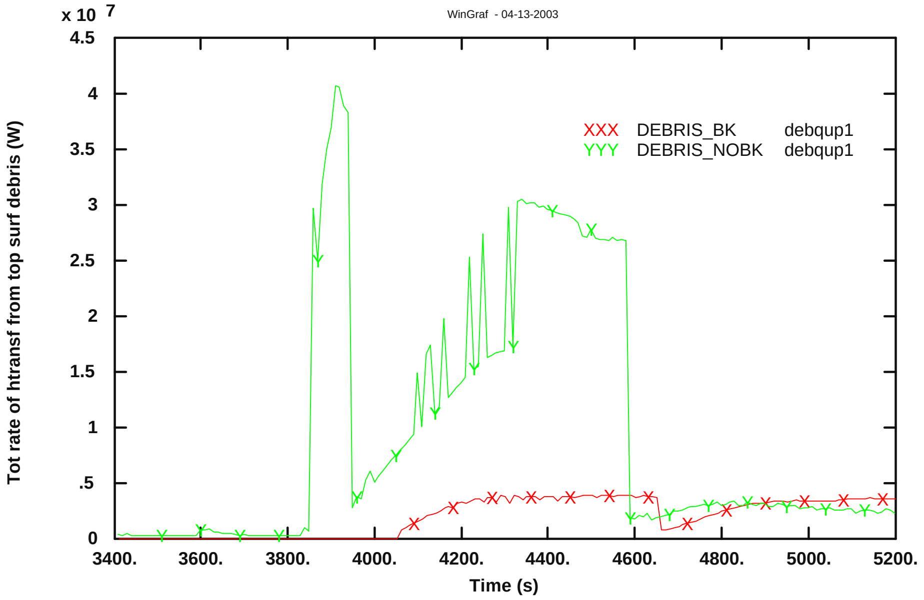

Figure 7.74 - Total rate of heat transfer by convection from top surface of debris (W) in MFCI SCDAP calculations

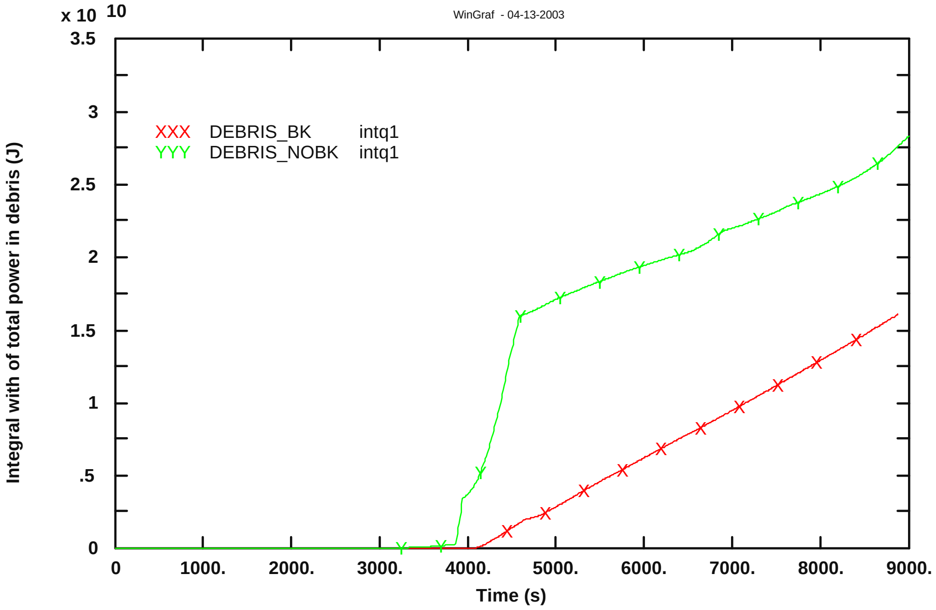

Figure 7.75 - Integral with respect to time of total transfer heat from debris and structural material to fluid at boundaries of debris and structural material (J) in MFCI SCDAP calculations

b) Core degradation, molten pool and slumping occurring. Cases with LPIS injection time = 1150s, 1200s, 1300s, 1500s and 2000s

Some sensibility cases are shown in this chapter in order to study the impact of LPIS. As it will be seen LPIS does not avoid (after core degradation) molten pool formation and subsequent slumping to the lower plenum. Cases are clearly far from core recovery: from case LPIS_1150, injection time 690s after the break (1150s from t = 0) up to LPIS_2000, injection time 1540s after the break (2000s from t = 0).

Base Case DEBRIS_NOBK (without LPIS) is shown in all plots together with the rest in order to verify if a late LPIS injection has similar consequences to a case without LPIS.

Bgmct0 (Figure 7.76) represents maximum temperature in the 5 fuel core components at all axial nodes, so it is an indicator of the hottest point in the core. From the figure it is shown that maximum temperature grows higher in LPIS cases compared to case without LPIS (DEBRIS_NOBK) because LPIS water powers the cladding oxidation producing H_2 at temperatures greater than about 1500K. This oxidation reaction is exothermic producing a lot of energy (586 KJ/mol) that makes maximum core temperature to reach 3000K in few seconds. Temperature decreases when molten pool slumps to lower head.

H_2 production rate (Figure 7.77) is more important in cases in which LIPS water arrives to the core when it has arrived to the threshold temperature for oxidation, about 1500K. Case without LPIS (DEBRIS_NOBK) produces much less H_2 at the beginning because the reaction it is not powered by additional LPIS water. It is also interesting to observe the integral of this quantity, which gives the H_2 accumulated (Figure 7.78).

In LPIS cases molten pool in the core (Figure 7.79, molten pool radius) is formed at about 1600s-1700s except for LPIS at 2000s that is similar to case without LPIS (DEBRIS_NOBK). It seems that LPIS delays molten pool slumping, except for LPIS at 2000s and LPIS at 1300s.

From Figure 7.80 to Figure 7.83 component masses of molten pool that slumped to lower plenum are represented, UO_2, ZrO_2, Zr and Ag. Although it is difficult to calculate exact masses and exact times of slumping, the figures purpose is to give an idea of the principal amounts that form the molten pool. These are principally UO_2 (about 60000-70000 kg), Zr (less than 5000 kg) and ZrO_2 (about 9000 kg). Ag mass (about 2000 kg) represents control material slumping the first. It is deduced that the rest of components (UO_2, ZrO_2, Zr) fall down later in the so-called slumping of molten pool and that once it occurs RELAP5/SCDAP 3.2 considers that almost all molten pool mass slumps. Almost all mass slumped to the lower plenum are present in the liquid phase (Figure 7.84).

From Figure 7.85 to Figure 7.90 the mass amounts are represented case by case. LPIS at 1300s is the case with less mass involved, molten pool is smaller and smaller slumping mass falls, ZrO_2 and Ag masses are similar to the rest. Zr mass is higher than ZrO_2 in all cases, different from what was experimented in the FARO facility, where molten pool was generally simulated with more ZrO_2 % (in mass) than Zr %. The first slump occurs when control material (Ag) falls into the lower plenum.

Figure 7.91 and Figure 7.92 show downcomer water level, which is something like water level in the core region. In the first part of the transient, after the break (460 s) downcomer level decreases quickly in all cases. At about 500s accumulators start to inject water recovering the water leak for some seconds, but it is the effect of LPIS injecting water in every case that recovers core cooling and downcomer level reaches its top. Obviously in case without LPIS (DEBRIS_NOBK) level continues to decrease. Figure 7.92 shows the consequence of the slumping. In case without LPIS (DEBRIS_NOBK) level increases because residual water in the lower plenum is pressed towards the downcomer. In the rest of cases level decreases because voiding produced in the lower plenum is transferred to downcomer.

Figure 7.93 shows void fraction in the lower plenum. Lower plenum is voided in case without LPIS and void fraction reaches 1.0 in few seconds. In the rest of cases the lower plenum is continuously filled up with LPIS water so void fraction oscillates.

Figure 7.94 and Figure 7.95 show pressure and water temperature in the lower plenum. Case without LPIS is almost in saturation conditions. The rest of cases are in subcooled conditions due to the LPIS that injects subcooled water into the vessel. When slumping occurs all cases reach saturation temperature in the lower plenum. Pressure at the moment of the slumping reaches (from 2.5 bar) about 4-5 bar in all cases.

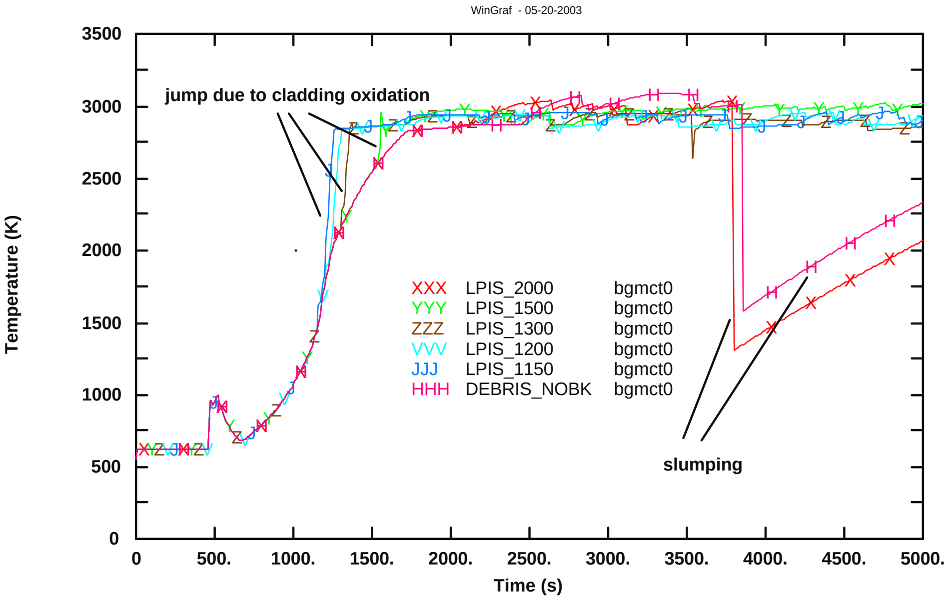

Figure 7.76 - Maximum core temperature in LPIS SCDAP calculations

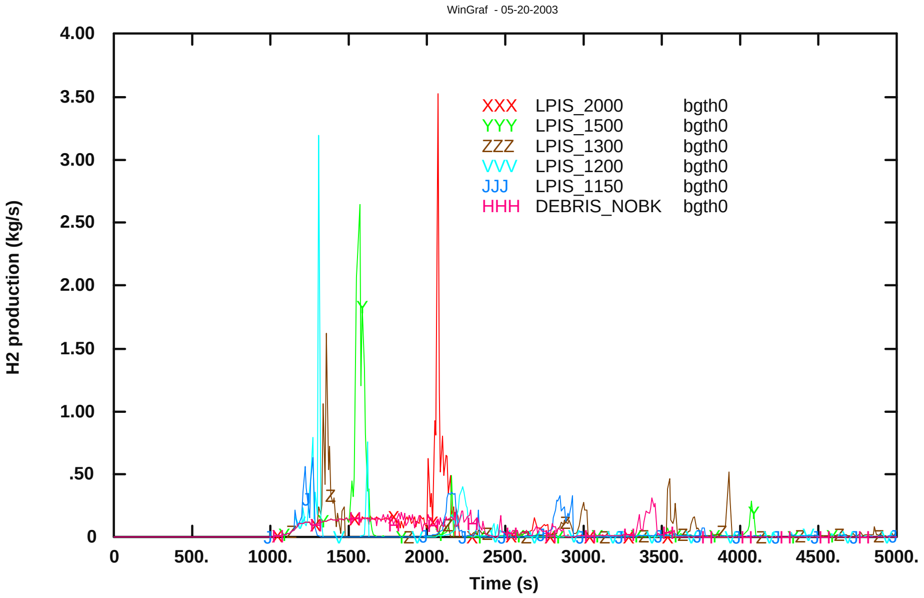

Figure 7.77 - H_2 production rate in LPIS SCDAP calculations

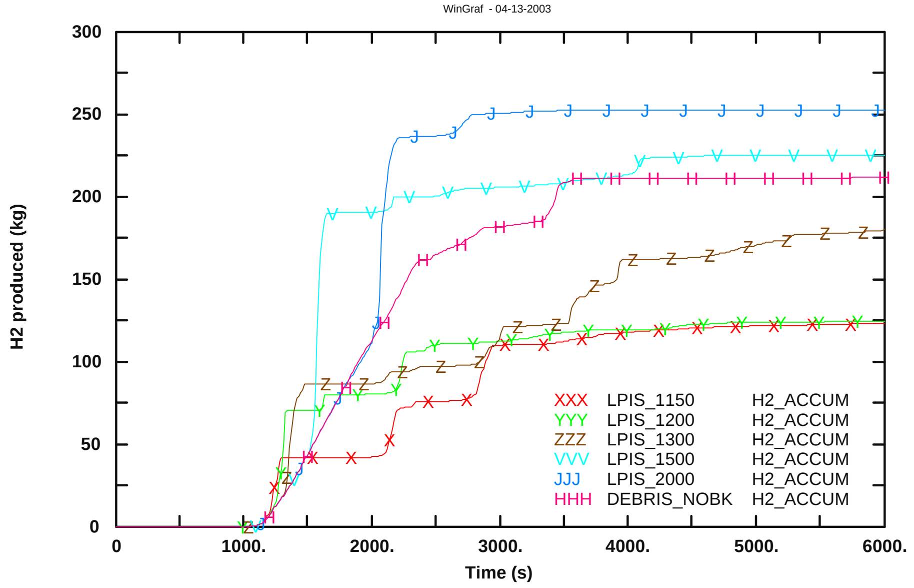

Figure 7.78 - H_2 accumulated in LPIS SCDAP calculations

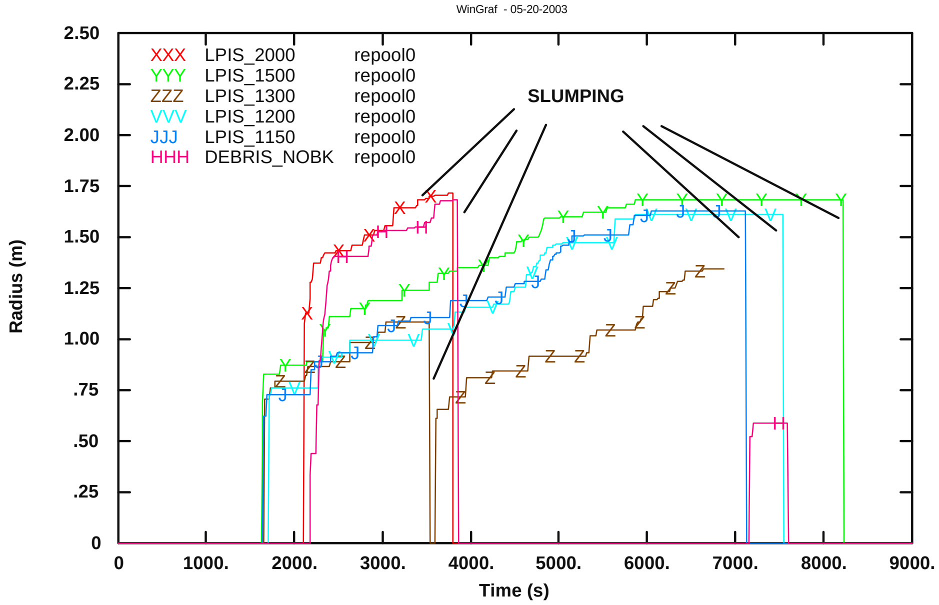

Figure 7.79 - Radius of molten pool in LPIS SCDAP calculations

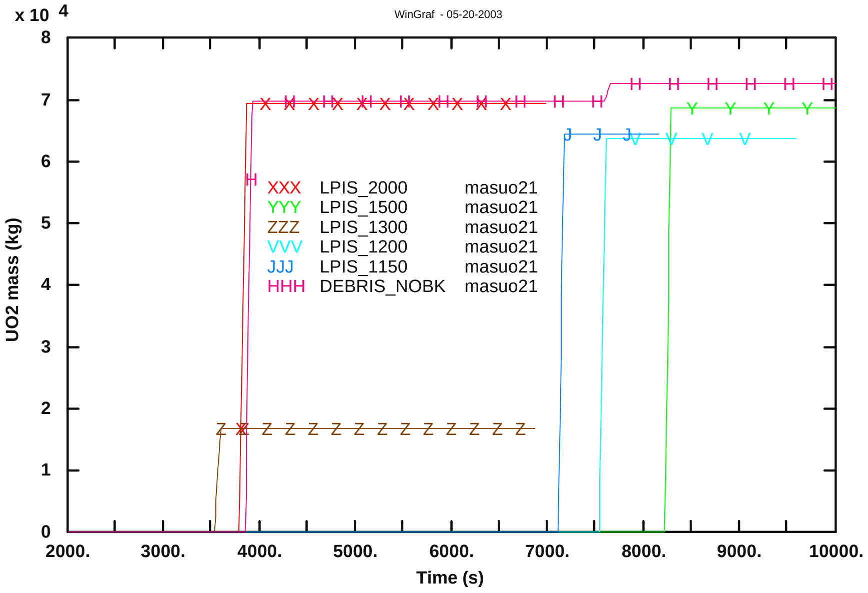

Figure 7.80 - Total UO_2 mass slumped in lower plenum in LPIS SCDAP calculations

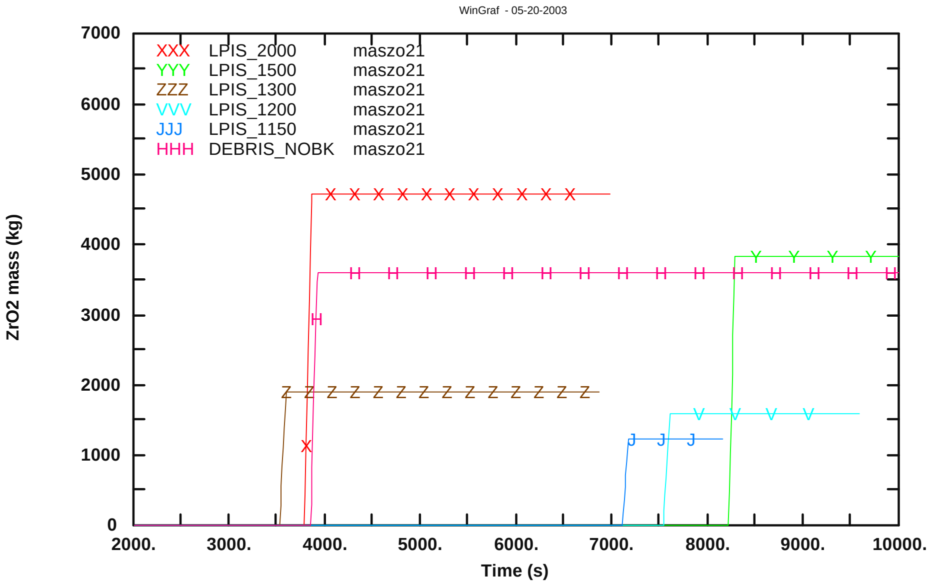

Figure 7.81 - Total ZrO_2 mass slumped in lower plenum in LPIS SCDAP calculations

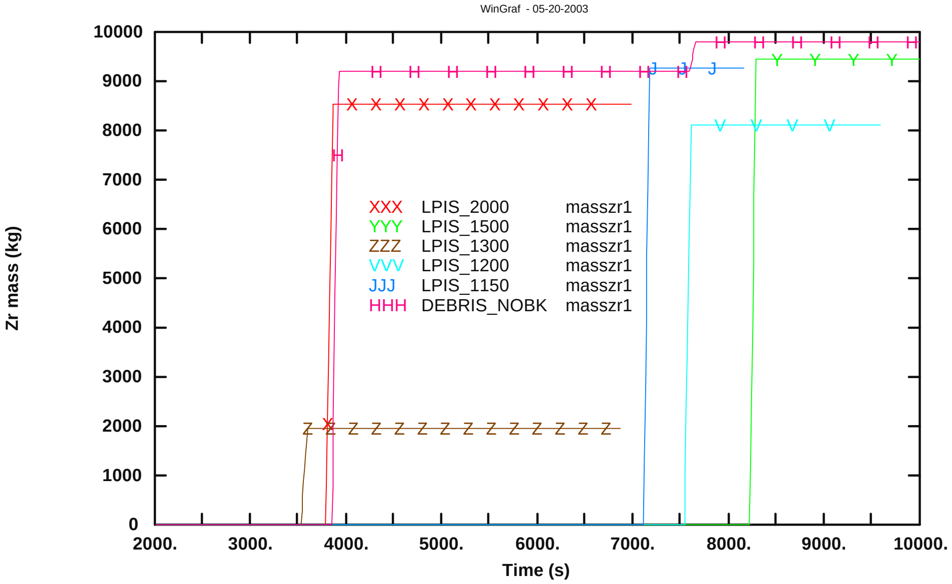

Figure 7.82 - Total Zr mass slumped in lower plenum in LPIS SCDAP calculations

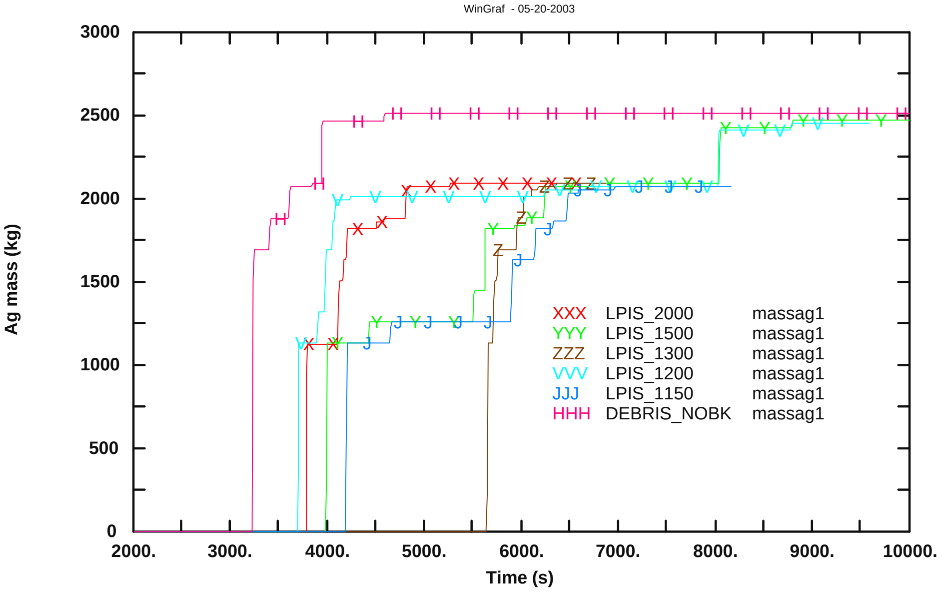

Figure 7.83 - Total Ag mass slumped in lower plenum in LPIS SCDAP calculations

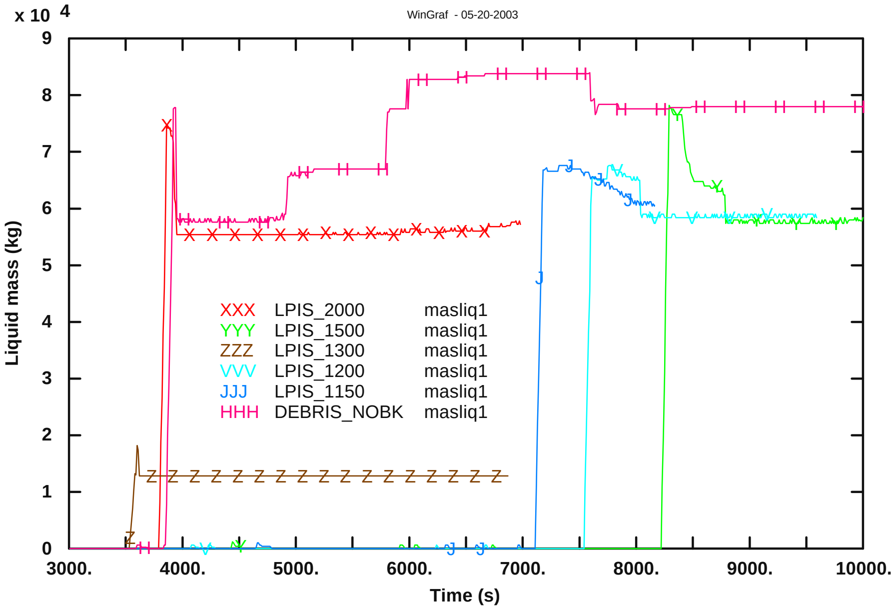

Figure 7.84 - Total Liquid mass in lower plenum in LPIS SCDAP calculations

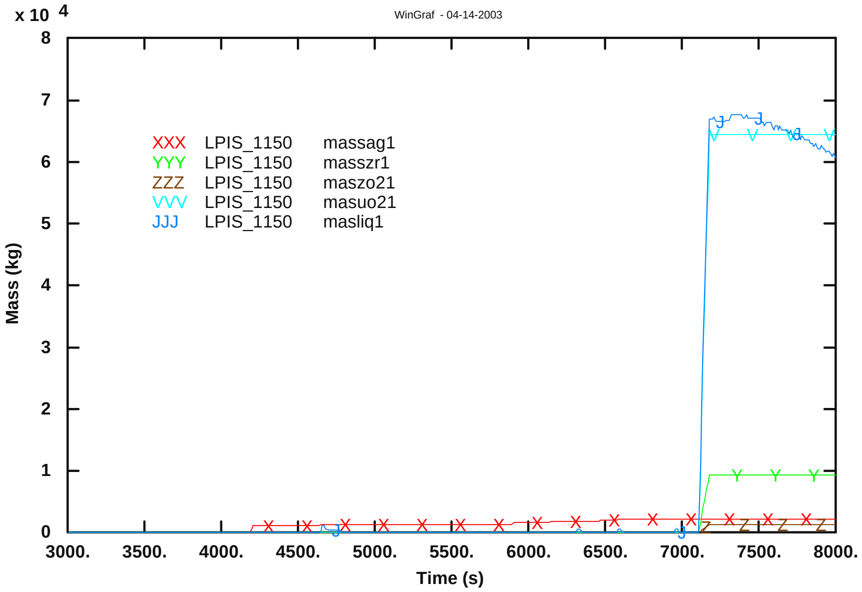

Figure 7.85 - Mass distribution in lower plenum in case LPIS_1150

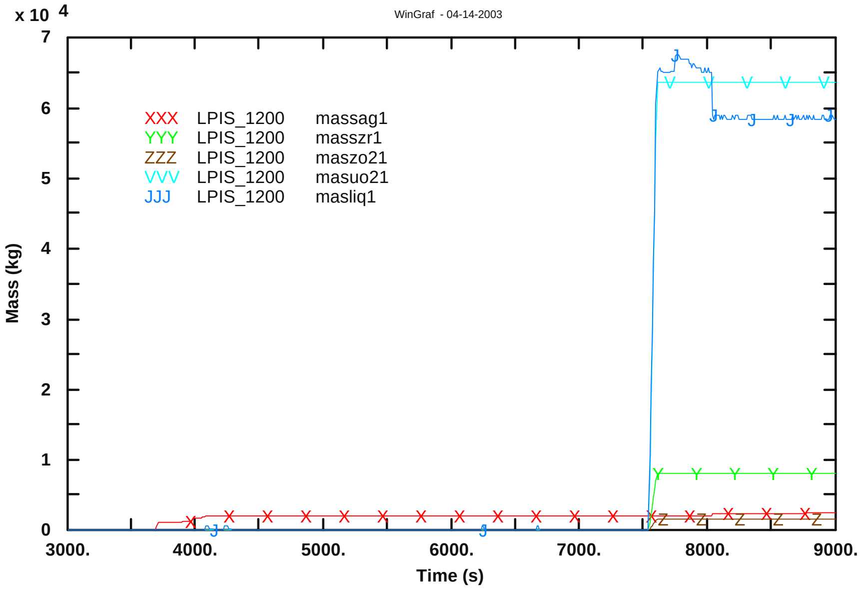

Figure 7.86 - Mass distribution in lower plenum in case LPIS_1200

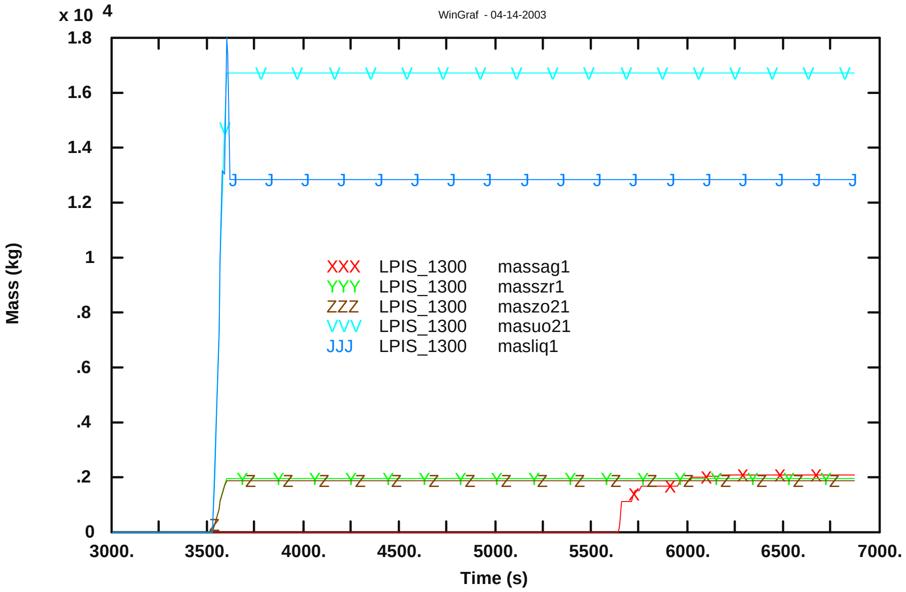

Figure 7.87 - Mass distribution in lower plenum in case LPIS_1300

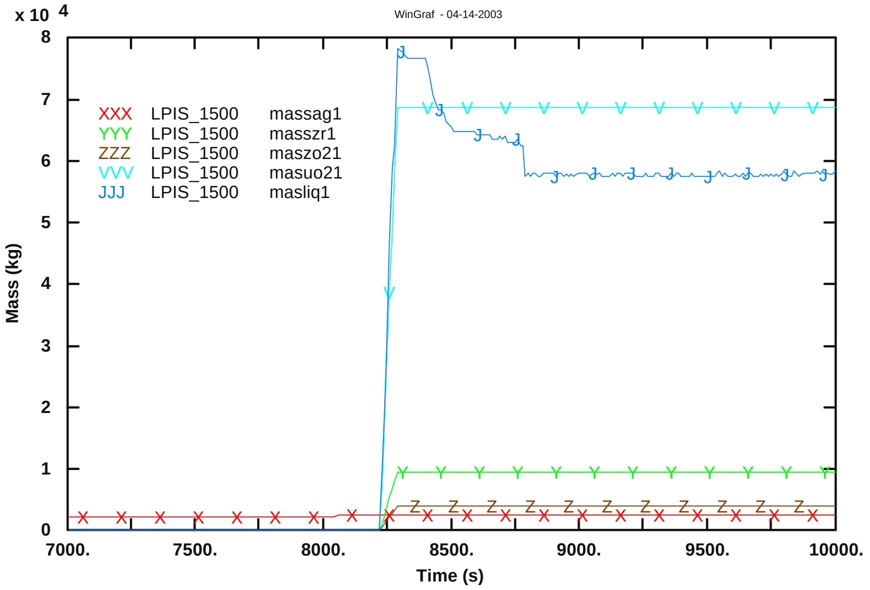

Figure 7.88 - Mass distribution in lower plenum in case LPIS_1500

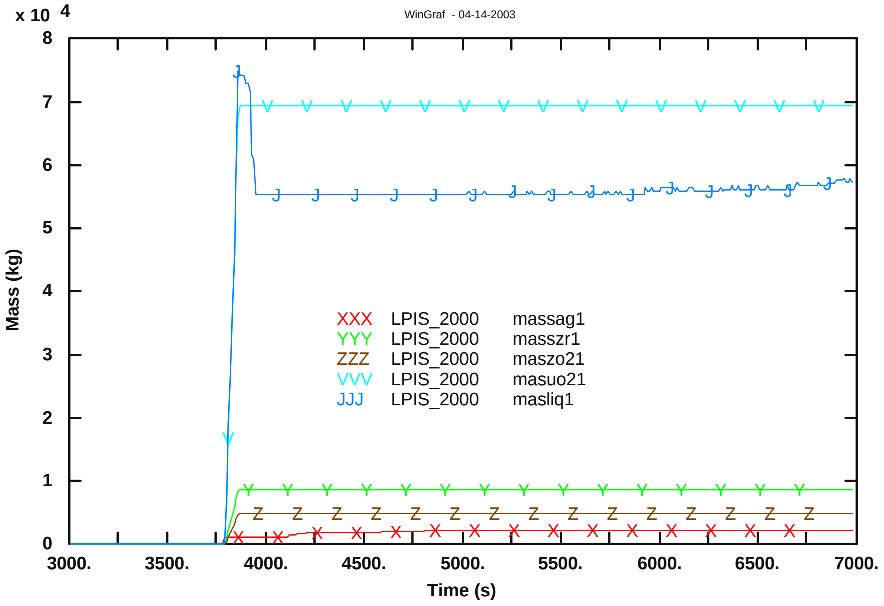

Figure 7.89 - Mass distribution in lower plenum in case LPIS_2000

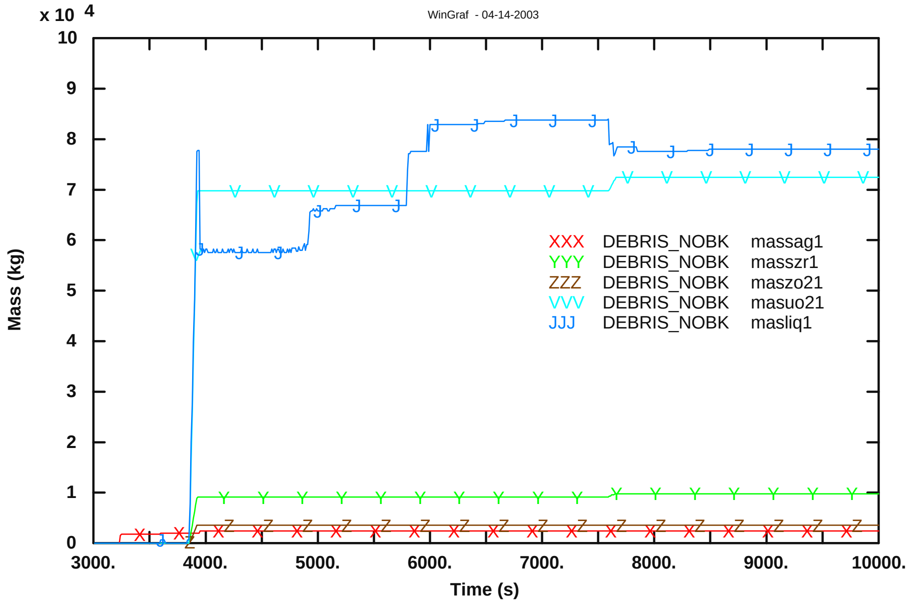

Figure 7.90 - Mass distribution in lower plenum in case DEBRIS_NOBK

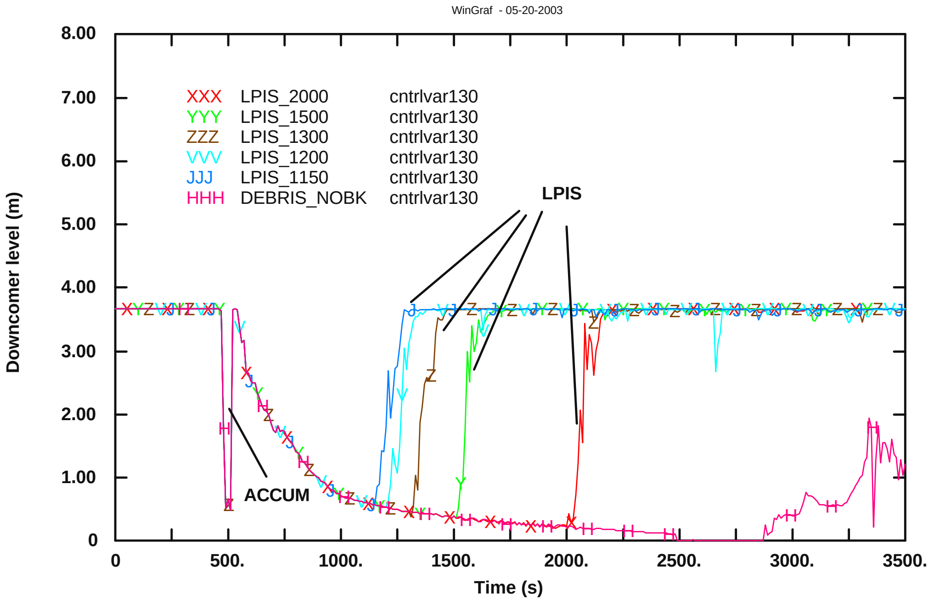

Figure 7.91 - Downcomer level before slumping in LPIS SCDAP calculations

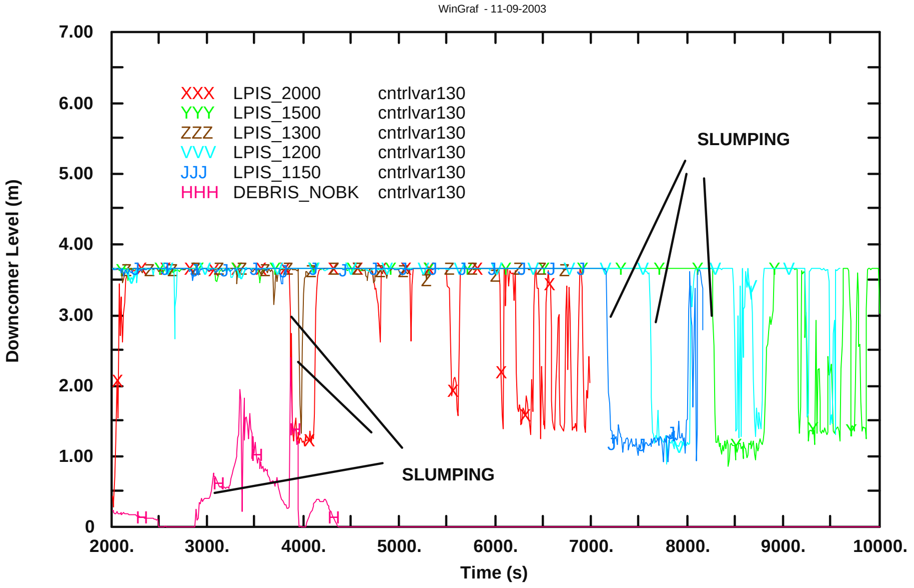

Figure 7.92 - Downcomer level after slumping in LPIS SCDAP calculations

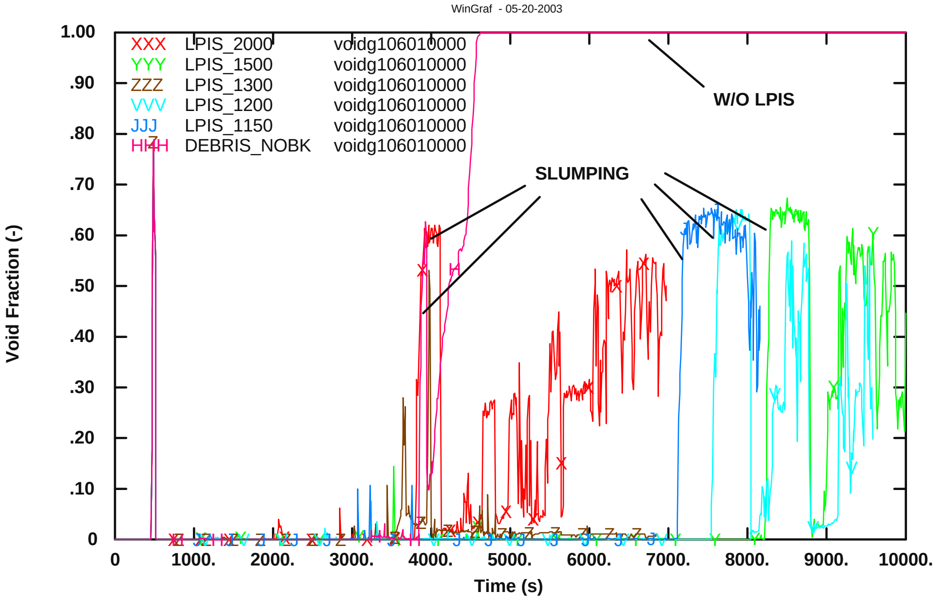

Figure 7.93 - Void fraction in the lower plenum in LPIS SCDAP calculations

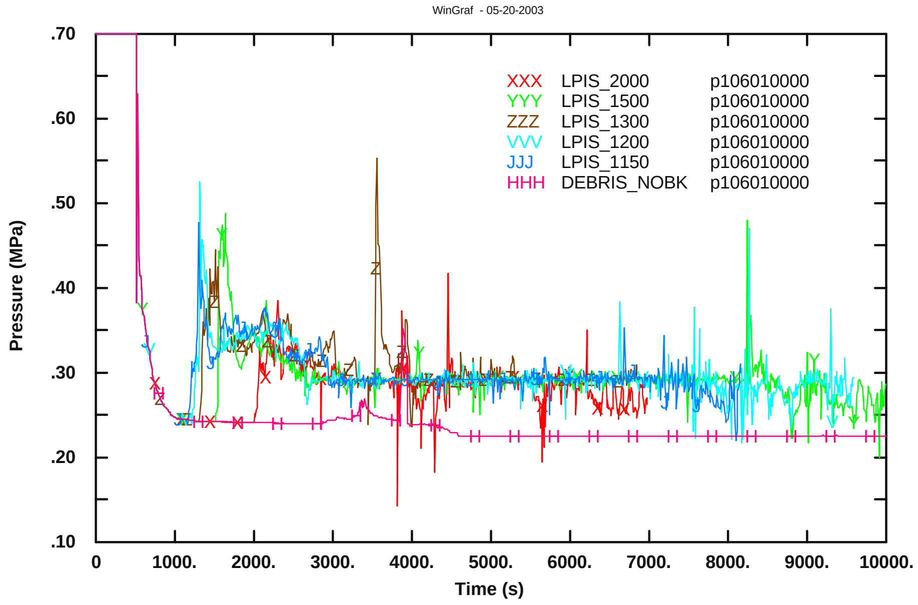

Figure 7.94 - Pressure in the lower plenum in LPIS SCDAP calculations

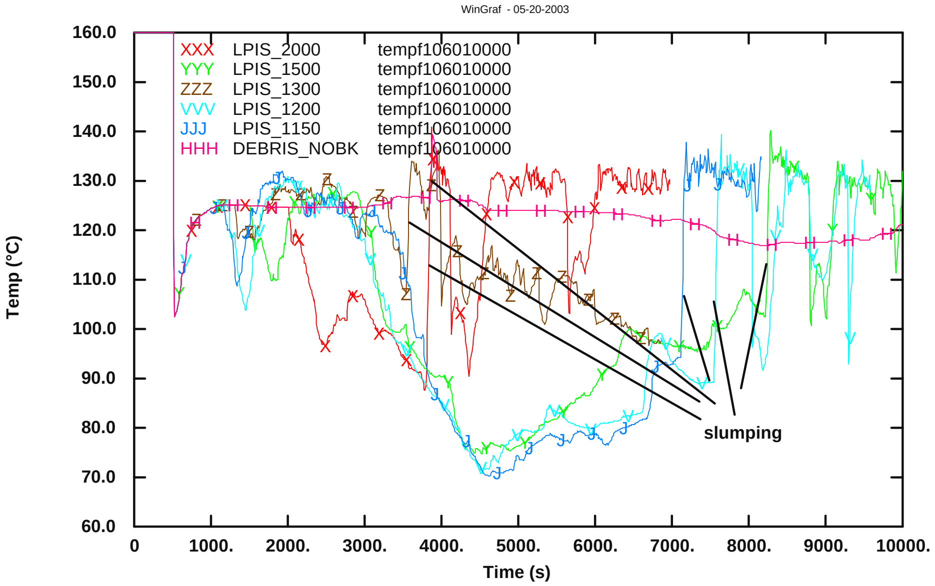

Figure 7.95 - Water temperature in the lower plenum in LPIS SCDAP calculations

c) Core degradation, molten pool and slumping occurring. Cases with LPIS injection time = 1120s, 1121s and 1125s

These three cases are closer to the core recovery. They are presented together (LPIS_1120, LPIS_1121 and LPIS_1125) in order to discuss the transient evolution after the LPIS injection time. Base Case DEBRIS_NOBK (without LPIS) is shown in all plots together with the rest.

Maximum core temperature (Figure 7.96) increases due to H_2 production at temperatures greater than about 1500K, powered by LPIS water. Although LPIS reaches to stop temperature increase at the beginning, the core recovery does not take place. The second increase (in cases LPIS_1120, LPIS_1121) at about 1600s is due to node covering by molten pool. Later on core degradation continues up.

Since bgmct0 quantity represents maximum temperature in the 5 fuel core components at all axial nodes, in case LPIS_1120 the exact maximum temperature (Figure 7.97) corresponds to axial position 9 fuel components 5 and 7, that are in the hydrodynamic channels 112 and 115 respectively (Figure 7.64), both in the radial external point. Temperature increase at about 1200s in component 7, axial position 9, is due to H_2 local production, as it can be observed from Figure 7.98. Figure 7.99 shows damage levels in these components, the damage starts when ballooning of cladding geometry, second step is fragmentation and they finally become molten pool.

In the same way for case LPIS_1121 maximum temperature (Figure 7.100) corresponds to radial external point fuel component 7, axial position 9 and fuel component 9, axial position 8. Those are included in the hydrodynamic channels 115 and 113 respectively. Figure 7.101 shows damage levels in these components, high temperature increase up to about 3000K in these components corresponds when they become molten pool.

H_2 production rate (Figure 7.102) as previous cases shows high peak production due to LPIS water injection.

Radius of molten pool (Figure 7.103) shows that slumping is delayed in cases LPIS_1120 and LPIS_1125 up to about 10000s compared to case without LPIS, which occurs at about 3900s as in LPIS_1121 case.

From Figure 7.104 to Figure 7.108 composition masses of molten pool slumped to the lower plenum are presented in all cases. LPIS_1121 case shows much less mass in the slumped molten pool than the rest.

Figure 7.109 shows downcomer water level, after the break, downcomer level decreases quickly in all cases. It is shown the effect of LPIS injecting water in every case that recovers core cooling and downcomer level reaches its top. After slumping level decreases in LPIS cases because voiding produced in the lower plenum is transferred to downcomer.

Figure 7.110 shows void fraction in the lower plenum. Lower plenum is voided in case without LPIS in few seconds. In LPIS_1120 and LPIS_1125 cases the lower plenum is continuously filled up with LPIS water so void fraction oscillates. In LPIS_1121 case only a small amount of mass slumps to the lower plenum so void fraction peak is also small.

Figure 7.111 and Figure 7.112 show pressure and water temperature in the lower plenum. When slumping occurs all cases reach saturation temperature in the lower plenum. Pressure jump at the time of the slumping reaches (from 3 bar) about 3.5-4 bar in all cases.

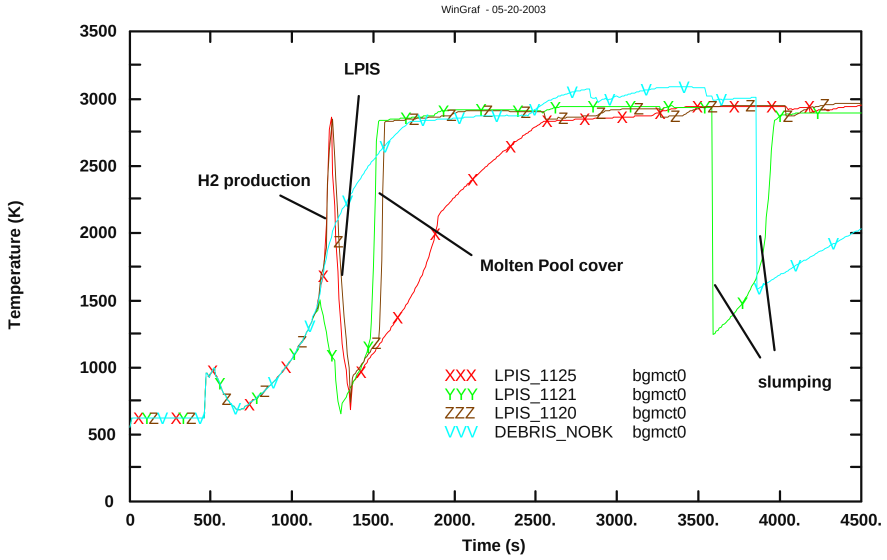

Figure 7.96 - Maximum core temperature in LPIS SCDAP calculations

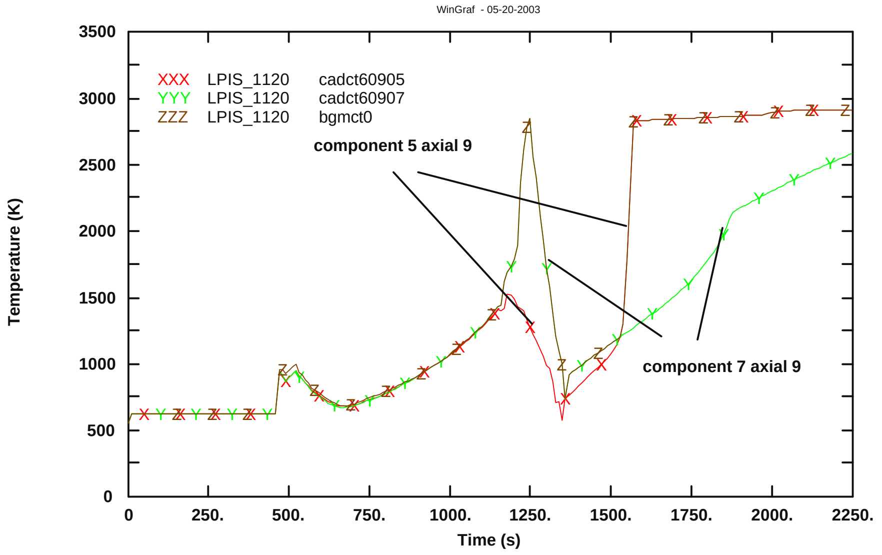

Figure 7.97 - Maximum core temperature in LPIS_1120 case

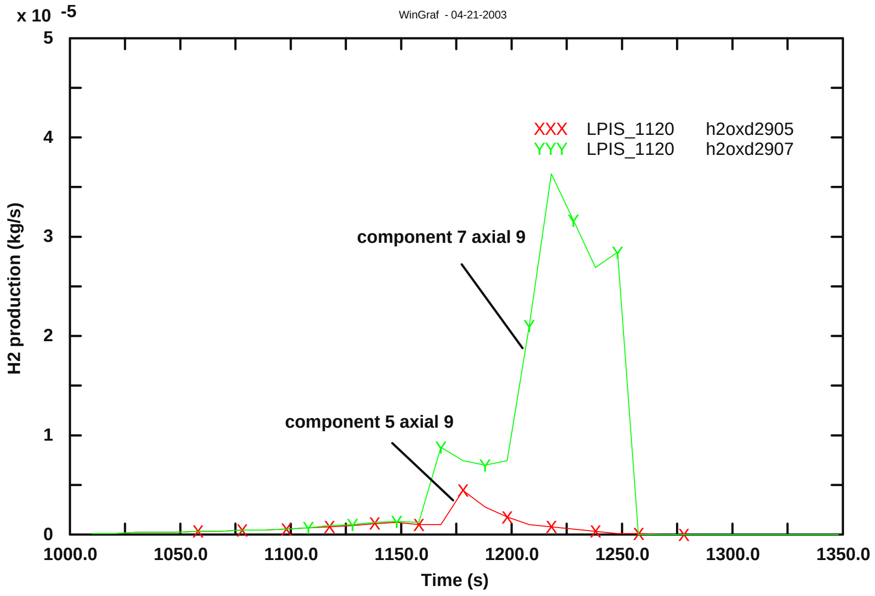

Figure 7.98 - Local H_2 production rate in case LPIS_1120

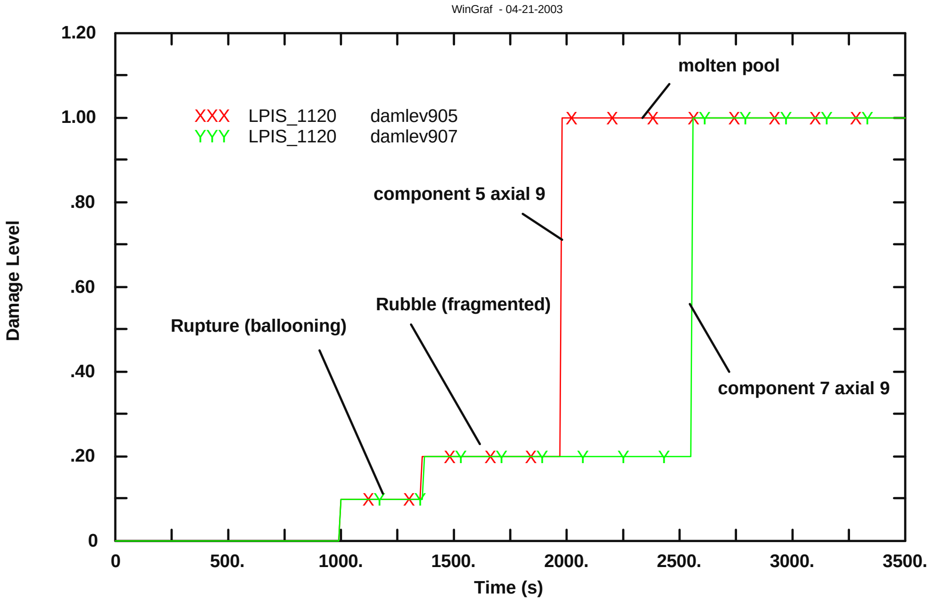

Figure 7.99 - Damage state in components 5 and 7 in LPIS_1120 case

<u>DAMLEV Damage state:</u>
0.0 Intact geometry
0.1 Rupture due to ballooning
0.2 Rubble (fragmented)
0.4 Cohesive debris
1.0 Molten pool

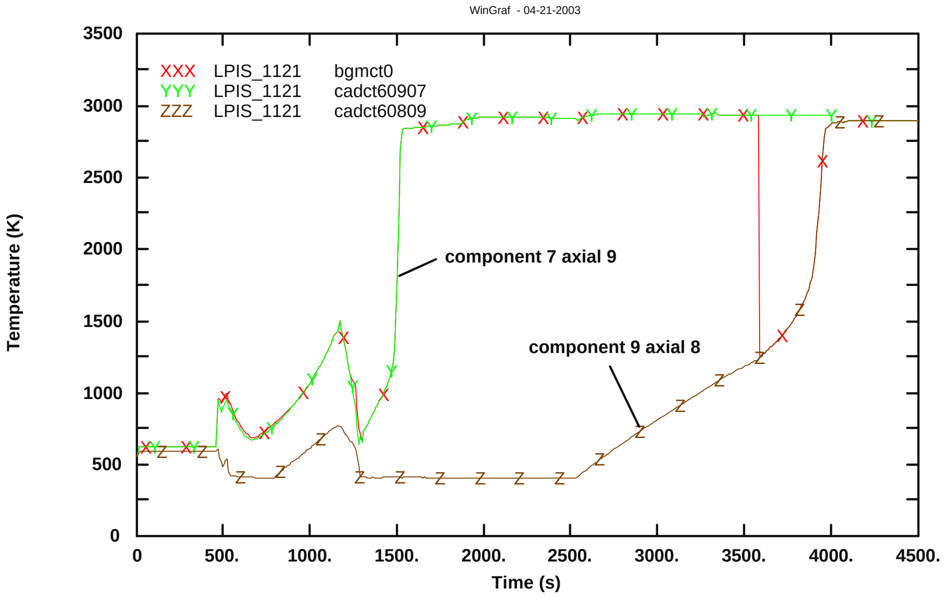

Figure 7.100 - Maximum core temperature in LPIS_1121 case

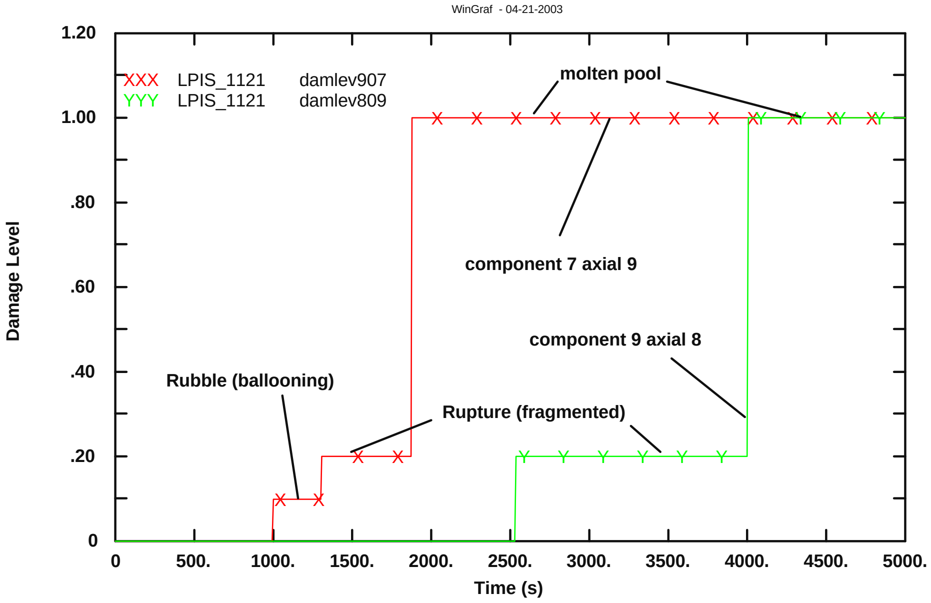

Figure 7.101 - Damage state in components 7 and 9 in LPIS_1121 case

<u>DAMLEV Damage state:</u>
0.0 Intact geometry
0.1 Rupture due to ballooning
0.2 Rubble (fragmented)
0.4 Cohesive debris
1.0 Molten pool

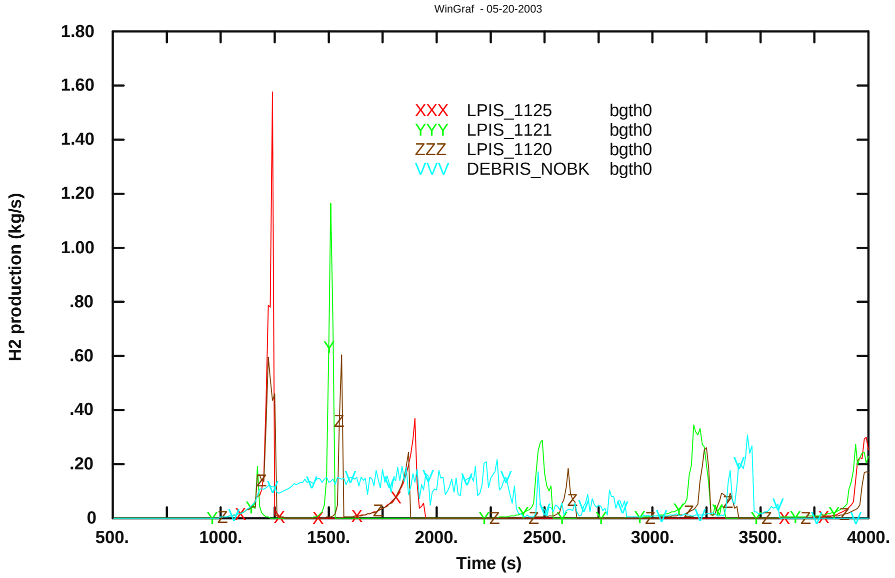

Figure 7.102 - H_2 production rate in LPIS SCDAP calculations

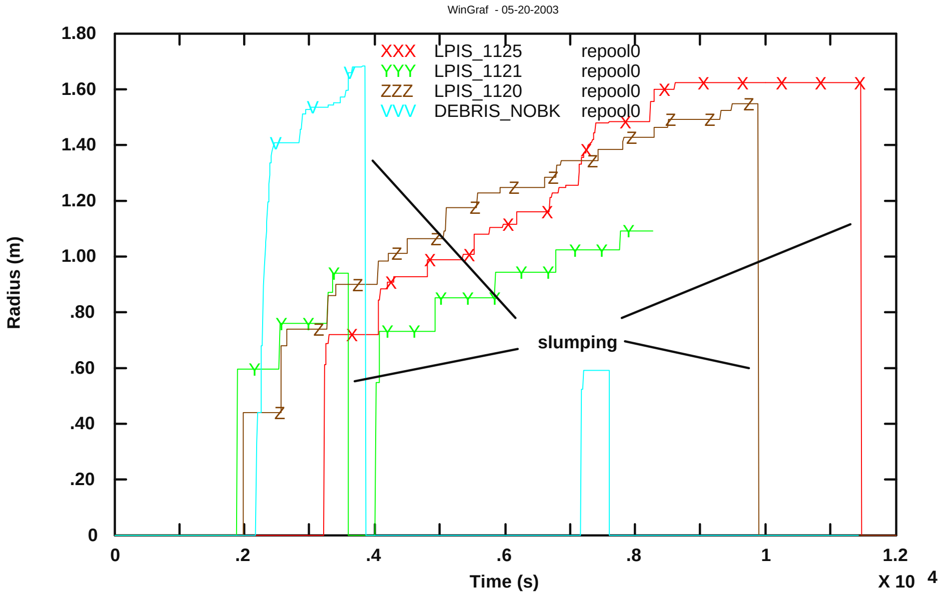

Figure 7.103 - Radius of molten pool in LPIS SCDAP calculations

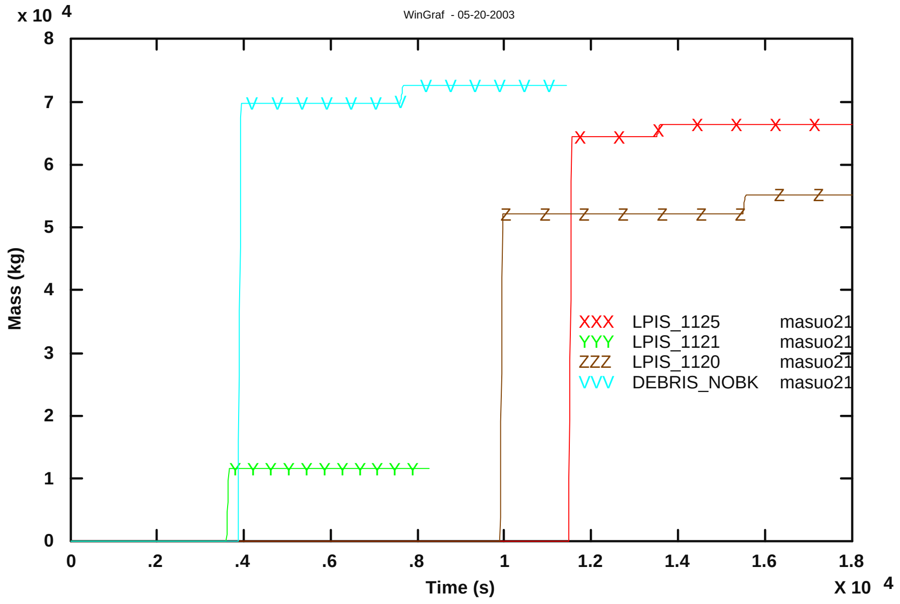

Figure 7.104 - Total UO_2 mass slumped in lower plenum in LPIS SCDAP calculations

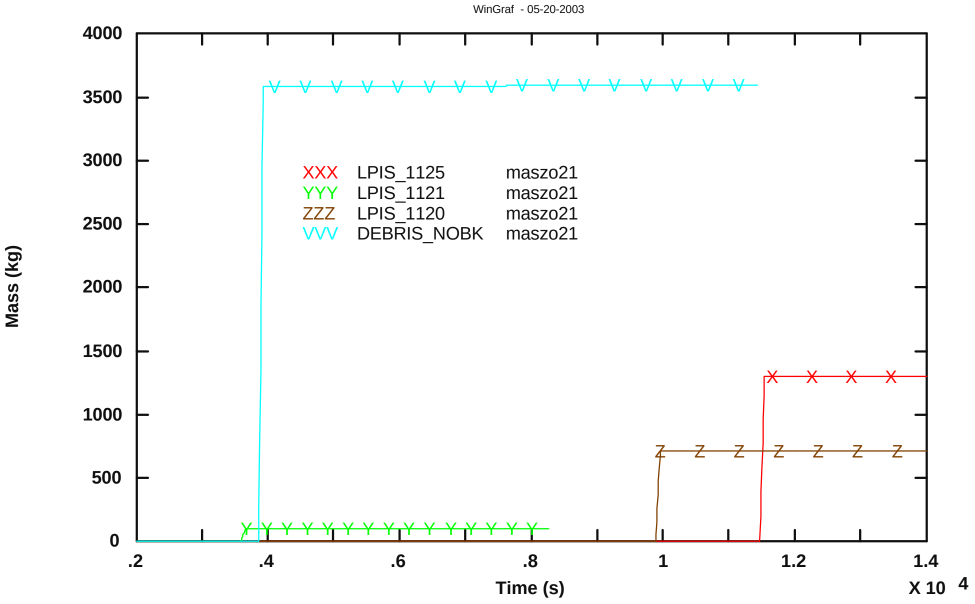

Figure 7.105 - Total ZrO_2 mass slumped in lower plenum in LPIS SCDAP calculations

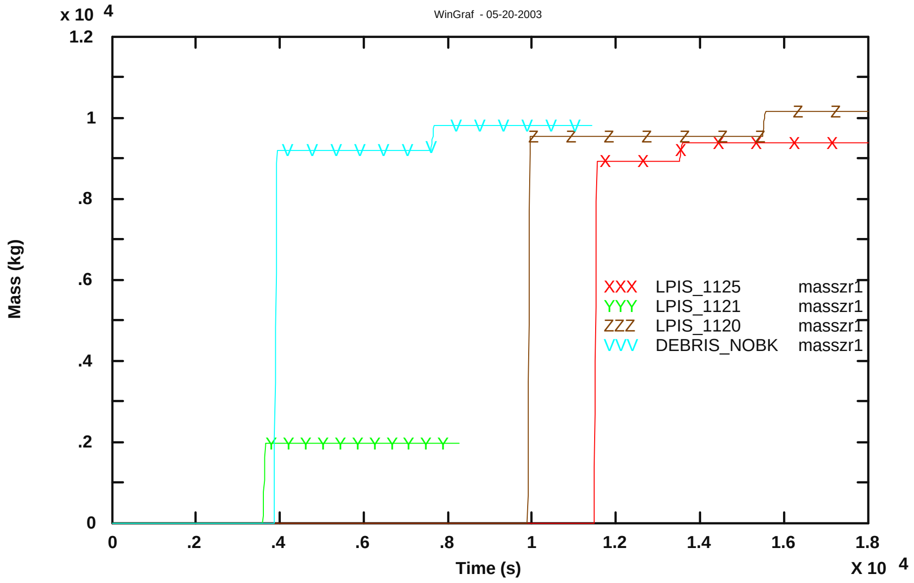

Figure 7.106 - Total Zr mass slumped in lower plenum in LPIS SCDAP calculations

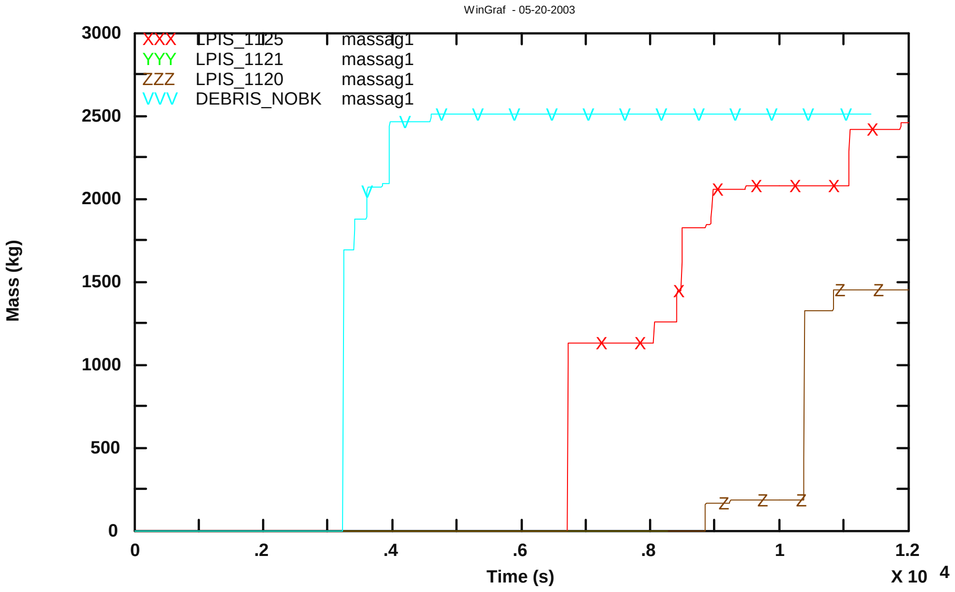

Figure 7.107 - Total Ag mass slumped in lower plenum in LPIS SCDAP calculations

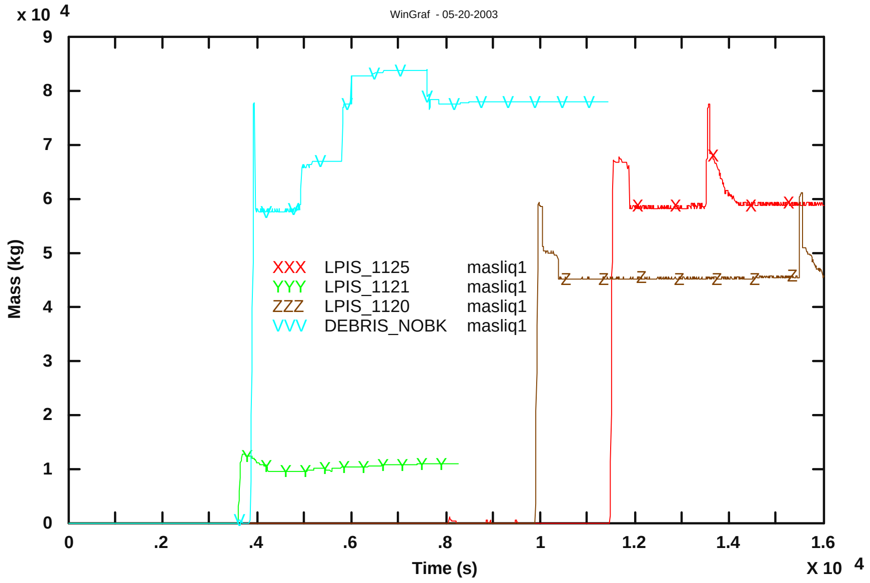

Figure 7.108 - Total Liquid mass in lower plenum in LPIS SCDAP calculations

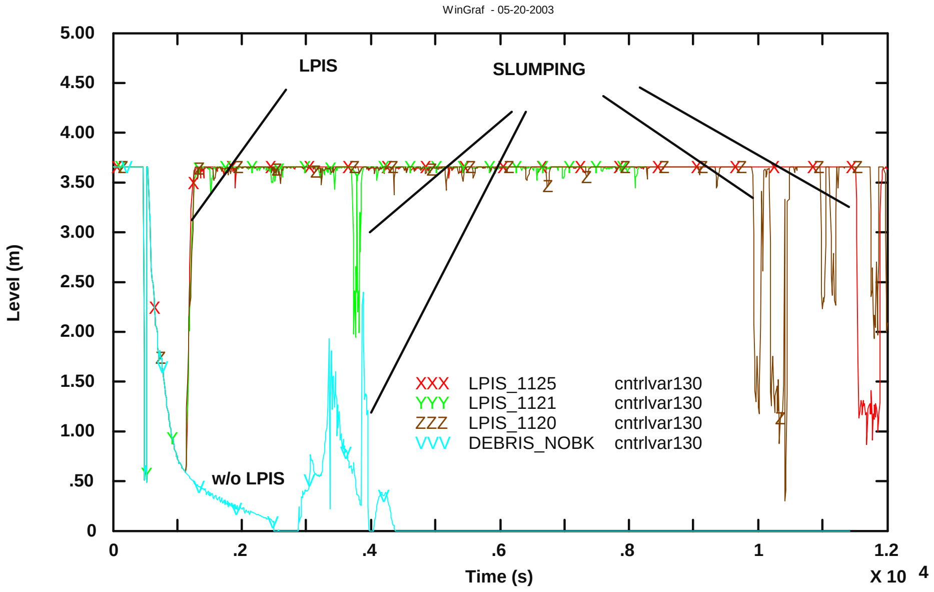

Figure 7.109 - Downcomer level in LPIS SCDAP calculations

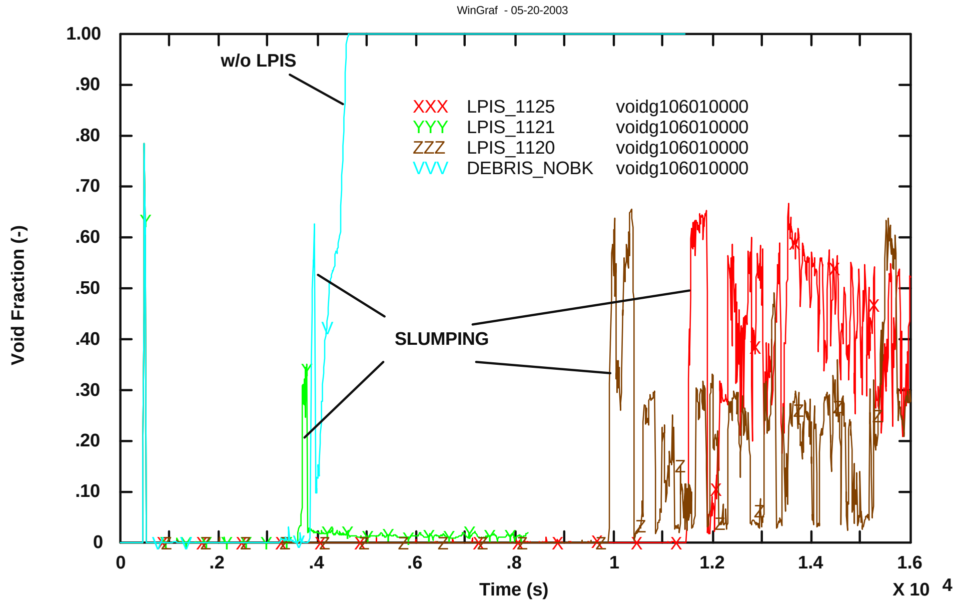

Figure 7.110 - Void fraction in the lower plenum in LPIS SCDAP calculations

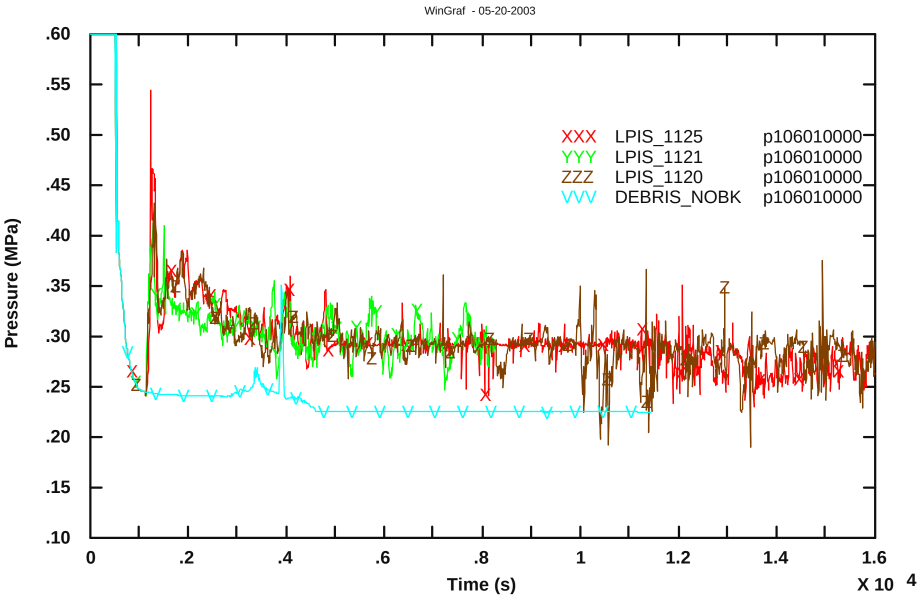

Figure 7.111 - Pressure in the lower plenum in LPIS SCDAP calculations

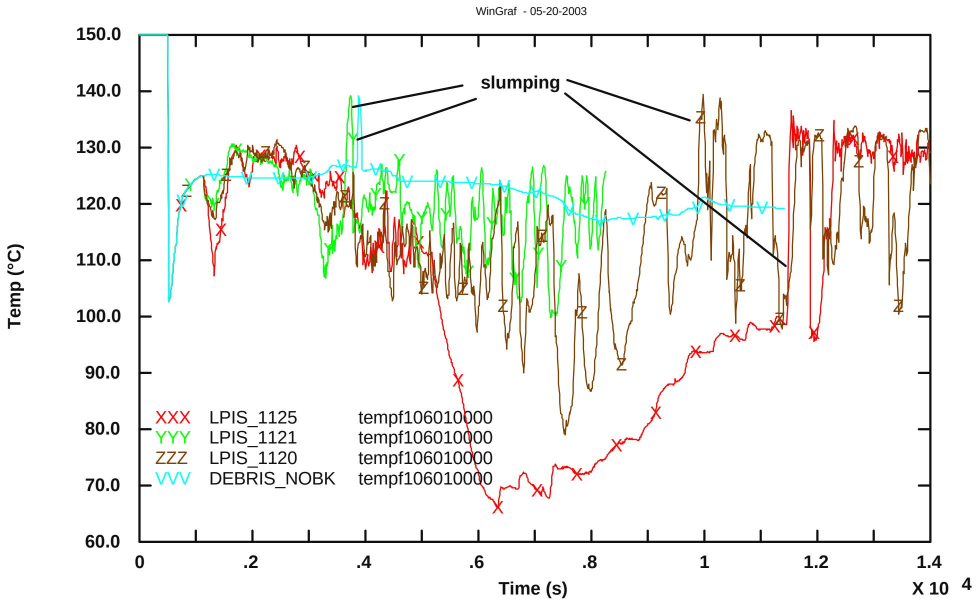

Figure 7.112 - Water temperature in the lower plenum in LPIS SCDAP calculations

d) Core degradation, molten pool and slumping avoided. Cases with LPIS injection time = 900s, 1100s, 1110s, 1115s and 1119s

In all these cases core is recovered due to the core emergency LPIS system, as it is observed in Figure 7.113. Only axial nodes 9 of components 1 to 7 in LPIS_1119 suffer break due to clad ballooning (Figure 7.114). H_2 is produced (Figure 7.115 and Figure 7.116) due to water injected but it is much less than in the core unrecovered cases.

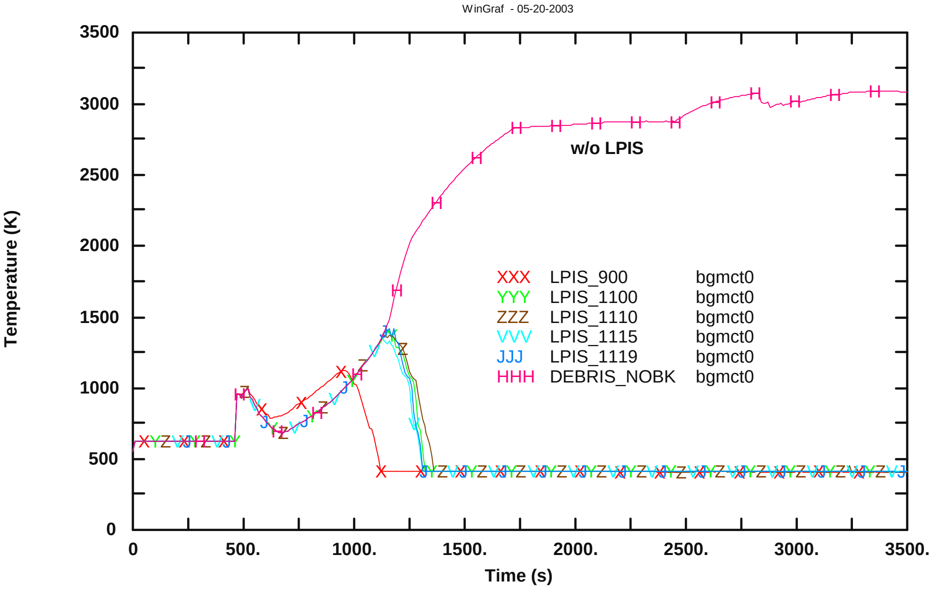

Figure 7.113 - Maximum core temperature in LPIS SCDAP calculations

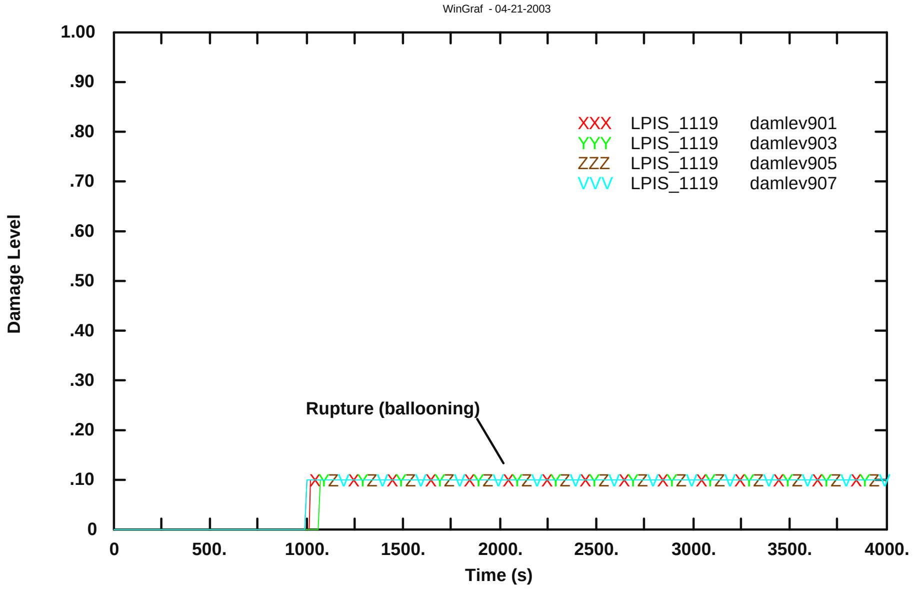

Figure 7.114 - Damage state in components 1, 3, 5 and 7 in LPIS_1119 case

<u>DAMLEV Damage state:</u>
0.0 Intact geometry
0.1 Rupture due to ballooning
0.2 Rubble (fragmented)
0.4 Cohesive debris
1.0 Molten pool

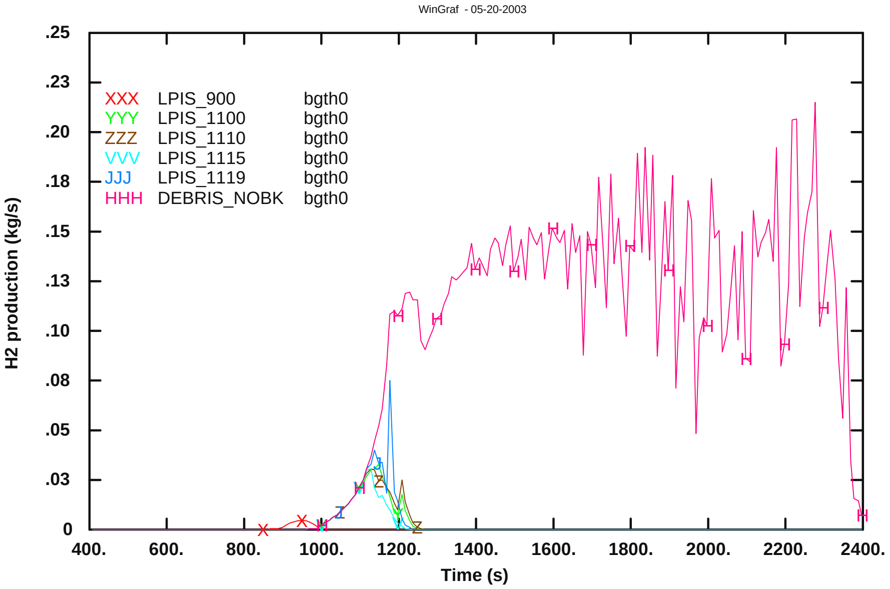

Figure 7.115 - H_2 production rate in LPIS SCDAP calculations

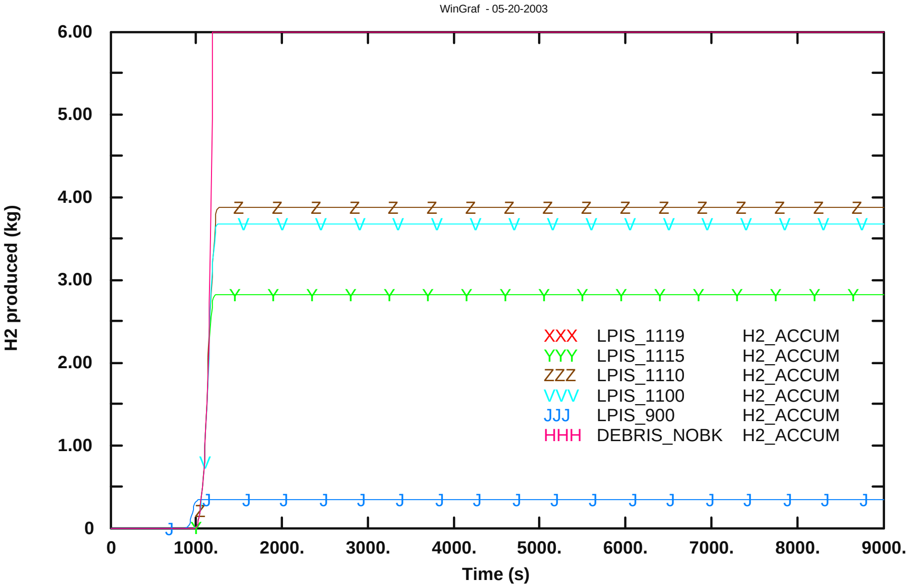

Figure 7.116 - H_2 accumulated in LPIS SCDAP calculations

7.5.6. INITIAL CONDITIONS FOR A MFCI DETAILED STUDY

From the performed RELAP5/SCDAP 3.2 calculations it is possible to obtain the conditions (system pressure, coolant temperature, molten mass temperature, molten mass composition, water level in the lower plenum, etc.) just before the molten pool slumping towards the lower plenum. These conditions can be used as initial conditions in a specific MFCI code input (as JRC-COMETA [6]) so a detailed MFCI study could be later performed.

Figure 7.117, Figure 7.118 and Figure 7.119 show volume, liquid and UO_2 mass in core region at the molten pool slumping time in all performed calculations, in which core degradation leads to a molten pool. Data have been retrieved from RELAP5/SCDAP 3.2 output files, that give every print out time the status, temperatures, pressures, mass components, etc. of the degraded core region.

Table 7.11 presents some quantities of cases DEBRIS_NOBK (Base case, without LPIS), LPIS_1120 and LPIS_1300 because they are the most representative. LPIS_1300 is different from the common trend, with very small molten pool mass. The last column shows system conditions used in the FARO melt fuel coolant interaction experiment Test L-11, where 151 kg of molten melt at 2800 K were poured in a pool of water at 4.9 MPa and saturation temperature.

Total mass of melt in the Base case is about 80000 kg, 69710 kg of which being UO_2, 3586 kg ZrO_2 and 9191 kg Zr. In general total mass or total volume of molten pool varies from about 60000 kg in the case with lower mass up to 80000 kg in the Base case. Melt mass is in calculated cases constituted most of UO_2 and Zr, FARO Tests were in general performed with a mixture of about 80% UO_2 and 20% ZrO_2, that it is a little different from results obtained in the proportion of Zr and ZrO_2. Melt mass temperature is similar in all cases about 2900 K. System pressure, about 0.2 MPa is result of LOCA depressurization.

It seems from figures that the effect of LPIS delays slumping of the molten pool from about 1 hour in the Base case up to about 11000s (3 hours) in case LPIS_1125, another effects are less molten mass produced and some degrees of subcooling of the residual water in the lower plenum. Cases LPIS_1121 and LPIS_1300 are far from the common trend, with early slumping time and small molten pool, reasons of the early slumping are not yet well identified and may be related to the large degree of uncertainty of the slumping time with RELAP5/SCDAP 3.2 code.

Specific MFCI calculation will also be useful to compare some quantities after slumping time, as lower plenum pressure, temperature or void fraction, but these detailed calculation are beyond the objectives of the presented study.

	Without LPIS BASE	**LPIS at 1300s**	**LPIS at 1120s**	**FARO Test L-11**
Mass UO_2 (kg)	69710	16700	51980	115
Mass ZrO_2 (kg)	3586	1891	707	29
Mass Zr (kg)	9191	1945	9535	7
% UO_2	84.51	81.32	83.54	76.16
%ZrO_2	4.35	9.21	1.14	19.21
%Zr	11.14	9.47	15.32	4.64
Tot mass melt (kg)	**82487**	**20536**	**62222**	**151**
T melt (K)	2973.00	2943.50	2977.60	2800
T system (dcmer) (K)	sat	387.65	sat	-
P lower plenum (Pa)	2.4E+05	2.8E+05	2.8E+05	49E+05
T lower plenum (K)	sat	381.15	391.34	sat
Subcooling (°C)	0	22.24	12.05	0
Slump at (minutes)	64.2	58.8	164.7	-

Table 7.11 - Initial conditions for a MFCI detailed calculation at the moment of slumping

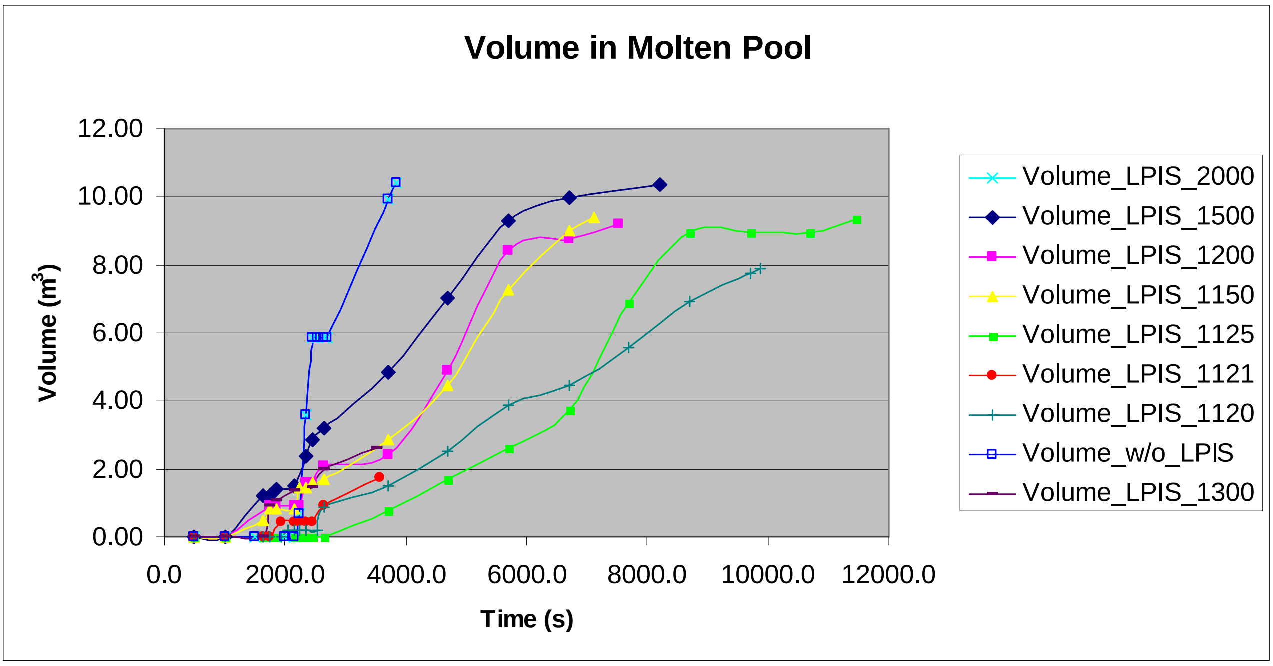

Figure 7.117 - Molten pool volume up to the slumping time in all SCDAP calculations

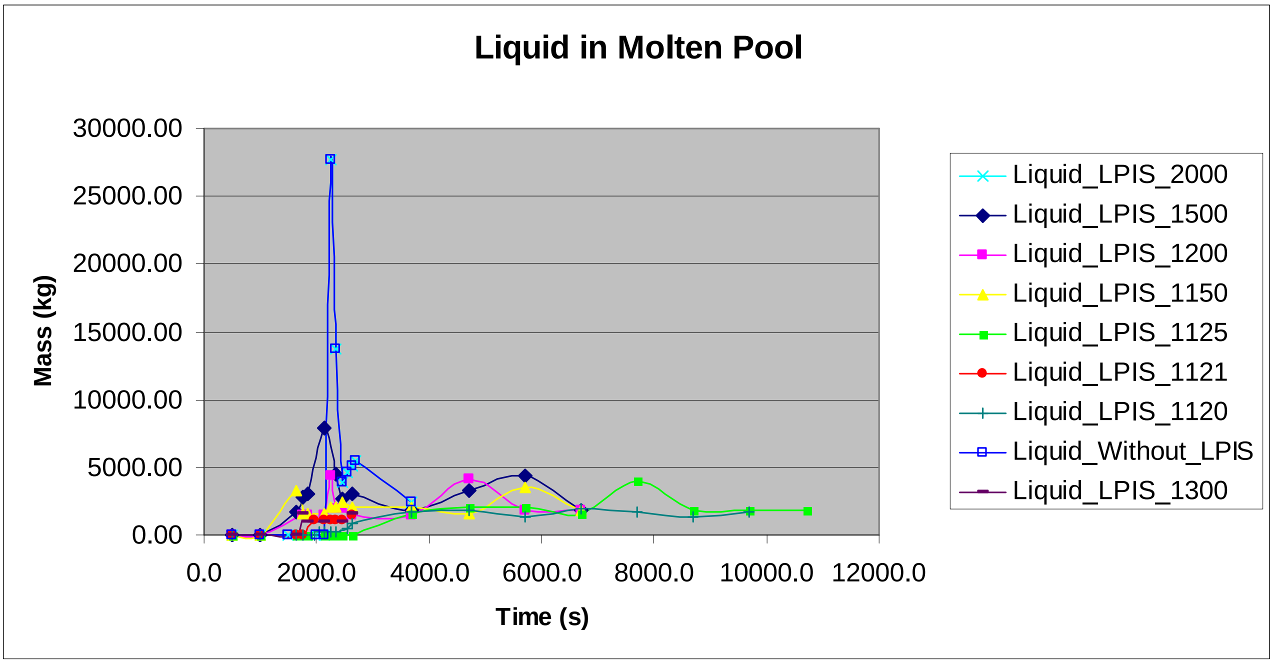

Figure 7.118 - Molten pool liquid phase up to the slumping time in all SCDAP calculations

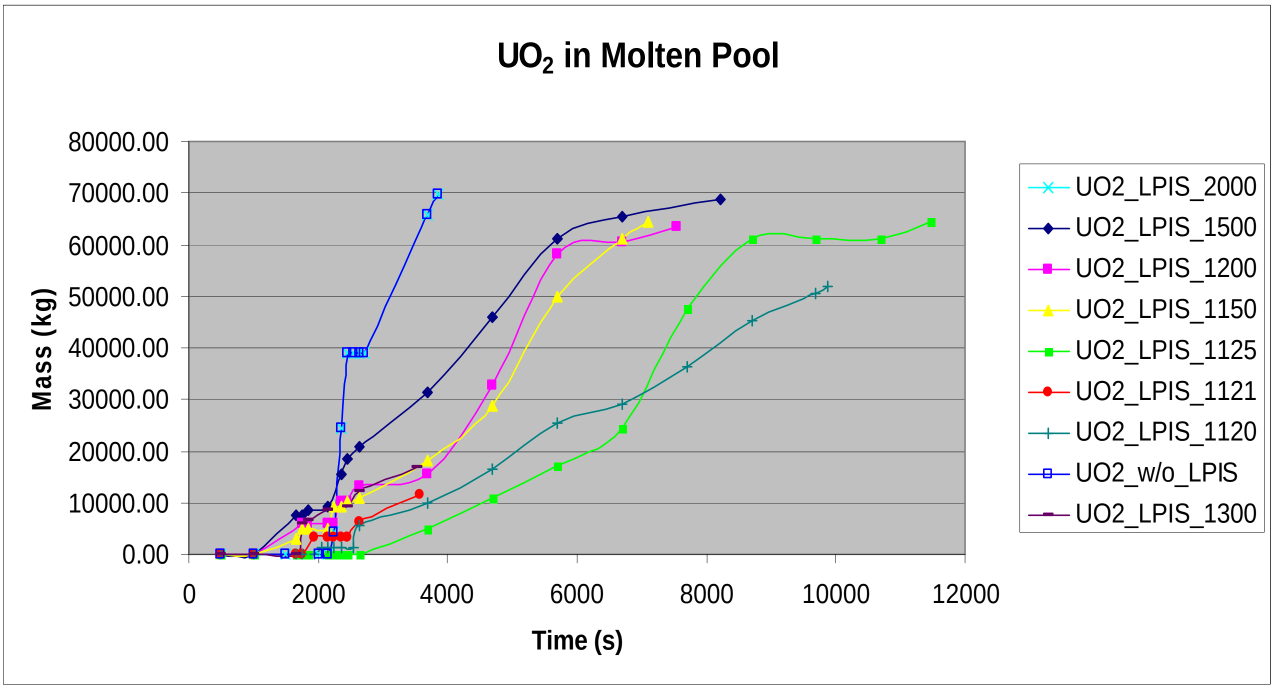

Figure 7.119 - Molten pool UO_2 mass up to the slumping time in all SCDAP calculations

7.5.7. CONCLUSIONS

Calculations show that the RELAP5/SCDAP 3.2 modelling theory in the late damage phase (as it is MFCI) reproduces phenomena as a function of the assumed option. The code assumes either *interaction* between molten mass and the residual water in the lower plenum or *no interaction at all*. In the latter the stored energy remains in the molten mass and is only removed by heat transfer from the surfaces of the resulting debris in the lower plenum.

Calculations have demonstrated that in order to perform a detailed MFCI study it is better to use a MFCI thermalhydraulic code in which the interaction grade is result from the initial conditions of the system, the molten pool conditions and the own interaction transient evolution and it is not an input parameter set by the code user. RELAP5/SCDAP 3.2 can be used to obtain the final conditions as initial conditions in a MFCI thermalhydraulic code. In that way RELAP5/SCDAP 3.2 and a detailed MFCI code can be seen as complementary tools.

Figure 7.65 shows that if LPIS injection time is lower than 659s after the break (case LPIS_1119) core temperature increase can be mitigated. The maximum time available for the operator to restore cooling conditions via the LPIS is about 10 minutes after the break (659s). Above this time meltdown cannot be avoided. Core temperature is powered due to the effect of the exothermic H_2 production when LPIS water reacts with cladding at temperatures above about 1500K (oxidation temperature).

Finally conditions up to the moment of the slumping are presented in order to select them as initial conditions for a detailed MFCI study.

8. COMETA CODE MODIFICATIONS

8.1. PREVIOUS COMETA LOGIC AND ACTUAL NEEDS

COMETA code was initially planned and developed for prediction of the thermalhydraulic behaviour of FARO facility, for design, definition of operational procedures and tests interpretation. The analytical activities were based on broad pre-test and post-test studies. The main objective of the code is to predict the behaviour of MFCI phenomena, including steam explosion events in any geometry 1d or 2d. The code is written in FORTRAN language and is structured in modules and subroutines depending on the functions and phenomena to deal with or simulate.

COMETA code is organized in a number of lumped volumes connected with junctions in the so-called 1d nodalization. A 2d nodalization can be built up connecting a number of macro-volumes (containing an arbitrary number of radial and axial volumes) and macro-junctions (Figure 6.1). The real conditions in every thermalhydraulic volume are used to set the drops conditions while they are in the volume.

An example of COMETA 1d nodalization used in the simulations for FARO geometry is presented in Figure 8.1 as a vertical cut. In some studies, however, for accuracy reasons a 2d nodalization is used. For example, FARO test L-33 uses such a nodalization to set the exact position of the trigger event. Figure 7.10 shows the real shape of 2d nodalization of FARO Test L-33 and Figure 7.29 the corresponding vertical cut.

A particular important issue concerning molten melt behaviour and its simulation with COMETA is the movement of the little *drops* formed due to the *jet* fragmentation when it enters into an hypothetical lower plenum water pool or in the water FARO release vessel. These particles float without any definite path in the water pool and fall down towards the vessel bottom, following the motion dynamic laws (gravity and friction).

In the previous COMETA logic the *drops* are considered to move or fall down with only a one-direction velocity, i.e. vertical coordinate and towards the vessel bottom. This occurred for any geometry 1d or 2d. In 1d geometry they could only fall down passing through the thermalhydraulic volumes (Figure 8.2 a). In the 2d geometry the original model assumed that *drops* were falling down in the central volumes without any radial component (Figure 8.2 b).

In FARO tests in which the initial jet size was relatively large (10 cm, versus a diameter of 70 cm) the 1d assumption was reasonable. As the jet size was reduced to 5 cm or in a real plant case, this assumption was no more applicable and it was necessary to model also the 2d flow and therefore it was necessary to include also the radial drops displacement.

It was therefore decided to modify the COMETA code subroutine that determines *drops* movement to include a radial velocity component (Figure 8.3). Changes are explained in the following subchapter.

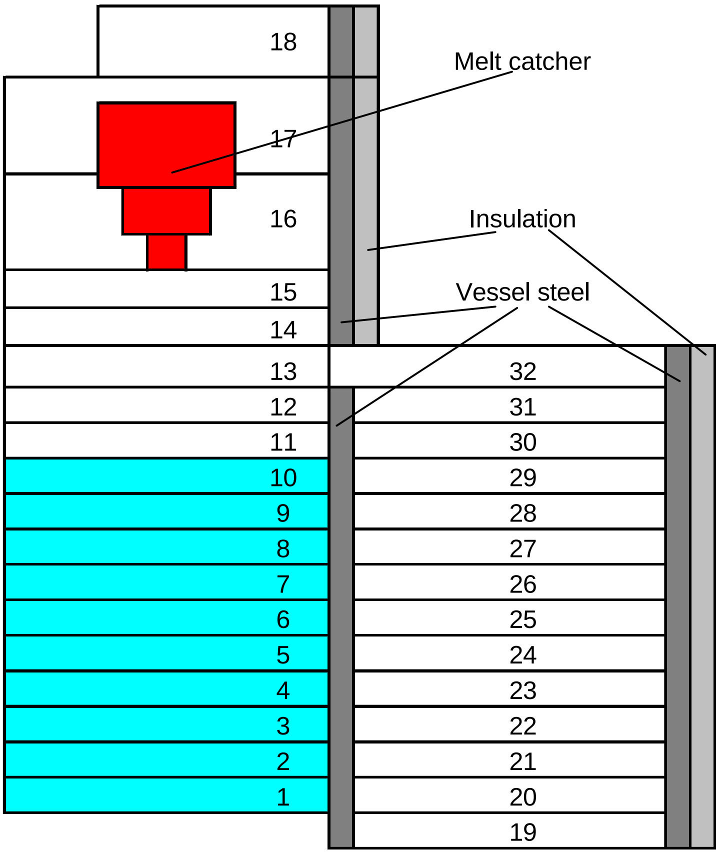

Figure 8.1 - COMETA nodalization 1d for FARO Test L-29

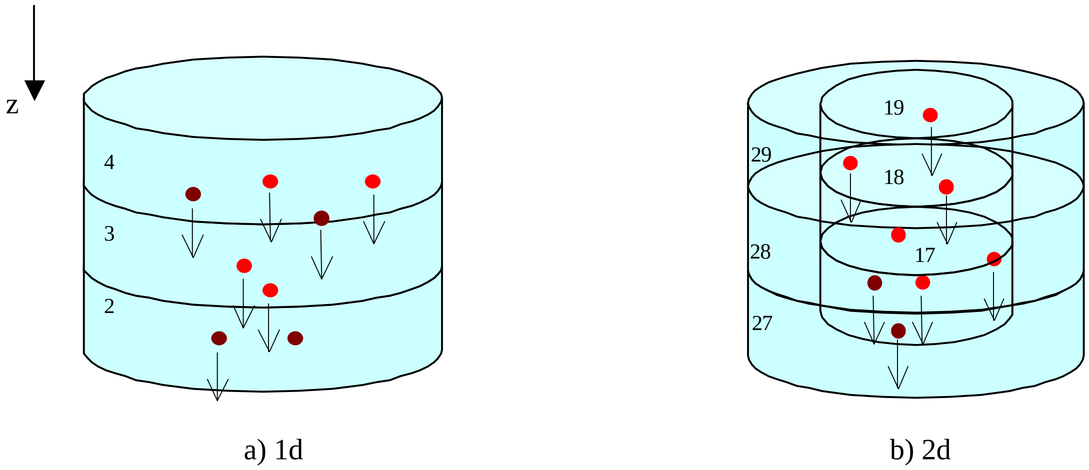

Figure 8.2 - Drops movement in thermalhydraulic volumes in 1d and 2d nodalization in previous COMETA logic

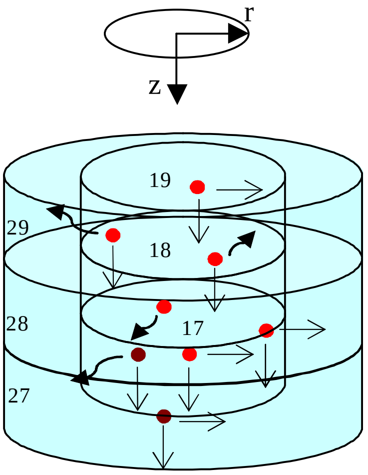

Figure 8.3 - Drops movement in thermalhydraulic volumes in 2d nodalization in present COMETA logic

8.2. MODIFIED COMETA. CHANGES INTRODUCED

The application of COMETA code to the prediction of tests performed in the FARO facility and the identification of problems in scale-up to reactor configurations, larger than scaled test facilities, lead to improve COMETA code lacks. The modifications performed in the code included part of engineering and part of computer programming analysis.

The *drops* movement subroutine (“*mapfrag*”) was modified in order to include the radial component (r). The aim of the subroutine is to determine from the *drop* position (coordinates x, r) the thermalhydraulic volume number in which the *drop* is positioned in the correspondent time step.

In that way for the 2d nodalization drops movement is not only restricted to central volumes but also to all lateral volumes.

The COMETA code is organized in explicit modules or subroutines that send and receive information from each other to calculate thermalhydraulic conditions in each time step (as a pure thermalhydraulic code) but also melt conditions are calculated in each time step for the three melt shapes of the melt field (*jet*, *drops* and *debris*).

Mainly in each global time step (t_1 = t_0+? t) both the thermalhydraulic equations and the melt fragmentation equations are solved separately in two modules (THSOLVER and FRASOLVER):

The so-called THSOLVER (built up of thermalhydraulic subroutines) solves equations obtaining 6 thermalhydraulic quantities for the time step t_1: pressure, internal energy for each phase (liquid and vapour), void fraction for each phase (liquid and vapour) and velocities for each phase (liquid and vapour). To solve equations it uses melt heat transfer calculated in the previous time step t_0.

The thermalhydraulic quantities found are used for the so-called FRASOLVER to solve melt conditions in the time step t_1 (3 melt quantities are obtained: heat transfer for *drops*, heat transfer for *jet* and heat transfer for *debris*). In general the time step interval ? t is equal for THSOLVER and FRASOLVER modules, but in some cases it is necessary to reduce global ? t for the melt conditions solving the melt quantities in shorter time steps.

The *drops* movement subroutine (“*mapfrag*”) is implicit to the FRASOLVER module, basically for each *drop* and its exact position the subroutine calculates the thermalhydraulic volume that contains the *drop* in the particular time step. Initially the subroutine was only taken into account the vertical volumes (z direction), central volumes in case of 2d nodalization. During the modifications radial component was added (r direction) so radial and not only central volumes were included in a 2d nodalization.

“*mapfrag*” receives as parameters for the calculation the following: position of the *drop* (components r and z). The returned variables are: the middle points of each thermalhydraulic volume (zmed, rmed), the number of the volume (jvol) where the *drop* is calculated to be in the time step and rmax that is the maximum radial distance of the volume (jvol).

In the subroutine first part, or *preparation* part, running a loop a matrix stores all limit coordinates (rmin, rmax, zmin and zmax) (Figure 8.4) of each thermalhydraulic volume (j) in the geometry (cylindrical or plenum shape).

In the second part or *running* part the code searches for the position of the *drop* using the *drops* coordinates received (r, z), i.e. running the loop for each thermalhydraulic volume (j) it is checked if the coordinate r is between rmin and rmax and coordinate z between zmin and zmax of the volume (j), if so the *drop* is in the volume (j) and the subroutine returns jvol=j and the middle points of the jvol volume (zmed, rmed).

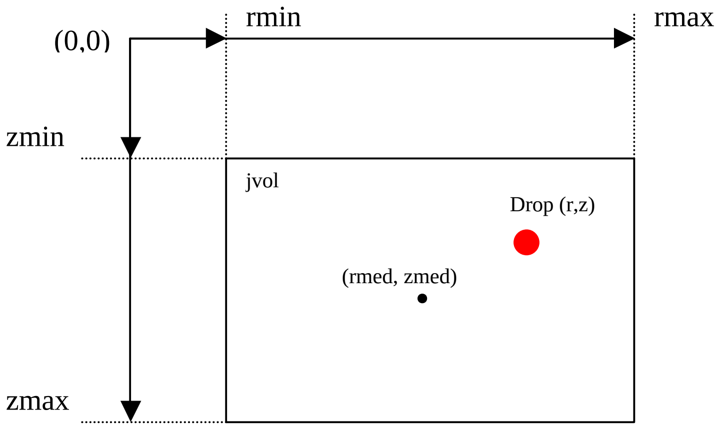

Figure 8.4 - Limit coordinates of the jvol volume and *drop* coordinates

The subroutine *"movedrrad"* is the one that really calculates *drops* relative movement and *drops* relative velocity.

This procedure calls "*mapfrag*" for every *drop* present and takes also into account if the *drop* position (x1) has overpassed the dimensions of the geometry (r>rmax), laterally or vertically and sets it symmetrically to the radial volume or to the upper volume inverting *drop* absolute radial velocities in both cases. This is the correspondent part of the code:

```
c check if reached the side, if yes vel=-vel
c
      if(x1.ge. rmax) then
        x1 = rmax ! max extension
        veldropRad(k) = -veldropRad(k)
      endif
```

If the *drop* position (x1) has reached the bottom it takes velocity=0. This is the correspondent part of the code:

```
c check if reached the center , if yes vel=0
c
      if(x1.le.0.0) then
        x1=0.e-4
        veldropRad(k)=0.0
      endif
```

Drops arrived to the bottom could be included in the fused *debris* conglomeration depending on its temperature.

The radial velocity of the (k) *drop* in the liquid phase (vfr) and in the gas phase (vgr) is calculated as:

vgr=vgradn(iv)+(rdrops(k)-deltar/2)*dvgdrn(iv) (Eq. 1)

vfr=vfradn(iv)+(rdrops(k)-deltar/2)*dvfdrn(iv) (Eq. 2)

where:

rdrops(k) is the radial position of the (k) *drop*
vfradn(iv) is the radial velocity of the volume (iv) liquid phase
vgradn(iv) is the radial velocity of the volume (iv) gas phase
deltar=rade(iv)-radi(iv) where rade is the external radius of the volume (iv) and radi the internal radius.

dvgdrn(iv) and dvfdrn(iv) are calculated in the subroutine "*velrad*"

dvfdrn(iv)=(vfo-vfi)/(rade(iv)-radi(iv)) (Eq. 3)

dvgdrn(iv)=(vgo-vgi)/(rade(iv)-radi(iv)) (Eq. 4)

where:

subscript o means out junctions
subscript i means inlet junctions

vfi is the liquid velocity of all inlet junctions of volume (iv) vfo is the liquid velocity of all outlet junctions of volume (iv)

vgi is the gas velocity of all inlet junctions of volume (iv)
vgo is the gas velocity of all outlet junctions of volume (iv)

These four velocities are calculated following the relationship between the velocities of inlet and outlet junctions in the gas or liquid phase and the mass flow that passes through the volume (iv):

$$v = \frac{M}{Aar}$$

where:

v is the junction velocity (m/s)
M is the mass flow (kg/s)
A is the inlet or outlet junction area (m^2)
a is the void fraction of liquid or gas
? is the density of liquid or gas (kg/m^3)
(vgr) and (vfr) are calculated solving (Eq.1 and Eq.2) and the average velocity is calculated as a weighted mean value of (vgr) and (vfr) in the gas, liquid and non-condensable phases in the volume (iv):

velmed=alfagn(iv)*vgr+alfafn(iv)*vfr +alfanc(iv)*vgr (Eq. 5)

where:

alfagn(iv) is the vapour void fraction in the volume (iv)
alfafn(iv) is the liquid void fraction in the volume (iv)
alfanc(iv) is the non-condensable void fraction in the volume (iv), non-condensable gases are assumed to have the vapour velocity

Finally the *drop* relative velocity (velr) is the sum of the velocity of the *drop* (veldropRad(k)) and the average velocity of the fluid in the volume (velmed) calculated before:

velr=veldropRad(k)+velmed (Eq. 6)

In the following subchapter the new version of the code including the modifications explained is tested versus FARO experimental data and compared to previous COMETA code non modified.

8.3. CALCULATIONS WITH MODIFIED COMETA LOGIC AND PREVIOUS COMETA LOGIC

L-28 was the FARO test chosen to perform two comparative calculations in order to demonstrate the different results achieved using the previous COMETA logic and the modified one. This was the first FARO test in which the jet size was reduced to 5 cm nozzle diameter from 10 cm (versus a vessel diameter of 70 cm) so the 2d nodalization assumption was the most reasonable, including the 2d flow and therefore the radial drops displacement. Figure 8.5 shows 2d nodalization for COMETA calculations. The conditions of the performed test are the following:

Mass:	174.9 kg
Melt Temperature	3052 K
Initial water Temperature	Tsat (saturation conditions)
Initial water level	1.44 m
Delivery nozzle diameter	0.044 m (5 cm jet versus FAT vessel 70 cm diameter)
Initial Pressure:	5.1 bar
Vessel geometry	FAT

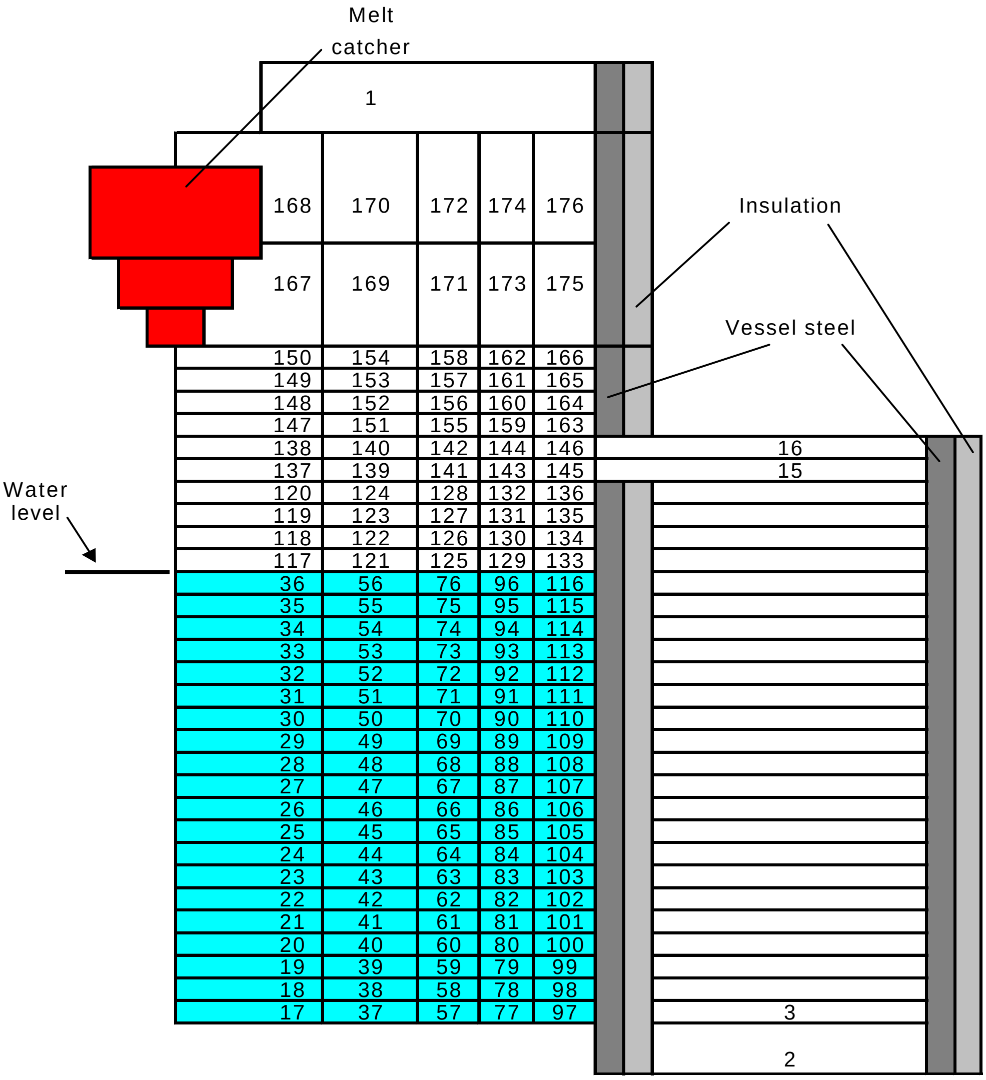

Figure 8.5 - COMETA 2d nodalization for FARO test L-28

Case L28denm is the calculation performed with the previous COMETA logic. In this case the *drops* generated in the *jet* interaction with the water present in the vessel are retained to move vertically in the central volumes (volume 17, bottom vessel, to volume 36 from Figure 8.5).

Case L28denh is the calculation performed with the modified COMETA logic, in this case the *drops* generated in the interaction have also the radial movement therefore they can travel from one internal volume to the laterals and vice versa. Their movement is free in all water volumes (volume 17, bottom vessel, to volume 116 from Figure 8.5).

Results of the calculations are presented in the following figures. Global pressure is presented in Figure 8.6. Pressure behaviour evolutions are compared to the experimental data, they follow the overall trend of the experimental data and both are similar in absolute values. The changes introduced in the code have not disturbed the general prediction of the experiment itself.

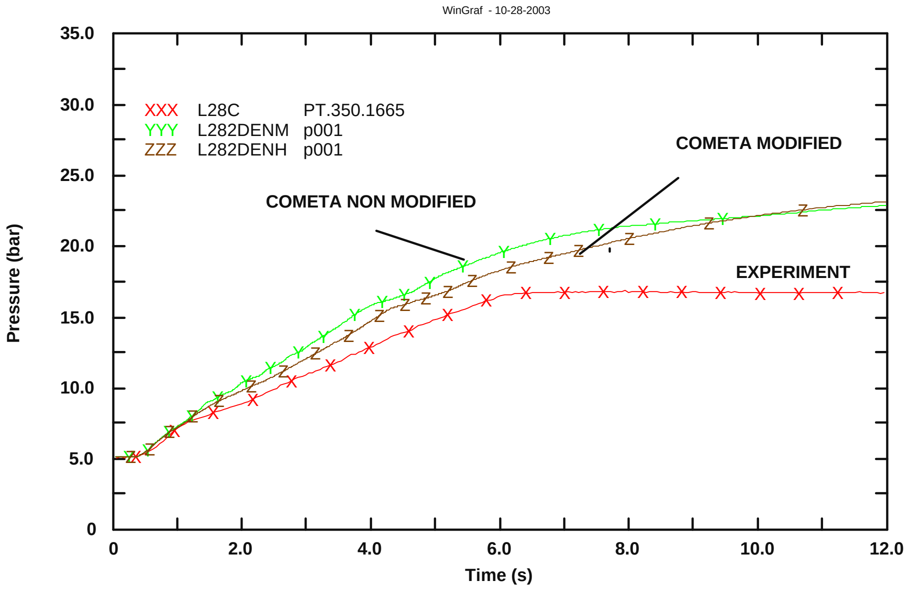

Figure 8.6 - Pressure behaviour in COMETA calculations for FARO test L-28

The comparison between both calculations to evidence the improvements in the code should be regarded in the local phenomena, i.e. local temperatures, local void fraction and local fragmented melt or *drops* distribution.

The local void fraction and fuel distribution inside a mixture strongly affects the pressure wave propagation and thus it has a strong importance in the evaluation of the explosivity and the effects of the explosion. Since the fuel distribution also affects the void distribution (steam + non-condensable gases) it is of decisive importance the correct local distribution of the fuel *drops*.

In a mixture where the *drops* fragment and distribute uniformly the explosion potential is higher if a trigger is applied. If the fuel fragments less, it is more likely that the application of a trigger does not determine an explosion. However a so called "stratitied explosion" can occur. That is when a trigger is applied to a layer of fuel with the water above.

From Figure 8.7 to Figure 8.14 water temperatures calculation results are plotted for different vertical and two radial positions in the vessel. They are compared to experimental data retrieved from the thermocouples placed into the FARO vessel during the experiment.

Results are compared in the so-called “stable melt discharge and quenching phase” of the experiment [Figure 9 of [37]] that is from 2s to about 6s. That period is the real situation in which a possible spontaneous explosion could take place.

It can be observed for most figures that the temperatures calculated with the COMETA modified are higher (due to the presence of *drops* in the lateral volumes) and closer to the experimental results in that period (2s-6s). So the code with the modifications included to take account of the *drops* radial movement has improved also the general prediction of the experiment in terms of temperature. This gives a further result of COMETA code assessment.

As it was discussed before, modifications in the code are very important for the prediction of local quantities (void fraction and *drops* distribution) critical in the evaluation of the explosivity and the effects of a possible steam explosion.

So void fraction and *drops* mass calculated quantities (in the correspondent volumes in which where compared the temperatures) are also presented in the report during the “stable melt discharge and quenching phase”. These quantities cannot be compared to experimental values but are very important in some studies. Local temperatures were compared and are in agreement with experimental values. As temperatures are partly a result of the local *drops* distribution and the void fraction, they contribute to assess code capabilities in the prediction of void fraction and *drops* distribution.

From Figure 8.15 to Figure 8.22 void fraction calculation results are plotted for different lateral volumes at four heights and two radial positions in the vessel. In general it can be observed that modified COMETA calculations reach a higher void fraction in all these volumes. Void fraction is influenced by a lot of parameters but also by the vapour produced by hot *drops* created in the central volumes, which with the new version of the code can travel to lateral volumes.

Finally the distribution of *drops* mass is plotted to verify the lateral presence of *drops* in the calculations performed with the modified code version. From Figure 8.23 to Figure 8.26 the mass of *drops* is shown in volumes at four heights and two radial positions in the vessel during the “stable melt discharge and quenching phase” (2s-6s).

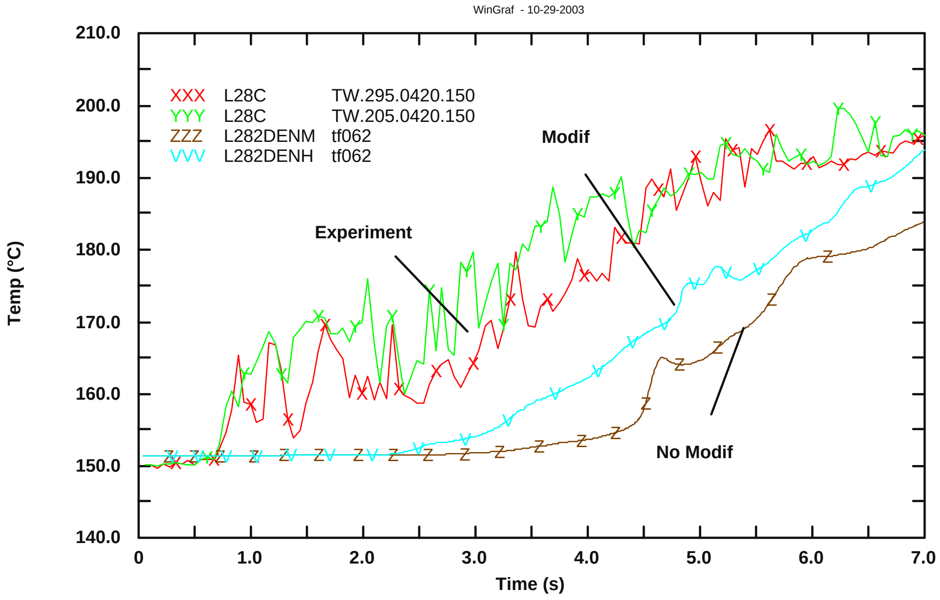

Figure 8.7 - Water temperature at height 0.420 m and 0.150 m radial vessel position

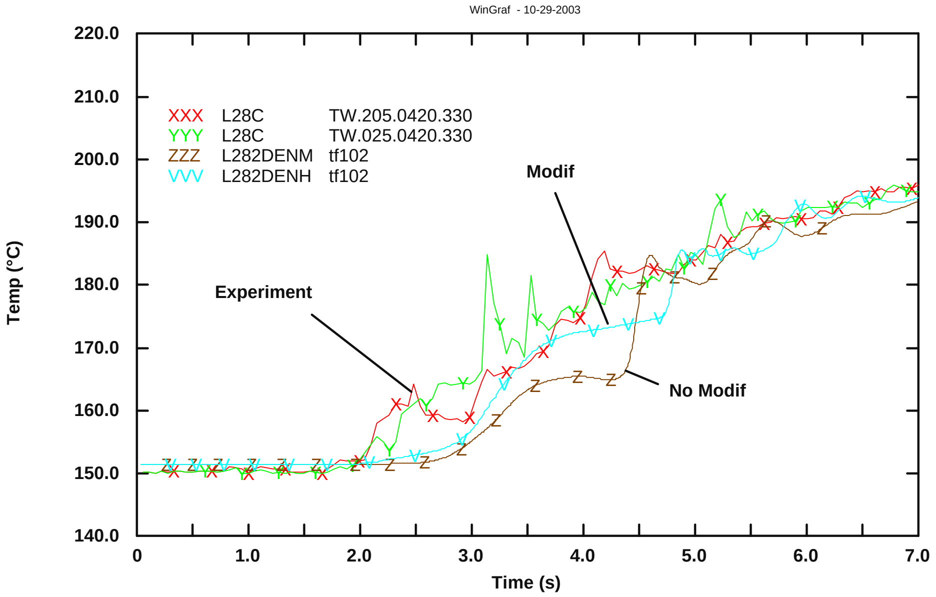

Figure 8.8 - Water temperature at height 0.420 m and 0.330 m radial vessel position

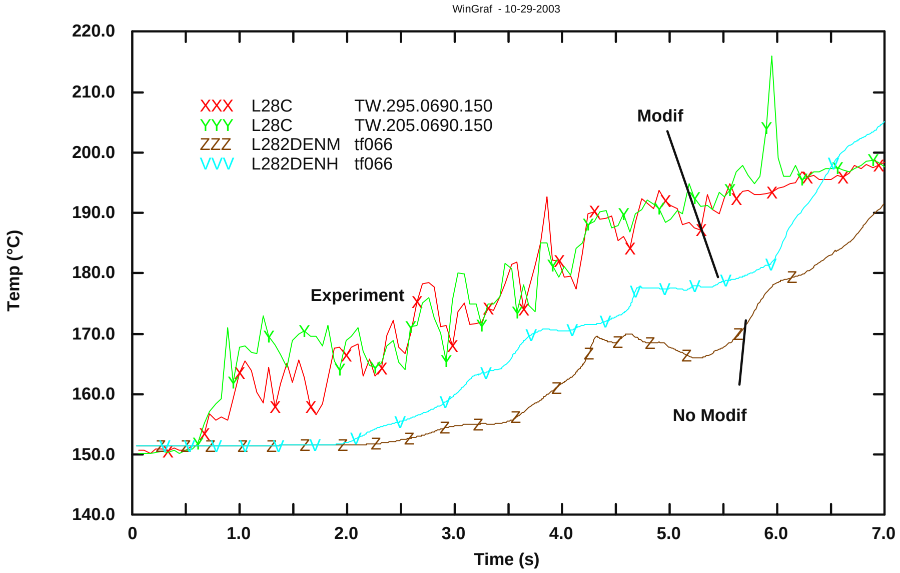

Figure 8.9 - Water temperature at height 0.690 m and 0.150 m radial vessel position

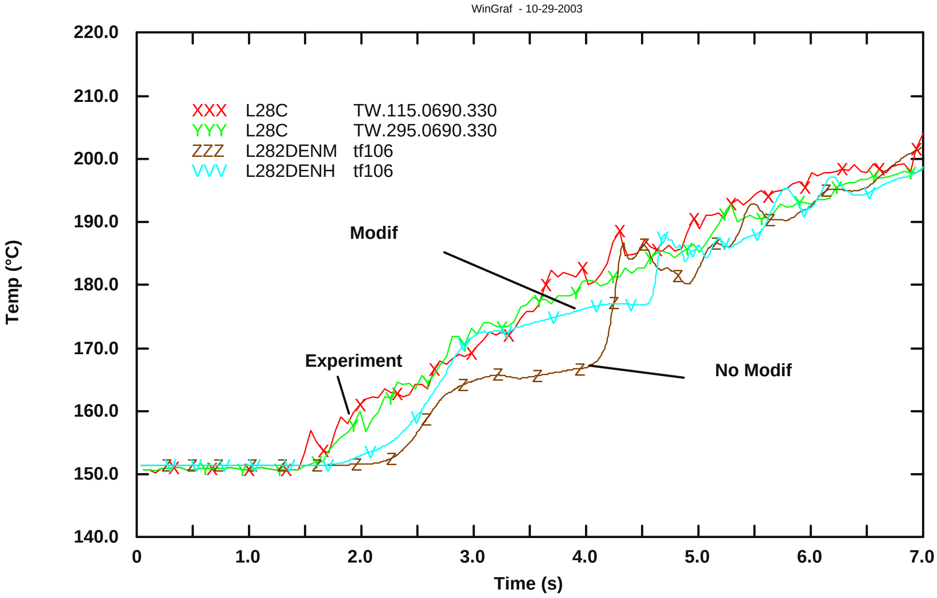

Figure 8.10 - Water temperature at height 0.690 m and 0.330 m radial vessel position

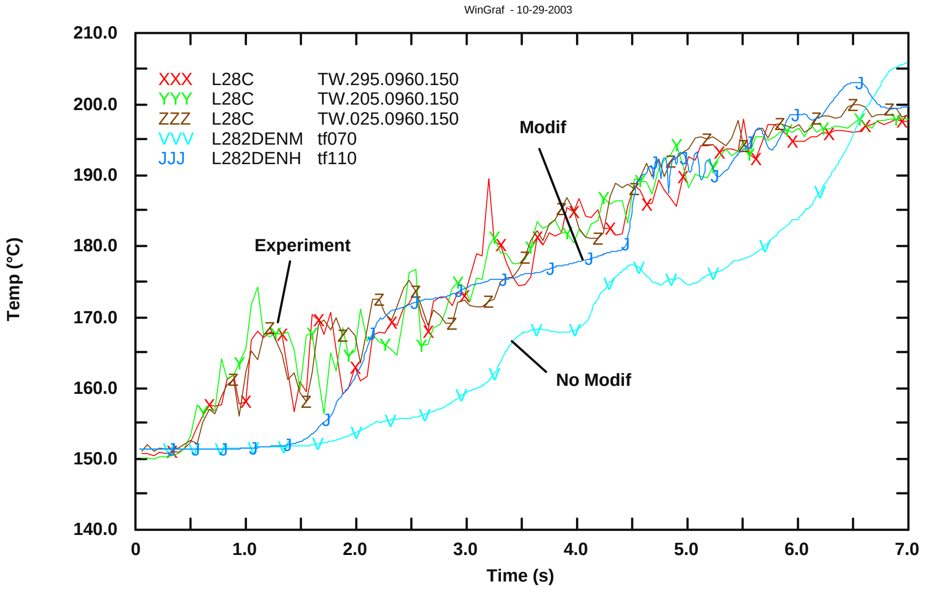

Figure 8.11 - Water temperature at height 0.960 m and 0.150 m radial vessel position

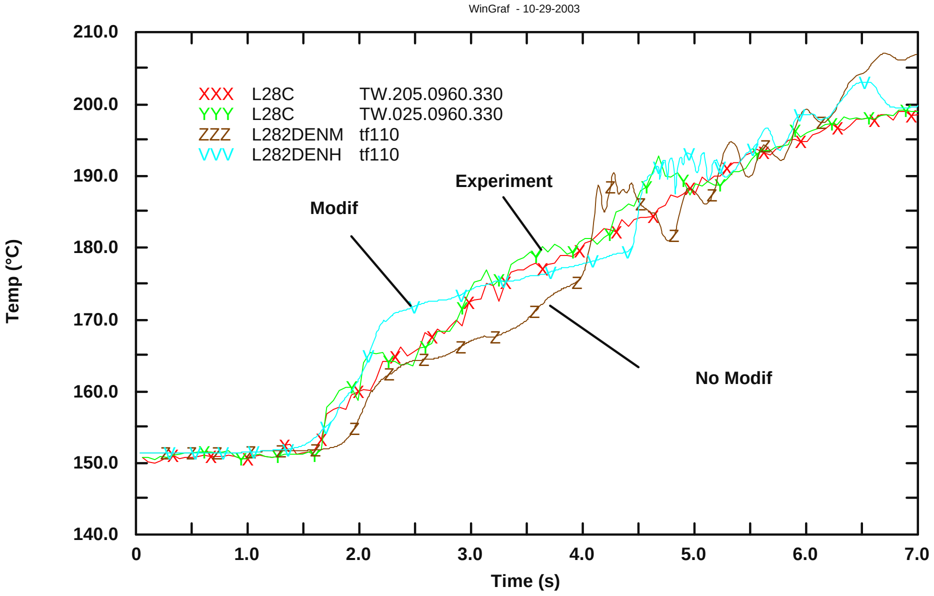

Figure 8.12 - Water temperature at height 0.960 m and 0.330 m radial vessel position

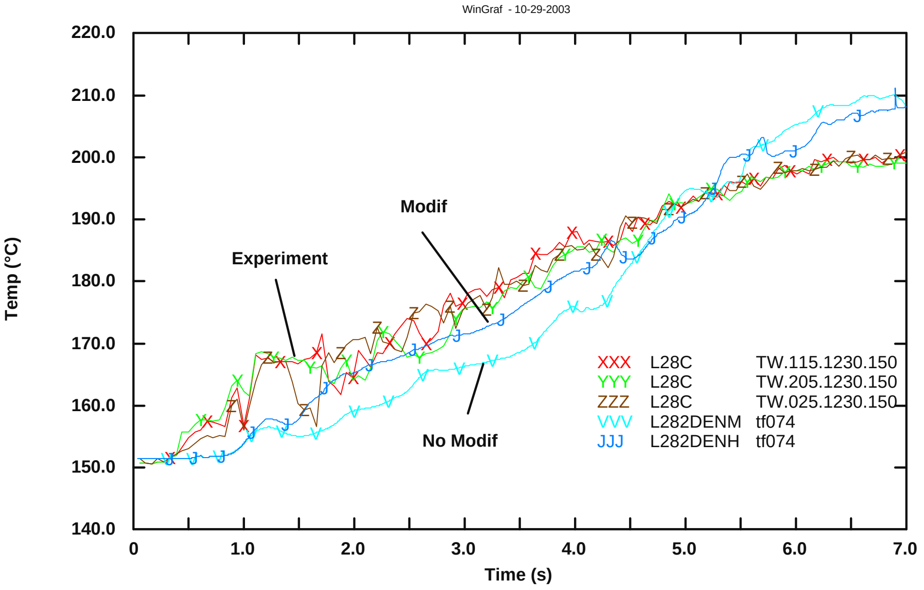

Figure 8.13 - Water temperature at height 1.230 m and 0.150 m radial vessel position

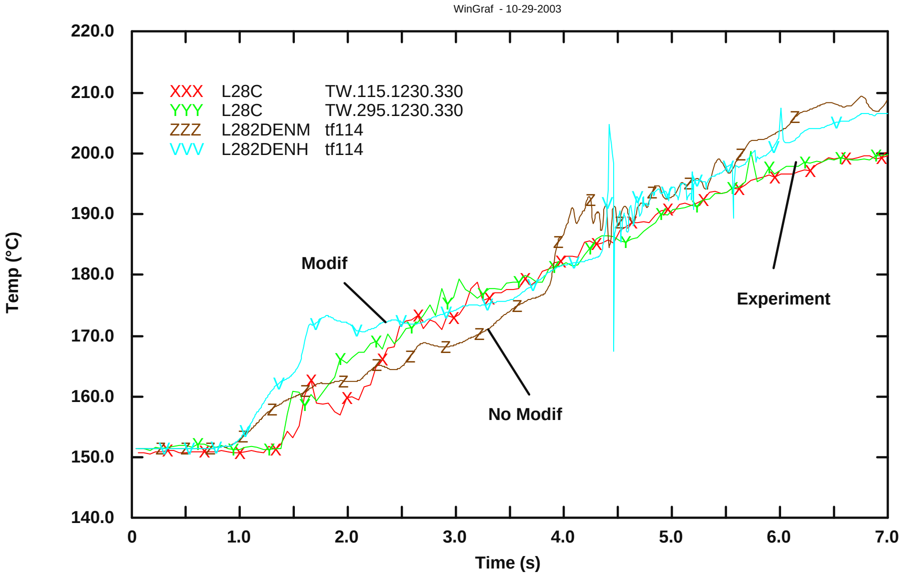

Figure 8.14 - Water temperature at height 1.230 m and 0.330 m radial vessel position

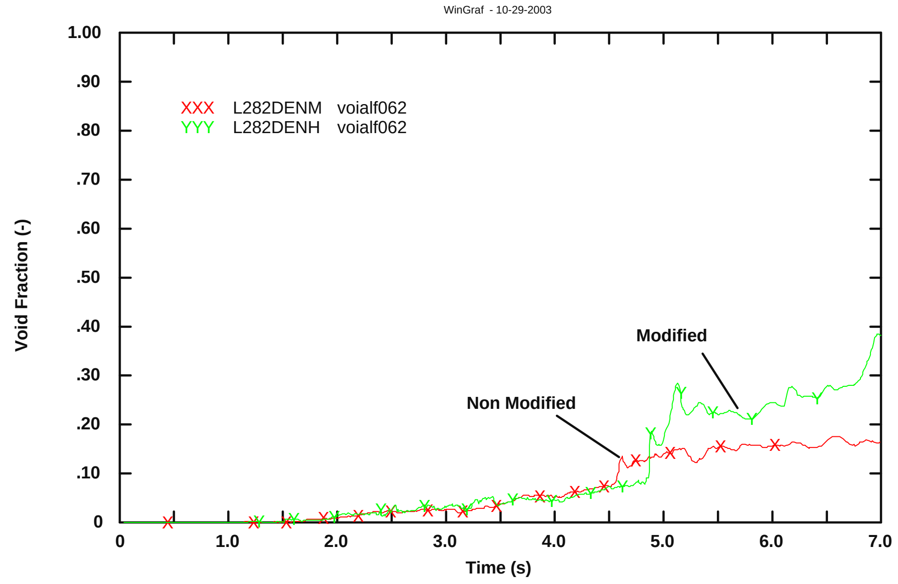

Figure 8.15 - Void fraction in volume 62 at 0.42 m height and 0.150 m radial position

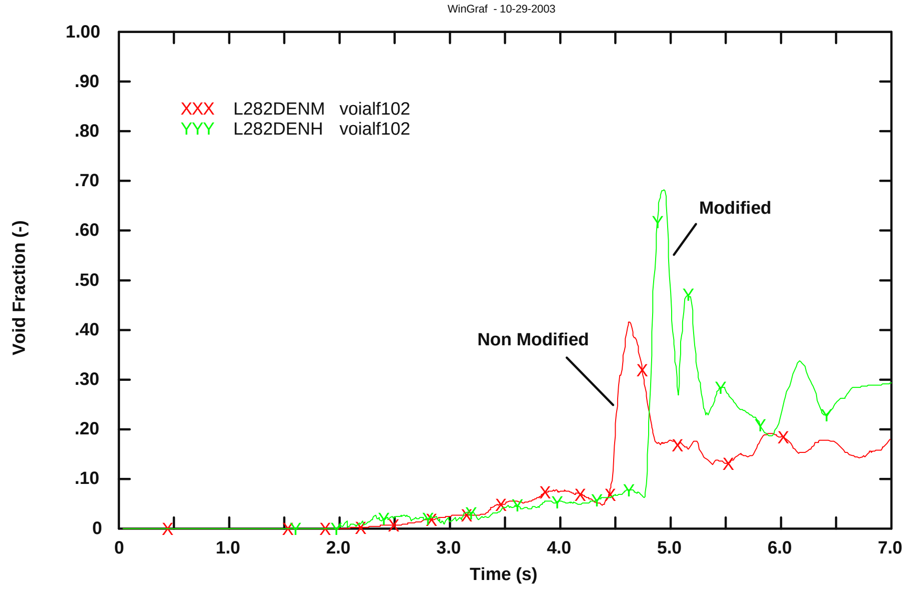

Figure 8.16 - Void fraction in volume 102 at 0.42 m height and 0.330 m radial position

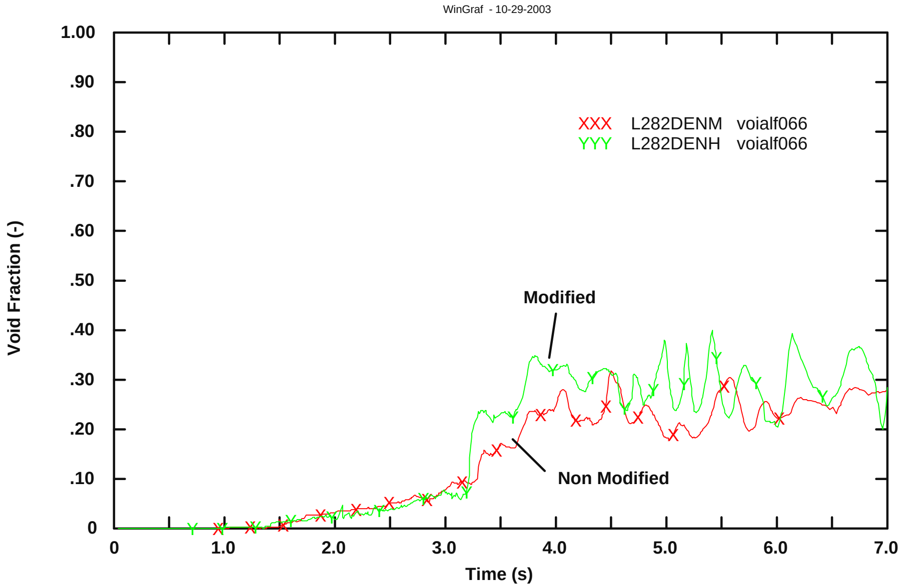

Figure 8.17 - Void fraction in volume 66 at 0.69 m height and 0.150 m radial position

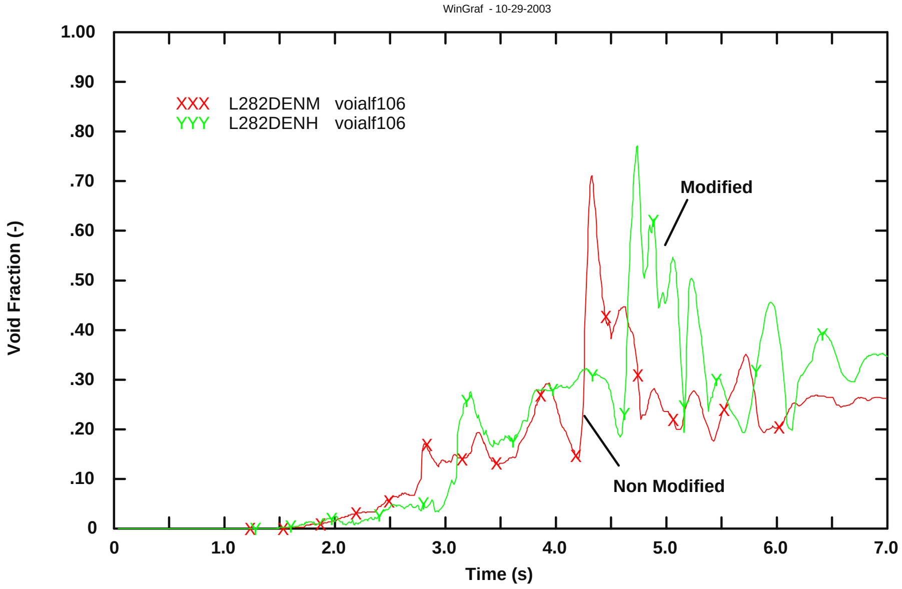

Figure 8.18 - Void fraction in volume 106 at 0.69 m height and 0.330 m radial position

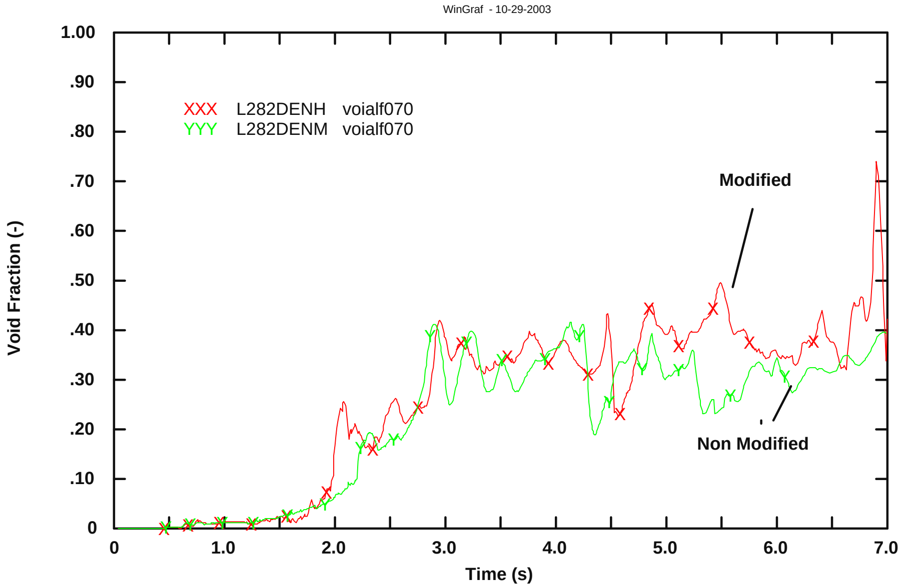

Figure 8.19 - Void fraction in volume 70 at 0.96 m height and 0.150 m radial position

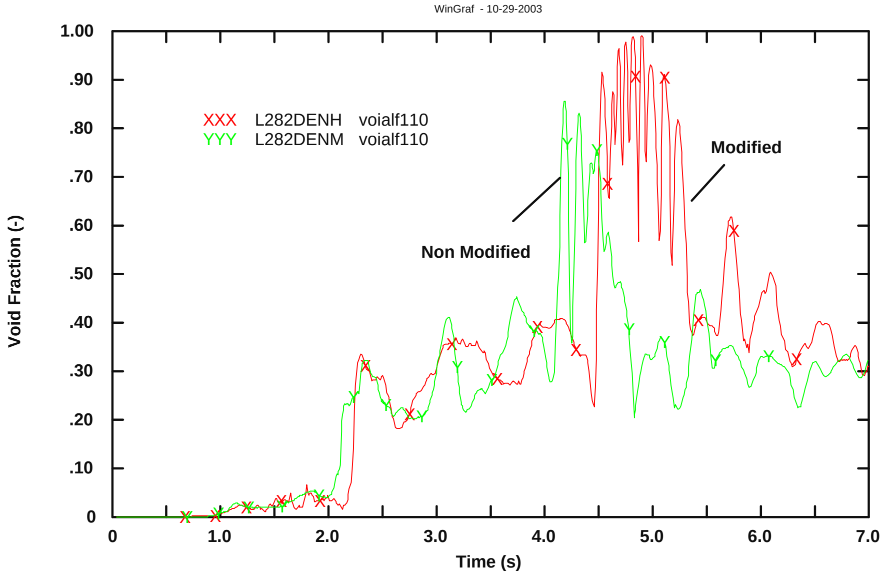

Figure 8.20 - Void fraction in volume 110 at 0.96 m height and 0.330 m radial position

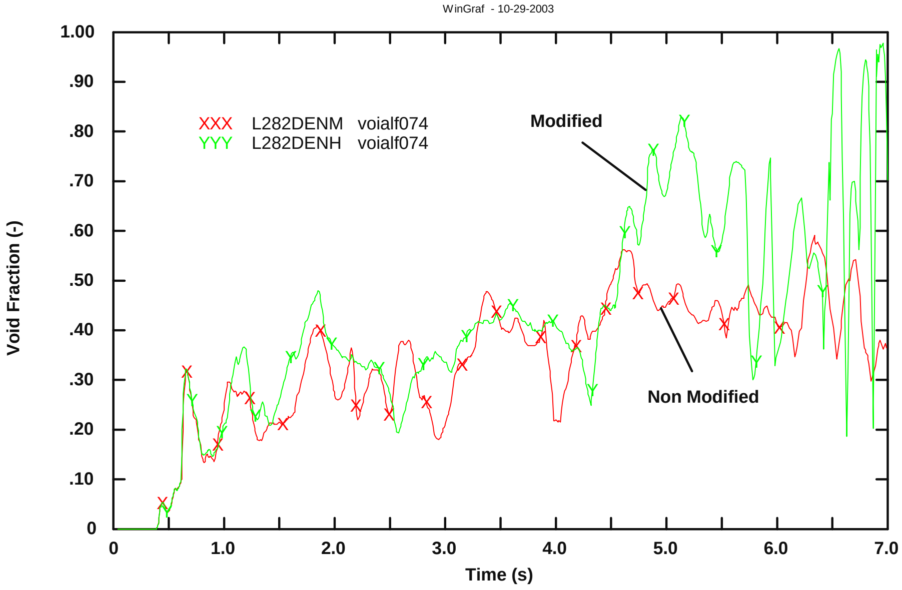

Figure 8.21 - Void fraction in volume 74 at 1.23 m height and 0.150 m radial position

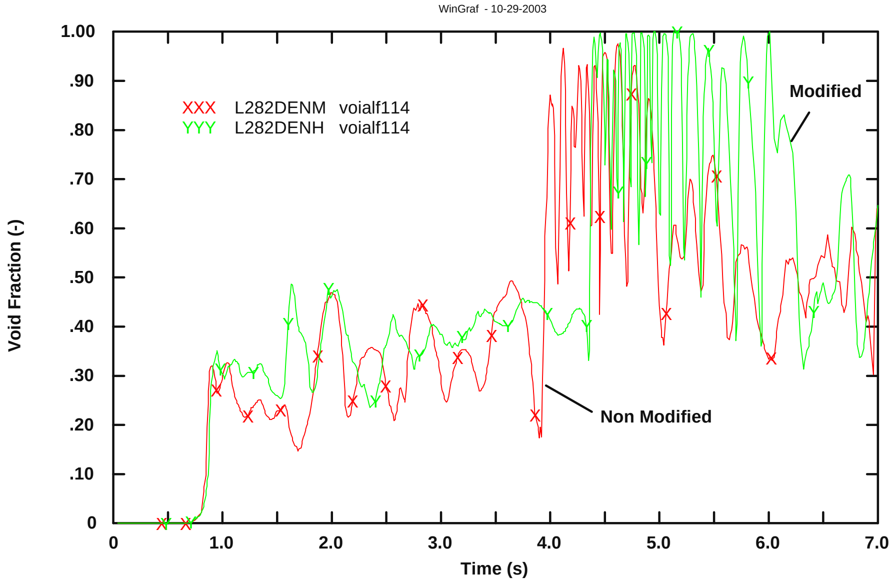

Figure 8.22 - Void fraction in volume 114 at 1.23 m height and 0.150 m radial position

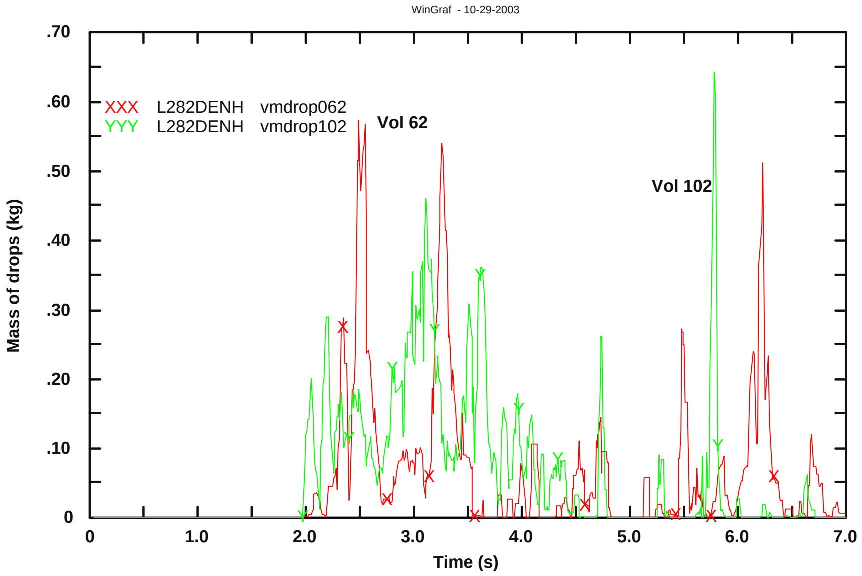

Figure 8.23 - Mass of drops distribution in lateral water volumes 62 and 102 at 0.42 m height in modified COMETA calculation

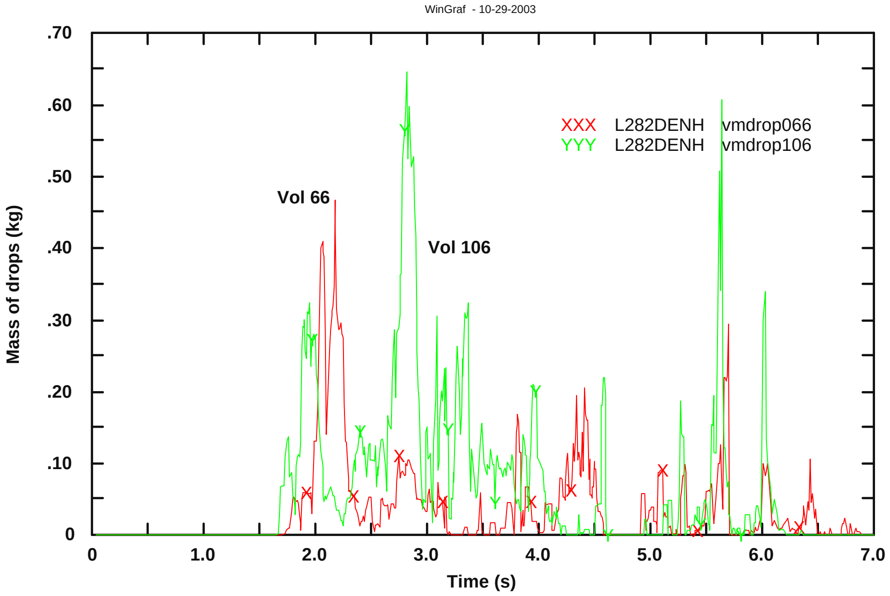

Figure 8.24 - Mass of drops distribution in lateral water volumes 66 and 106 at 0.69 m height in modified COMETA calculation

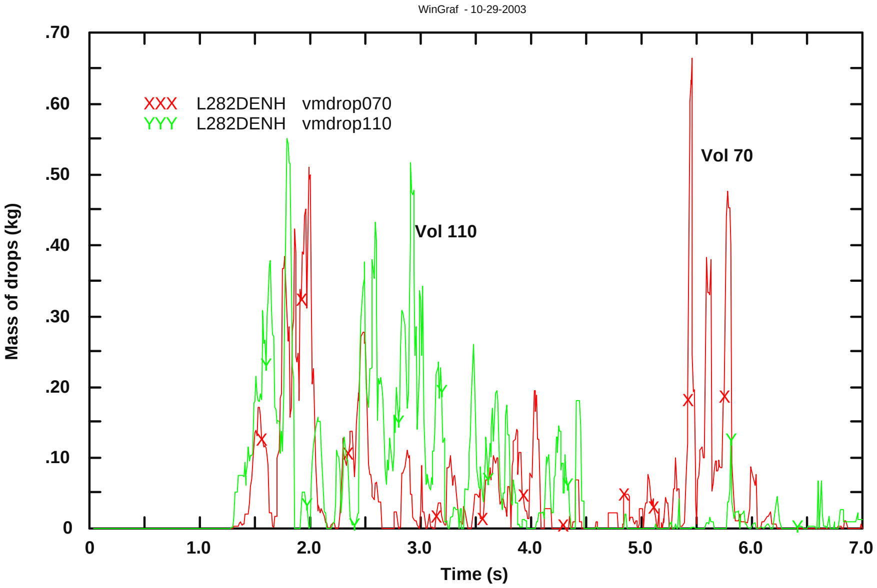

Figure 8.25 - Mass of drops distribution in lateral water volumes 70 and 110 at 0.96 m height in modified COMETA calculation

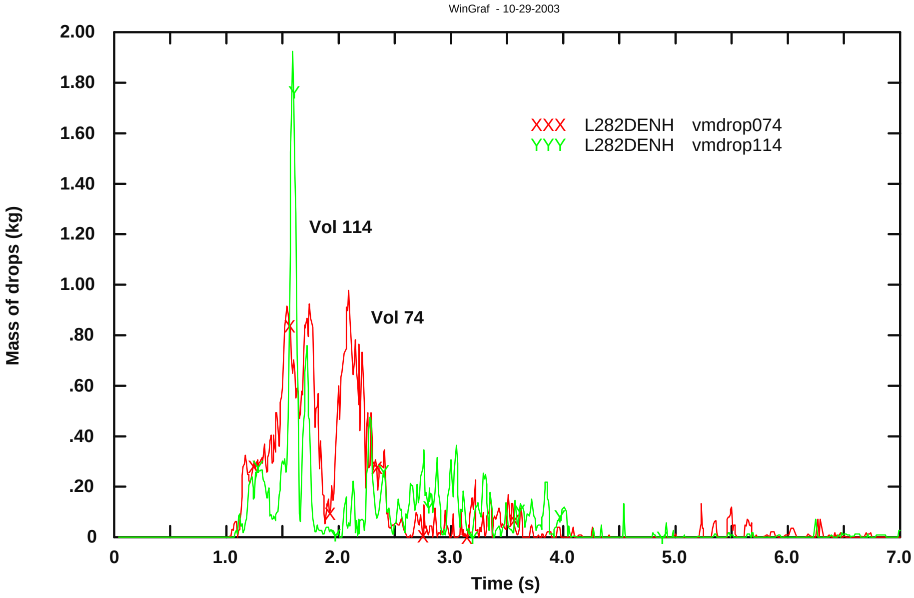

Figure 8.26 - Mass of drops distribution in lateral water volumes 74 and 114 at 1.23 m height in modified COMETA calculation

8.4. CONCLUSIONS

COMETA code source has been modified in order to include the radial movement of the melt *drops* produced in the interaction when the melt *jet* penetrates into the water and along its travel to the bottom vessel through the vessel central section. In the old version of the code *drops* movement was simulated restricted only vertically in the central volumes.

This modification has been found to be a good improvement in the prediction and assessment of the code and essential in some studies where local quantities are critical in the evolution of the transient (as local void fraction and *drops* distribution are for vapour explosions studies).

The modified COMETA code has been tested against FARO test L-28 experimental data and compared to old version. In the results 3 local parameters were presented: temperatures were compared to experimental values and gave improved results in the prediction. Void fraction and *drops* distribution were plotted in order to evidence the differences using the old and the new version of the code.

OVERALL CONCLUSIONS

In the context of the prediction through computer codes of the progression and consequences of severe accidents in water cooled reactors the following achievements were reached:

- The COMETA code was successfully applied for the prediction of FARO tests under conditions not experimented before: subcooling in test L-29, vapour explosion in test L-33.

  In the subcooled test option it was shown the effect on the global void fraction of the selection of different pressure and /or temperature. The results indicate that the greater influence on the void fraction is caused by the pressure level (1 to 5 bar), which compressing the non-condensable void fraction, induces remarkable change in the global void fraction. No major influence is present in the quenching rate. Also, in subcooled conditions no significant difference resulted from the adoption of the standard or enhanced fragmentation model.

  The code was able to calculate the subcooled conditions without innerving in major stability problems. It was found a point that needed improvement in the code: the jet parcels description in order to properly account for velocity differences among them.

  The COMETA code was able to calculate the conditions foreseen for the FARO Test L-33. The code was also applied to simulate the triggering and the response due to a possible explosion. No propagation was calculated if the H_2 generation model was the same as applied for previous saturated tests. If the amount is reduced to values typical of the last subcooled Test L-31 or even less a propagation of the explosion seems possible.

- The code was applied to large scale configurations (ASCÓ NPP reactor) clarifying phenomena (thermalhydraulic equilibrium) and size effects. All the cases shown decreasing fragmentation and energy production as the initial water level in the core inlet and lower plenum was reduced. The relation between the void fraction and the quenching rate was clarified. An equilibrium value is generally attained and is possible only if increase and decrease of void fraction is allowed; that is if the mixture level is at or above the injection point (flooded regime). On the contrary, if the mixture level is too low, the power exchanged will continuously decrease and tend to zero as the water level decreases (depleted regime).

  Problems in scale-up to reactor configurations were identified in the application of COMETA code and leaded to improve COMETA code lacks. For example COMETA logic related to drops movement in 2d nodalization was changed and adapted to large reactor configurations. The implementation of two-dimensional equational model has revealed as absolutely necessary for reproducing the detailed movement of the drops in particular applications where detailed knowledge of local phenomena is absolutely needed. The hypotheses used for the improvement implemented in the COMETA code, formulated in the equations that this Thesis proposes, have resulted useful for the fitting description of the fragmented melt during the MFCI.

- Assessment and qualification of the COMETA code: Simulations performed with old versions were unified with the present code version. Results were improved and consolidated. Guides to perform simulations were given to advise code users when selecting 1d or 2d geometries.

- Calculations to understand the RELAP5/SCDAP 3.2 modelling theory in the late damage phase were performed. They revealed that in order to perform a detailed MFCI study it is better to use a MFCI thermalhydraulic code in which the interaction grade is result from the initial conditions of the system, the molten pool conditions and the own interaction transient evolution and it is not an input parameter set by the code user. RELAP5/SCDAP 3.2 can be used to obtain the final conditions as initial conditions in a MFCI thermalhydraulic code. In that way RELAP5/SCDAP 3.2 and a detailed MFCI code can be seen as complementary tools. The maximum time available for the operator to restore cooling conditions via the LPIS after a LOCA was acquired from the calculations. Above this time meltdown could not be avoided. Finally conditions up to the moment of the slumping were presented in order to select them as initial conditions for a detailed MFCI study.

In general the main objective of the PhD research was achieved **expanding the general knowledge in Melt Fuel Coolant Interaction**. The knowledge was complemented **collaborating and complementing** the application of COMETA code under conditions not experimented before, **developing and improving** COMETA code sources and **verifying the code consistency, analysing and unifying** the COMETA simulations carried so far.

A further analytical study was carried out in order to underline the MFCI inside the general overview of a NPP severe accident progression.

BIBLIOGRAPHY AND REFERENCES

[1] A. Annunziato, S. Barsotti - *“Assessment and Improvements of the COMETA Condensation Model in Presence of Non-Condensable Gases”* - JRC - Technical Note No.I.94.90. June 1994.

[2] F. Reventós, J. Sánchez-Baptista, A. Pérez-Navas, P. Moreno - “*Assessment and application of blackout transients at Ascó nuclear power plant with relap5/mod2*” - International agreement report nureg/ia-119-June 1993.

[3] C. Addabbo, A. Annunziato, R. Silverii, D. Magallon - “*COMETA analysis of system pressure effect in FARO Melt Quenching tests*” - Proceedings of the ICONE 6 - 6335 - May 10-14, 1998.

[4] A. Annunziato, C. Addabbo - “*COMETA (Core Melt Thermalhydraulic Analysis) a computer code for Melt Quenching Analysis*” - International Conference on New Trends in Nuclear System Thermalhydraulics. Pisa, May-June 1994.

[5] A. Annunziato, C. Addabbo, H. Hohmann, D. Magallon - “*COMETA code calculation of FARO Melt Quenching Tests*” - International Conference on New Trends in Nuclear System Thermalhydraulics. Pisa, May-June 1994.

[6] A. Annunziato, C. Addabbo - *“COMETA (Core Melt Thermalhydraulic Analysis): Code User’s Manual”* - JRC - Special Publication No.I.98.130. October 1998.

[7] A. Annunziato - *“COMETA v0.4 Pre Test Calculation of FARO Base Case Test”* - JRC - Technical Note No.I.93.114. August 1993.

[8] S. Bocci, A. Cirigliano, G. Forasassi, G. Fruttuoso, A. Manfredini and F. Oriolo - *“Core coolability and corium retention in a LWR”* - Università di Pisa. Dipartimento di Ingegneria Meccanica, Nucleare e della Produzione.

[9] A. Annunziato - *“The effect of H_2 production on the propagation of Energetic Fuel Coolant Interaction in UO_2/ZrO_2 Mixtures”* - JRC - Technical Note No.I.96.108. June 1996.

[10] A. Annunziato, C. Addabbo - “*Effect of uncondensables in Fuel Coolant Interaction and Quenching*” - Proceedings of the ICONE 5 - 2593 - May 26-30, 1997 Nice, France.

[11] G. Albrecht (FZK-D), A. Annunziato (JRC-EC), P. Giordano (IRSN-F), D. Magallon (CEA-F), L. Meyer (FZK-D), S. Park (RIT-SE), P. Piluso (CEA-F), R. Seghal (RIT-SE), W. Schütz (FZK-D). *“EUROPEAN NETWORK FOR THE REDUCTION OF UNCERTAINTIES IN SEVERE ACCIDENT SAFETY ISSUES (EURSAFE). ASSESSMENT OF CURRENT PRACTICES FOR PRESERVATION AND MAINTENANCE OF Severe Accident DATA”*. January 2003.

[12] H.J. Allelein, K.Neu, J.P. Van Dorsselaere, K. Müller, P. Kostka, M. Barnak, P. Matejovic, A. Bujan, J. Slaby. - *“European validation of the integral code ASTEC (EVITA)”*. - Nuclear Engineering and Design 221 (2003) 95 - 118.

[13] A. Annunziato - “*Evaluation of melt final superheat with Metal Zr mixtures*” - Internal JRC Note. October 1998.

[14] M. SAITO et al. - *“Experimental study on penetration behaviors of Water Jet into Freon-11 and Liquid Nitrogen”* - ANS Proc. 1988 Nat.l Heat Transfer Conf., Houston.

[15] A. Annunziato, A. Yerkess, C. Addabbo - *“FARO and KROTOS code simulation and analysis at JRC Ispra”* - Nuclear Engineering and Design 189 (1999), 359 - 378.

[16] A. Annunziato, C. Addabbo - "*FARO Base Case Post-Test Analysis by COMETA Code*" - Seventh International Topical Meeting on Nuclear Reactor Thermal Hydraulics (NURETH-7). Saratoga, 1995.

[17] D. Magallon - "*FARO LWR Programme. Scoping Test Data Report*" - JRC - Technical Note No.I.92.135. 1992.

[18] M. Dehn, D. Magallon - "*FARO LWR Programme Base Case Test L-11 Data Report*" - JRC - Technical Note No.I.94.147. 1994.

[19] A. Benuzzi, D. Magallon - "*FARO LWR Programme Base Case Test L-11 Quick Look Report*" - JRC - Technical Note No. I.94.55. 1994.

[20] R. Silverii, D. Magallon - "*FARO LWR Programme Test L-27 Data Report*" - JRC - Technical Note No.I.99.194. 1999.

[21] R. Arroyo, J. A. Martínez, C. Vicente, P. Villalibre - "*Fenomenología de degradación del núcleo. Comparación con una simulación predictiva para un PWR comercial*" - Revista Sociedad Nuclear Española, January 1991.

[22] M. Alconero, A. I. Alvárez, J. A. Bagües, J. C. García, J. González, A. Lantaron, J. Saiz, O. Villegas - *"Herramientas de análisis e interpretación de fenomenología de degradación del núcleo"* - Revista Sociedad Nuclear Española, January 1991.

[23] A. Franceschini - *"Interazione Combustibile Refrigerante in un reattore nucleare ad acqua legera in condizioni inzidentali severe"* - Università degli Studi di Pisa. Facoltà di Ingegneria. Nuclear Engineering Final Project. 1998 - 1999.

[24] A. Alonso - *"La investigación sobre accidentes severos"* - Revista Sociedad Nuclear Española, October 1989.

[25] A. Annunziato, C. Addabbo - *"JRC STRESA Web site: http://asa2.jrc.it/stresa*".

[26] *"Loss of Coolant Accident by W.L. Riebold"*. - Nuclear Reactor Safety Transfer. Ed. Mc. Graw-Hill. ISBN 0-89116-224-0.

[27] A. Maréchal, A. Annunziato - *"Modification of the Corium Physical Properties in the COMETA Code"* - JRC - Technical Note No.I.94.98. July 1994.

[28] NEA Committee on the Safety of Nuclear Installations (CSNI) - Senior Group of Experts on Nuclear Safety Research Facilities and Programmes (SESAR/FAP) *"Nuclear Safety Research in OECD Countries: Summary Report of Major Facilities and Programmes at Risk"* - 2001 Report.

[29] A. Annunziato, C. Addabbo, A. Yerkess, R. Silverii, W. Brewka, G. Leva - "'*OECD/CSNI International Standard Problem 39 on FARO Test L-14 on Fuel Coolant Interaction and Quenching - Comparison Report, Volume I: Analysis of the Results*" - NEA/CSNI/R (97)31. 1997.

[30] *"Oecd-loft lp-fp-2 code comparison report vol i: thermal-hydraulic comparisons compiled by: d.c.mecham, m.merilo t.sirkia, j.j.peña, s.enciso, f. reventós, f.oriolo, e.coryell, s.güntay"* - OECD-LOFT project report - April 1989.

[31] F. Reventós, J. J. Peña, S. Enciso - *"Oecd-loft experiment lp-fp-2 calculation using relap5/mod2"* - International code assessment and application program specialist meeting. Winfrith- UK - January 1987.

[32] C. Pretel, F. Reventós - "*Prediction of unusual occurrence of core dryout in sbloca scenarios of the Ascó npp*" - 6th international conference on nuclear engineering-icone6 - San Diego-California-Usa - May 1998.

[33] F. Reventós, J. Sánchez-Baptista, A. Pérez-Navas, P. Moreno - "*Primary feed&bleed thermal-hydraulic analysis for asco nuclear power plant*" - Relap5 international users seminar - Boston-Massachusetts-Usa - July 1993.

[34] A. Alonso, L. Rebollo, R. Salve - *"El proyecto Phebus - CSD en el marco de la investigación sobre accidentes severos"* - Revista Sociedad Nuclear Española, January 1991.

[35] Comité de Dirección del Consorcio - "*El proyecto Phebus - CSD y el consorcio Phebus- España"* - Revista Sociedad Nuclear Española, January 1991.

[36] B. Adroguer, C. Gonnier, J. A. Martínez - "*El proyecto Phebus. La instalación, la matriz experimental y el análisis de los resultados"* - Revista Sociedad Nuclear Española, January 1991.

[37] A. Annunziato, C. Addabbo, D. Magallon - "*FARO Test L-28 Quick Look Report*" - JRC - Technical Note No.I.99.74. 1999.

[38] The SCDAP/RELAP5 Development Team - "*SCDAP/RELAP5/MOD3.2 CODE MANUAL VOLUME II: DAMAGE PROGRESSION MODEL THEORY"* - NUREG/CR-6150 INEL-96/0422 Revision 1 Volume II. October 1997.

[39] The SCDAP/RELAP5 Development Team - "*SCDAP/RELAP5/MOD3.2 CODE MANUAL VOLUME III: USER'S GUIDE AND INPUT MANUAL"* - NUREG/CR-6150 INEL-96/0422 Revision 1 Volume III. November 1997.

[40] The SCDAP/RELAP5 Development Team - "*SCDAP/RELAP5/MOD3.2 CODE MANUAL VOLUME V: DEVELOPMENTAL ASSESSMENT"* - NUREG/CR-6150 INEL-96/0422 Revision 1 Volume V. October 1997.

[41] Emmanuell Gailliez, Jean-Calude Micaelli - "*Séminaire ICARE/CATHARE"* - Institut de Protection et de Sûreté Nucléaire (IPSN).

[42] H.J. Allelein, J. Bestele, K. Neu, F. Jacq, M. Kissane, W. Plumecocq, J.P. Van Dorsselaere. - *"Severe accident code ASTEC development and validation"*.

[43] J. C. Latché - IPSN/DRS, A. Breest, H.J. Allelein - GRS - "*Status of the Simulation of Melt Spreading and Melt Coolability within the Containment*".

[44] M. Epstein, H.K. Fauske - "*Steam film instability and the Mixing of the Core-Melt Jets and Water"* - ANS Proc., 1985 Nat.l Heat Transfer Conf., Denver

[45] A. Annunziato, C. Addabbo, W. Brewka - *"The STRESA (Storage of Reactor Safety) Database (Web page: http://asa2.jrc.it/stresa)*" - ICONE 9 - 818 - 2001.

[46] J. J. Peña, S. Enciso, F. Reventós - "*Thermal-hydraulic post-test analysis of lp-fp-2 experiment*" - OECD loft project-Spanish consortium final report-November 1987.

[47] J. J. Peña, S. Enciso, F. Reventós - "*Thermal-hydraulic post-test analysis of oecd-lp-fp-2 experiment*" - International agreement report nureg/ia-0049-April 1992.

[48] L. Batet; C. Pretel; C. Llopis, A. Cuadra, JL. Gago, F. Reventós - "*Thermal-hydraulic code assessment activities of the technical university of Catalonia* " - 2002 relap5 international users seminar - Park City-Utah-Usa - September 2002.

[49] F. Reventós, J. Sánchez-Baptista, A. Pérez-Navas, P. Moreno - "*Transient analysis for Ascó npp using relap5/mod2*" - Relap5 user's seminar college station-Texas-Usa, February 1989.

[50] F. Reventós, J. Sánchez-Baptista, A. Pérez-Navas, P. Moreno - "*Transient analysis in the Ascó npp using relap5/mod2*" - Nuclear Technology volume 90, number 3, June 1990.

[51] H. S. Park, R. Chapman, M. L. Corradini (University of Wisconsin, Madison) - *"Vapor Explosions in a One-Dimensional Large-Scale Geometry with Simulant Melts"*. NUREG/CR-6623. October 1999.

[52] M. L. Corradini (University of Wisconsin, Madison) - *"Vapor Explosions: A Review of Experiments for Accident Analysis"*. Nuclear Safety, vol. 32.No 3, July-September 1991.

PUBLICATIONS

[1] "Characterizing Melt Fuel - Coolant Interaction in a NPP context with RELAP5/SCDAP 3.2 code". CD-Rom for the 29th Annual Meeting of the Spanish Nuclear Society, Zaragoza, October 2003. P. Pla, F. Reventós, A. Annunziato.

[2] "Use of STRESA (Storage of Reactor Safety) Web platform for Remote Codes Input deck Preparation and Execution". CD-Rom for the 27th Annual Meeting of the Spanish Nuclear Society, Valencia, October 2001. P. Pla, A. Annunziato, C. Addabbo.

[3] "COMETA Code Calculations of the FARO Quenching Tests". JRC EUR 19761 EN, March 2001. P. Pla, A. Annunziato, C. Addabbo.

[4] "Simulación mediante el código de cálculo COMETA de los experimentos de interacción combustible fundido-refrigerante realizados en la instalación FARO". CD-Rom ISSN. 1575-3204 for the 26th Annual Meeting of the Spanish Nuclear Society, León, October 2000. P. Pla, A. Annunziato, C. Addabbo.

[5] "COMETA code Analysis of Fuel Coolant Interaction Phenomena in a Reactor Geometry" - Ninth International Topical Meeting on Nuclear Reactor Thermal Hydraulics (NURETH-9), San Francisco, California, October 3 - 8, 1999. A. Annunziato, C. Addabbo, P. Pla.

[6] "COMETA v.1 Pre-Test Calculation of FARO Test L-33". JRC Technical Note No I.99.163, September 1999. A. Annunziato, P. Pla, C. Addabbo.

[7] "COMETA v.1 Pre-Test Calculation of FARO Test L-29". JRC Technical Note No I.99.44, March 1999. A. Annunziato, P. Pla, C. Addabbo.

[8] "Analysis of Fuel-Coolant Quenching Phenomena by COMETA code in Reactor Geometry". JRC Technical Note No I.99.48, March 1999. P. Pla, A. Annunziato, C. Addabbo.

[9] "Análisis de la fenomenología de interacción combustible fundido-refrigerante mediante el código COMETA". CD-Rom ISSN. 1137-2885 for the 24th Annual Meeting of the Spanish Nuclear Society, Valladolid, October 1998. P. Pla, A. Annunziato.

LIST OF FIGURES

LIST OF TABLES